FINAL REPORT

Behavior of Perfluoroalkyl Chemicals in Contaminated Groundwater

SERDP Project ER-2126

FEBRUARY 2016

Christopher P. Higgins, Ph.D.
John E. McCray, Ph.D.
Robert L. Siegrist, Ph.D., P.E.
Jonathan O. Sharp, Ph.D.
Jennifer G. Sepulvado
Tess Weathers
David Azzolini
Kaneen Christensen
Erica McKenzie
Simon Roberts
Colorado School of Mines

Distribution Statement A
This document has been cleared for public release

SERDP
DOD ▪ EPA ▪ DOE

Page Intentionally Left Blank

This report was prepared under contract to the Department of Defense Strategic Environmental Research and Development Program (SERDP). The publication of this report does not indicate endorsement by the Department of Defense, nor should the contents be construed as reflecting the official policy or position of the Department of Defense. Reference herein to any specific commercial product, process, or service by trade name, trademark, manufacturer, or otherwise, does not necessarily constitute or imply its endorsement, recommendation, or favoring by the Department of Defense.

Page Intentionally Left Blank

REPORT DOCUMENTATION PAGE

Form Approved
OMB No. 0704-0188

The public reporting burden for this collection of information is estimated to average 1 hour per response, including the time for reviewing instructions, searching existing data sources, gathering and maintaining the data needed, and completing and reviewing the collection of information. Send comments regarding this burden estimate or any other aspect of this collection of information, including suggestions for reducing the burden, to Department of Defense, Washington Headquarters Services, Directorate for Information Operations and Reports (0704-0188), 1215 Jefferson Davis Highway, Suite 1204, Arlington, VA 22202-4302. Respondents should be aware that notwithstanding any other provision of law, no person shall be subject to any penalty for failing to comply with a collection of information if it does not display a currently valid OMB control number.
PLEASE DO NOT RETURN YOUR FORM TO THE ABOVE ADDRESS.

1. REPORT DATE *(DD-MM-YYYY)*	2. REPORT TYPE	3. DATES COVERED *(From - To)*
02/19/2016	FINAL Report	04/27/2011-02/19/2016

4. TITLE AND SUBTITLE
Behavior of Perfluroalkyl Chemicals in Contaminated Groundwater

5a. CONTRACT NUMBER
W912HQ-11-C-0052

5b. GRANT NUMBER

5c. PROGRAM ELEMENT NUMBER

6. AUTHOR(S)
Christopher P. Higgins, John E. McCray, Robert L. Siegrist, Jonathan O. Sharp, Jennifer Guelfo, Tess Weathers, Kaneen Christensen, Erica McKenzie, Simon Roberts

5d. PROJECT NUMBER
ER-2126

5e. TASK NUMBER

5f. WORK UNIT NUMBER

7. PERFORMING ORGANIZATION NAME(S) AND ADDRESS(ES)
Colorado School of Mines
1500 Illinois Street
Golden, CO 80401

8. PERFORMING ORGANIZATION REPORT NUMBER
ER-2126

9. SPONSORING/MONITORING AGENCY NAME(S) AND ADDRESS(ES)
Strategic Environmental Research & Development Program
4800 Mark Center Drive, Suite 17D08
Alexandria, VA 22350

10. SPONSOR/MONITOR'S ACRONYM(S)
SERDP

11. SPONSOR/MONITOR'S REPORT NUMBER(S)
ER-2126

12. DISTRIBUTION/AVAILABILITY STATEMENT
DISTRIBUTION STATEMENT A. Approved for public release: distribution unlimited.

13. SUPPLEMENTARY NOTES

14. ABSTRACT
This project evaluated physicochemical and biological parameters for determining the fate and transport of PFAAs in groundwater relevant to AFFF-impacted sites in the presence of co-contaminants and during their remediation. Results indicate PFAA transport can be retarded by NAPLs. PFAAs do not appear to significantly affect hydrocarbon degradation, though they do induce biofilm formation and interfere with microbial dehalogenation. ISCO can result in increased PFAA sorption. Many PFAAs rapidly desorb from AFFF-impacted soils, though PFAA precursors desorb more slowly. Advective studies support the strong role of pH on PFAA sorption. Finally, ISCO may facilitate conversion of precursors to PFAAs.

15. SUBJECT TERMS
Perfluoroalkyl Chemicals, Contaminated Groundwater

16. SECURITY CLASSIFICATION OF:			17. LIMITATION OF ABSTRACT	18. NUMBER OF PAGES	19a. NAME OF RESPONSIBLE PERSON
a. REPORT	b. ABSTRACT	c. THIS PAGE			Christopher P. Higgins
					19b. TELEPHONE NUMBER *(include area code)*
U	U	U	U	249	(720) 984-2116

Page Intentionally Left Blank

TABLE OF CONTENTS

Abbreviations and Acronyms vii
Acknowledgements ix
Executive Summary x

1. INTRODUCTION AND PROJECT SCOPE 1
   1.1 PFAA Transport and Retardation 1
   1.2 Potential Interactions with NAPL Co-Contaminants 4
   1.3 Potential Impacts of Co-Contaminant Remediation Technologies 5
   1.4 ER 2126 Project Goals and Approach 7

2. METHOD REFINEMENT AND VERIFICATION 10
   2.1 Introduction (Task 1) 10
   2.2 Method Refinement and Verification Experimental Approach 12
      2.2.1 Overview 12
      2.2.2 Aqueous Spike Recovery Protocol 13
      2.2.3 Solid Phase Spike Recovery Protocol 14
      2.2.4 Solid and Aqueous Phase Sample Analysis 15
   2.3 Results and Discussion 16
      2.3.1 Aqueous Spike Recovery Experiments 16
      2.3.2 Solid Phase Spike Recovery Experiments 17

3. BATCH PARTIONING EXPERIMENTS 19
   3.1 Introduction (Task 2) 19
   3.2 Experimental Methods and Approach 21
      3.2.1 Materials 21
      3.2.2 Batch Sorption Experiments 22
      3.2.3 Aqueous Sample Preparation 23
      3.2.4 Soil Extractions 24
      3.2.5 LC-MS/MS Analysis 25
      3.2.6 Quality Assurance/Quality Control Measures 25
   3.3 Results and Discussion 27
      3.3.1 PFAA Sorption 27
      3.3.2 Impact of NAPL 30
      3.3.3 Impact of SDS 34
      3.3.4 Impact of AO 37
   3.4 Implications 38

4. BATCH CO-CONTAMINANT REMEDIATION EXPERIMENTS 40
   4.1 Introduction (Task 3) 40
   4.2 Enhanced Biofilm Production by a Toluene-Degrading Rhodococcus Observed After Exposure to Perfluoroalkyl Acids (Task 3a) 40

4.2.1 Background 40
4.2.2 Materials and Methods 42
4.2.2.1 PFAA Preparation and Aqueous Analysis 42
4.2.2.2 Cellular Preparation, Harvest, and Protein Measurements 43
4.2.2.3 Toluene Biodegradation 43
4.2.2.4 Growth and EPS Production 44
4.2.2.5 Soil Enrichments 45
4.2.2.6 Quantification of Gene Expression 45
4.2.3 Results and Discussion 50
4.2.3.1 Effect of PFAAs on Toluene Degradation 50
4.2.3.2 Effect of PFAA Presence on Growth and Biofilm Formation ... 52
4.2.3.3 Expression of Stress Genes 55
4.2.4 Environmental Implications 56
4.3 Perfluoroalkyl acids inhibit reductive dechlorination of trichloroethene by repressing Dehalococcoides (Task 3b) 58
4.3.1 Background 58
4.3.2 Materials and Methods 59
4.3.2.1 PFAA preparation and aqueous analysis 59
4.3.2.2 Cellular preparation 60
4.3.2.3 Reductive dechlorination with the mixed culture 60
4.3.2.4 Dechlorination measurements 60
4.3.2.5 Phylogenetic sequencing 61
4.3.3 Results and Discussion 62
4.3.3.1 Effect of PFAAs on reductive dechlorination by a |mixed culture 62
4.3.3.2 Effects of PFAA exposure on community structure 64
4.3.3.3 Reductive dechlorination of axenic Dehalococcoides 69
4.3.4 Environmental Implications 70
4.4 Impacts of ISCO on PFAA Sorption in Batch Systems (Task 3c) 71
4.4.1 Background 71
4.4.2 Experimental Conditions 72
4.4.2.1 Materials 72
4.4.2.2 Experimental Conditions 72
4.4.3 Results and Discussion 73
4.4.3.1 PFAA Sorption 73
4.4.3.2 Impact of Permanganate 74
4.4.3.3 Impacts of Persulfate 75
4.4.3.4 Data Considerations and Conclusions 77

5. FLOW-THROUGH TRANSPORT AND REMEDIATION EXPERIMENTS 78
5.1 Introduction (Task 4) 78
5.2 Relevant Advective Transport Theory 78
5.3 Transport Potential of Perfluoroalkyl Acids (PFAAs) at AFFF-impacted Sites: Column Experiments and Modeling (Task 4a) 80

5.3.1 Background 80
5.3.2 Experimental Methods and Approach 81
5.3.2.1 Materials 81
5.3.2.2 Column Design 82
5.3.2.3 Bromide Tracer Tests 82
5.3.2.4 PFAA Column Tests 83
5.3.2.5 Sample Preparation and Analysis 84
5.3.2.6 Equilibrium PFAA Sorption 84
5.3.2.7 Data Analysis 86
5.3.2.8 Contaminated Aquifer Simulations 87
5.3.3 Results and Discussion 88
5.3.3.1 Qualitative Trend in PFAA Advective Transport 88
5.3.3.2 Evaluation of Equilibrium Transport 89
5.3.3.3 Flow Interruption Experiments 90
5.3.3.4 Continuous Flow vs. Flow Interruption Kinetic Parameters 92
5.3.3.5 Factors Impacting PFAA Mass Transfer 95
5.3.3.6 Implications for PFAA Remediation 97
5.3.4 Conclusions 98
5.4 PFAA Transport with Active Microbial Communities (Task 4b) 99
5.4.1 Background 99
5.4.2 Materials and Methods 99
5.4.3 Results 101
5.4.4 Conclusions 103
5.5 Effects of chemical oxidants on PFAA transport in columns (Task 4c) 103
5.5.1 Background 103
5.5.2 Experimental Methods and Approach 105
5.5.2.1 Experimental design 105
5.5.2.2 Materials 105
5.5.2.3 Column packing and characterization 107
5.5.2.4 Column experiments, sample collection, and supporting batch experiments 107
5.5.2.5 Analytical procedures 109
5.5.2.6 PFAA data analysis 110
5.5.3 Results and Discussion 111
5.5.3.1 PFAA transport through unoxidized porous media 111
5.5.3.2 PFAA fate during ISCO application to the porous media 113
5.5.3.3 Aqueous chemistry effects on PFAA sorption 120
5.5.3.4 Effects of oxidant species and altered geochemistry on PFAA transport 121
5.5.3.5 Effects of oxidized porous media on PFAA transport 122
5.5.4 Conclusions 126
5.6 The influence of a non-aqueous phase liquid (NAPL) and chemical oxidant application on perfluoroalkyl acid (PFAA) fate and transport (Task 4c) 127
5.6.1 Background 127

5.6.2 Materials and Methods 129
5.6.2.1 Experimental design 129
5.6.2.2 Materials 130
5.6.2.3 Column packing, characterization, and TCE application 132
5.6.2.4 Column experiments and sample collection 133
5.6.2.5 Ancillary batch experiments 134
5.6.2.6 Analytical procedures 135
5.6.2.7 Data analysis 135
5.6.3 Results and discussion 138
5.6.3.1 1-D column studies water quality 138
5.6.3.2 PFAA sorption by TCE 143
5.6.3.3 PFAA fate and transport during chemical oxidant treatment (phases ii and iii) 147
5.6.3.4 PFAA transport in oxidized porous media (phases iv – vi) 153
5.6.3.5 Post-experiment PFAA partitioning coefficients 157
5.6.4 Conclusions 159

6. DESORPTION OF PFASs FROM AFFF-IMPACTED SOIL 160
6.1 Introduction 160
6.2 Background 160
6.3 Materials and Methods 162
6.3.1 Materials 162
6.3.1.1 Soils 162
6.3.1.2 Soil and Aquifer Solid Characterization 162
6.3.1.3 Solids Extraction 162
6.3.1.4 Analytical Standards and Methods 163
6.3.1.5 PFAA Precursor Oxidation 163
6.3.1.6 Analytical Methods 163
6.3.2 Experimental Approach 163
6.3.2.1 Batch Desorption Experiments 163
6.3.2.2 Batch System Modeling 164
6.3.2.3 Column Experiments 164
6.4 Results and Discussion 165
6.4.1 Analysis of Fresh Soils and Aquifer Soils 165
6.4.2 PFAA Desorpiton in Batch Systems 166
6.4.3 Modeling of Batch Systems 167
6.4.3.1 Fast and Slowly Desorbing Modeled Fractions 172
6.4.3.2 Chain Length Effects 173
6.4.5 PFAA Desorption from Columns 175
6.4.5.1 Untreated Columns 175
6.4.5.2 Columns Treated with Chemical Oxidants 177
6.4.5.3 Column Desorption Conclusions 179

6.4.6 Overall Conclusions and Implications 179
6.4.6.1 Desorption 179
6.4.6.2 Implications for Source Zones 180

7. REPORTING, DISSEMINATION, AND CONCLUSIONS 182
7.1 Reporting and Dissemination 182
7.1.1 Reporting 182
7.1.2 Dissemination 182
7.2 Summary and Conclusions 186

8. REFERENCES 188

APPENDICES 210
Appendix A-1 Soil Isotherm Parameters and Interpolated K_d Values 211
Appendix A-2 Summary of Freundlich n-values measured in PFAS and PFAS+ Co-contaminated Isotherms 218
Appendix A-3 Aqueous PFAS Concentrations measured in the Presence of Varying Concentrations of SDS 219
Appendix A-4 Aqueous PFAS Concentrations measured in the Presence of Varying Concentrations of AO 221
Appendix B Dual-Indexed Primer Specification used in Chapter 4 223

ABBREVIATIONS AND ACRONYMS

1D	one dimensional
ADE	advection-dispersion equation
AGW	artifical groundwater
AO	n,n-dimethyldodecylamine n-oxide
AFB	Air Force Base
AFCEC	Air Force Civil Engineering Center
AFFF	Aqueous film forming foam
au	arbitrary unit
BAA	broad area announcement
BTC	breakthrough curve
BTEX	benzene, toluene, ethylbenzene, xylene
cDCE	cis-dichloroethene
CMC	critical micelle concentration
COC	chemical of concern
CSM	Colorado School of Mines
CTAB	cetyltrimethylammonium bromide
DNA	deoxyribonucleic acid
DD	Dodecane
DoD	U.S. Department of Defense
EPS	Extracellular polymeric substance
ERD	enhanced reduction dechlorination
ESTCP	Environmental Security Technology Certification Program
f_{oc}	fraction organic carbon
FPTA	fire protection training area
GC	gas chromatography
ICP-AES	inductively coupled plasma atomic emission spectroscopy
ISCO	*in situ* chemical oxidation
Kd	solid-water distribution coefficient
Koc	organic-carbon-water distribution coefficient
LB	Luria-Bertani
LC-MS/MS	liquid chromatography tandem mass spectrometry
mg/L	milligrams per liter
mL	milliliter
mm	millimeter
mM	millimolar
MNA	monitored natural attenuation
m/z	mass to charge ratio
NAPL	nonaqueous phase liquid
ng/L	nanograms per liter

ng/g	nanograms per gram
nM	nanomolar
NOM	natural organic matter
OTU	operational taxpnomic unit
PAH	polycyclic aromatic hydrocarbons
PCB	polychlorinated biphenyl
PCE	perchloroethylene
PFAA	perfluoroalkyl acid
PFAS	poly- and perfluoroalkyl substance
PFBA	perfluorobutanoate
PFBS	perfluorobutane sulfonate
PFCA	perfluorocarboxylate
PFDA	perfluorodecanoate
PFHpA	perfluoroheptanoate
PFHpS	perfluoroheptane sulfonate
PFHxA	perfluorohexanoate
PFHxS	perfluorohexane sulfonate
PFNA	perfluorononanoate
PFOA	perfluorooctanoate
PFOS	perfluorooctane sulfonate
PFPeA	perfluoropentanoate
PFSA	perfluorosulfonate
PFUnA	perfluoroundecanoate
pK_a	acid dissociation constant
RCF	relative centrifugal force
rpm	rotations per minute
RNA	ribonucleic acid
RSD	relative standard deviation
RT-qPCR	reverse transcriptase quantitative polymerase chain reaction
SEM	scanning electron microscopy
SDBS	sodium dodecylbenzene sulfonate
SDS	sodium decyl sulfate
SERDP	Strategic Environmental Research and Development Program
TCE	trichloroethylene
TOC	total organic carbon
USEPA	United States Environmental Protection Agency
µg/L	micrograms per liter
µL	microliter
µm	micrometer
V	volt
VC	vinyl chloride

ACKNOWLEDGMENTS

The research described in this interim report was supported by the U.S. Department of Defense, through the Strategic Environmental Research and Development Program (SERDP). Dr. Andrea Leeson and other SERDP staff are gratefully acknowledged for their assistance and support.

EXECUTIVE SUMMARY

The overall goal of this research was to evaluate the relative importance of key physicochemical and biological parameters in determining the fate and transport of perfluoroalkyl acids (PFAAs) in groundwater in the presence of co-contaminants and during remediation of co-contaminants. The presence of specific PFAAs and their polyfluorinated precursors in groundwater, notably the PFAAs at aqueous film-forming foam (AFFF)-impacted fire training areas, has raised concerns about the risk these PFAAs may pose to human health. Unfortunately, there are serious data gaps with respect to our understanding of the behavior of poly- and perfluoroalkyl substances (PFASs), which include PFAAs, in groundwater systems, particularly in the presence of co-contaminants present at AFFF-impacted sites. Moreover, very little is known about how PFAA fate and transport will be affected when sites are subject to *in situ* remediation aimed at attenuating the co-contaminants also present. Thus, understanding the interplay between the co-contaminants typically present at AFFF-impacted sites, the biogeochemical changes brought about by their remediation, and the transport potential of PFAAs is crucial in designing and implementing any remediation strategies aimed at PFAAs. This study endeavored to understand the fundamental processes governing PFAA fate and transport in the presence of co-contaminants and during co-contaminant remediation by integrating batch and flow-through laboratory experiments.

In theory, PFAAs transport potential at AFFF-impacted sites can both increase and decrease due to the presence of co-contaminants such as fuel hydrocarbons and the implementation of co-contaminants remediation strategies, such as bioremediation and in situ chemical oxidation (ISCO). The co-contaminants, if present as non-aqueous phase liquids (NAPLs), may serve as an additional phase into which PFAAs could partition, or may block sorption sites for PFAAs, increasing their transport potential. In addition, other non-fluorinated components of AFFF, such as hydrocarbon surfactants, can exert similar effects. Questions also arise as to the impacts of biomass growth in the subsurface as a result of bioattenuation of co-contaminants (i.e., monitored natural attenuation [MNA] or enhanced reductive dechlorination [ERD]) on PFAA transport, as PFAAs are known to have strong affinities for proteins. When remediation strategies such as ISCO are employed, this may not only impact PFAA transport through alterations in the PFAA-co-contaminant interactions, but also through the extreme changes in subsurface geochemistry that can arise as a result of ISCO. For example, ISCO could both destroy a potentially-sorptive phase for PFAAs by degrading the NAPL and/or soil organic carbon, but the lower pH that often results from ISCO may increase PFAA sorption potential.

The goals of this research were twofold: to conduct PFAA sorption and transport studies under conditions representative of AFFF-impacted sites before and after co-contaminant remediation, and to gain a fundamental understanding of the processes governing these interactions. With respect to co-contaminant remediation strategies, evaluating all likely scenarios and geochemical conditions would be an immense task, and was beyond the scope of this project. Specifically, we endeavored to determine the impacts of aerobic and anaerobic co-contaminant bioremediation strategies (for toluene and trichloroethylene [TCE], respectively, as model co-contaminants) as

well as ISCO (using permanganate, activated persulfate, or catalyzed hydrogen peroxide [CHP]) on PFAA transport. With respect to transport under unaltered conditions (i.e., in the absence of the implementation of a co-contaminant remediation strategy), we endeavored to identify the impacts of co-contaminants and potential sorption kinetic limitations on PFAA transport by conducting transport studies at the batch and column scale. This results of this research should allow us to move closer to modeling PFAA plumes at AFFF-impacted sites. With further study, the results of this project should meaningfully contribute to modeling and site assessment guidelines that can be used by engineers and contaminant hydrologists for practical implementation.

Project Goals and Specific Research Questions

The principal goal of this project was to examine the fundamental processes impacting PFAA fate and transport in AFFF-impacted groundwater. Thus, investigation of the relative importance of various physicochemical and biological parameters on PFAA transport under natural and remediation-induced conditions was the primary focus of this research. The ultimate goal was to provide an understanding of the key processes and associated parameters and thereby enable informed and improved remediation strategy decisions for U.S. Department of Defense (DoD) sites where groundwater is contaminated by PFAAs and co-contaminants.

In pursuit of these goals, the specific questions addressed were:

- What are the effects of PFAA concentration and presence of aqueous and NAPL-phase contaminant mixtures (PFAAs and co-contaminants) on PFAA partitioning and retardation in subsurface porous media, particularly as they relate to potential differential transport in the source zone versus a downgradient plume?
- How do biogeochemical conditions, porous media properties, and the presence of co-contaminants (fuel mixtures and residues or chlorinated solvents) affect PFAA transport behavior prior to (or in the absence of) in situ remediation?
- What are the impacts of co-contaminant in situ remediation (MNA, ERD, ISCO) on PFAA fate and transport?
- How can an understanding of PFAA behavior be incorporated into quantitative assessment reflecting the complexity of conditions likely present at DoD contaminated sites?

Experimental Tasks and Findings

To answer these specific questions, the following experimental project tasks were delineated:

Analytical Method Refinement and Verification (Task 1)

Existing analytical methodologies for quantifying PFAAs in aqueous and solid phases were refined and verified. This focused on both direct-injection of aqueous samples for liquid chromatography tandem mass spectrometry (LC-MS/MS) analysis and extraction of solid phases

for LC-MS/MS. Matrices tested represented the extreme geochemical conditions that may be present during co-contaminant remediation.

The specific findings related to this work are:

- To ensure adequate method performance, aqueous-phase analysis of PFAAs by LC-MS/MS requires pH adjustment for samples that exhibit significant deviations from typical ambient pH conditions. This is particularly true for samples that have been impacted by the application of ISCO.
- For most PFAAs in most aqueous matrices (i.e. ISCO-treated), the isotope-dilution-based direct injection LC-MS/MS approach is suitable for PFAA analysis. However, due to analytical variability, it is recommended that each user reconfirm the accuracy of the method in their specific matrix prior to initiation of experiments.
- For most PFAAs in most solid phases (i.e., with NAPL, NAPL + ISCO, etc.), the isotope-dilution-based solvent extraction and LC-MS/MS analysis approach is suitable. However, as with aqueous sample analysis, due to analytical variability, it is recommended that each user reconfirm the accuracy of the method in their specific matrix prior to initiation of experiments.

Finally, since the initiation of this project, additional analytical and isotopically labeled standards have been made commercially available and should be employed, whenever possible, for all future analytical work for both solid and aqueous samples.

Batch Partitioning Experiments (Task 2)

Bench-scale batch sorption experiments and NAPL-partitioning experiments were conducted to evaluate the impact of a wide array of variables on PFAA sorption. These included: a) evaluating varying geochemical conditions representative of un-remediated AFFF-impacted sites; b) evaluating competitive effects in PFAA mixtures and at the high aqueous PFAA levels observed at many AFFF-impacted sites; and c) evaluating the effects of co-contaminants such as NAPL and other AFFF-components on PFAA sorption.

The specific findings related to this work are:

- Sorption of PFAAs in the absence of co-contaminants generally follows previously-determined paradigms, with the notable exception of the short-chain perfluorocarboxylates (PFCAs). Specifically, perfluorobutanoate (PFBA) and perfluoropentanoate (PFPeA) sorbed much more strongly than otherwise predicted based on their perfluorocarbon chain length.
- Competition between PFAAs for sorption sites to environmental solid phases is generally minimal, and is only slightly evident in low f_{oc} materials.
- PFAA sorption to NAPL is generally independent of NAPL type (i.e., model fuel NAPL, chlorinated solvent NAPL).
- The presence of TCE NAPL in solid phases generally led to an increase in PFAA sorption linearity. In addition, the sorption of the shorter-chain PFCAs generally

increased in the presence of NAPL. In contrast, for the longer-chain PFAAs and higher f_{oc} materials, the presence of NAPL generally had no effect or decreased the sorption of PFAAs.

- A linear-sum model accounting for a PFAA's organic-carbon-based sorption coefficient (i.e., K_{oc}) and a NAPL partitioning coefficient (i.e., K_{NAPL}) was insufficient to predict sorption in the presence of NAPL, as it consistently underpredicted sorption. This is likely due to both adsorption of PFAAs to the interface as well as absorption into the NAPL itself.
- The impacts of non-fluorochemical-based AFFF surfactant components on PFAA sorption were mixed. Sodium decyl sulfate (SDS) had no impact on PFAA sorption in a positively-charged solid (i.e. rich in Fe and Al oxides) and led to slight increases in sorption for the shorter-chain PFAAs in negatively-charged solids. As with NAPL, no changes or slight decreases in sorption were observed for the long chain-length PFAAs, suggesting a potential for competition between longer chain-length PFAAs and SDS for sorption sites.
- A model amphoteric non-fluorochemical-based AFFF surfactant, n,n-dimethyldodecylamine n-oxide (AO), resulted in slight increases in sorption for shorter chain-length PFAAs for negatively-charged solids. AO had little impact on sorption of longer chain-length PFAAs in these materials. In contrast, the presence of AO in the positively-charged soil led to increases in sorption for the longer chain-length PFAAs.

In brief, sorption and transport of PFAAs will be impacted by the presence of co-contaminants, particularly NAPLs. Interactions between PFAAs, co-contaminants, and environmental solids are complex, but the overall data suggest that NAPL presence at a site may further retard PFAA transport, assuming limited mobility of the NAPL.

Batch Co-Contaminant Remediation Experiments (Task 3)

Bench-scale experiments evaluated the impacts of co-contaminant remediation on PFAA sorption. Specific in situ remediation approaches employed for co-contaminants that were evaluated included aerobic biotransformation (i.e., MNA), ERD, and ISCO. The range of conditions explored attempted to mimic the range of conditions likely present within a source zone and groundwater plume during in situ remediation. Specifically, we addressed: a) natural attenuation conditions associated with hydrocarbon degradation; b) ERD conditions simulating TCE biodegradation; and c) ISCO conditions representative of TCE oxidation.

The specific findings related to this work are:

- The presence of high-concentrations of PFAAs has no impact on the degradation of a model fuel contaminant (toluene) by a model soil microbe (RHA1). Neither the kinetics of degradation nor the induction time for toluene were impacted by the presence of PFAAs. However, exposure during growth to aqueous PFAA concentrations above 1 mg/L each of 11 PFAAs was associated with enhanced aggregation of bacterial cells. This flocculation was accompanied by increased production (~2.5x) of extracellular

polymeric substances (EPS). In addition, significant increases in the expression of genes related to stress responses were also observed.

- Reductive dechlorination of TCE by a methanogenic, mixed culture was significantly inhibited when exposed to concentrations representative of PFAA source zones (>66 mg/L total of 11 PFAA analytes, 6 mg/L each). TCE dechlorination, cis-dichloroethene, and vinyl chloride production and dechlorination, and ethene generation were all inhibited at these PFAA concentrations. Phylogenetic analysis revealed that the abundances of 65% of the operational taxonomic units (OTUs) changed significantly when grown in the presence of PFAAs. Notably, there was significant repression of *Dehalococcoides* coupled with a corresponding enhancement of methane-generating *Archaea*. Growth and dechlorination by axenic cultures of Dehalococcoides mccartyi strain 195 were similarly repressed under these conditions, confirming an inhibitory response of this pivotal genus to PFAA presence. These results suggest that chlorinated solvent bioattenuation rates could be impeded in subsurface environments near PFAA source zones.
- Batch experiments with ISCO oxidants indicate that slight changes to sorption coefficients (i.e., K_d values) can be expected when permanganate is added to the system, though the impact depends on the PFAA and whether or not NAPL is present. In contrast, the addition of persulfate increased the K_d values for nearly all PFAAs, though the effects were more pronounced for the longer chain-length PFAAs. The increased sorption upon the addition of persulfate can generally be attributed to the lower pH upon persulfate addition and previous observations of increased sorption of PFAAs at lower pH values.

In brief, prior to the start of this project, little was known about how PFAA fate and transport would be affected when AFFF-impacted sites are subject to *in situ* remediation aimed at attenuating co-contaminants. When microbial co-contaminant remediation technologies are employed, the interactions between PFAAs and the microbial populations are complex. For hydrocarbon-degrading populations, PFAAs do not appear to significantly affect hydrocarbon degradation, though the PFAAs do appear to induce biofilm formation which may subsequently impact PFAA transport. Surprisingly, high levels of PFAAs appear to interfere with microbial dehalogenation reactions. Finally, ISCO appears to impact PFAA sorption in batch systems, with permanganate generally having minimal to no impact, whereas persulfate generally increasing sorption for many PFAAs due to lower pH values.

Flow-through Transport and Remediation Experiments (Task 4)

Information and understanding gained from PFAA sorption batch tests was confirmed in bench-scale flow-through experiments using one-dimensional (1-D) columns. These experiments aimed to examine the validity of employing PFAA-transport data obtained from batch experiments for simulating behavior in model groundwater systems during ambient conditions or those imposed during remediation. Specifically, experiments evaluated: a) PFAA transport under unaltered conditions both in the presence and absence of co-contaminant; b) PFAA transport simulated MNA conditions aimed at aerobic bioattenuation of co-contaminants; and c) PFAA transport during ISCO treatment of co-contaminant NAPLs.

The specific findings related to this work are:

- Continuous flow 1-D column experiments confirmed chain length-dependent transport of longer (>6 CF_2 groups) PFAAs. At higher flows, transport trends with porous media organic carbon content were unclear, indicating possible nonequilibrium conditions. Measured column sorption coefficients ($K_{d,col}$) were smaller than $K_{d,eq}$ for some PFAAs and in porous media with higher f_{oc} values, further suggesting the potential for nonequilibrium conditions. Equilibrium transport generally was applicable in low f_{oc} media. Flow interruption of high-flow experiments confirmed rate-limited sorption of some PFAAs under advective conditions.
- Simulated MNA column experiments suggest that continued biological activity will occur in the presence of high concentrations of PFAAs (110 mg/L total), and that this biological activity, particularly in the presence PFAAs, may reduce the permeability of the porous media. This may be a result of increased biofilm formation as a stress response activated upon PFAA exposure. This biofilm formation may, in turn, increase the retardation of PFAAs in the subsurface.
- Flow-through 1-D column experiments which included the application of ISCO (i.e., activated persulfate, potassium permanganate, or CHP) suggest that standard ISCO is not a viable remediation strategy for PFAA destruction. However, substantial changes in PFAA transport were observed upon and following ISCO application. Generally, activated persulfate decreased PFAA transport, while permanganate and CHP increased PFAA transport. The changes in PFAA mobility were greater than would be predicted based on aqueous chemistry considerations alone, suggesting that ISCO application results in changes to the porous media matrix that also influence transport. ISCO application is likely to result in changes in PFAA transport, where the direction (increased or decreased transport) and magnitude are dependent on PFAA characteristics, oxidant characteristics, and site-specific factors.
- Observed retardation factors from column experiments using saturated porous media containing residual TCE indicate that TCE provides additional sorption capacity that can increase PFAA retardation under advective conditions. As with the no TCE systems, ISCO impacts on PFAA transport and sorption were apparent, with substantially enhanced sorption in the persulfate-treated columns. In contrast, PFAA transport was accelerated in permanganate- and CHP-treated columns.

In brief, these studies indicate that while equilibrium transport of PFAAs may be appropriate for low f_{oc} materials and low flow conditions, nonequilibrium transport of some PFAAs may be evident for high groundwater velocities and higher f_{oc} materials. Simulated MNA flow-through experiments suggest that the increased EPS production observed in batch systems may also result in decreased permeability (and likely PFAA transport) under advective conditions. Advective studies further support earlier work indicating that PFAA transport may be impeded by NAPL. Finally, the application of ISCO under advective conditions indicates that ISCO, particularly the application of persulfate and permanganate, will significantly impact PFAA fate and transport. Notably, in the case of persulfate, the effects appear to be primarily driven by the low pH that results from persulfate application.

Desorption from AFFF-impacted soil (Task 7)

The desorption of PFAAs and PFAA precursors (as determined via the total oxidizable precursor [TOP] assay) from field-collected AFFF-impacted soils and aquifer sediment materials was evaluated in both batch and bench-scale column experiments. Specific conditions evaluated included: a) unaltered conditions (batch and column); and b) desorption in the presence of chemical oxidants (column experiments).

The specific findings related to this work are:

- Batch desorption experiments using field-collected AFFF-impacted materials indicate that PFCAs and perfluorosulfonates (PFSAs) have similar desorption rates for equivalent perfluorinated carbon chain lengths, with both classes of PFAAs exhibiting decreasing desorption rates with increasing perfluorinated chain length. PFAA precursors, as measured by the TOP assay, desorbed more slowly than PFAAs from the contaminated materials.
- In flow-through (unsaturated) column desorption experiments, some PFAAs are rapidly released from AFFF-impacted soils, while others (particularly PFOS and PFHxS) are released much more slowly. An important factor controlling the rate of release appears to be solution pH, with lower pH conditions resulting in slower and less complete release of PFAAs from the solid phase.
- In flow-through (unsaturated) column desorption experiments when chemical oxidants are added (permanganate and persulfate), persulfate appears to impact the release of PFAAs from AFFF-impacted soils primarily through pH effects. In contrast, permanganate appears to enhance both the release of PFAAs as well as the conversion of some PFAA precursors to PFAAs.

In short, many PFAAs, with the notable exceptions of PFOS and perhaps PFHxS, are relatively rapidly desorbed from AFFF-impacted solids. PFAA precursors, however, appear to desorb much more slowly. Advective experiments support the results from the batch studies, but also indicate the strong role of pH on PFAA desorption. Finally, chemical oxidants impact PFAA desorption primarily through pH effects, though permanganate appears to not only mobilize PFAAs from AFFF-impacted soil, but also facilitate significant conversion of some polyfluorinated precursors to PFAAs.

Dissemination of Research Results and Impact on Ongoing SERDP/ESTCP Projects

In addition to the experimental work summarized above, significant effort was expended ensuring the results were appropriately disseminated. This included at least 30 public presentations at local, state, national, and international meetings and conferences. In particular, the results were highlighted as part of the SERDP and ESTCP Webinar Series held on January 28, 2016.

The findings of this work have also been published in five peer-reviewed journals (to date):

1. McKenzie, E.R., Siegrist, R.L., McCray, J.E. and C.P. Higgins. 2016. The influence of a non-aqueous phase liquid (NAPL) and chemical oxidant application on perfluoroalkyl acid (PFAA) fate and transport. *Water Research.* 92: 199-207. DOI:10.1016/j.watres.2016.01.025
2. Weathers, T.S., Harding-Marjanovic, K., Higgins, C.P., Alvarez-Cohen, L., and J.O. Sharp. 2016. Perfluoroalkyl acids inhibit reductive dechlorination of TCE by repressing Dehalococcoides. *Environmental Science & Technology.* 50 (1): 240-248. DOI:10.1021/acs.est.5b04854
3. Weathers, T.S., Higgins, C.P., and J.O. Sharp. 2015. Enhanced biofilm production by a toluene degrading Rhodococcus observed after exposure to perfluoroalkyl acids. *Environmental Science & Technology,* 49 (9): 5458–5466 DOI:10.1021/es5060034
4. McKenzie, E.R., Siegrist, R.L., McCray, J.E. and C.P. Higgins. 2015. Effects of Chemical Oxidants on Perfluoroalkyl Acid (PFAA) Transport in 1-D Porous Media Columns. *Environmental Science & Technology.* 49 (3): 1681–1689 DOI:10.1021/es503676p
5. Guelfo, J.L. and C.P. Higgins. 2013. Subsurface transport potential of perfluoroalkyl acids at aqueous film-forming foam (AFFF)-impacted sites. *Environmental Science & Technology,* 47 (9):4164–4171. DOI:10.1021/es3048043

In addition, a number of manuscripts are still being refined, and will be submitted for publication in the near future:

1. Guelfo, J.L., Wunsch, A., McCray, J.E. and C.P. Higgins. Transport Potential of Perfluoroalkyl Acids (PFAAs) at AFFF-impacted Sites: Column Experiments and Modeling. *Manuscript in Preparation.*
2. Azzolini, D.C., Roberts, S.R. and C.P. Higgins. Desorptive behavior of perfluoroalkyl acids and perfluoroalkyl acid precursors from aqueous film-forming foam impacted soils. *Manuscript in Preparation.*
3. Weather, T.S.., Higgins, C.P., and J.O. Sharp. Interactions between a common soil microbe and perfluoroalkyl substances in batch systems. *Manuscript in Preparation.*

Finally, the results of this project are directly contributing to two new and/or imminent ESTCP projects, ER-201574-T2 and ER-201633. In addition, it is anticipated that these results will contribute to a number of ongoing and/or future SERDP projects (i.e., SERDP ER-2128, SERDP ER-2424, etc.).

1. INTRODUCTION AND PROJECT SCOPE

As a result of the extensive use of aqueous film forming foams (AFFF) by the U.S. military and the need to ensure adequate training of personnel, soil and groundwater at many fire training facilities potentially have been contaminated with perfluoroalkyl acids (PFAAs) and other poly- and perfluoroalkyl substances (PFASs). Given the orders of magnitude differences between the concentrations observed at some fire-training sites (µg/L to mg/L) and the provisional health advisory levels adopted by the U.S. Environmental Protection Agency (USEPA) (~ng/L), there is a critical need to both understand the behavior of these chemicals in groundwater systems under ambient conditions as well as those imposed during in situ remediation. Complicating our ability to predict the behavior and remediation of PFAAs in groundwater is the fact that by their very nature, many AFFF sites suspected of PFAA contamination are likely also contaminated with other chemicals of concern (COCs). In particular, fuel hydrocarbons were intentionally applied and ignited at many sites and extinguished with PFAA-bearing AFFF products (Levine *et al.*, 1997). Other possible co-contaminants, such as chlorinated solvents, have been detected at sites associated with fire-training facilities (e.g., McCray and Brusseau, 1998; McCray *et al.*, 2010b) and the presence of complex organic contaminant mixtures at these sites, including chlorinated solvents such as perchloroethylene (PCE) and trichloroethylene (TCE), is common (McCray and Brusseau, 1999). Fuel hydrocarbons such as benzene, toluene, ethylbenzene, and xylene (BTEX) compounds have been detected in groundwater at AFFF-impacted sites at levels up to 2 mg/L (with aqueous phase total organic carbon reaching 225 mg/L), and in some locations, non-aqueous phase liquids (NAPLs) and tar-like residuals were present (Moody *et al.*, 2003).

The impact of the co-contaminants and co-contaminant remediation strategies on PFAA surfactant fate and transport in the subsurface is an area where little data exist. Moreover, the processes impacting PFAA behavior will likely vary substantially from the source zone to the edge of a contaminated groundwater plume (**Figure 1-1**). For example, co-contaminants may be present at high levels in the source zone prior to remediation and biogeochemical conditions and COC concentration can be different in the source zone when compared to the plume edge. Co-contaminant levels and biogeochemical conditions may be dramatically altered during and following in situ remediation. The more recalcitrant and mobile PFAAs may be transported downgradient under ambient conditions and experience enhanced transport as a result of in situ remediation.

1.1 PFAA Transport and Retardation

PFAAs are unique environmental contaminants in that they are both bioaccumulative and relatively mobile. The specific PFAAs under investigation in this project (**Table 1-1**) are expected to exist as anions at circumneutral pH values. While the exact acid dissociation constants (i.e., pK_a values) of some PFAAs are the subject of much debate (Goss 2008), it is anticipated that they will also be present as organic anions at the typical pH values observed in groundwater. This has important implications for the transport of PFAAs in groundwater, as the electrostatic repulsion of these organic anions from negatively charged natural organic matter

(NOM), biofilms, clay, and mineral surfaces would be expected to lead to minimal sorption and retardation. However, as discussed below, there are several mitigating factors that may affect PFAA transport and retardation in groundwater.

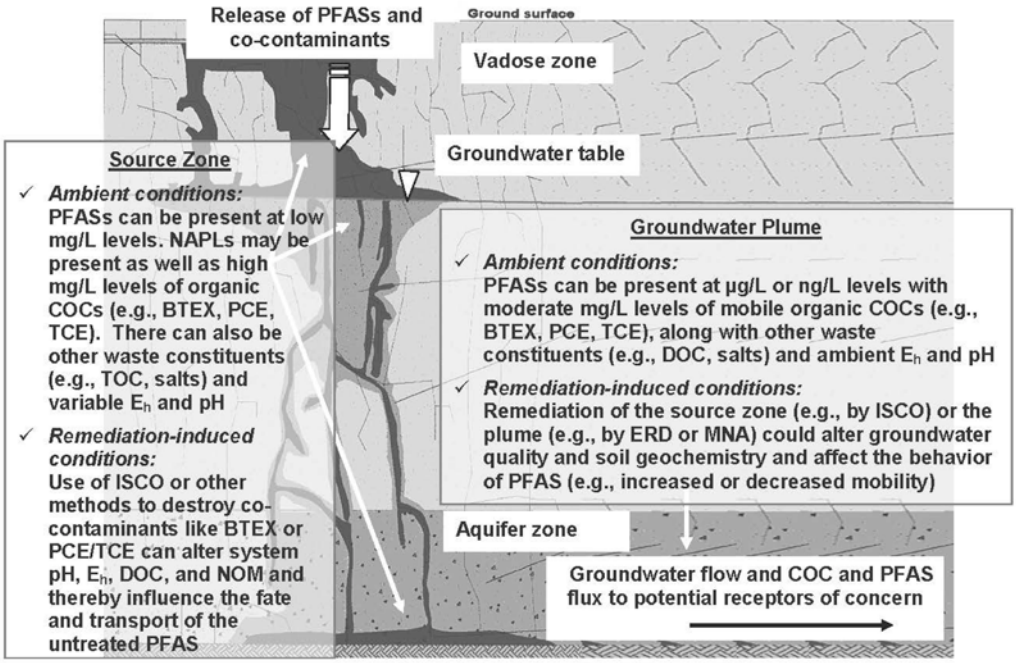

Figure 1-1. Processes affecting PFAS behavior and remediation in a contaminated groundwater system.

Several previous sorption studies for PFAAs focused on aquatic sediments (Higgins and Luthy, 2006; Higgins and Luthy, 2007; Johnson *et al.,* 2007), though some studies have also been conducted for biosolids-amended soils (Sepulvado *et al.,* 2011) or oil-contaminated soils (Chen *et al.,* 2009). Although these studies did not focus on aquifer materials, they have led to some important insights with respect to PFAA transport in groundwater. For example, the extent of sorption for all PFAAs is strongly dependent on the length of the perfluoroalkyl tail, with each CF_2 group increasing the sediment-water equilibrium distribution coefficient (K_d) value by a factor of ~3.5 (Higgins and Luthy, 2006). Though the current regulatory focus is on PFOA and PFOS, shorter chain length PFCAs and PFSAs have been detected at AFFF sites (Moody and Field, 1999; Moody *et al.,* 2003) and these PFAAs would be expected to be comparatively more mobile.

Table 1-1. PFAAs evaluated in this project

Chemical Name	Chemical Class	Concentration in AFFF-impacted Groundwater
PFBS	PFSAs	nd to 210 µg/L[c]
PFHxS	PFSAs	9 to 120 µg/L[b]
PFOS	PFSAs	6 to 110 µg/L[b]
PFBA	PFCAs	nd
PFPeA	PFCAs	nd
PFHxA	PFCAs	nd to 372 µg/L[a]
PFHpA	PFCAs	nd to 149 µg/L[a]
PFOA	PFCAs	nd to 6570 µg/L[a]
PFNA	PFCAs	nd

[a] Moody and Field, 1999;
[b] Moody *et al.,* 2003;
[c] Schultz *et al.,* 2004;
nd = not detected

Higgins and Luthy (2006) also demonstrated that within natural materials, PFAAs appear to preferentially partition into NOM, resulting in fairly consistent organic carbon-normalized K_d values (i.e., K_{oc} values). For example, the log K_{oc} values determined for PFOS and PFOA in the 0.5-100 µg/L range was 2.57 and 2.06, respectively (Higgins and Luthy, 2006). This suggests that these PFAAs may undergo retardation in groundwater similar to COCs such as TCE (Jeong *et al.,* 2008). Importantly, compared to the role of NOM, Higgins and Luthy (2006) showed that positively charged mineral surfaces had little impact on the sorption of these anionic PFAAs, a finding that has been confirmed by others (Johnson *et al.,* 2007). This result somewhat contradicts what might be expected based on analytical chemical methods, where weak anion exchange solid-phase extraction columns, which are typically positively charged at circumneutral pH, have been shown to be extremely effective for concentrating trace levels of PFAAs in aqueous samples (Taniyasu *et al.,* 2008).

Solution chemistry has been shown to play a role in the sorption of PFAAs both to natural materials (Higgins and Luthy, 2006; Johnson *et al.,* 2007) as well as adsorbents such as activated carbon and anion exchange resin (Yu *et al.,* 2009). In all cases, the pH effects observed were primarily attributed to alterations in the charge of the sorbent. However, the very low pH values (pH 3) tested for the adsorbents may have been close enough to the pK_a of PFOA for the neutral, protonated PFOA to become important. For the natural materials, an increasing concentration of divalent metal cations such as Ca^{2+} from 0.1-50 mM increased the sorption of all PFAAs (Higgins and Luthy, 2006). Consistent with other recent studies of organic anion sorption to NOM (Tulp *et al.,* 2009), subsequent modeling efforts concluded this effect was primarily due to a reduction in the negative charge of the NOM by the binding of the metal cations (Higgins and Luthy, 2007). These findings have clear implications with respect to the range of conditions that may be present at untreated AFFF sites and sites that have been subjected to various remedial technologies. For example, while no studies to date have examined the effect of NAPLs on PFAA sorption, the surfactant nature of PFAAs may result in significant partitioning into a NAPL or a NAPL-water interface if NAPL is present at the site, thereby affecting retardation of PFAAs in groundwater.

Surfactants such as PFAAs are known to exhibit unique sorptive behavior at various concentrations due to the formation of micelles and hemimicelles at the solid-water interface (Gaudin and Fuerstenau, 1995). Even at concentrations 1000-fold lower than the critical micelle concentration (CMC), hemimicelle formation at this interface may lead to increased sorption and retardation (Schwarzenbach *et al.,* 2003). Thus, the concentration dependence of the sorption of PFAAs to aquifer materials may be significant, and this has important implications with respect the validity of using the same transport parameter values across the source zone and groundwater plume. Interestingly, log K_{oc} values for PFOS of up to 3.1 have been reported based on isotherms conducted in the low mg/L range (Johnson *et al.,* 2007); although as with the study conducted in the low µg/L range (Higgins and Luthy, 2006), nonlinear isotherms were evident. Johnson and colleagues (2007) concluded that although the concentration of NOM was clearly the dominant parameter impacting sorption, monolayer coverage of the mineral surfaces with PFOS had been exceeded for some of the materials, which in turn gave rise to the highly nonlinear isotherms observed. A highly nonlinear isotherm was also evident in a recent study of PFOS sorption onto

a natural sediment with a relatively low NOM content (f_{oc} = 0.0075) also conducted in the low mg/L range (Pan *et al.,* 2009). Understanding the source of this nonlinearity, particularly in light of the likely variations in PFAA concentrations in the source zone as compared to an associated groundwater plume (**Figure 1-1**), is important to understanding the transport of PFAAs at AFFF-impacted sites.

Field observations with respect to PFAA transport in groundwater are extremely limited. Push-pull tests have been conducted in an aquifer with PFOS present at relatively high levels (26 mg/L; Moody and Field, 2000), though this level is within the range of concentrations of PFOS detected at AFFF-impacted sites (Moody *et al.,* 2003). While no detailed characteristics of the aquifer were provided, the PFOS breakthrough curve was nearly identical to the bromide tracer curve, suggesting no retardation of PFOS in that system under the conditions of the push-pull test. As some sorption of PFOS to NOM is expected based on the studies highlighted above, it is unclear which processes (e.g. rate-limited sorption) may have caused a lack of PFOS retardation.

Transport of PFASs via groundwater advection is likely occurring at some DoD sites, as revealed by individual PFASs as high as 33 µg/L that were measured several hundred meters downgradient from an AFFF-impacted fire training pad (Moody *et al.,* 2003). However, despite continual use of PFCA- and PFSA-based AFFF products at Wurtsmith Air Force Base (AFB), a significantly uneven spatial distribution of these PFAAs in groundwater downgradient from the fire-training pit was evident (Schultz *et al.,* 2004).

1.2 Potential Interactions with NAPL Co-Contaminants

At AFFF-impacted sites, PFAA surfactants in groundwater may interact with co-contaminants such as NAPLs via various complex mechanisms that can influence the mobility of the NAPL, the transport of solubilized contaminants associated with the NAPL, and transport of the PFAAs themselves. These interactions can be particularly complex when the NAPL is a mixture of chemicals. The commonly acknowledged interactions between surfactants and NAPLs is related to the ability of surfactants, when present above the CMC, to enhance the solubility of contaminants in the NAPL and thus affect NAPL dissolution and the transport of NAPL constituents (Sabatini *et al.,* 1999). However, when considering the effects of NAPLs on the transport of surfactants, the NAPL-groundwater interfacial area becomes a key parameter. Surfactants can partition to the NAPL-water interface, though partitioning into the bulk NAPL as reverse micelles is also possible (Sabatini *et al.,* 1999; McCray *et al.,* 2000). Indeed, the retardation of anionic surfactants in the presence of NAPLs has been used to estimate the interfacial area of the NAPL (Cho *et al.,* 2005; Schaefer *et al.,* 2009). Different surfactants will experience different degrees of retardation for the same NAPL because interfacial partitioning coefficients are likely to vary considerably due to slight differences in surfactant size, structure, and hydrophobicity. For NAPL mixtures, the interfacial area is a function of mixture composition (Seo and McCray, 2002). Thus, as the NAPL ages, the effect of the NAPL in retarding surfactant transport via partitioning to the bulk NAPL as well as the NAPL-water interface will also change in a complex manner that has not been previously studied. Thus, the presence of NAPL at AFFF-impacted sites may have an impact on PFAA partitioning, retardation, and transport, but the mechanisms by which this may occur have not been examined.

Prior to the initiation of this research, only one published study was identified that investigated the interactions between PFAAs and NAPL. This study examined only PFOS, and found that PFOS sorption increased in the presence of crude oil (Chen *et al.*, 2009). Other studies have examined PFAA interactions with polycyclic aromatic hydrocarbons (PAHs) likely present in NAPLs at AFFF-impacted sites (An and Jeong, 2001; An *et al.*, 2002). These studies found increased solubilization of PAHs by PFOS and PFOA micelles, suggesting interactions between the perfluoroalkyl tails of PFAAs and hydrocarbons are possible. It is unlikely that individual PFAA micelles will be present in groundwater (typically PFAA CMCs are ~ high mg/L), but the presence of PFAA mixtures, the potential presence of hydrocarbon surfactants (Moody and Field, 2000), and the dependence of CMC values on aquatic chemical conditions suggest enhanced solubilization of NAPLs is possible at AFFF-impacted sites. If hydrocarbon surfactants co-applied as part of the AFFF-mixtures are not rapidly degraded, their presence may also directly impact PFAA mobility. One recent study investigated the effects of the presence of both anionic (sodiumdodecylbenzene sulfonate; SDBS) and cationic (cetyltrimethylammonium bromide; CTAB) surfactants on the sorption of PFOS to sediments (Pan *et al.*, 2009). CTAB significantly enhanced the sorption of PFOS to the sediment materials and the authors also reported significant hysteresis as CTAB concentrations increased. The results for SDBS were inconsistent: lower concentrations (< 5 mg/L) of SDBS increased the sorption of PFOS, but higher concentrations resulted in significantly less sorption, as well as significant hysteresis. While likely not directly applicable to AFFF-impacted sites, this study clearly indicates that the presence of co-contaminants can both increase and decrease the retardation of PFAAs in groundwater, depending on the type and concentration of the co-contaminants.

1.3 Potential Impacts of Co-Contaminant Remediation Technologies

In situ remediation of PFAAs in contaminated groundwater is challenging. Indeed, PFAAs are remarkably stable in the environment. Research conducted to date suggests that limited to negligible biotransformation of PFAAs such as PFOS is anticipated under typical environmental conditions (Key *et al.,* 1998). While the development of novel *in situ* PFAA remediation strategies is not the focus of this project, a central goal of this project is to understand the potential for altered behavior of PFAAs under conditions which can occur during commonly employed approaches for *in situ* remediation of hydrocarbons and chlorinated solvents. The *in situ* technologies under examination in this project for impacts on PFAA fate and transport include monitored natural attenuation (MNA), enhanced reductive dechlorination (ERD), and *in situ* chemical oxidation (ISCO).

In some cases, the best remediation strategy for COCs present at AFFF-impacted sites may be MNA, a strategy by which COCs are allowed to degrade (primarily via aerobic biological mechanisms) over time under natural conditions. MNA has often been advocated as a favored strategy for hydrocarbon-based COCs in groundwater, and has been employed at AFFF-impacted DoD sites (e.g., Levine *et al.,* 1997). When used, MNA will likely result in the degradation of the most readily degradable hydrocarbons, including other components of AFFF-formulations. Biodegradation of contaminant plumes in the subsurface follows a thermodynamic cascade starting with the most favorable electron donor/acceptor couple. This process results in redox zones along a contaminant plume that sequentially exhaust electron acceptors while consuming

the most readily degraded organics as electron donors (Cozzarelli *et al.,* 2001; Alvarez and Illman, 2006). In addition to alterations in redox, the microbial respiration processes occurring through MNA may influence the pH through the evolution of CO_2 and release of H^+. In these cases, the mineralization or partial degradation of total hydrocarbon loading (including alkanes and other organics) anticipated at AFFF-impacted sites may also impact the sorptive properties of the soils and aquifer solids. Impacts can be due to changes in the structure and availability of carbon in the subsurface, the enhanced biomass resulting from microbial respiration, and alterations in subsurface pH and redox, all of which are anticipated to influence PFAA transport. At present, it is unclear whether the potential impacts of MNA biodegradation processes will increase or decrease PFAA transport in groundwater.

If chlorinated solvents are present at AFFF-impacted sites, the potential application of microbially-mediated ERD for remediation of these COCs would likely be considered. ERD has been extensively used for *in situ* treatment and polishing of chlorinated ethane contaminated aquifers and dense NAPL (DNAPL) source zones, but essentially no data are available to understand how ERD may or may not impact the fate and transport of PFAAs. For PCE and other chlorinated ethenes such as TCE, *Dehalococcoides*-containing consortia facilitate microbial reduction by sequential dehalogenation (Fennell *et al.,* 2001). Low Eh conditions such as those observed during methanogenesis are required for this to proceed (Freedman and Gossett, 1989). When employed *in situ*, ERD is likely driven by obligate anaerobic consortia utilizing H_2 as an electron donor and TCE as the electron acceptor (Ballapragada *et al.,* 1997). Biostimulation and augmentation can facilitate ERD by introducing acclimated consortia and/or electron donor and nutrients such as lactate, yeast extract, ammonia, and phosphate into the subsurface (Ellis *et al.,* 2000). Due to alterations in subsurface geochemical conditions and potential sorptive properties of contaminated soils and aquifer sediments as a result of ERD, it is expected that ERD impacts on PFAA fate and transport may be substantial. A recent study suggests changes in redox conditions may alter the mobility of PFAAs in groundwater. Though the mechanism responsible for these observations is not understood, both PFOS and PFOA were slowly released from sediments in spiked anaerobic microcosms over a two-year period (Ferrey *et al.,* 2012). While redox conditions became more reducing over the course of the experiment, the pH of the microcosms also rose, which may have contributed to PFAA desorption. Additional data on the effects of redox conditions (particularly those induced during ERD) on the mobility of PFAAs are needed to develop an accurate understanding as to how specific co-contaminant remediation technologies such as ERD may impact PFAA fate and transport.

Over the past decade, ISCO has undergone substantial research and development and is now proven to be a useful technology for the remediation of groundwater contaminated by a wide variety of organic contaminants (Siegrist *et al.,* 2001; ITRC, 2005; Huling and Pivetz, 2006; Siegrist *et al.,* 2008, Siegrist *et al.,* 2011). As of 2010, the chemical oxidants that have been investigated and become widely used for ISCO are hydrogen peroxide (H_2O_2), potassium and sodium permanganate ($KMnO_4$, $NaMnO_4$), sodium persulfate ($Na_2S_2O_8$), and ozone (O_3). Many chlorinated solvents, petrochemicals, energetic compounds, and polymers have been shown to be susceptible to oxidative degradation through reactions with one or more of these oxidants (Smith *et al.,* 2008; Siegrist *et al.,* 2010). Aqueous-phase PFOS and PFOA appear susceptible to

oxidative degradation under specialized conditions using activated persulfate and possibly catalyzed hydrogen peroxide (Vecitis *et al.,* 2009 and references therein). However, compared to the common COCs within the chlorinated solvent and petrochemical classes, the reaction mechanisms for PFAAs such as PFOA are poorly understood and the reactions may be too slow for practical application via ISCO (Vecitis *et al.,* 2009). While an array of organics can be destroyed by oxidants, ISCO has been most widely investigated and deployed for treatment of sites contaminated by chlorinated solvents (e.g., PCE, TCE) and petroleum hydrocarbons (e.g., total petroleum hydrocarbons, BTEX); in contrast, very limited information is available concerning the application of ISCO for treatment of PFAAs in groundwater. Similarly, essentially no data are available regarding the behavior of PFOS and PFOA under conditions imposed by ISCO (e.g., aqueous phase pH depression or destruction and/or alteration of NOM and other organic COCs). Yet, ISCO can be used to treat what have historically been the prime COCs at fire-training sites and other locations (e.g., TCE, BTEX) where PFAAs may also be present. Thus, further research is warranted to understand: 1) if and how ISCO can be used to destroy PFAAs and under what optimum conditions; and 2) even if the form of ISCO employed does not successfully destroy the PFAAs, how the conditions imposed by ISCO, when applied to other co-contaminants, affect PFAA transport. The impact on transport is particularly important in light of the extreme biogeochemical conditions (e.g., pH 2 to 3 near NAPL interfaces, Eh of +600 to +800 mV) often created as a result of ISCO implementation.

1.4 ER 2126 Project Goals and Approach

The principal goal of this project was to examine the fundamental processes impacting PFAA fate and transport in AFFF-impacted groundwater. Thus, investigation of the relative importance of various physicochemical and biological parameters on PFAA transport under natural and remediation-induced conditions was the primary focus of this research. The ultimate goal was to provide an understanding of the key processes and associated parameters and thereby enable informed and improved remediation strategy decisions for DoD sites where groundwater is contaminated by PFAAs and co-contaminants.

In pursuit of these goals, the specific questions addressed were:

- What are the effects of PFAA concentration and presence of aqueous and NAPL-phase contaminant mixtures (PFAAs and co-contaminants) on PFAA partitioning and retardation in subsurface porous media, particularly as they relate to potential differential transport in the source zone versus a downgradient plume?
- How do biogeochemical conditions, porous media properties, and the presence of co-contaminants (fuel mixtures and residues or chlorinated solvents) affect PFAA transport behavior prior to (or in the absence of) *in situ* remediation?
- What are the impacts of co-contaminant *in situ* remediation (MNA, ERD, ISCO) on PFAA fate and transport?
- How can an understanding of PFAA behavior be incorporated into quantitative assessment reflecting the complexity of conditions likely present at DoD contaminated sites?

To achieve these goals and answer these questions, the following experimental project tasks were delineated:

Task 1- Method Refinement and Verification: Existing analytical methodologies for quantifying PFAAs in aqueous and solid phases were refined and verified. This focused on both direct-injection of aqueous samples for liquid chromatography tandem mass spectrometry (LC-MS/MS) analysis and extraction of solid phases for LC-MS/MS. Matrices tested represented the extreme geochemical conditions that may be present during co-contaminant remediation.

Task 2 - Batch Partitioning Experiments: Bench-scale batch sorption experiments and NAPL-partitioning experiments were conducted to evaluate the impact of a wide array of variables on PFAA sorption. These included: a) evaluating varying geochemical conditions representative of un-remediated AFFF-impacted sites; b) evaluating competitive effects in PFAA mixtures and at the high aqueous PFAA levels observed at many AFFF-impacted sites; and c) evaluating the effects of co-contaminants such as NAPL and other AFFF-components on PFAA sorption.

Task 3 - Batch Co-Contaminant Remediation Experiments: Bench-scale experiments evaluated the impacts of co-contaminant remediation on PFAA sorption. Specific in situ remediation approaches employed for co-contaminants that were evaluated included aerobic biotransformation (i.e., MNA), ERD, and ISCO. The range of conditions explored attempted to mimic the range of conditions likely present within a source zone and groundwater plume during in situ remediation. Specifically, we addressed: a) natural attenuation conditions associated with hydrocarbon degradation; b) ERD conditions simulating TCE biodegradation; and c) ISCO conditions representative of TCE oxidation.

Task 4 - Flow-through Transport and Remediation Experiments: Information and understanding gained from PFAA sorption batch tests was confirmed in bench-scale flow-through experiments using 1D columns. These experiments aimed to examine the validity of employing PFAA-transport data obtained from batch experiments for simulating behavior in model groundwater systems during ambient conditions or those imposed during remediation. Specifically, experiments evaluated: a) PFAA transport under unaltered conditions both in the presence and absence of co-contaminant; b) PFAA transport during simulated MNA conditions aimed at aerobic bioattenuation of co-contaminants; and c) PFAA transport during ISCO treatment of co-contaminant NAPLs.

In response to initial results from a companion Strategic Environmental Research and Development Program (SERDP) project (ER-2128, led by Prof. Jennifer Field) as well as results from a field site characterization study funded by the U.S. Air Force (AFCEC BAA 689; McGuire *et al.*, 2014), an additional experimental task was added to begin to understand desorption of PFAAs from field-collected material:

Task 7 - Desorption from AFFF-impacted soil. This task used batch and bench-scale experiments to examine PFAA and PFAA precursor desorption from AFFF-impacted soil under various conditions. Specific conditions evaluated included: a) unaltered conditions (batch and column); and b) desorption in the presence of chemical oxidants (column experiments).

This Final Report describes the technical accomplishments made during SERDP Project ER-2126, by describing the approach, experimental methods, and results for each experimental task described above.

2. METHOD REFINEMENT AND VERIFICATION

2.1 Introduction (*Task 1*)

The analysis of poly- and perfluoroalkyl substances (PFASs) and PFAAs (a subclass of PFASs) in water and solid environmental samples is not as simple as one might expect. For aqueous samples, direct injection of PFAS samples onto a LC-MS/MS system is relatively simple, and yet this approach had not been tested in the aqueous matrices that might be encountered in the experiments outlined for this work (i.e., very low pH, oxidant levels, residual NAPLs, etc.). In addition, soil and aquifer sediment must be extracted prior to LC-MS/MS analysis, again using a protocol that has not been tested under the method. To this end, it was necessary to confirm that the standard analytical protocols developed and applied at the Colorado School of Mines (CSM) are applicable to these complex matrices. The PFASs selected for this method verification (**Table 2-1**) include the perfluorocarboxylates (PFCAs) and perfluorosulfonates (PFSAs). The PFCAs and PFSAs are of various change lengths, and most have been detected at AFFF-impacted sites.

Table 2-1. Names, structures, and properties of PFAAs used in this study

Compound	Abbreviation	Structure	Properties
PERFLUOROSULFONIC ACIDS (PFSAs)			
Perfluorobutane sulfonate	PFBS	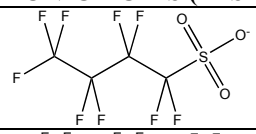	Mol. Wt.: 299.09 S_w: N/A CMC: N/A
Perfluorohexane sulfonate	PFHxS	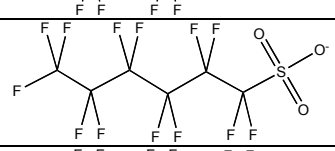	Mol. Wt.: 399.11 S_w: N/A CMC: N/A
Perfluoroheptane sulfonate	PFHpS	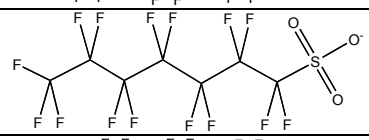	Mol. Wt.: 449.11 S_w: N/A CMC: 7859 mg/L [1]
Perfluorooctane sulfonate	PFOS	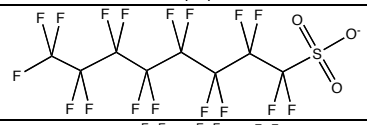	Mol Wt.: 499.12 S_w: N/A CMC: 3781 mg/L [1]
Perfluorodecane sulfonate	PFDS	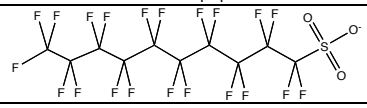	Mol Wt.: 599.14 S_w: N/A CMC: N/A

Table 2-1. Names, structures, and properties of PFAAs used in this study (cont.)

Compound	Abbreviation	Structure	Properties
PERFLUOROCARBOXYLIC ACIDS (PFCA)			
Perfluorobutanoic acid	PFBA	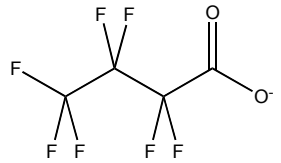	Mol. Wt.: 213.03 S_w: Miscible [3] CMC: 156222 mg/L [1]
Perfluoropentanoic acid	PFPeA	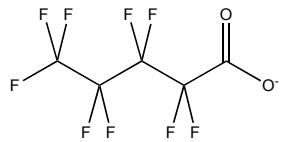	Mol. Wt.: 263.04 S_w: N/A CMC: 139411 mg/L [1]
Perfluorohexanoic acid	PFHxA	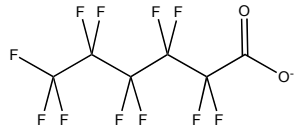	Mol. Wt.: 313.05 S_w: N/A CMC: 20818 mg/L [1]
Perfluoroheptanoic acid	PFHpA	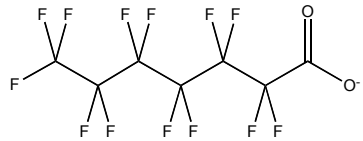	Mol. Wt.: 363.05 S_w: Miscible [3] CMC: 18153 mg/L [1]
Perfluorooctanoic acid	PFOA	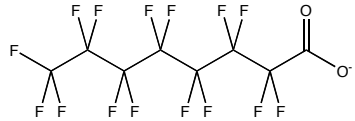	Mol. Wt.: 413.06 S_w: 9500 mg/L [3] CMC: 3800 mg/L [1]
Perfluorononanoic acid	PFNA	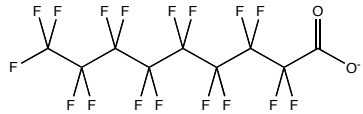	Mol. Wt.: 463.07 S_w: N/A CMC: 1945 mg/L [1]
Perfluorodecanoic acid	PFDA	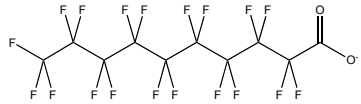	Mol. Wt.: 513.08 S_w: 5131 mg/L [3] CMC: 431 mg/L [1]
Perfluoroundecanoic acid	PFUnA	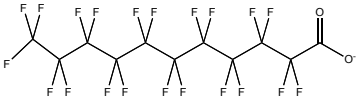	Mol. Wt.: 563.08 S_w: N/A CMC: N/A

Miscible indicates that at 25°C, it was miscible in water in all proportions.
All CMCs were collected at temperatures ranging from 2.5°C to 100°C.
[1] Kissa (2001)
[2] Arp *et al.*, (2006)
[3] Kauck and Diesslin (1951)

The aqueous and solid phase methods initially tested were derived from previous work (Schultz *et al.,* 2004; Higgins *et al.,* 2005; Higgins and Luthy, 2006; Sepulvado *et al.,* 2011). Briefly, LC-MS/MS calibration standards (9-12 concentrations spanning 2-3 orders of magnitude) are prepared from stock solutions purchased from Wellington Laboratories. Stock solution of these analytes and the surrogate standards were prepared in a 70/30 (v/v) methanol/aqueous ammonium hydroxide (0.01%) solution (70/30). Whenever possible, stable isotope surrogate and/or internal standards are employed (**Table 2-2**). A set of calibration standards is analyzed before and after every batch of LC-MS/MS samples to eliminate day-to-day variability.

Table 2-2. PFAAs and surrogate standards used in this study

Analyte	Surrogate Standard
PFBA	[$^{13}C_4$] PFBA
PFPeA	[$^{13}C_3$] PFPeA
PFHxA	[$^{13}C_2$] PFHxA
PFHpA	[$^{13}C_4$] PFHpA
PFOA	[$^{13}C_4$] PFOA
PFNA	[$^{13}C_5$] PFNA
PFDA	[$^{13}C_2$] PFDA
PFUnA	[$^{13}C_2$] PFUnA
PFBS	[$^{18}O_2$] PFHxS
PFHxS	[$^{18}O_2$] PFHxS
PFOS	[$^{13}C_4$] PFOS

Appropriate blanks are analyzed at least once each working day or with each batch of samples. Unless otherwise noted, all samples are analyzed in triplicate. To confirm laboratory method precision, triplicate aliquots of aqueous samples should have a relative standard deviation (RSD) of <10%, while triplicates of solid samples should have a RSD of <20%.

To confirm that this analytical approach is sound for all experimental tasks, this task focused on method refinement and validation of various soil and water samples. The focus of this work was expected "worst case" matrices (i.e., with the greatest potential for analytical interferences or artifacts), primarily those involving high levels of chemical oxidants and co-contaminants. The experimental approach and results from this work are provided below.

2.2 Method Refinement and Verification Experimental Approach

2.2.1 Overview

Aqueous and solid phase PFAS spike recovery experiments were conducted in the following mixed systems with aqueous and soils (only) as well as experiments for aqueous, soils and the following:

1. Iron (II) activated sodium persulfate ($Na_2S_2O_8$, 10 g/L)
2. Iron (II) activated hydrogen peroxide (H_2O_2, at 5 g/L)
3. Potassium permanganate ($KMnO_4$ at 10 g/L)
4. TCE NAPL and $Na_2S_2O_8$ (10 g/L)
5. Dodecane NAPL and $Na_2S_2O_8$ (10 g/L)
6. TCE NAPL and H_2O_2 (5 g/L)
7. Dodecane NAPL and H_2O_2 (5 g/L)
8. TCE NAPL and $KMnO_4$ (10 g/L);
9. Dodecane NAPL and $KMnO_4$ (10 g/L)

The focus was on systems containing NAPL and/or oxidant, as these systems were expected to lead to the greatest deviations from "standard" conditions (i.e., multiple phases, extreme pH values, Eh conditions, etc.) All the experimental combinations were prepared in 500 mL amber glass bottles and mixed for at least 24 hours (oxidant) but up to 96 hours (NAPL systems) using a shaker table. Each experimental system contained 20 grams of loamy sand soil (Soil A) and 500 mL of artificial groundwater (AGW; systems with NAPL contained 485 mL of AGW and 15 mL of NAPL). Soil A was purchased from Agvise Laboratories, and was dry sieved (2mm) prior to use. **Table 2-3** provides the composition of the AGW, while **Table 2-4** provides a summary of the oxidation methods tested in the spike recovery experiments.

Table 2-3. Composition of artificial groundwater

Component	Concentration (mg/L)	Concentration (mM)
$MnSO_4 \cdot H_20$	1	0.01
Na_2SO_4	180	1.27
NaCl	113	1.93
$NaHCO_3$	40	0.48
HCl	pH to 6.5	N/A

Table 2-4. Summary of oxidant conditions tested for method refinement and verification

Oxidant	Molecular Weight (g/mol)	Activation Method	Activation Molar Ratio or Concentration (M)	Oxidant Concentration (g/L)
$KMnO_4$	158.04	None	n/a	10
$Na_2S_2O_8$	238.03	$FeCl_2$ and citric acid	10:1:5	10
H_2O_2 (30%)	34.015	Fe2SO4	0.005	5

2.2.2 Aqueous Spike Recovery Protocol

Once the experimental systems were mixed for the designated time (24 hours for systems with oxidants and 96 hour for systems with NAPLs), the mixtures in each of the bottles were decanted into approximately eight 50 mL polypropylene Falcon tubes. The eight Falcon tubes for each mixture were centrifuged at 2700 rpm for 20 minutes to separate the aqueous and solid phases. Once centrifuged, the aqueous phase was poured into six Falcon tubes (filled to 50 mL). Three of these six falcon tubes (for each mixture) were spiked with the PFAS native mixture (to 1000 ng/L) and vortexed, while the unspiked Falcon tubes mixtures were used as controls. Native spiking solutions contained all PFASs listed in **Table 2-2**.

Once spiked, all six Falcon tubes were immediately sampled. As the focus was on systems containing oxidants, the aqueous phase samples were then prepared with a methanol-based method prior to analysis via LC-MS/MS. The primary purpose of using methanol method (i.e., a 1:1 dilution of aqueous sample with methanol) was to quench the oxidation reactions. An isopropanol-based method, which is employed when oxidants are not present, was separately validated when employed (i.e., for *Task 2*, etc.). Samples prepared using the methanol method contained 675 µL of sample, 675 µL of optima-grade methanol and 150 µL of isotope surrogate solution (70/30) in a 2 mL microcentrifuge tube. Preparation of oxidant samples required the use of basic or acidic methanol to maintain a pH of 3 to 10 in the samples. **Table 2-5** summarizes the required pH adjustments in sample preparation.

Table 2-5. Summary of oxidant sample pH and methanol adjustments required for aqueous sample preparation

Oxidant Conditions	Initial pH	Reaction Quenched and pH adjusted using:	Adjusted pH
H_2O_2	5.0	Methanol	5.0
H_2O_2 – TCE	5.8	Methanol	5.8
H_2O_2 – Dodecane	1.6	Methanol + 1% NH_4OH	5.2
$Na_2S_2O_8$	2.9	Methanol + 1% NH_4OH	8.8
$Na_2S_2O_8$ – TCE	2.8	Methanol + 1% NH_4OH	8.9
$Na_2S_2O_8$ – Dodecane	2.3	Methanol + 1% NH_4OH	3.9
$KMnO_4$	7.5	Methanol	7.5
$KMnO_4$ – TCE	10.7	Methanol + 1 % CH_3COOH	5.0
$KMnO_4$ – Dodecane	7.1	Methanol	7.1

Following sample preparation in the microcentrifuge tube, all samples were microcentrifuged for 30 minutes at 1330 rotations per minute (rpm). The centrifuged samples were then placed in a 2 mL auto-sampler vial for analysis by LC-MS/MS.

For all aqueous samples, LC-MS/MS analysis was conducted similar to methods reported in Hansen *et al.,* (2002) and Higgins *et al.,* (2005). Briefly summarized, chromatography was performed using 10 mM ammonium acetate aqueous and methanol gradients delivered at a flow rate of 250 µL/min by a Shimadzu LC system. Samples and standards were injected (1 mL) by a CTC auto-sampler onto a 50 by 4.6 mm Phenomenex column (3 µm pore size) equipped with a C18 guard column. Initial eluent solutions were 5% methanol, ramped to 100% methanol over 4.75 minutes and held at 100% for 3.5 min before reverting to 10% at 10 minutes. An AB SCIEX triple quadrupole LC-MS/MS system operating in negative electrospray ionization multiple reaction-monitoring (MRM) mode was employed for sample analysis. Two MRM transitions were acquired for all analytes. Quantitation was performed using an inverse weighted (1/X) internal standard calibration curve with calibration standards prepared with aqueous ratios corresponding to the sample preparation; isopropanol standards were prepared with 1053 µL of milliQ water, 117 µL of isopropanol and 130 µL of standard solution containing surrogate and methanol standard were prepared with 585 µL of milliQ water, 585 µL of optima-grade methanol and 130 µL of standard solution containing surrogate. For each analyte all calibration points were within 30% of the actual calibration values and the R^2 of the calibration curve was 0.99 for all samples.

2.2.3 Solid Phase Spike Recovery Protocol

Using the solid-phases prepared as described above (i.e., soil + TCE, soil + TCE + $KMnO_4$, etc.) solid-phase spike recovery experiments were conducted to confirm the existing solid-phase protocols (Sepulvado *et al.,* 2011) provided sufficient accuracy and precision for PFAS analysis. Briefly, 1 g of the appropriately-prepared solid phase was placed in each of six 50 mL Falcon tubes. Three of the six tubes were spiked with 20 µL of the 50 ng/mL native PFAS mixture (**Table 2-2**) and 20 µL of the 100 ng/mL surrogate solution, with the remaining three tubes only received surrograte solution (i.e., they served as background measurements to control for

potential PFAS contamination). The solid-phases were then extracted as described below and analyzed PFAS concentrations by LC-MS/MS.

For the solid phase extraction procedure, a solvent mixture of 99:1 (v/v) methanol and ammonium hydroxide was employed for each extraction. Ten mL of the solvent mixture was added to each tube prior to vortexing and placement of each tube in a heated (30°C) sonication bath (Fisher Scientific FS110H, Pittsburg, PA) for one hour. Each tube was subsequently removed and placed on a shaker table for two hours. The samples were then centrifuged at 2,700 rpm for 20 minutes (1467 relative centrifugal force; RCF), and the extract was decanted into a clean, glass 20-mL scintillation vial. This procedure was repeated twice for a total of three extraction cycles. After each round of extraction, the extract was evaporated to dryness under nitrogen (Organomation Associates Inc. N-EVAP 112, Berlin, MA) and after the final extraction was reconstituted with 700 µL of 99:1 (v/v) methanol and acetic acid (acidic methanol). The reconstituted extract was transferred to a microcentrifuge tube containing 20-40 mg of ENVI-Carb (Supelco Inc., Bellefante, PA), vortexed by hand for thirty seconds, and centrifuged at 17,000 RCF for 30 minutes. An aliquot of cleaned extract was then used to prepare a 1500 µL final sample for analysis in an autosampler vial. Autosampler vials were vortexed 30 seconds prior to LC-MS/MS analysis.

2.2.4 Solid and Aqueous Phase Sample Analysis

Chromatography was performed using an aqueous ammonium acetate (10 mM) and methanol (10mM) gradient delivered at a flow rate of 800 µL/min by a Shimadzu LC system (Shimadzu LC-20AD) pump controlled by Shimadzu controller (Shimadzu CBB-20A). Samples and standards were injected (1 mL) by a CTC Analytics LEAP Technologies autosampler onto a 50 mm x 4.6 mm Gemini C18 column (3-micron particle size, Phenomenex, Torrance, CA) equipped with a C18 Guard Column and Guard Cartridge (Higgins Analytical). For analysis of soil extracts, initial eluent conditions were 50% methanol and 50% water. The percent methanol was ramped to 95% over 4 min, held at 95% over 4 min, ramped down over 1.5 min, and held at 50% for 2.5 min. For analysis of aqueous samples, initial eluent conditions were 5% methanol and 95% water. The percent methanol was ramped to 60% over 0.75 min, ramped to 100% over 4 min, held at 100% over 3 min, ramped down to 5% over 0.5 min, and held at 5% for 1.75 min. A MDS Sciex Applied Biosystems 3200 mass spectrometer (MDS Sciex, Ontario) operating in negative electrospray ionization scheduled multiple reaction monitoring (MRM) mode was employed for sample analysis. Two MRM transitions were acquired for all analytes. The monitored transitions were analyte dependent and are the same or similar to those used previously for PFASs (Higgins *et al.,* 2005). For PFASs, these transitions correspond to decarboxylation transitions, while the monitored PFAS transitions were the formation of the FSO_3^- ion (m/z = 99). Monitored SDS transitions were the formation of the HSO_4^- (m/z = 97) ion. Quantitation was performed using Analyst®, with calibration curves generally having r^2 values greater than 0.98 and the accuracy of each calibration point within 30% of its expected value. Limits of quantitation were analyte, matrix, and run-dependent but were approximately 0.02-0.5 ng/g in soil and 2-9 ng/L in aqueous samples. All values reported are corrected for recovery of surrogate standards, which were generally greater than 60% for all samples and matrices, except where otherwise noted.

Optimal instrumental source parameters were determined and are as follows: ionspray voltage -4,000 V, curtain gas flow 35 arbitrary units (au), nebulizer gas flow 50 au, turbo gas flow 50 au, medium collision gas flow, and source temperature 650 °C. Zero air provided by a Parker-Balston Source 5000 Zero Air Generator was used for the nebulizer and drier gas, and nitrogen was used as the curtain and collision gas.

2.3 Results and Discussion

2.3.1 Aqueous Spike Recovery Experiments

In general, the pH-adjusted methanol quenching method performed quite well for most PFASs analyzed in this task. Example spike-recovery data are provided in **Figure 2-1**. Briefly, recovery was acceptable (i.e., between 70-130% of the spiked amount) under most conditions for most analytes. As is clear from **Figure 2-1**, significant variability was often observed between replicate samples, and even between replicate experiments and different users. While the method clearly works well for the key analytes targeted in this study (i.e., PFOS and PFOA), the inter- and intra-experiment variability suggests for subsequent tasks, initial method validation will be required for all users in the specific matrices being examined to ensure validity of their experimental results.

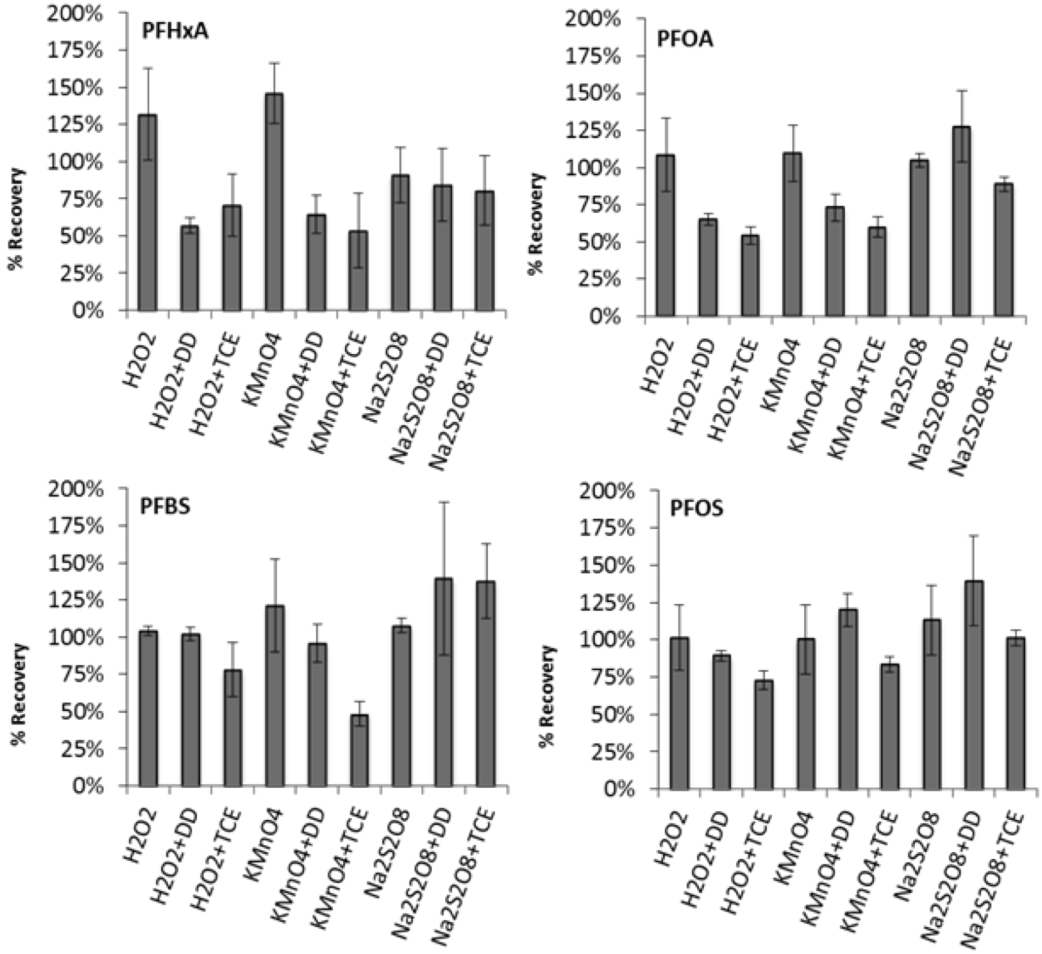

Figure 2-1. Example spike-recovery data for aqueous PFAS analysis in complex matrices.

2.3.2 Solid Phase Spike Recovery Experiments

In general, the solid-phase spike-recovery experiments yielded much more consistent and less variable results that the aqueous-phase analysis. Example spike-recovery results for solid-phase PFAS analysis are provided in **Figure 2-2**. While over and under-recovery was still an issue in some matrices, the inter-experiment variability, particularly for key analytes such as PFOS and PFOA, appeared to be considerably lower, with the vast majority of all results falling within the acceptability window of 70-130%. However, as with the aqueous analysis, these data demonstrate the need for each user to verify that the analytical method works well for the matrices specifically-under investigation within their task or sub-task. Nevertheless, no major method modifications were identified as part of the method refinement and validation for solid-phase PFAS analysis.

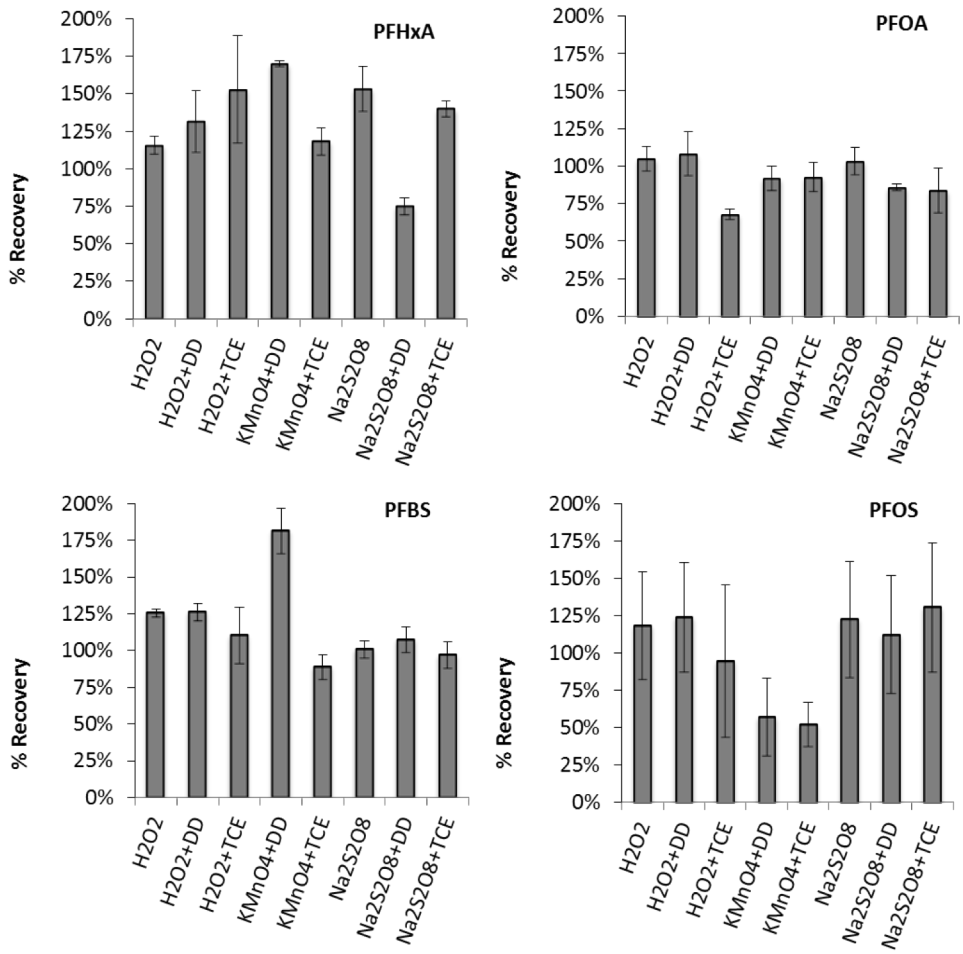

Figure 2-2. Example spike-recovery data for solid-phase PFAS analysis in complex matrices.

3. BATCH PARTIONING EXPERIMENTS

3.1 Introduction (*Task 2*)

AFFF formulations are complex, proprietary, and often include solvents and both fluorinated and hydrocarbon surfactants (Moody and Field, 1999). Transport of PFASs, including PFAAs, in groundwater at fire protection training areas (FPTAs) may thus be impacted by other AFFF components and by co-contaminants released during training exercises, such as fuels or chlorinated solvents, which may exist as NAPLs. Previous work has investigated sorption of PFOS to crude oil-contaminated soil and in the presence of non-fluorinated surfactants (Chen *et al.,* 2009; Pan *et al.,* 2009). To the best of our knowledge, behavior of multiple PFAAs in the presence of NAPL or non-fluorinated AFFF surfactants has not been documented.

Multiple mechanisms may influence PFAA sorption at AFFF-impacted FPTAs (**Figure 3-1**). The presence of multiple PFASs may lead to competitive sorption amongst PFASs. Previous work showed no competition when multiple PFAAs were present below 1 µg/L (Higgins and Luthy, 2006) but competition at higher concentrations applicable to AFFF-impacted FPTAs has not been investigated. Fuels or chlorinated solvents may have a varied effect on sorption. TCE, selected as a model NAPL for this study, has been documented in groundwater at FPTAs along with fuel components such as benzene, toluene, ethylbenzene, and xylenes (Kao and Prosser, 1999; Bugna *et al.,* 2005). These components may compete with PFASs for sorption sites, but when present at high enough concentrations to exist as a NAPL, may also act as an additional sorbent (Jonker and Barendregt, 2006; Jonker *et al.,* 2003). For example, NAPL led to increases in sorption of both PAHs and polychlorinated biphenyls (PCBs), and in some cases these compounds had a higher affinity for NAPL than for soil organic carbon (Jonker and Barendregt, 2006; Jonker *et al.,* 2003). Previous work found PFOS sorption increased in the presence of crude oil, (Chen *et al.,* 2009) but behavior of other PFAAs in the presence of other NAPLs is uncertain, especially given their hydrophobic and oleophobic nature. Hydrocarbon surfactants in AFFF that may also be present in groundwater

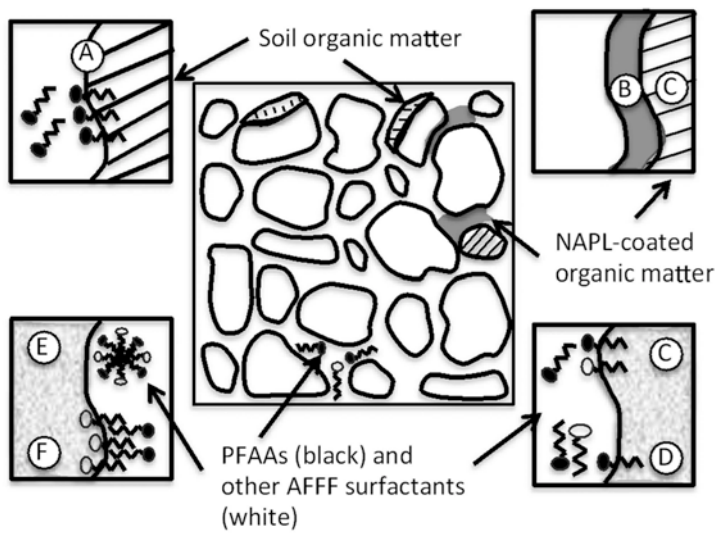

Figure 3-1. A conceptual model of the processes that may impact PFAS sorption at AFFF-impacted sites.
A.) Competitive sorption among PFASs; B.) NAPL as a sorbent; C.) Co-contaminant interference at PFAS sorption sites; D.) Hydrocarbon surfactant-enhanced PFAS solubility. E.) Hydrocarbon surfactant/PFAS mixed hemimicelles increasing sorption; and F.) Hydrocarbon surfactants as a sorbent.

include anionic sodium decyl sulfate (SDS) and n,n-dimethyldodecylamine n-oxide (AO) (3M, 2005; Fire, 2010). These surfactants may have varied effects on PFAA sorption. Sorption of atrazine increased in the presence of a nonionic surfactant and decreased in the presence of cationic and anionic surfactants (Tao *et al.*, 2006). PFOS sorption has been shown to increase in the presence of a cationic surfactant and decrease when an anionic surfactant was present (Pan *et al.,* 2009). To the best of our knowledge, the impacts on PFAA sorption of non-fluorinated surfactants specific to AFFF remain unexplored.

The objective of this task was to determine the groundwater transport potential of PFAAs by studying sorption in mixed PFAA and co-contaminant systems using batch studies. Bench-scale batch sorption experiments and partitioning experiments were conducted to evaluate the impact of a wide array of variables on PFAA sorption. All natural solids were microbially inactivated to reduce variations in biogeochemical conditions. A minimum of five initial aqueous concentrations were used to construct all isotherms. Appropriate controls were employed to quantify any sorptive losses to the vial walls or air/water interface. Specifically, we tested sorptive behavior of perfluorocarboxylic acids (PFCAs) and perfluorosulfonic acids (PFSAs) in single-PFAA vs. mixed-PFAA systems to examine competitive effects. PFAA sorption was studied in soils amended with NAPL, and in systems containing representative non-fluorinated AFFF surfactants. Conceptual models were developed to provide potential explanations for the observed changes in PFAA sorption. Lastly, initial predictions of relative advective transport of PFAAs were made based on the results of this task.

The specific subtasks conducted as part of this task include:

Task 2a: Evaluation of Varying Geochemical Conditions. Batch sorption experiments were conducted to examine the effects of soil grain size, mineralogy, and NOM content as well as groundwater pH and hardness on the equilibrium sorption of PFAAs of various classes and chain lengths in the µg/L range.

Task 2b: Evaluation of Varying PFAA Concentrations and Mixtures. Using a subset of materials and conditions evaluated in *Task 2a*, isotherms covering a wider range of initial aqueous PFAA concentrations (ng/L to mg/L) were generated for PFOS and PFOA as representative PFAAs. Each chemical was tested alone and then in combination to examine the potential effects of competitive or enhanced sorption when PFAA mixtures are present.

Task 2c: Effects of Co-Contaminants on PFAA Sorption. This subtask evaluated the impact of partitioning to NAPL, NAPL-water interfaces, and porous media in the presence of co-contaminants. When the NOM content of the aquifer material is low, this organic phase may represent a significant sorbent for PFAAs in the subsurface. Using a subset of conditions evaluated in *Task 2a*, partitioning of PFAAs to various NAPLs in the presence and absence of aquifer materials was investigated.

For clarity, the specific experimental protocols and initial results of all three subtasks are presented in the following sections.

3.2 Experimental Methods and Approach

3.2.1 Materials

Calibration standards of perfluorobutanoate (PFBA), perfluoropentanoate (PFPeA), perfluorohexanoate (PFHxA), perfluoroheptanoate (PFHpA), PFOA, perfluorononanoate (PFNA), perfluorodecanoate (PFDA), perfluoroundecanoate (PFUnA), perfluorobutanesulfonate (PFBS), perfluorohexanesulfonate (PFHxS), and PFOS, as well as stable-isotope surrogate standards (**Tables 2-1 and 3-1**) were purchased from Wellington Laboratories. Spiking solutions for all experiments were prepared from standards of PFCAs and PFSAs purchased from Sigma-Aldrich. The hydrocarbon surfactants SDS and AO were purchased from Alfa Aesar. Stock solution of calibration standards, spiking standards (purity-corrected), surfactants (purity-corrected) and surrogate standards were prepared in a 70/30 (v/v) methanol/aqueous solution. Unless otherwise noted, all experiments utilized a spiking solution containing all PFAAs. Unless otherwise specified, all other chemicals were of reagent grade and were purchased from Fisher Scientific, Mallinckrodt Chemicals, or Sigma Aldrich.

Table 3-1. PFAAs and surrogate standards used in this study

Analyte	Surrogate Standard
PFBA	[$^{13}C_4$] PFBA
PFPeA	[$^{13}C_3$] PFPeA
PFHxA	[$^{13}C_2$] PFHxA
PFHpA	[$^{13}C_4$] PFHpA
PFOA	[$^{13}C_4$] PFOA
PFNA	[$^{13}C_5$] PFNA
PFDA	[$^{13}C_2$] PFDA
PFUnA	[$^{13}C_2$] PFUnA
PFBS	[$^{18}O_2$] PFHxS
PFHxS	[$^{18}O_2$] PFHxS
PFOS	[$^{13}C_4$] PFOS

Solid phases used in this study were selected to represent a variety of geochemical and physical characteristics (**Table 3-2**). Preliminary studies showed no appreciable sorption of PFAAs to sorbents (e.g. sand) without any organic matter, so solid phases with varying f_{oc} were selected. These preliminary experiments were conducted in sands of varying sizes with no f_{oc}, so it is unlikely that there is a relationship between PFAA sorption and grain size. Additionally, f_{oc} values up to 1.35% have been measured in aquifer sediments at an AFFF-impacted FPTA (McGuire *et al.*, 2014). A loamy sand (A) and loam (B) were purchased from Agvise Laboratories, and a sandy clay loam (C) was donated. Soil C likely exhibits a net positive charge due to high iron oxide content (**Table 3-3**). All soils were dry sieved (2 mm) prior to use. To study NAPL impacts on PFAA transport, some experiments utilized soils amended with TCE as a model NAPL. To ensure TCE was present as NAPL, 1 mL of TCE was added to 15 g of soil to achieve a TCE concentration of ~100 g/kg and stirred vigorously prior to use. Artificial groundwater (AGW) was made by modifying deionized water with ions typically found in groundwater and was used as the aqueous phase for all experiments (**Table 3-3**).

Table 3-2. Solid phase characteristics

Solid Phase	f_{oc}[1] %	Sand %	Silt %	Clay %	ρ_b (g/cm^3)	pH	Major Cations (mg/kg)					Fe[2] (g/kg)	Al[2] (g/kg)
							K	Ca	Mg	Na	H		
Soil A (Loamy Sand)	1.7	81	1	9	1.14	6.1	319	1084	171	11	33	2.21	0.93
Soil B (Loam)	4.5	33	42	25	0.92	7.8	888	4418	607	14	21	6.14	1.67
Soil C (Sandy Clay Loam)	0.8	47	20	33	1.11	5.2	73	272	76	20	NM	24.17	3.99

[1] Walkley-Black;
[2] Citrate-Bicarbonate-Dithionite (CBD) extractable;
NM = not measured

3.2.2 Batch Sorption Experiments

All sorption isotherms were measured as 5-point isotherms with initial aqueous concentrations (C_w^i) of 0.5, 5, 50, 500, and 1000 µg/L. Triplicate reactors were prepared for each soil type (soils A, B, and C) and concentration point by transferring 15 g soil and 40 mL artificial groundwater (**Table 3-3**) with 1 g/L of sodium azide to a 50 mL polypropylene tube to achieve a soil-water ratio of 0.375 g/mL. Reactors were then spiked with 20 µL of an appropriate concentration of PFAA mix spiking solution prepared in 70/30 such that methanol comprised only ~0.04% of the aqueous phase. Reactors were vortexed and placed on a shaker table (VWR 5000 STD 120V) for a period of 10 days based on previous work (Higgins and Luthy, 2006; Sepulvado *et al.,* 2011). Prior to sampling, the reactors were centrifuged (Eppendorf 5810, Hamburg, Germany) at 2,700 rpm (1467 RCF), for 20 min. At the completion of the 10-day sorption experiments, the aqueous phase was sampled and removed and the solid phase from all reactors was extracted to determine residual fraction of PFAAs in the solid phase and to enable the completion of mass balance calculations. Batch sorption isotherms with PFAA mix were measured in soils A, B, and C.

Table 3-3. Composition of artificial groundwater

Component	Concentration (mg/L)	Concentration (mM)
$MnSO_4 \cdot H_20$	1	0.01
Na_2SO_4	180	1.27
NaCl	113	1.93
$NaHCO_3$	40	0.48
HCl	pH to 6.5	N/A

A series of sorption experiments was also conducted to study competitive effects, the impacts of NAPL, and the impacts of other AFFF hydrocarbon surfactants on PFAA sorption. To determine if there were any competitive effects amongst PFAAs, batch sorption isotherms with PFOA or PFOS only were measured in soils A and B. These reactors were prepared as described above but were spiked with 20 µL of a spiking solution in 70/30 that contained either PFOS or PFOA only. To determine the impacts of NAPL on PFAA sorption, isotherms were repeated for soils A and B; however the solid phase of these reactors was modified with 1 mL of TCE and stirred vigorously prior to the addition of aqueous phase or PFAA mix. Finally, sorption experiments in the presence of other AFFF surfactants were completed in soils A, B, and C. Reactors for these experiments were prepared as described above but were consecutively spiked with 20 µL of a spiking solution in 70/30 containing either SDS or AO. These surfactants were selected because of their presence in some AFFF formulations (3M, 2005; Fire, 2010). Reactors were spiked with 100 mg/L of either SDS or AO.

Prior to completing the isotherms with SDS and AO, preliminary single-point K_d measurements of PFAA sorption were completed in reactors with soils A and B spiked with 500 µg/L of PFAAs and either 0.5, 10, 50, 100 mg/L of either SDS or AO. PFAA results from these experiments were preliminary and were not utilized in this work; however reactors from these experiments were retained and analyzed for SDS or AO as appropriate to serve as a 4-point isotherm for these surfactants to serve as a semi-quantitative analysis of SDS or AO sorption relative to PFAAs. Unfortunately, matrix interference prevented use of analytical results of AO concentrations and those results were removed from further consideration. Because SDS analysis

did not employ a stable-isotope surrogate standard, quantitative use of these results should be treated with caution. Additionally, the solid phase of these reactors was not extracted for SDS, so all sorption results are based on the aqueous loss method as described in previous work (Higgins and Luthy, 2006).

Finally, to understand the impacts of NAPL on PFAA sorption the partitioning of PFAAs in NAPL-water only systems was studied. Two model NAPLs, TCE and dodecane (DD), were selected. Though DD was not used in batch isotherms, PFAA-DD partitioning was studied to determine how NAPL type my impact PFAA sorptive behavior in the presence of NAPL. NAPL-water partitioning experiments were conducted in 50 mL glass centrifuge tubes with an actual capacity of 63 mL and were prepared with 12.5 mL of TCE and 50 mL of artificial groundwater, yielding a NAPL-water ratio of 0.25 mL/mL. Experiments in glass tubes were designed to minimize the air space in the glass centrifuge tubes as PFAA loss to glass reactors appears to be controlled by the amount of surface area available for a meniscus to form (unpublished data). All NAPL-water experiments were spiked to a C_w^i of 500 µg/L and allowed to equilibrate on a shaker table for 3-days based on previous work (Jonker *et al.,* 2003). At the end of the 3-day period, reactors were allowed to sit for 30 minutes prior to sampling the aqueous phase. Because DD is a light NAPL (LNAPL), DD was siphoned from the top of batch reactors using a Pasteur pipet prior to sampling the aqueous phase. Residual DD remained after this process was complete; however, aqueous phase samples were taken from the center of the water column using a pipet extended through the residual DD phase.

3.2.3 Aqueous Sample Preparation

To ensure that aqueous sample concentrations fell within the linear range of the calibration curve during analysis, each point in the batch isotherm was prepared with a specific dilution scheme (**Table 3-4**). In general, an aliquot of aqueous phase from each batch reactor was diluted in a 2-mL microcentrifuge tube to create a 1500 µL interim sample. These interim samples were vortexed for 30 seconds and centrifuged (Fisher Scientific, accuSpin Micro 17) at 17,000 RCF for 30 minutes. An aliquot of the interim sample was then used to prepare a 1500 µL final sample for analysis in an autosampler vial. Autosampler vials were vortexed 30 seconds prior to direct injection LC-MS/MS analysis. Sample dilutions were designed assuming that none of the PFAA mass partitioned to the solid phase, thereby including a worst-case scenario to ensure final sample concentrations were within calibration range. Interim dilutions were 91% aqueous phase and 9% isopropanol. Final samples for analysis were 82% aqueous phase, 8% isopropanol and 10% 70/30 containing 0.3 ng surrogate standard.

Samples for SDS analysis were prepared from interim samples that were initially prepared for PFAA analysis using the 500µg/L preparation scheme (**Table 3-4**). Final samples for SDS analysis were prepared from these interim samples with dilution factors of 0.36, 0.05, 0.01, and 0.005 for reactors with initial aqueous concentration of SDS of 0.5, 10, 50, and 100 mg/L respectively. Final samples were prepared in autosampler vials with 9% isopropanol and 91% aqueous phase. Results were intended for semi-quantitative use only; therefore, no internal standard was used during these analyses.

Table 3-4. Aqueous sample preparation scheme for batch sorption experiments

	0.5 µg/La	5 µg/L	50 µg/L	500 µg/L	1000 µg/L
Interim Sample Preparation:					
H2O from batch reactor	NA	1215	900	150	25
Milli Q water	NA	150	465	1215	1340
Isopropanol	NA	135	135	135	135
Final Sample Preparation:					
H2O from interim sample	NA	550	137	150	450
Diluent (MilliQ+9% isopropanol)	NA	800	1213	1200	900
Surrogate solution in 70/30	NA	150	150	150	150

All units are in µL.

[a] Interim sample preparation was not required for this sample to be in calibration range and final sample was prepared directly from batch reactor as follows: 1215 µL of batch reactor aqueous phase, 135 µL of isopropanol, and 150 µL of surrogate solution.

3.2.4 Soil Extractions

Moisture content of each sample was separately measured by drying overnight in an oven at 105°C to enable reporting of the results on an oven-dry dry weight basis. After being sampled, the aqueous phase of batch sorption reactors was poured off and the remaining solid phase extracted in the 50 mL polypropylene conical tubes. A solvent mixture of 99:1 (v/v) methanol and ammonium hydroxide was employed for each extraction. Ten mL of the solvent mixture was added to each tube prior to vortexing and placement of each tube in a heated (30°C) sonication bath (Fisher Scientific FS110H, Pittsburg, PA) for one hour. Each tube was subsequently removed and placed on a shaker table for two hours. The samples were then centrifuged at 2,700 rpm for 20 minutes (1467 RCF), and the extract was decanted into a clean, glass 20-mL scintillation vial. This procedure was repeated twice for a total of three extraction cycles. After each round of extraction, the extract was evaporated to dryness under nitrogen (Organomation Associates Inc. N-EVAP 112, Berlin, MA) and after the final extraction was reconstituted with 700 µL of 99:1 (v/v) methanol and acetic acid (acidic methanol). The reconstituted extract was transferred to a microcentrifuge tube containing 20-40 mg of ENVI-Carb (Supelco Inc., Bellefante, PA), vortexed by hand for thirty seconds, and centrifuged at 17,000 RCF for 30 minutes. To ensure that soil extract concentrations fell within the linear range of the calibration curve during analysis, each point in the batch isotherm was prepared with a specific dilution scheme (**Table 3-5**). In general, an aliquot of cleaned extract was transferred and diluted in a 2-mL microcentrifuge tube to create an 1800 µL interim sample. These interim samples were vortexed, and an aliquot of the interim sample was then used to prepare a 1500 µL final sample for analysis in an autosampler vial. Autosampler vials were vortexed 30 seconds prior to direct injection LC-MS/MS analysis. All interim dilutions were 70% acidic methanol and 30% dilution water (0.01% ammonium hydroxide in Milli-Q water). All final samples were 8.6% of a solution of 70/30 made with acidic methanol and dilution water, 1.4% of 70/30 containing 0.3 ng of surrogate solution, and 90% Milli-Q.

Table 3-5. Solid extract preparation scheme for batch sorption experiments

	0.5 µg/L[a]	5 µg/L	50 µg/L	500 µg/L	1000 µg/L
Interim Sample Preparation: Solid extract	NA	120	20	20	20
Acidic methanol	NA	1140	1240	1240	1240
Dilution water	NA	540	540	540	540
Final Sample Preparation: Interim Sample	NA	118	130	23	20
70% acidic MeOH 30% Dilution H_2O	NA	12	0	107	110
Milli-Q	NA	1350	1350	1350	1350
Surrogate solution in 70/30	NA	20	20	20	20

All units are in µL.

[a] Interim sample preparation was not required for this sample to be in calibration range and final sample was prepared directly from soil extract as follows: 39 µL of soil extract, 91 µL of 70% acidic methanol/30% dilution water solution, 20 µL of surrogate solution, and 1350 of Milli-Q.

3.2.5 LC-MS/MS Analysis

Aqueous samples were analyzed directly via LC-MS/MS as described in *Task 1*. Briefly, An Applied Biosystems 3200 mass spectrometer (MDS Sciex) was used to monitor two transitions for each analyte. Quantitation was performed using Analyst. Limits of quantitation were analyte, matrix, and run-dependent but were approximately 0.02-0.5 ng/g in soil and 2-9 ng/L in aqueous samples. All values reported are corrected for recovery of surrogate standards, which were generally greater than 60% for all samples and matrices.

3.2.6 Quality Assurance/Quality Control Measures

To account for variations in the samples, batch sorption reactors were prepared in triplicate and the aqueous phase and solid extracts analyzed from all reactors. In all cases, analytical results are reported as the average of the three values. If one of the three values was below detection then the average value was reported as below detection.

Control isotherms were prepared for sorption experiments by preparing triplicate control reactors as described above for batch sorption isotherms but with no solid phase. These reactors were placed on the shaker table and sampled on the final day. If losses for an analyte were greater than 10%, then these results were used to calculate the mass of PFAA lost to the reactor so that this could be accounted for in mass balance calculations of PFAAs recovered in the solid phase, aqueous phase, and reactor. Mass lost to the reactor was calculated similar to previous work (Higgins and Luthy, 2006) as follows:

$$f_w = \frac{M_w}{M_T} = \frac{M_w}{M_w + M_v} = \frac{C_w V_w}{C_w V_w + \sigma_v A_v} \qquad \text{(eqn. 3-1)}$$

where M_w is the mass of analyte in water, M_T is the total mass, M_v is the mass lost to the reactor (i.e. vial), C_w is the measured aqueous concentration of the analyte, V_w is the volume of water in

the control reactor, σ_v is the surface area normalized concentration of analyte on the vial, and A_v is the surface area of the vial. If we divide this equation by C_wV_w:

$$f_w = \frac{1}{1+\frac{\sigma_v A_v}{C_w V_w}} = \frac{1}{1+K_v r_{av}} \qquad \text{(eqn. 3-2)}$$

where K_v is the vial-water distribution coefficient, and r_{av} is the ratio of vial surface area to aqueous phase (A_v/V_w). In control vials, f_w can be calculated because a known amount of PFAA is spiked into the vial and the analyte mass recovered in the aqueous phase is measured during aqueous phase analysis. Since f_w is calculated this way, the equation can be rearranged to solve for K_vr_{av}. Because r_{av} is constant for all reactors, the K_vr_{av} term from control reactors can be used to solve for PFAA mass lost to the vial in batch sorption isotherms:

$$K_v r_{av} = \frac{\sigma_v A_v}{C_w V_w} = \frac{M_v}{M_w} \qquad \text{(eqn. 3-3)}$$

The K_vr_{av} term is determined in control reactors and M_w in isotherm batch reactors with solid phase is measured by aqueous phase analysis. Therefore, this equation can be rearranged to solve for M_v, which can be incorporated into mass balance equations.

Control reactors were also prepared in glass centrifuge vials to account for losses to this type of vial in NAPL-water partitioning experiments. Vials were prepared as described above for NAPL-water batch experiments except with no NAPL phase. Mass lost to the vial was calculated as described above.

Finally, in this study, all solid and aqueous phase concentrations were measured enabling completion of mass balance calculations for recovery of PFAAs between the solid phase, aqueous phase, and vial (**Table 3-6**). If the average recovery for any single concentration point in an isotherm was above 130%, that point was removed from consideration in the isotherm and subsequent regressions. All mass balance results below are the average recovery for all PFAA concentrations and solid phases of points that were included in the isotherms for each set of experiments. For instance, PFAA only mass balances are the average of each PFAA that was recovered in the A, B, and C soils in experiments that contained no co-contaminants. AO mass balance results were anomalous and are discussed in more detail below. It should be noted that low recovery of longer chain-length PFAAs is thought to be the result of underestimation of the PFAA mass lost to the vial. Because all solid and aqueous phase concentrations were measured (as opposed to estimating solid phase via aqueous loss), these analytes were still considered in this study.

As mentioned, AO mass balance data showed anomalous over recovery of PFAAs. Exceptionally high K_v values were obtained from the control isotherms containing 100 mg/L AO and these lead to high estimates of M_v for the mass balances, resulting in the over recovery reflected. Isotherms containing AO were conducted simultaneously with isotherms containing no co-contaminant and

Table 3-6. Mass balance results for batch isotherms

Analyte	PFAA only			PFAA + NAPL		PFAA + SDS			PFAA + AO			PFAA + AO corrected		
	mass balance (%)	± (%)	n	mass balance (%)	n	mass balance (%)	± (%)	n	mass balance (%)	± (%)	n	mass balance (%)	± (%)	n
PFBA	111	7	3	102	2	97	5	3	106	4	3	108	6	3
PFPeA	109	9	3	105	2	101	1	3	111	10	3	107	8	3
PFHxA	110	7	3	113	2	111	5	3	129	7	3	122	8	3
PFHpA	117	9	3	118	2	118	18	3	131	20	3	116	17	3
PFOA	102	5	3	108	2	124	20	3	175	47	3	110	21	3
PFNA	84	6	3	75	2	87	16	3	245	136	3	76	20	3
PFDA	66	7	3	53	2	67	13	3	626	207	3	60	16	3
PFUnA	53	-	1	35	1	47	-	1	NM	-	-	NM	-	-
PFBS	116	16	3	132	2	113	14	3	152	25	3	137	19	3
PFHxS	111	6	3	105	2	100	15	3	214	70	3	107	16	3
PFOS	76	15	3	80	2	77	17	3	621	572	3	77	13	3

NM = not measured
± is the standard deviation

all were spiked simultaneously. No anomalous recovery issues were reflected in data from isotherms with no co-contaminant, suggesting experimental errors with the PFAA spiking solution were unlikely. Additonally, analytical data met all data quality criteria, indicating that this is likely not an analytical artifact. It is possible that the presence of the AO in the control reactors led to additional losses of PFAAs to the vial through the formation of hemimicelles on the vial wall. One would expect this effect to be lessened in vials containing soil, as some of the AO would partition to the solid phase. Therefore, AO mass balances were repeated using K_v values from control vials containing no co-contaminant. The resulting corrected mass balances showed recovery more typical of other mass balances and AO results were still considered in this study. It should be noted that the value used for K_v affects only the mass balance results and not the results of soil-water partitioning coefficients. This is because both solid and aqueous phase PFAA concentrations were measured and so estimates of M_v were not needed to calculate partitioning coefficients.

3.3 Results and Discussion

3.3.1 PFAA Sorption

In some cases, PFAA sorption was found to be non-linear; therefore PFAA sorption isotherms were fit with the Freundlich equation (r^2 >0.95, **Appendix A-1**):

$$C_s = K_f C_w^n \qquad \text{(eqn. 3-4)}$$

where C_s is the concentration in the soil, K_f is the Freundlich sorption coefficient, and *n* describes isotherm linearity. Nonlinearity is thought to arise because there are multiple types of sites that have different sorption free energies. The linear portion of the isotherm implies

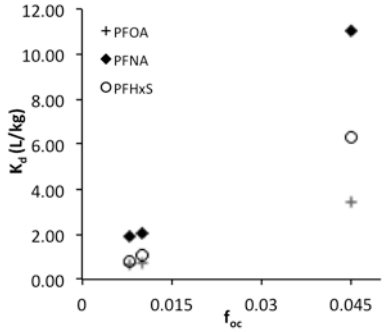

Figure 3-2. Trends of select PFASs with soil f_{oc}.

constant free energy of sorption (Schwarzenbach *et al.*, 2003). In this study, values for *n* were 0.7-1.1 (**Appendix A-1**), consistent with previous studies (Higgins and Luthy, 2006). Because sorption of some PFAAs was nonlinear and to facilitate comparison of sorption between PFAAs and soils, concentration-specific solid-water distribution coefficients (K_d values; L/kg) were calculated for each PFAA and soil at two aqueous concentrations. Interpolated values were calculated at a concentration of 5 nM as done in prior work to facilitate comparison of results (Higgins and Luthy, 2006) and at a concentration of 0.35 mg/L to represent differing trends at the upper end of the isotherm at concentrations more typical of AFFF-impacted sites. K_d values at 5 nM were normalized to f_{oc} to obtain concentration-specific K_{oc} (L/kg$_{oc}$) values. Consistent with previous work, (Higgins and Luthy, 2006) K_d values increased with increasing f_{oc} (**Figure 3-2**), confirming the importance of hydrophobic interactions in PFAA sorption. Where available, K_{oc} values (**Table 3-7**) compared well with prior work and also increase with increasing PFAA chain length (Higgins and Luthy, 2006). Exceptions to this trend were observed for PFBA and PFPeA, as will be discussed.

Table 3-7. Log K_{oc} values calculated in this work and compared to previous studies

Analyte Name	Tail Length[a]	Average Log K_{oc}	±	n[b]	Log K_{oc} Prev. Work (Higgins and Luthy, 2006)	±
PFBA	3	1.88	0.11	3	N/A	
PFPeA	4	1.37	0.46	3	N/A	
PFHxA	5	1.31	0.29	3	N/A	
PFHpA	6	1.63	0.15	3	N/A	
PFOA	7	1.89	0.02	3	2.06	
PFNA	8	2.36	0.04	3	2.39	0.09
PFDA	9	2.96	0.15	3	2.76	0.11
PFUnA	10	3.56		1	3.3	0.11
PFBS	4	1.79	0.10	3	N/A	
PFHxS	6	2.05	0.08	3	N/A	
PFOS	8	2.80	0.08	3	2.57	0.13

[a] Length of fluorocarbon tail;
[b] n= number of soils included in average

Previous work found no competitive effects for PFOS when sorption occurred in a PFAA-mix vs. a PFOS only system, but the systems studied used fewer PFAAs and a lower concentration range than included herein (Higgins and Luthy, 2006). Single-solute isotherms for PFOA and PFOS were compared to PFOA/PFOS isotherms measured in a mixed-PFAA system (**Figure 3-3**). In soil B, there was no statistical difference between sorption of either PFOA or PFOS in single vs. mixed-PFAA systems (**Figure 3-3**). Minor competitive effects were evident in both PFOA and PFOS in soil A. Because f_{oc} of the loamy sand is much lower than that of the loam

(**Table 3-2**), competitive effects in the loamy sand may arise due to a more limited number of sites available for sorption. This indicates that competitive effects amongst PFAAs may be a factor in low f_{oc} environments; however overall effects observed in this study were considered to be minor and remaining experiments were conducted with a mix of the 13 PFAAs considered.

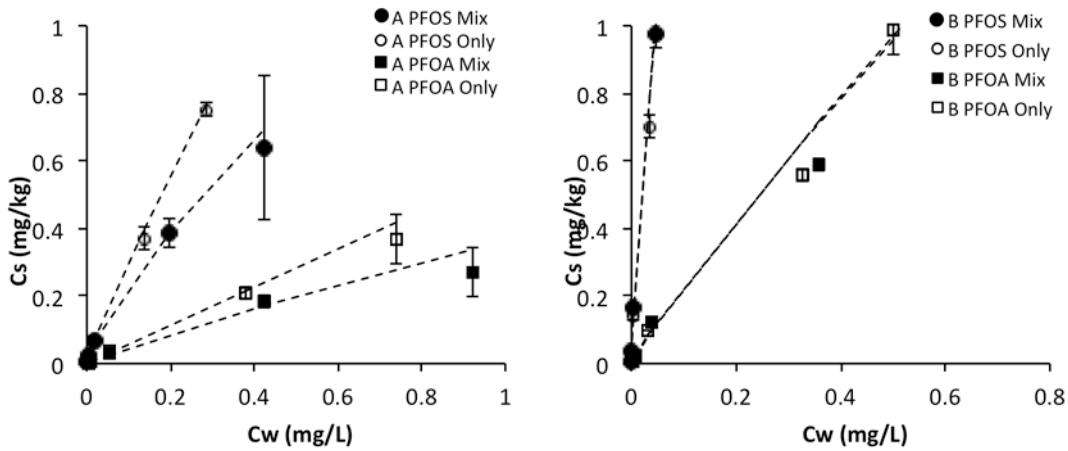

Figure 3-3. Sorption of PFOA and PFOS to soils A and B in both mixed-PFAS (closed symbols) and single solute (open symbols) systems. Dashed lines are fitted Freundlich isotherms.

Previous work observed a ~0.55 log unit increase in K_d per addition of each CF_2 group to the fluorocarbon tail based on K_d measurements for PFCAs with 7 CF_2 groups (C7) to C10 PFCAs (Higgins and Luthy, 2006). This study included regressions of K_d values with chain length for C3 to C10 PFCAs in soils A and B and found similar Log K_d increases of 0.45 (± 0.04) and 0.51 (± 0.04) per CF_2 group in soils A and B, respectively, for C5 to C10 PFCAs (**Figure 3-4**). C3 and C4 PFCAs, however, did not follow this trend. Regressions of C7-C9 PFCA K_d values vs. chain length in soil C yielded a slope of 0.46 (± 0.01). Small deviations from this slope were observed for C5-C6 in the soil C; however, C3 and C4 PFCAs were again exceptions to the trend. Sorption of these compounds was much higher than would be expected based on extension of chain length-Log K_d regressions. As both solid and aqueous phase concentrations were measured and mass balances of PFBA and PFPeA in the soil, aqueous phase, and reactor were 109-111% (**Table 3-6**) for all isotherms, it is very unlikely that these deviations resulted from experimental artifacts.

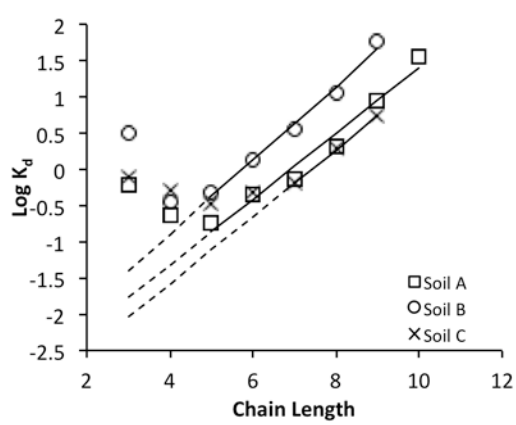

Figure 3-4. Log K_d values for PFCAs of varying chain length in A, B, and C soils. Solid lines are regressions of chain length vs. Log K_d ($r^2 > 0.95$) for C5-C10 (soils A and B) or C7-C9 (soil C) PFCAs. Slopes of the solid lines are 0.45 (± 0.04), 0.51 (± 0.04), and 0.46 (± 0.01) for the A, B, and C soils, respectively. Dashed lines are extrapolations of the regressions to the smaller chain lengths.

The chain length-K_d relationship indicates the importance of van der Waals effects (e.g. hydrophobic effects) in PFAA sorption, so exceptions observed in PFBA and PFPeA suggest a different mechanism may be relatively more important for shorter chain length PFAAs. Electrostatic effects may play a relatively more important role for these PFAAs, but as anomalous trends were observed in negatively charged A and B soils as well as the positively charged C soil, this is unlikely. Additionally, sorption of both PFBA and PFPeA was dependent on soil f_{oc}, suggesting hydrophobic effects are still important. Another possibility is that there is a subset of sorptive sites in organic matter available only to smaller molecules (i.e., a steric effect). If this were true, K_d values would be higher for smaller PFAAs and, in fact, Log K_d values do decrease with increasing size from C3 to C5 PFCAs before increasing for C6 and higher PFCAs. This is also consistent with dependency of PFBA and PFPeA sorption on f_{oc} as these sites would likely be more abundant in higher f_{oc} soils. This suggests sorption of PFBA, PFPeA, and potentially PFHxA is impacted by steric effects as well as hydrophobic effects. It is important to note anomalous behavior, as recent PFAA production has moved from long-chain (>7 CF_2 groups) PFAAs such as PFOS to short-chain PFAAs such as PFBA, which were widely believed not to undergo significant sorption. These results suggest non-negligible sorption of these compounds does occur. Further mechanistic studies, such as those conducted by Tulp *et al.*, (2009) of sorption of these short chain PFAAs to organic matter are needed to confirm and explain this behavior.

3.3.2 Impact of NAPL

Behavior of PFAAs in the presence of NAPL was investigated by measuring PFAA sorption in both A and B soils amended with TCE (**Figure 3-5**, **Appendix A-2**). The impacts of NAPL on PFAA sorption varied between PFAAs and soils. In soil A (1.7 % f_{oc}), the presence of NAPL phase TCE generally led to an increase in isotherm linearity (**Appendix A-2**) and thus a concentration-dependent effect on sorption. Sorption was not impacted or slightly decreased at lower PFAA concentrations and increased at higher concentrations (**Figure 3-5**). PFBA, PFPeA, and PFHxA were exceptions to this trend. Sorption of these compounds increased across the entire concentration range when TCE was present. In soil B (4.5 % f_{oc}), sorption was unchanged or decreased in the presence of NAPL. PFBA, PFPeA, and PFHxA were again exceptions. For these compounds, sorption increased over all or part of the concentration range (**Figures 3-5 and 3-6**).

Multiple factors may influence PFAA sorption in the presence of NAPL (Jonker *et al.,* 2003). Previous work with PAHs and PCBs indicated an increase in sorption when oil is present above the critical separate phase concentration (CSPC), which is the concentration (C_{NAPL}) where oil will exist as a NAPL, typically at 1000-3000 mg/kg (Jonker *et al.,* 2003; Sun and Boyd, 1991). The exact CSPC is dependent on the soil f_{oc} because a NAPL will only form if the soil organic carbon is saturated with NAPL components: more NAPL is required in systems with higher f_{oc} (Jonker *et al.,* 2003) CSPCs typically occur at approximately 15% of oil in organic carbon (w/w) (Jonker *et al.,* 2003). Based on an f_{oc} of 1.7% for soil A, the CSPC would be approximately 255 mg/kg, which is approximately 400 times lower than the C_{NAPL} employed here. Above the CSPC,

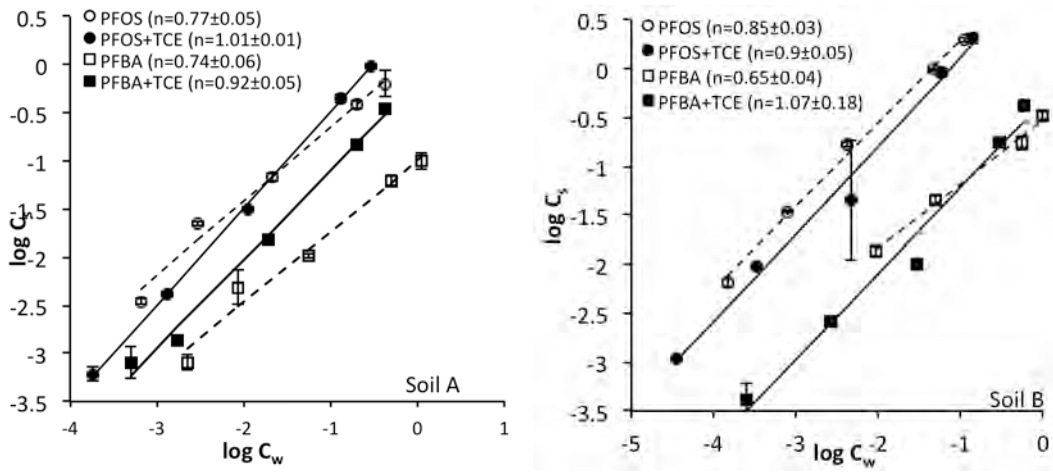

Figure 3-5. Sorption of PFBA (squares) and PFOS (circles) in the presence (closed symbols) and absence (open symbols) of TCE to soils A and B. Solid lines are fitted Freundlich isotherms for closed symbols and dashed lines are fitted Freundlich isotherms for open symbols. Error bars represent relative error in triplicate measurements of C_s.

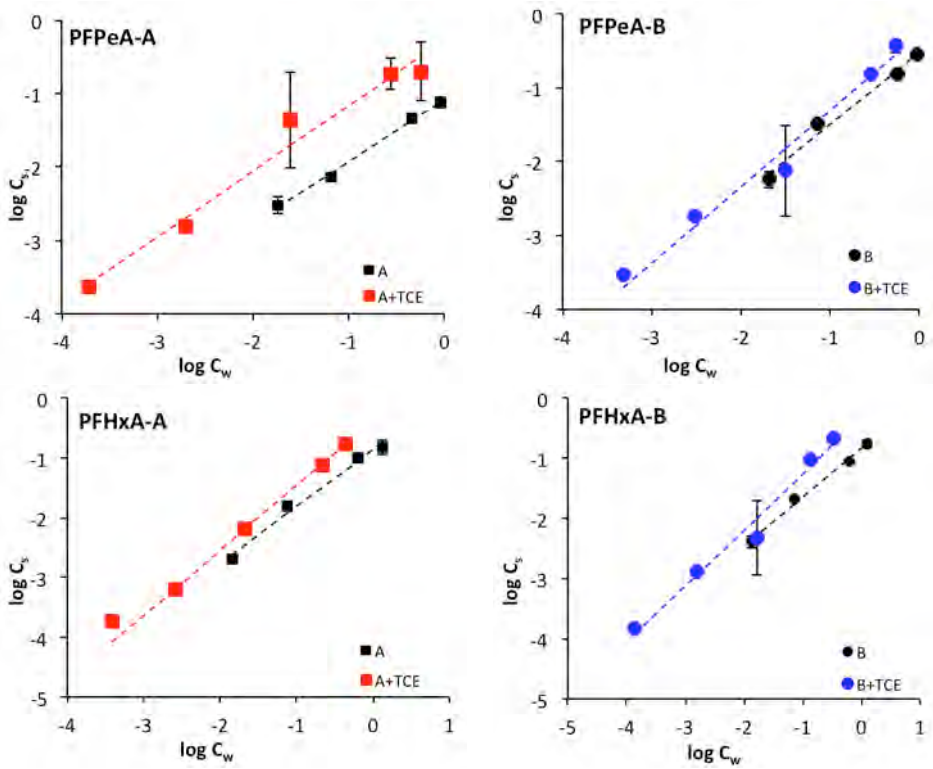

Figure 3-6. Sorption of PFBA, PFPeA, and PFHxA to A (squares) and B (circles) soils in the absence (black) and presence (red) of TCE. Dashed lines are fitted Freundlich isotherms. Error bars represent relative error in triplicate measurements of C_s.

NAPL may serve as an additional sorbent (Jonker *et al.,* 2003; Sun and Boyd, 1991). NAPL may also reduce sorption by blocking access to organic matter sorption sites (Jonker *et al.,* 2003; Sun and Boyd, 1991). A combination of these mechanisms may explain the varied effects of NAPL on PFAA sorption. PFAA sorption to soil A without NAPL was low (i.e. PFOS Log K_d=0.72) and in some cases fairly nonlinear (i.e. PFOS n=0.77±0.05; Table S9) suggesting different types of organic matter sorption sites are available, including high affinity sites in the lower end of the isotherm and lower affinity sites in the upper end. In the lower end of soil A isotherms, PFAA sorption in the presence of NAPL was unchanged or slightly decreased, suggesting PFAAs either had access to an adequate number of high affinity sites or, in some cases, were blocked from sorption sites by NAPL. In the upper end of the isotherms, small increases in sorption were observed when TCE was present and isotherm linearity generally increased (i.e. PFOS n=1.01±0.01; **Appendix A-2**). Consistent with the lower f_{oc} of soil A, these data suggest NAPL acted as a sorbent and increased the number of sorption sites at high concentrations of PFAAs.

Sorption of PFAAs to soil B without NAPL was stronger (i.e. PFOS Log K_d=1.54) than to soil A, consistent with its higher f_{oc}. Addition of TCE to soil B caused no change or decreases in PFAA sorption, with only minor changes in linearity (i.e. PFOS+TCE n=0.85±0.03 vs. 0.90±0.05 without TCE). Where PFAA sorption was unchanged by NAPL, an adequate number of higher affinity sorption sites were likely still present. Decreases in sorption were chain-length dependent, with the magnitude of sorptive decreases increasing from C7 to C9 PFCAs, and were likely the result of TCE blocking access to organic matter sorption sites in soil B. This suggests that blocking of sorption sites by NAPL has more of an impact on stronger sorbing PFAAs. These results are consistent with the higher f_{oc} of soil B. Because higher affinity sorption sites were more abundant in this soil and isotherms fairly linear, NAPL provided no additional sorptive capacity and may have in fact reduced the sorptive capacity, likely through blocking of organic matter sites.

As with sorption in the absence of NAPL, changes in sorption of short-chain PFAAs in the presence of TCE NAPLs were unexpected. Sorption of PFBA, PFPeA, and PFHxA generally increased over the entire concentration range in soils A and B **(Figures 3-5 and 3-6**). Previous work found affinity of smaller PAHs for weathered oils was higher than for larger PAHs, and similar results were found for PCBs (Jonker and Barendregt, 2006; Jonker *et al.,* 2003). The authors hypothesized a steric effect wherein smaller molecules were better able to fit into the complicated weathered oil matrix (Jonker and Barendregt, 2006; Jonker *et al.,* 2003). Therefore, it is possible that trends observed for PFBA, PFPeA, and PFHxA to TCE are a steric effect.

Some have proposed that sorption when unweathered NAPL is present can be described as the linear sum of sorption to the soil and sorption to NAPL as follows (Jonker *et al.,* 2003):

$$K_d = f_{oc}K_{oc} + f_{NAPL}K_{NAPL} \qquad \text{(eqn. 3-5)}$$

where f_{NAPL} is the fraction of NAPL in the soil and K_{NAPL} (L/kg) is the NAPL-water partition coefficient. Moreover, sorptive losses to different kinds of unweathered NAPLs should be similar, suggesting K_{NAPL} values will be consistent among varying NAPL types (Jonker *et al.,* 2003; Ortiz, Kraatz, and Luthy, 1999). This study measured single-point K_{NAPL} values in NAPL-water batch systems for both DD and TCE (**Table 3-8**). Overall, sorption of PFAAs to NAPL appears to have a chain-length dependent trend; however the trend is somewhat unclear for C5-C8 PFAAs (**Figure 3-7**). Additionally, K_{NAPL} values for TCE and DD were not statistically different, suggesting NAPL type may not be a determining factor in PFAA NAPL sorption. K_{NAPL} values for TCE and DD were used with K_{oc} values to calculate predicted K_d values for PFCAs in soil A at aqueous PFAA concentrations of 0.35 mg/L, where sorptive increases were observed in the presence of TCE NAPLs (**Figure 3-8**). In general, equation 2 under predicted sorption in the presence of NAPL. Many values were within a factor of two of those measured; however K_{NAPL} values under predicted sorption of long-chain PFAAs by an order of magnitude or more. These results suggest that even though NAPL is present as a separate phase in these systems, pure NAPL-water partitioning cannot be used to predict sorptive increases of PFAAs in soil A.

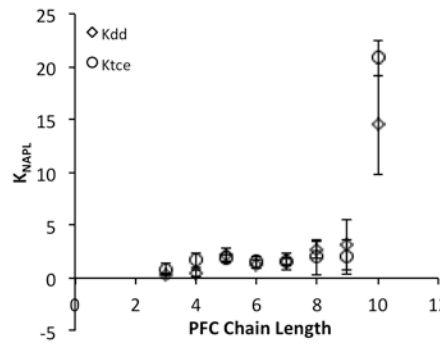

Figure 3-7. Measured values for K_{NAPL} with PFAS chain length for PFCAs. Diamonds are values measured for DD (K_{DD}) and circles are values measured for TCE (K_{TCE}).

Table 3-8. K_{NAPL} values measured for DD and TCE.

Analyte Name	K_{DD} (L/kg)	±	K_{TCE} (L/kg)	±
PFBA	0.23	0.24	0.86	0.60
PFPeA	0.50	0.34	1.72	0.72
PFHxA	2.20	0.60	1.85	0.37
PFHpA	1.32	0.35	1.50	0.59
PFOA	1.53	0.32	1.58	0.84
PFNA	2.66	0.81	1.98	1.73
PFDA	3.16	2.39	2.00	1.62
PFUnA	14.52	4.71	20.85	1.70
PFBS	NM	NM	0.19	0.17
PFHxS	NM	NM	0.22	0.22
PFOS	0.24	0.16	0.67	0.64

NM = no aqueous loss was measured

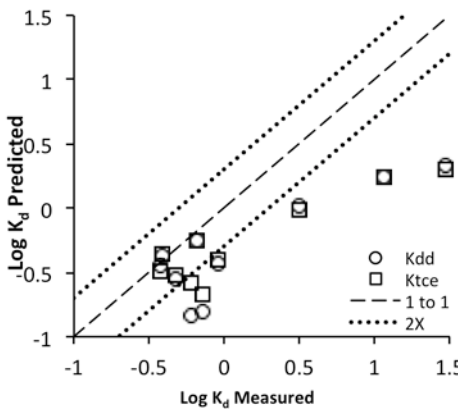

Figure 3-8. Modeled vs. measured Log K_d values in the presence of TCE. Circles represent values modeled with K_{DD} and squares represent values modeled with K_{TCE}.

Previous work reported Log K_{NAPL} values of 4.16 L/kg for PFOS in crude oil using equation 2 at a PFOS concentration of 5µg/L (Chen *et al.,* 2009). Though this would account for any soil-NAPL-water interactions, it is much higher than the Log K_{NAPL} of -0.18 L/kg for TCE measured herein. If **Equation 3-5** is solved for K_{NAPL}, the resulting values are higher than those measured in water-NAPL systems. For example, at aqueous PFAA concentrations of 0.35 mg/L, the calculated PFOS Log K_{TCE} value is 2.0 L/kg. Though this is still lower than values reported for crude oil, this value is more consistent with what was observed previously. NAPL or soil type may help explain additional differences between the two studies. While this study found similarities in PFAA sorption to DD and TCE, it should be noted that crude oil and NAPLs present in the environment are often complex mixtures that change composition with weathering, and some organic contaminants have a higher affinity for weathered vs. unweathered NAPL (Jonker and Barendregt, 2006; Jonker *et al.,* 2003). Overall, PFAA transport in the subsurface with NAPL may not depend primarily on NAPL type, but may be impacted by other factors such as soil f_{oc}.

3.3.3 Impact of SDS

PFAA isotherms were measured in soils A, B, and C in the presence of 100 mg/L SDS, results were fit with the Freundlich isotherm, and K_d values interpolated at PFAA concentrations of 0.35 mg/L (**Appendix A-2**). In the presence of SDS, PFAA sorption was essentially unchanged in soil C (**Figure 3-9, Figure 3-10**), and the impacts of SDS on PFAA sorption were chain length-dependent in soils A and B (**Figure 3-9, Figure 3-10**). In soils A and B, SDS caused increases in PFAA sorption in short-chain PFAAs such as PFPeA. These increases diminished in magnitude with increasing chain-length such that there was no change in sorption for some compounds such as PFOA, and decreases in sorption were observed with SDS for the largest PFAAs such as PFDA (**Figure 3-9**).

SDS may influence PFAA sorption in multiple ways. Even at concentrations below the CMC, surfactants and organic compounds may have a partition-like interaction between nonionic portions of the surfactant and organic compounds (Tao *et al.*, 2006; Kile and Chiou, 1989). These interactions may take place between the organic compound and surfactant in solution, leading to an increase in apparent solubility and a decrease in sorption. This has been observed with DDT and trichlorobenzene in the presence of multiple nonionic surfactants and with PFOS in the presence of the anionic surfactant sodium dodecylbenzene sulfonate (Pan *et al.,* 2009; Kile and Chiou, 1989). At concentrations of about 0.001-0.01 of the CMC, surfactants may also form hemimicelles near a solid surface, (Schwarzenbach *et al.*, 2003). which, when coupled to sorbate interactions with surfactants (including mixed hemimicelle formation), may lead to increases in

apparent sorption of the sorbate (Tao *et al.*, 2006). Surfactants may also decrease sorption if they compete for sorption sites.

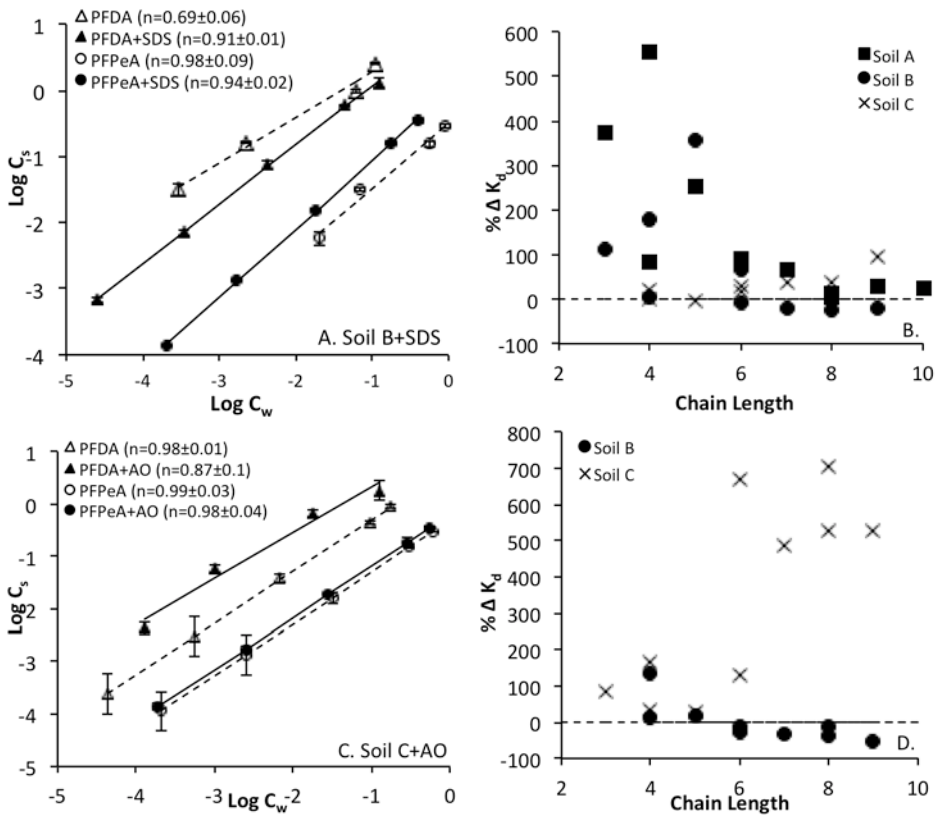

Figure 3-9. A.) Sorption of PFPeA (circles), PFOA (squares), and PFDA (triangles) in the presence (closed symbols) and absence (open symbols) of SDS to soil B. B.) The percent change in K_d values between systems with no SDS and 100 mg/L SDS vs. PFAS chain length in soils A, B, and C. C.) Sorption of PFPeA (circles) and PFDA (triangles) in the presence (closed symbols) and absence (open symbols) of AO to soil C. D.) The percent change in K_d values between systems with AO and 100 mg/L AO vs. PFAS chain length in soils B and C. In all isotherms, solid lines are fitted Freundlich isotherms for closed symbols and dashed lines are fitted Freundlich isotherms for open symbols, and error bars represent relative error in triplicate measurements of C_s.

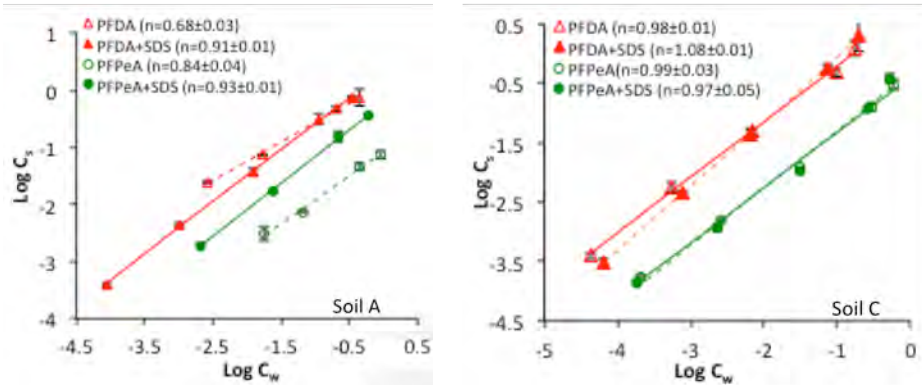

Figure 3-10. Sorption of PFPeA (circles) and PFDA (triangles) in the presence (closed symbols) and absence (open symbols) of SDS to soils A and C. Solid lines are fitted Freundlich isotherms for open symbols and dashed lines are fitted Freundlich isotherms for closed symbols. Error bars represent relative error in triplicate measurements of C_s.

SDS led to increases in sorption of PFBA, PFPeA, PFHxA, PFHpA, and PFBS in the A and B soils as well as PFOA in the B soil. Because SDS was present at concentrations where hemimicelle formation is possible, increases in sorption may be due to mixed hemimicelle formation with SDS. SDS had no effect on, and in some cases decreased, sorption of long-chain PFAAs in A and B soils. Specifically, sorption decreased for PFNA, PFDA, and PFOS. Sorption of PFHxS in soil A and PFOA and PFHxS in soil B was unchanged. This study did not directly measure SDS impacts on PFAA solubility; however, preliminary control experiments with PFAAs and varying concentrations of SDS (no soil) implied little impact of SDS on aqueous PFAA concentrations.

Hemimicelle formation with SDS may play a role in sorptive increase of short-chain PFAAs, but it is possible that formation of mixed hemimicelles with SDS is not favorable for larger PFAAs due to increased oleophobicity of the larger fluorocarbon tail. Finally, semi-quantitative SDS sorption isotherms indicate a log K_{oc} for SDS of approximately 5 vs. 2.8 for PFOS (**Figure 3-11**), so it is possible SDS outcompetes stronger-sorbing, long-chain PFAAs. Where sorption was unchanged, it is likely that multiple competing processes result in no net change to overall PFAA affinity for the soil. Such was likely for soil C, for which no changes in PFAA sorption were observed with SDS. Soils A and C have similar f_{oc}, so similar changes to sorption with SDS might be expected; however, soil C is positively charged, which may lead to increased importance of electrostatic effects. For example, the anionic sulfonate group of SDS may

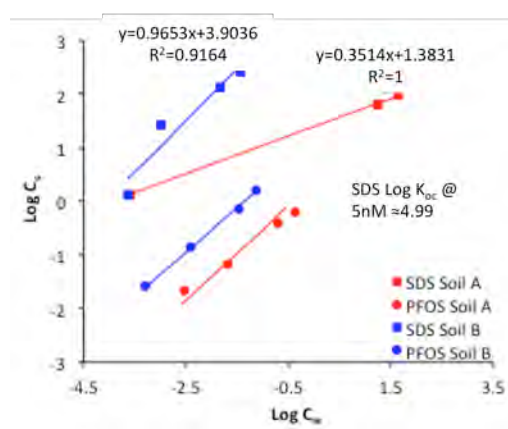

Figure 3-11. SDS sorption isotherms for SDS (squares) and PFOS (circles) in soils A (red) and B (blue). Lines are are fitted Freundlich isotherms. Isotherm parameters and r^2 values for SDS are shown and are available for PFOS in **Appendix A-2**. Average Log K_{oc} for SDS at 5 nM is approximately 4.99 L/kg_{oc}.

interact electrostatically with the soil C surface, such that sorption is a combination of interactions with organic matter and the positive C surface. This combination of mechanisms may dilute SDS distribution in the soil matrix and reduce potential for hemimicelle formation. These results indicate nonfluorinated, anionic AFFF components may have a chain-length dependent impact on PFAA transport and, importantly, may slow transport of relatively more mobile PFAAs in negatively charged soils. The degree of impact will vary with soil f_{oc}.

3.3.4 Impact of AO

PFAA sorption was also measured in soils A, B, and C in the presence of 100 mg/L AO, results were fit with the Freundlich isotherm, and K_d values interpolated (Appendix A-2). Addition of AO led to sorption increases for PFPeA and PFHxA in soils A and B. Addition of AO did not lead to significant changes to sorption of the remaining PFAAs in soil B, excepting PFBA where effects were concentration dependent and PFDA, where a decrease in sorption was observed (**Figures 3-9 and 3-12**). In soil A, concentration-dependent changes to sorption of all remaining PFAAs were observed when AO was added (**Figure 3-12**). In soil C, chain-length dependent effects were observed (**Figure 3-9**). PFBA and PFPeA sorption was unchanged, but increases in sorption were observed for the longer-chain PFAAs.

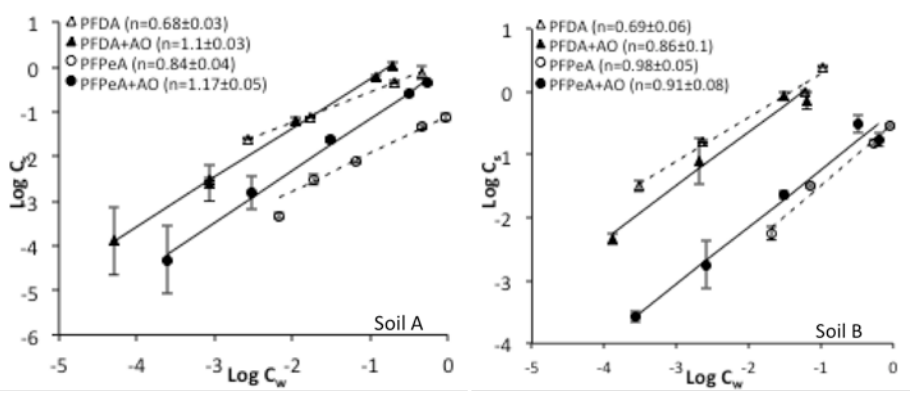

Figure 3-12. Sorption of PFPeA (circles) and PFDA (triangles) in the presence (closed symbols) and absence (open symbols) of AO to soils A and B. Solid lines are fitted Freundlich isotherms for closed symbols and dashed lines are fitted Freundlich isotherms for open symbols. Error bars represent relative error in triplicate measurements of C_s.

As with SDS, AO may influence PFAA sorption via changes to solubility, hemimicelle formation, or competitive sorption. Aqueous PFAA measurements in control (no soil) reactors with PFAA and varying amounts of AO were used to understand AO-PFAA interactions in solution. As the aqueous concentration of AO increased, aqueous PFAA concentrations decreased, with larger differences observed for longer chain length PFAAs (**Appendix A-4**). This implies a greater affinity of longer-chain PFAAs for interfaces when AO is present. If this mechanism was the dominant process impacting PFAA sorption to AO-contaminated soils, sorption would likely increase with increasing PFAA chain length in the presence of AO. This was observed in soil C, suggesting amphoteric AO does not interact with a positive surface in a manner that elicits competitive sorption effects. As mentioned previously, matrix interference during analysis prevented the evaluation of AO K_{oc} values and thus its competitive potential. Competition, however, would not completely explain changes in PFAA sorption observed in

soils A and B with AO. Concentration-dependent effects in soil A suggest that, similar to NAPL, AO is outcompeting PFAAs for higher energy sorption sites at the lower end of the isotherm. However, at the upper end of the isotherm, sorbed AO may create an environment favorable for PFAA sorption, possibly through formation of mixed hemimicelles. This would explain increases in linearity of PFAA isotherms (**Appendix A-2**) and increases in sorption of PFAAs in the upper end of the isotherm where lower affinity sites are the only remaining sites in soil A. This effect is likely not apparent in soil B due to the higher f_{oc} and greater number of high affinity sites available for sorption. Collectively, these data suggest that amphoteric AFFF surfactants could have a varied effect on groundwater transport of PFAAs depending on PFAA chain length as well as surface charge and soil f_{oc}.

3.4 Implications

Impacts of co-contaminants on groundwater transport potential of PFAAs at AFFF-impacted sites are quite complex and not easily generalized. They may depend on factors such as f_{oc}, PFAA chain length, PFAA concentration, and solid phase surface charge. To illustrate this potential variability, concentration-specific K_d values were used to calculate retardation factors (R_f) for soil A at two PFAA concentrations (1 and 500 µg/L, **Table 3-9**) as follows:

$$R = 1 + \frac{\rho_b}{\theta} K_d \qquad \text{(eqn. 3-6)}$$

where ρ_b is the soil bulk density (1.14 g/cm^3) and θ is the porosity (0.53).

Table 3-9. Soil A R_f for select PFAAs in the presence and absence of co-contaminants.

	R 1 µg/L	R+TCE 1 µg/L	R+SDS 1 µg/L	R+AO 1 µg/L	R 500 µg/L	R+TCE 500 µg/L	R+SDS 500 µg/L	R+AO 500 µg/L
PFBA	2.67	4.06	2.75	3.17	1.33	2.91	2.69	3.83
PFPeA	1.67	4.06	3.58	1.89	1.25	2.57	2.69	3.52
PFHxA	1.52	1.64	3.26	1.52	1.39	2.04	2.35	2.77
PFHpA	2.26	1.75	2.68	1.58	1.77	2.08	2.50	2.63
PFOA	3.18	4.27	3.36	1.73	2.06	2.70	2.80	4.40
PFNA	7.54	6.40	4.40	3.40	2.99	3.73	3.33	6.39
PFDA	32.82	18.80	11.58	10.14	5.42	9.45	7.14	18.13
PFBS	3.34	2.78	3.46	2.53	1.72	2.43	2.37	3.70
PFHxS	4.25	2.93	3.76	2.75	1.95	2.71	2.83	4.21
PFOS	18.47	9.54	9.08	12.15	5.27	9.95	5.63	10.58

Concentrations of 1 and 500 µg/L refer to the aqueous concentration of PFAA modeled. R is the retardation factor. R+ is the retardation factor in the presence of the respective co-contaminant.

Rf provides an indication of contaminant transport relative to groundwater with a value of one indicating conservative transport. In the absence of co-contaminants, PFAA transport is expected to be chain-length dependent, with the exception of PFBA and PFPeA. The Rf values for the smallest PFAAs (e.g. PFBA, PFPeA) generally increase in the presence of TCE, SDS, or AO,

indicating that these co-contaminants may reduce smaller PFAA groundwater transport. For other PFAAs, the effect of co-contaminants on R varies based on the PFAA concentration. Rf values for PFOS at 1 μg/L decrease when TCE is present, though the opposite is seen at PFOS concentrations of 500 μg/L, where Rf values increase when TCE is present. Similar trends are observed with SDS and AO. Various mechanisms may be responsible for sorptive changes, and until these mechanisms are better understood, it may be necessary to have a detailed understanding of site characteristics (e.g. soil characteristics, co-contaminants present) to predict PFAA transport. Further work is also needed to understand impacts to PFAA transport when multiple co-contaminants are present under nonequilibrium conditions. Given the complex nature of PFAA and co-contaminant interactions and the recent push towards regulation, these results emphasize the need for additional research on subsurface transport of PFAAs.

4. BATCH CO-CONTAMINANT REMEDIATION EXPERIMENTS

4.1 Introduction (*Task 3*)

Due to their co-application during fire training exercises, PFAAs co-occur with traditional contaminants such as fuel hydrocarbons and chlorinated solvents. In many cases, these co-contaminants may have been (or are currently) the targets of remediation strategies. The impacts of co-contaminant remediation strategies on PFAA fate and transport in the subsurface is expected to be related to alterations of the aquifer solids and NAPL interfacial properties as well as the changes to the solution and solid-phase chemistry. As part of this project, bench-scale experiments were conducted to examine the impact of different *in situ* remediation approaches employed for contaminants of concern at DoD sites including MNA, ERD, and ISCO on the transport potential of PFAAs. The range of conditions explored mimic the range of conditions likely present within a source zone and groundwater plume during *in situ* remediation.

More specifically, this task is composed of three subtasks:

Task 3a: Natural Attenuation. While biodegradation of PFAAs is not anticipated under passive attenuation conditions (i.e., MNA), microbial respiration of hydrocarbons (jet fuels and/or diesel NAPLs) may impact PFAA retardation via biogeochemical and/or physicochemical alterations. Model hydrocarbon biodegradation was assessed under oxic and microaerophillic conditions. Thus, the interactions of PFAAs with hydrocarbon degrading communities was assessed.

Task 3b: Enhanced Reductive Dechlorination. ERD represents a viable *in situ* remediation technology for chlorinated solvents at AFFF-impacted sites. The biodegradation of TCE during ERD was assessed in the presence of PFAAs. Bioaugmentation using a *Dehalococcoides* consortium was used to simulate ERD in laboratory batch studies.

Task 3c: In Situ Chemical Oxidation. The effects of ISCO on PFAA behavior was investigated in batch reactors containing aqueous PFAAs, NAPLs, and oxidants. Batch tests were conducted at various timepoints to examine the kinetic effects of oxidants on PFAA sorption behavior.

4.2 Enhanced Biofilm Production by a Toluene-Degrading *Rhodococcus* Observed After Exposure to Perfluoroalkyl Acids (*Task 3a*)

4.2.1 Background

PFASs are emerging contaminants that are widespread in many facets of the environment: surface water, soil, air, and groundwater (Hansen *et al.*, 2002). Advances in detection and quantification have led to growing concerns of exposure. Within the broader class of PFASs, a subset of PFAAs are environmentally persistent, toxic, and can bioaccumulate (Van de Vijver *et al.* 2003; Moody *et al.*, 2002; Higgins *et al.*, 2007). These molecules have been detected in human kidneys, livers, and blood serum (Van de Vijver *et al.*, 2003; Key *et al.*, 1997; USEPA,

2012; Kuklenyik *et al.*, 2004). To mitigate exposure, the U.S. Environmental Protection Agency has set provisional drinking water health advisories for two common PFAAs: 0.4 µg/L for perfluorooctanoate (PFOA) and 0.2 µg/L for perfluorooctane sulfonate (PFOS; USEPA 2009).

PFAAs are fully fluorinated carbon chains of varying lengths and two primary classes: carboxylates and sulfonates (Prevedouros *et al.*, 2006). These chemicals possess distinctive properties: they have hydrophobic and oleophobic tails, and tend to form micelles (Higgins *et al.*, 2007). Due to these unique aspects, PFAAs are used in many industrial applications, such as non-stick coatings, fire retardants, and pesticides (Keyt *et al.*, 1997; USEPA 2012). Some PFAAs, as well as their precursors, are critical components of AFFF used for fire suppression Prevedouros *et al.*, 2006; Moody and Field, 2000; moody and Field, 1999; Moody *et al.*, 2003). Extensive use of AFFF for military firefighter training has led to the significant introduction of PFAAs into groundwater in sites that are often contaminated with other chemicals, such as chlorinated solvents or hydrocarbons (Moody and Field, 1999; Moody and Field, 2000)

The biodegradation of recalcitrant hydrocarbons commonly found at AFFF-impacted sites (i.e., BTEX: benzene, toluene, ethylbenzene, and xylene), has been extensively documented and provides a long-term mechanism for attenuation (Deeb *et al.*, 2002; Patterson *et al.*, 1993) Bacterial strains of *Rhodococcus*, a genus of common soil microbes, have been particularly noted for their resistance to toxicity and ability to degrade a range of organic compounds with bioremediation and industrial applications. They are also noted for their utility for mechanistic exploration in laboratory investigations due to genetic annotation and a diversity of biodegradation pathways (Sharp *et al.*, 2007; Sivan *et al.*, 2006; LeBlanc *et al.*, 2008; Perry *et al.*, 2007; Vandergeize *et al.*, 2004; McLeod *et al.*, 2006; Sharp *et al.*, 2010; Homme and Sharp, 2013). To date, it remains unclear to what extent PFAAs may impact microorganisms relevant to hydrocarbon bioremediation. While biodegradation of PFAAs is not expected, in part due to increased rigidity of the fluorinated chain that may enable resistance to enzymatic interactions (Key *et al.*, 1997). Concerns regarding potential adverse effects from PFAA exposure on microbial populations and subsequent co-contaminant degradability have been expressed and could complicate remediation efforts in contaminated subsurface systems (Moody and Field, 1999).

The objective of this study (*Task 3a*) was to examine the interactions between a suite of 11 PFAAs and microbes as they relate to contaminant metabolism and cellular growth in aqueous batch systems. First, we evaluated the effects of PFAA concentrations on toluene degradation and induction time by a well-characterized soil bacterium, *Rhodococcus jostii* strain RHA1 (Goncalves *et al.*, 2006). Next, we followed the growth of this microorganism during PFAA exposure and analyzed the subsequent flocculation and production of extracellular polymeric substances (EPS), a component of biofilms, which was also observed during growth of soil-derived communities. Finally, reverse transcriptase quantitative polymerase chain reactions (RT-qPCR) were utilized to quantify the upregulation of stress-associated genes for cells grown in the presence of PFAAs. Collectively, this study assessed possible changes in subsurface bioremediation potential of co-contaminants, as well as impacts on microbial behavior including biofilm production and stress responses that may be elicited by exposure to PFAAs.

4.2.2 Materials and Methods

4.2.2.1 PFAA Preparation and Aqueous Analysis

Purity-corrected stock solutions of an eleven-analyte mixture were made using salts from Sigma-Aldrich in a 70/30 v/v methanol/aqueous solution (Guelfo and Higgins, 2013). The components in this mixture were: PFBA, PFPeA, PFHxA, PFHpA, PFOA, PFNA, PFDA, PFUnA, perfluorobutane sulfonate (PFBS), perfluorohexane sulfonate (PFHxS), and PFOS). This mixture was used in the following experiments unless otherwise noted. The appropriate volume of the PFAA mixture in 70/30 v/v methanol/aqueous solution was added to experimental vessels to achieve target aqueous concentrations and left overnight or until the methanol from the spiking solution had evaporated to minimize residual methanol that could be utilized as a carbon source for microbial respiration. Initial control experiments indicated insignificant losses of PFAAs from this evaporation step (**Figure 4-1**).

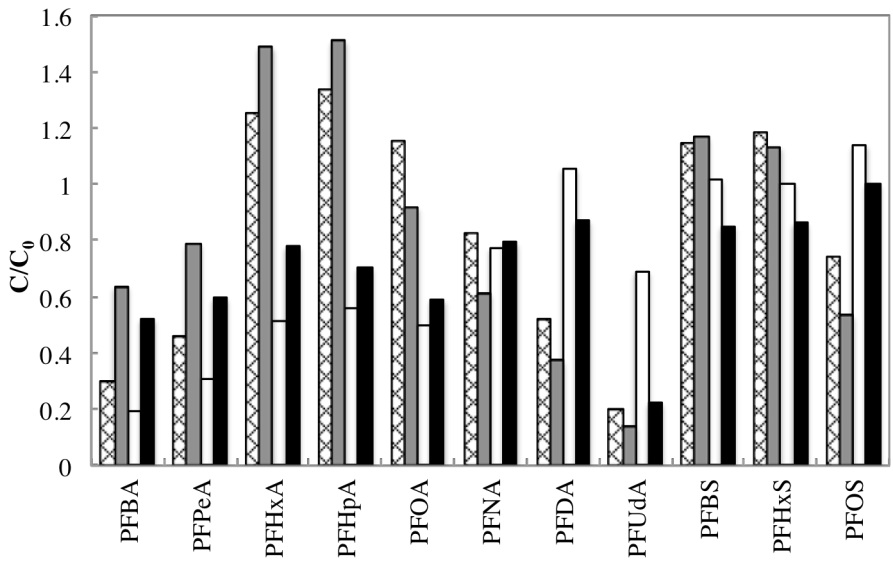

Figure 4-1. Final PFAA concentrations remain quantifiable, even after an evaporation step (cross hatches, white) for two different concentrations: 0.1 mg/L of each analyte (cross hatches, gray) and 1 mg/L (white, black) in glass bottles sealed with butyl rubber stoppers.

To verify PFAA concentrations in aqueous suspensions, samples were centrifuged to remove particulates, sampled, and diluted as appropriate according to published methods (Guelfo and Higgins, 2013), followed by measurement via LC-MS/MS utilizing stable-isotope surrogate standards purchased from Wellington Laboratories. An Applied Biosystems 3200 mass spectrometer (MDS Sciex) was utilized with Analyst for quantitation. Control experiments were performed to ensure that PFAA losses due to experimental setup (i.e. vessel type, stopper type, sampling procedure) were quantifiable and repeatable (i.e., **Figure 4-1**). This control experiment was performed under the same conditions as the toluene degradation experiments (discussed below) but without cellular material and toluene. Recovery after evaporation actually increased for shorter chain acids, and slightly decreased for most sulfonates. Because the final PFAA concentrations remain quantifiable, we are able to utilize the evaporation step in future experiments (**Figure 4-1**). Additionally, though some losses to the air-water interface were observed when using glass bottles, the final aqueous concentration is still quantifiable, even at concentrations lower than those utilized for the 10 mg/L experiments.

4.2.2.2 Cellular Preparation, Harvest, and Protein Measurements

Bacterial cultures of *Rhodococcus jostii* RHA1 were archived at -80°C and maintained axenically using Luria-Bertani (LB) agar plates (Sharp *et al.*, 2007). Liquid LB (Difco) cultures were grown in either 500 mL or 1 L glass flasks using a volume to liquid ratio of 5:1. Subsequent generations were propagated with 1 or 10% liquid inoculum. For cells grown on toluene (Pharmco-Aaper, HPLC UV-grade, 99.7%), 500 mL capped pyrex bottles with 100 mL of minimal salts media were inoculated directly from the plate (Sharp *et al.*, 2007). Toluene (20 µL) was supplied to a glass test tube resting in the pyrex bottle and allowed to mix via headspace. For induction and degradation experiments, cells were harvested and washed using 0.1 M potassium-phosphate buffer (pH ~7.0; Finette *et al.*, 1984). Harvested cells were then added to experimental vessels at target specific protein concentrations after PFAA addition, methanol evaporation, and media equilibration. All growth and assay experiments occurred at 30°C and 150 rpm unless otherwise described. To quantify cellular protein, aliquots of 0.5 or 1 mL were centrifuged at 15,000 x g for 3 minutes, decanted, and stored at -80°C until analysis. Protein extraction included NaOH digestion, physical disruption, and heated incubations at 100°C as described elsewhere (Sharp *et al.*, 2007). Cellular protein was quantified using the colorimetric Coomassie Plus Assay Reagent (Bradford) with bovine serum albumin (BSA) as the standard (Thermo Scientific).

4.2.2.3 Toluene Biodegradation

Batch systems containing toluene and a PFAA mixture (no PFAAs in the control) were designed to assess the degradation rates of this model substrate. Degradation experiments were performed in 60 mL amber glass bottles and sealed with non- poly tetrafluoro ethylene (PTFE) containing butyl rubber stoppers. Experiments were performed in triplicate in 0.1 M potassium-phosphate buffer (pH 7; 50 mL total) for toluene degradation. This buffer was chosen to reduce interference during LC-MS/MS analysis of PFAAs. PFAAs were added as described above to achieve a target final concentration of 10 mg/L for each analyte (110 mg/L total PFAAs), followed by the addition of potassium-phosphate buffer and neat toluene through the butyl rubber stopper with a 5 µL high precision glass syringe (Hamilton). Toluene partitioned into the aqueous phase via headspace, resulting in an initial aqueous concentration of 34.6 mg toluene per L (Sharp *et al.*, 2005). This mixture was allowed to equilibrate for at least 12 hours prior to the addition of toluene-grown, washed, and harvested cells of *Rhodococcus jostii* (an initial quantity of 22 mg/L protein approximated from optical density (OD) measurements and OD-protein correlations established from growth experiments discussed herein). Headspace samples of 50 µL were removed approximately every hour until at least 50% toluene degradation was observed. Gas phase toluene concentrations were measured using a Hewlett Packard 5890 Series II Plus gas chromatograph flame ionization detector (GC-FID) with a 0.25 µm Rxi-5ms fused silica column (Restek). A standard curve was developed with known aqueous toluene standards that were created, stored, and sampled in the same manner as the reaction vessels. Concentration in the headspace was extrapolated to the liquid phase using a dimensionless Henry's Law constant of 0.337 for a 30°C system (Robbins *et al.*, 1993).

To evaluate the potential lag in degradation for cells newly introduced to toluene as the only carbon source, a similar procedure was used as described above. Cells were added from a washed culture grown in LB broth with an initial protein content of 55 mg/L approximated as discussed above. Headspace was immediately sampled after inoculation, and was sampled approximately every 4 hours until at least 50% toluene degradation was observed. Induction times were calculated by evaluating the slope by linear regression of the degradation period (between hours 4 and 8) and calculating the intersection of this slope with the average toluene concentration of early linear data points (hours 0 to 4) to avoid bias based on sampling times. The calculated intersection represents the time to induction, or the approximate time at which significant toluene degradation began.

4.2.2.4 Growth and EPS Production

Growth experiments were performed in one liter sealed polypropylene bottles in triplicate containing PFAAs, LB media, and a liquid inoculum of *R. jostii* RHA1 (~0.2 mg/L initial protein concentration) with a 1:10 liquid to headspace ratio. To evaluate the effects of varied PFAA concentrations, this experiment was also performed at 0.1, 0.2, 0.5, 1, 2, 5, and 10 mg/L of each PFAA analyte wherein 50 µL of inoculum was transferred to 4.95 mL LB media in 50 mL polypropylene tubes sealed with parafilm and placed at an angle of 10°. A single sample was taken after three days of growth for this entire range of concentrations and analyzed for optical density.

Optical density was measured using a Jenway 6505 UV/Vis Spectrophotometer. EPS production was quantified by using a modified anthrone reagent (Fisher Scientific) total sugar and polysaccharide assay with glucose (Sigma Aldrich) as a standard (Morris 1948; Meuser *et al.*, 2011). Prior to polysaccharide analysis, samples were centrifuged at 15,000 x g for 3 minutes. The supernatant was decanted and stored at 4°C. EPS was harvested by adapting two methods that account for loosely and tightly bound EPS. Both resulted in agreement of trends, however, the method using NaCl (Aguilera *et al.*, 2008) produced greater EPS yields and is presented herein (results from a comparison of the method using EDTA (Zhang *et al.*, 1999) are found in **Figure 4-2**). This extraction includes a room temperature incubation to release loosely bound EPS, followed by a heated incubation with 20 g/L NaCl to release tightly bound EPS (Aguilera *et al.*, 2008). The following modifications were implemented: initially, a cellular aliquot was weighed and transferred to a 15 mL polypropylene conical tube with 5 mL of MilliQ^{TM} water per 1.5 g cells, and only NaCl was used for the chemical extraction.

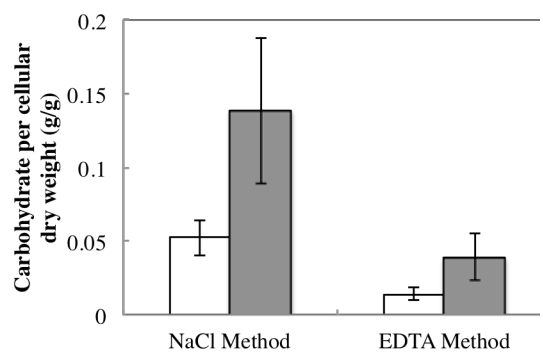

Figure 4-2. EPS extraction using the EDTA method was used as described elsewhere (Zhang et al. 1999) with the use of 10 mL of 10mM EDTA per sample. EPA as measured by a carbohydrate assay with glucose as a standard is more abundant in the presence of PFAAs (gray) than without PFAAs (white) for two types of extraction methods.

Light microscopy images were generated with 20 µL of liquid sample on glass slides performed with an Olympus CX41 light microscope. To prepare the cells for scanning electron microscopy (SEM) with a Hitachi TM3000 SEM, 1 mL aliquots were sampled after 4 days of growth when the differences in degree of flocculation were largely apparent. These aliquots were stored at 4°C until dehydration and fixing; a visualization protocol was adapted (Neeves *et al.*, 2010).

4.2.2.5 Soil Enrichments

Cultures derived from circumneutral pH soil were harvested from below turf grass at a depth of 7.5 to 10 cm in Golden, Colorado. Following sample collection, 5 g soil was placed into 100 mL LB media at a volume to liquid ratio of 5:1. Every 12 hours, 0.5 mL of liquid inoculum was moved to fresh LB media with a 10:1 volume to liquid ratio and incubated as described above. After 4 generations, 50 µL of inoculum was transferred to 4.95 mL LB media in 50 mL polypropylene tubes containing 10 mg/L of each PFAA (110 mg/L total) or no PFAAs prepared as described previously. Tubes were prepared in triplicate, sealed with parafilm, and placed at an angle of 10° within the incubation conditions. Flocs from each replicate were measured and counted using an Olympus CX41 light microscope with a Bright-Line Hemacytometer counting chamber and Infinity Analyze software.

4.2.2.6 Quantification of Gene Expression

To evaluate genetic upregulation, 50 µL of strain RHA1 grown in minimal media with 40 mM sodium pyruvate (Sigma Aldrich; Sharp *et al.*, 2007; Goncalves *et al.*, 2006) was transferred to 50 mL polypropylene tubes containing either 10 mg/L of each PFAA (110 mg/L total) or no PFAAs and 4.95 mL fresh media in triplicate. A parallel set grown with LB was also performed. Tubes were sealed with parafilm and placed at an angle of 10° in a 30°C incubator at 150 rpm. Samples were aerated on day 2, 3, and 5 by opening the tube and gently pipetting in order to ensure ample oxygen transfer into the medium. When flocculation was most apparent (day 6) samples were centrifuged, decanted, resuspended in 2 mL RNALater (Ambion), and stored at 4°C until RNA extraction. RNA from 1.5 mL well-mixed aliquots was extracted using the MoBio PowerBiofilm RNA Isolation Kit (VWR). The manufacturer protocol was followed with a final elution of 100 µL prior to DNAse treatment and removal using the Turbo DNA-free Kit (Ambion). DNAse treated RNA was concentrated to a final volume of 40 µL as described in the MoBio PowerBiofilm RNA Isolation Kit procedure. RNA was quantified using a Qubit 2.0 Fluorometer with a Qubit RNA HS Assay Kit. All purified RNA was stored at -80°C until use.

Two primer sets for stress-related genes were utilized: *sigF3* (LeBlanc *et al.*, 2008) and *prmA* (Sharp *et al.*, 2007) *GyrB* (Kita *et al.*, 2009; Taki *et al.*, 2006) was used as a reference gene with primers as described for *Rhodococcus opacus* and adjusted for RHA1 specificity using GenBank Primer-BLAST (Ye *et al.*, 2012). *SigF3* and *prmA* primers were designed using Geneious version 6.1 (Kearse *et al.*, 2012) tested for specificity using GenBank Primer-BLAST, and synthesized by Integrated DNA Technologies (**Table 4-1**). Amplification was performed in triplicate for each biological replicate in 96-well plates using a Roche LightCycler 480II. Wells were prepped with qScript One-Step SYBR Green qRT-PCR Kit (Quanta Biosciences). Each 25 µL reaction contained 2 µL of extracted RNA, 0.4 µM each of a forward and reverse primer, 8

µL nuclease free water, 12.5 µL SYBR Green Master Mix, and 0.5 µL qScript Reverse Transcriptase. Quantification protocols were adapted from Sharp *et al.* (2007) reverse transcription occurred for 10 minutes at 50°C, followed by initial denaturation for 5 minutes at 95°C. All temperature ramping occurred at 4.4°C/s unless otherwise specified. Amplification followed with 40 cycles of a 95°C hold for 10 seconds, 30 seconds at 55°C (2.2°C/s ramp rate), and quantification after 1 minute at 72°C. The absolute quantification/second derivative maximum method was used for quantification within the Roche LightCycler 480II version 1.5 software. To test for DNA contamination, each sample was also amplified in duplicate without the reverse transcriptase enzyme in addition to a triplicate negative control with nuclease free water.

Table 4-1. Primer specifications

Primer Name	Gene ID	Amplicon Length	Sequence	GC Content (%)	T_m (°C)
sigF3 119F	ro04728 (LeBlanc *et al.*, 2008)	323	5'TGG GTC ATG TTG CCG AAG AA3'	50	57.0
sigF3 441R			5'GAA CTG CAC CTC TCC CTC AC3'	60	57.6
prmA 394F	ro00441 (Sharp *et al.*, 2007)	210	5'ACG ATC CAG ATG AAC CTC AAG AA3'	43.5	55.8
prmA 603R			5'TAC GAA CAG GGT GTT GGT GAA C3'	50	57.2
gyrB 607F	ro008268 (Kita *et al.*, 2009)	121	5'GTC TAC AGC TTC GAG ACG3'	55.6	54.7
gyrB 727R			5'TGA CGA CCT CTT CCG TG3'	58.8	55.7

RNA extractions were performed on 1.5 mL aliquots of 5 mL sample resuspended in 2 mL RNAlater for samples grown in minimal media. All samples were tested for inhibition by running dilutions, no inhibition effects were observed. Primers were ordered from Integrated DNA Technologies prepared as Lab Ready with standard desalting. Primer details can be found in **Table 4-1.** PCR product was analyzed via gel electrophoresis to verify primer specificity in tandem with melt-curve genotyping. All positive samples amplified above the limits of detection. Melt curves were generated with a 5 minute hold at 95°C, followed by one minute at 65°C (2.2°C/s ramp rate), and finally quantification every 5°C during a 1.1°C /s ramp up to 98°C. The program ended with 10 seconds of cooling to 37°C at 2.2 °C /s. Melt curves are shown in **Figure 4-3** and depict uniform peaks at the appropriate temperature for the product length for both samples and standards. Earlier peaks correspond to negative controls. LightCycler® 480 version 1.5.0 (Roche) was used to program thermal cycling and to calculate errors and efficiencies with the Absolute Quantification/Second Derivative Maximum algorithm. Errors, efficiencies, standard curve slopes and y-intercepts are shown in **Table 4-2**. DNA was quantified using a NanoDrop Light Spectrophotometer (Thermo Scientific) using the dsDNA protocol. Yield was negligible and purity (A260/A280) was within the limits as recommended within the MoBio Biofilm RNA Extraction protocol for samples diluted with nuclease free water.

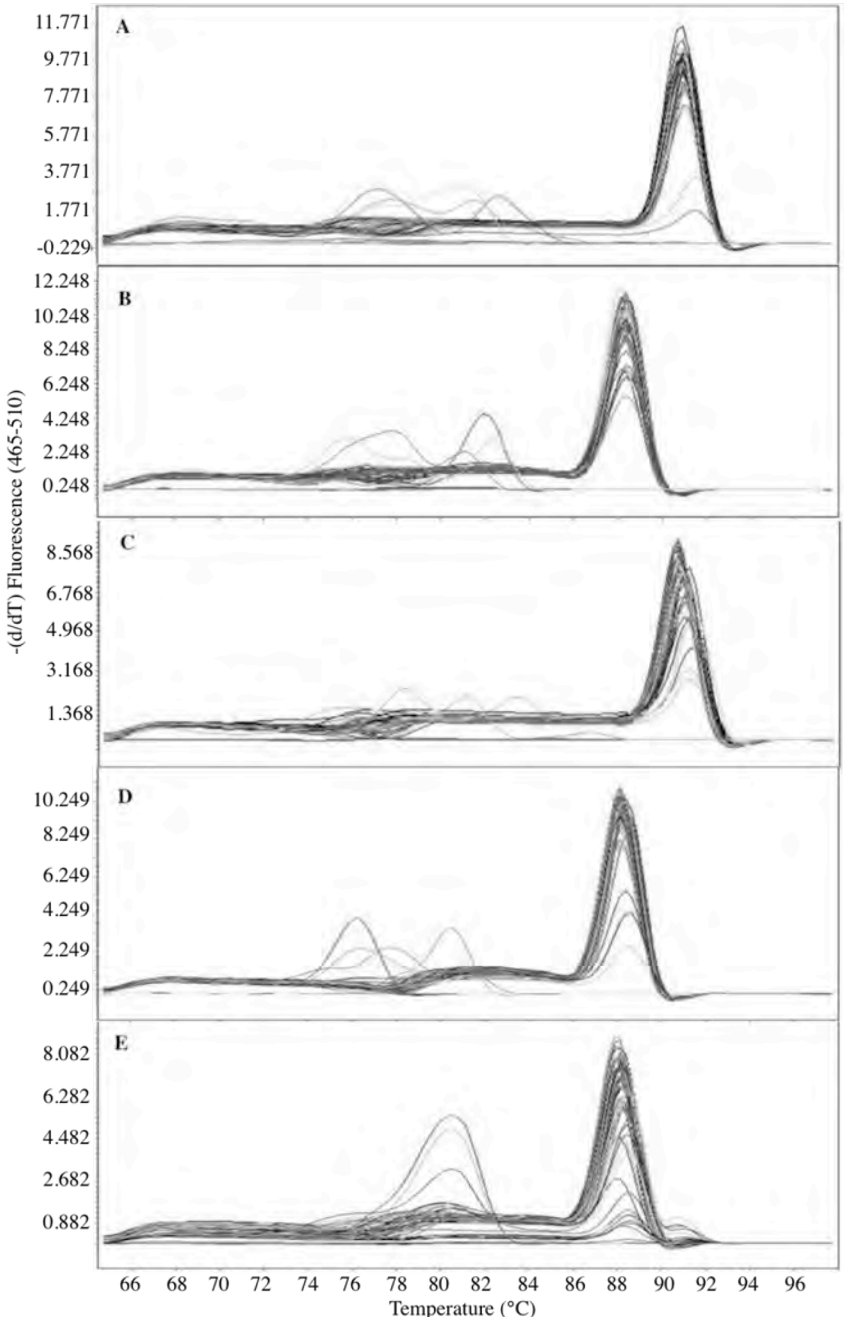

Figure 4-3. Melt curve analysis for (A) LB grown *sigF3* (B) LB grown *prmA*, (C) sodium pyruvate grown *sigF3*, (D) sodium pyruvate grown *prmA*, and (E) *gyrB* for both types of samples depict uniform melting and amplicon lengths. The early outlier peaks in all cases are negative controls.

Table 4-2. Errors, efficiencies, slopes, and intercepts for each gene and media

Growth Media	Gene	Error	Efficiency	Slope	Y-Intercept
Both	gyrB	0.014	2.018	-3.279	30.93
LB	sigF3	0.0104	2.062	-3.182	37.28
	prmA	0.0236	1.917	-3.538	35.95
Minimal	sigF3	0.0129	2.052	-3.204	29.66
	prmA	0.0149	1.948	-3.453	31.52

Standard curves for *prmA, gyrB*, and *sigF3* were developed by bead purifying the PCR product amplified from experimental template using Agencourt AMPure XE (Beckman Coulter). Purity was verified using gel electrophoresis to obtain a single band of the target length. Purified DNA was then quantified and diluted as appropriate for each standard curve, with the exception of the *sigF3* standard curve used for LB grown samples.. Standards and PCR products were stored at -20°C. Testing for DNA contamination was performed by performing controls on each sample in duplicate without the reverse transcription enzyme. For the LB grown samples, each RT control was below detection or amplified with high uncertainty as shown in **Table 4-3** with the exception of a single well for LB grown No-PFAA *sigF*, sample 7. Because no DNA contamination was observed in the corresponding replicate sample, we assumed the DNA contamination only occurred in that specific well and that the corresponding sample template was not compromised. For the samples grown on minimal media, all RT controls were below detection, measured with high uncertainty, or amplified after the negative controls, with the exception of No-PFAA *sigF* samples 7, 8, and 9. Because every replicate of this negative control amplified above the limit of detection, this entire sample has been removed from the analysis.

RNA from 1 mL well-mixed aliquots from the samples grown in LB was extracted using the Qiagen RNEasy RNA Extraction kit. Protocols involving enzymatic lysis, proteinase K digestion, mechanical disruption, and purification of total RNA from bacterial lysate were performed prior to DNAse treatment and removal using the Turbo DNA-free Kit (Ambion).

A set of standard curves for s*igF3* (used only for cells grown on LB) were developed from extracted genomic DNA from RHA1 using the PowerSoil DNA Isolation Kit (MoBio). The target gene was amplified from the genomic DNA using the amplification protocol described herein, followed by gel electrophoresis on the PCR product. The target band was extracted from the gel using E.Z.N.A. Gel Extraction Kit (Omega bio-tek), quantified using Qubit dsDNA HS Assay Kit, and diluted as necessary. Standards for *sigF3* derived through extraction and purification of the gel band were utilized for the LB grown cells instead of the bead-purified set due to the reproducibility at the lower bounds of detection, as can be seen in **Figure 4-3**. For measurement of *prmA,* samples were diluted as necessary to fall between a range of 1 – 2 ng/µL RNA.

Table 4-3. CP cycles for negative RT-qPCR controls

Sample	Replicate	*prmA* Cq or CP (cycles)	*sigF3* Cq or CP (cycles)	gyrB Cq or CP (cycles)
LB No PFAA-RT Control	1	ND	35[a]	35[a]
	2	ND	35[a]	ND
	4	ND	ND	ND
	5	ND	ND	ND
	7	ND	22.13	35[a]
	8	ND	23.70[a]	ND
LB 110 mg/L PFAA-RT Control	1	ND	ND	ND
	2	ND	ND	ND
	4	ND	ND	35[a]
	5	ND	33.18[a]	35[a]
	7	ND	ND	35[a]
	8	ND	ND	35[a]
LB Negative Control	1	35[a]	35[a]	N/A
	2	35[a]	32.89[b]	N/A
	3	35[a]	33.01[b]	N/A
Minimal Media No PFAA-RT Control	1	ND	35[a]	35[a]
	2	--	35[a]	35[a]
	4	35[a]	33.97	30.85[c]
	5	35[a]	35[a]	30.54[c]
	6	35[a]	33.49	33.33[c]
	8	35[a]	33.04	32.97[c]
Minimal Media 110 mg/L PFAA -RT Control	1	ND	35[a]	35[a]
	2	ND	35[a]	ND
	4	ND	33.32	33.15[c]
	5	ND	35[a]	33.44[b]
	6	ND	34.51	35[a]
	8	ND	35[a]	35[a]
Minimal Media Negative Control	1	35[a]	ND	30.67[b]
	2	35[a]	ND	30.32[b]
	3	35[a]	35[a]	--

ND = non dectected
[a] High uncertainty
[b] Nonspecific binding (multiple melt curve peaks)
[c] Amplification after negative control

To calculate statistical significance, samples were compared to a set of gene specific DNA standard curves and normalized to total RNA concentration as recommended elsewhere (Saleh-Lakha *et al.*, 2011; Bustin *et al.*, 2002). Student's t-tests for samples with unequal variance were performed on analytical triplicates to encompass both biological and technical sources of error as done elsewhere (Sharp *et al.*, 2007). Upregulation-fold change calculations were performed by utilizing a relative expression model that includes a correction for variations in real-time efficiencies (Sharp *et al.*, 2007; Pfaffl 2001). An additional evaluation for significance utilizing randomization tests within the Relative Expression Software Tool (REST; Pfaffl *et al.*, 2002) was also performed. The upregulation ratio, R, was calculated according to **Equation 4-1** (Pfaffl 2001):

$$R = \frac{E_{targ}^{Cq_{targ,control} - Cq_{targ,sample}}}{E_{ref}^{Cq_{ref,control} - Cq_{ref,sample}}} \qquad \text{(eqn. 4-1)}$$

where E is the efficiency of the target or reference gene, Cq is the average quantification cycle for the control replicates (in this case no PFAAs) or the sample replicates (110 mg/L PFAAs). A randomization approach using the Relative Expression Software Tool (REST; Pfaffl *et al.*, 2002) was used to calculate statistical significance. In this approach, Cq values are randomly and repeatedly reallocated between control and sample with a new R value calculated at each step.

After the specified number of iterations (2000 – 10,000), the probability that the control and sample groups are significantly different, or if the target gene is upregulated or downregulated, is provided.

The student's t-test for samples with unequal variance was also performed on this dataset. For this evaluation, copy numbers per sample were normalized to the mass of RNA present in the sample prior to amplification. The student's t-test was performed on 9 replicates (three biological replicates with three technical replicates) to encompass the variability inherent in both facets of the experiment, as executed in Sharp *et al.* (2007). Normalization to the reference gene and statistical analysis using REST was not performed on the *prmA* gene on samples grown in LB due to minimum sample volume requirements. Statistical significance on RNA normalized expression using student's t-test was performed.

4.2.3 Results and Discussion

4.2.3.1 Effect of PFAAs on Toluene Degradation

If the presence of PFAAs affects microbial processes, it may be manifested as changes in toluene degradation rates or variations in induction time needed for the synthesis of toluene-degrading enzymes. Toluene was selected as a representative recalcitrant hydrocarbon, as similar metabolic machinery is utilized for the aerobic biodegradation of all BTEX compounds by oxygenase-type enzymes (Deeb *et al.*, 2001). The genes responsible for toluene degradation are hypothesized to be part of the ethylbenzene dioxygenase pathway (Goncalves *et al.*, 2006; Kita *et al.*, 2009) and are found in two of the linear plasmids within the RHA1 genome (McLeod *et al.*, 2006). In our experiments, near-complete toluene degradation by strain RHA1 was observed regardless of the presence of PFAAs at collective concentrations as high as 110 mg/L. Cultures that were grown on toluene as the sole electron acceptor prior to harvest exhibited a rapid onset of aerobic toluene biodegradation with no visible lag in batch assays. Just 5.7±0.3% of the initial toluene remained after 6.5 hours for the systems with PFAAs versus 3.3±2.3% for the systems without PFAAs (**Figure 4-4**). The protein normalized rate of toluene degradation for the system with PFAAs was

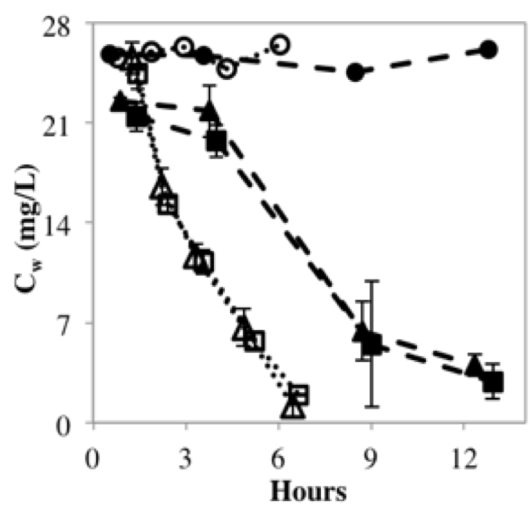

Figure 4-4. Toluene concentration over time for toluene grown systems (open symbols, initial protein ~22 mg/L) and induction time and concentrations for those grown on Luria-Bertani broth (closed symbols, initial protein ~55 mg/L) are not affected by the presence of PFAAs. Points represent the triplicate average toluene concentration in the liquid phase (C_w) calculated from headspace measurements using Henry's Law constant of 0.337 for systems with PFAAs (squares) and without (triangles), error bars represent the standard deviation. Abiotic controls are shown with circles.

0.183±0.009 mg toluene / mg protein per hour; without PFAAs the degradation rate was 0.200±0.007 mg toluene / mg protein per hour. These values are not significantly different ($p > 0.05$), strongly suggesting that the presence of high concentrations of PFAAs does not affect enzymatic affinity for toluene degradation nor does it exhibit any clear short-term toxicological effect on cells acclimated to the presence of toluene.

An analogous experiment was then conducted to understand whether the presence of PFAAs inhibits the synthesis of enzymes involved in aerobic toluene degradation. Strain RHA1 grown in LB media and then introduced to toluene as the sole carbon source after harvesting did not exhibit significant differences in rates or induction times with PFAA exposure (**Figure 4-4**). After about 13 hours, 7.9±3.8% of the toluene remained in the systems with PFAAs, and 11.5±2.3% of the toluene remained in systems without PFAAs. Induction times, which represent a transcription / translation response to the presence of toluene as a target substrate, were not significantly different: 3.65±0.33 hours for systems with PFAAs versus 3.65±0.17 hours for systems without PFAAs. After the induction time had passed, the rates of toluene degradation were similar in both systems regardless of PFAA presence: the rate for PFAA systems was 0.051±0.026 mg toluene / mg protein per hour while the rate for systems without PFAAs was 0.056±0.003 mg toluene / mg protein per hour. These rates are slower than those observed for the system grown on the target substrate for both cases with and without PFAAs, which can be expected if *R. jostii* is still in the process of acclimatizing to toluene as the sole carbon source. This suggests that the rate of degradation should increase over time, however that degree of resolution was not observed as a result of experimental confines.

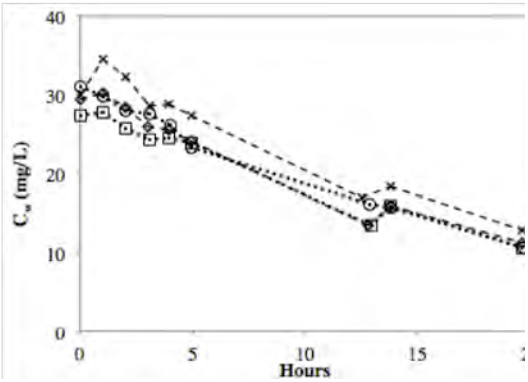

Figure 4-5. Toluene degradation is not affected by an 11-component PFAA mixture (open squares), by PFOS alone (open diamond), or by PFOA alone (x) as compared to a control without PFAAs (open circle). The average degradation rate is 1.02 ± 0.07 mg/L toluene per hour.

Three sets of toluene degradation control experiments were also performed including 0.1M potassium-phosphate buffer (pH ~ 7) and either PFOA, PFOS, or the entire 11 analyte mix at 10mg/L each. Another set included *Rhodococcus sp.*, toluene, and either PFAA, PFOS, or the entire 11 analyte mix at 10 mg/L each. The final set included only *Rhodococcus sp*. and either PFAA, PFOS, or the entire 11 analyte mix at 10 mg/L each. These experiments were set up as described for the toluene degradation experiment. Aqueous PFOS and PFOA independently yielded similar results to the PFOS and PFOA within the mix, implying competitive effects between PFAAs are not a concern for these systems (**Figure 4-5**).

As there were no significant alterations in degradation rate or induction time at 10 mg/L of each PFAA (110 mg/L total), effects at lower concentrations are unlikely. Field concentrations of PFAAs in groundwater have been measured up to 7 mg/L for a single analyte; a choice of 10 mg/L of each analyte may be representative of an environmental worst-case scenario (Moody

and Field, 2000). The similarities in toluene degradation rates and induction times further support the inference that strain RHA1 could continue to degrade toluene when exposed to high concentrations of individual components or mixtures of PFAAs.

4.2.3.2 Effect of PFAA Presence on Growth and Biofilm Formation

While a metabolic impact was not observed for cells grown and then subsequently exposed to PFAAs and toluene, significant differences in optical density trends and values were observed for *R. jostii* strain RHA1 during the exponential phase of growth in the presence of similarly high concentrations of PFAAs (**Figure 4-6A**). This anomaly was attributed to cellular flocculation associated with the presence of PFAAs, which was visibly observed in all replicates. Optical density is a common proxy for measuring microbial growth in liquid media but one that loses quantitative meaning when refractive particle sizes differ. For an alternative representation of biomass accumulation, the protein contents at various points throughout the growth curves were analyzed (**Figure 4-6B**). In contrast to optical density, quantified protein extracted from biomass grown in the absence and presence PFAAs were not significantly different, thus the actual quantity of cellular biomass was not affected by the presence of the PFAAs. When exploring the effects of varied PFAA concentrations, growth after three days exhibited a decrease in optical density relating to flocculation interference at total PFAA concentrations in excess of 22 mg/L (**Figure 4-7**).

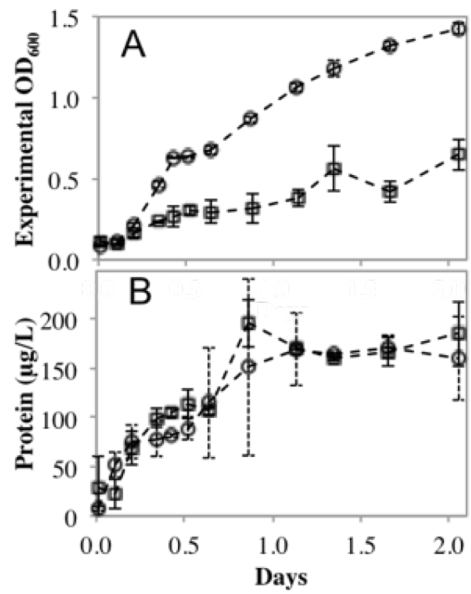

Figure 4-6. Visible cellular flocculation results in lower optical density readings for cells grown in the presence of PFAAs (panel A, open squares) than for those grown in the absence of PFAAs (panel A, open triangles). However, protein content trends remain similar between cells grown in the presence of PFAAs (panel B, open squares) and those grown in the absence of PFAAs (panel B, open triangles).

This flocculation was not observed when PFAAs were added to harvested cells during toluene degradation experiments described in the previous section. Additionally, the flocs that formed during exponential growth broke apart after approximately 7 days in a more stationary phase (**Figure 4-8**) without any change in PFAA concentration. These results suggest that flocculation was associated with a biological response rather than surfactant-derived chemical interactions with PFAAs. The presence of

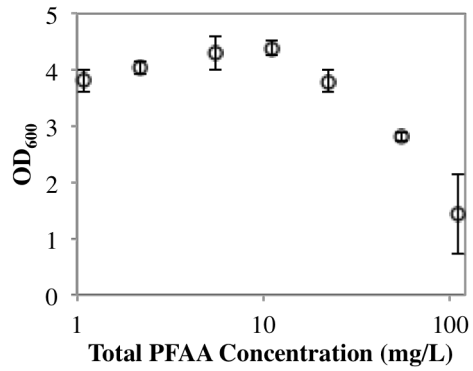

Figure 4-7. Flocculation response at different PFAA concentrations (1-110 mg/L total) as represented by optical density (OD). A drop in OD correlating with flocculation occurs above 22 mg/L total PFAAs.

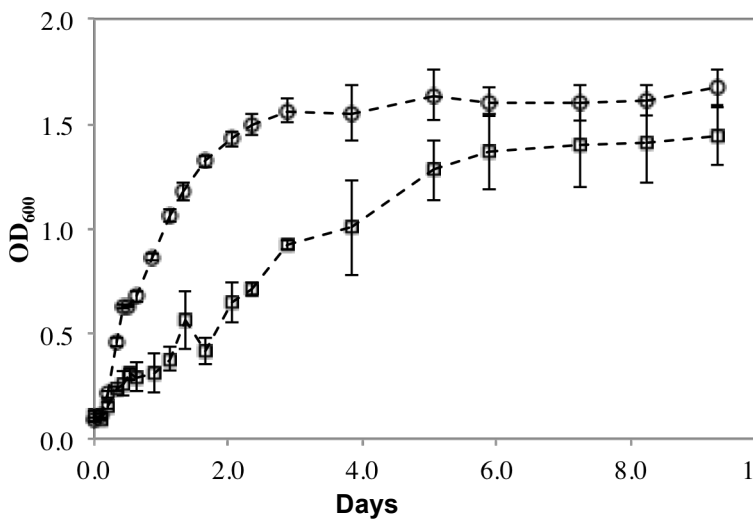

Figure 4-8. Long-term growth curves of RHA1 grown with PFAAs (squares) and without PFAAs (circles) show an eventual leveling off of growth. The late increase in growth in the presence of PFAAs to within a standard deviation of the case without PFAAs is caused by an eventual breakup of the cellular aggregates.

PFAAs, at least at these very high concentrations, impacts the manner of *R. jostii*'s growth with enhanced potential for biofilm formation and cellular aggregation.

To test whether the flocculation phenomena was a result of enhanced EPS production, a combination of microscopy and quantitation by carbohydrate analysis was employed. Photographs of liquid samples (**Figure 4-9A**) and light micrographs of *R. jostii* depict homogenously distributed cells in solution without PFAAs (**Figure 4-9C**). The system with PFAAs, however, exhibits large and dense cellular clumps with little to no free-floating cells (**Figure 4-9B**, **Figure 4-9D**). SEM also captures differences between the systems grown with PFAAs and those without. When grown in the absence of PFAAs, cells were more uniform in size with an average cellular length of approximately 1.8±0.82 µm (**Figure 4-9E**). In contrast, when grown in the presence of PFAAs, the average cellular length doubled to approximately 3.4±1.6 µm (**Figure 4-9F**). This lengthening is potentially end-to-end adhesion as a result of EPS production or an artifact of incomplete cell division, as has been observed in resource limited systems and linked to a stress response (Pfeiffer and Bonhoeffer, 2003). SEM images of strain RHA1 grown in the presence of PFAAs also capture collapsed EPS (**Figure 4-9F**). The EPS is typically a highly hydrated substance, but after the dehydration steps necessary for SEM visualization, EPS can be observed as a collapsed structure (Hassan *et al.*, 2002).

Extraction of EPS from the cellular matrix yielded statistically significant ($p < 0.05$) increases in carbohydrates for the systems grown with PFAAs. In the case without PFAAs, 0.052±0.012 g carbohydrates / g cellular dry weight was recovered, versus 0.139±0.050 g carbohydrates / g cellular dry weight for the case with 10 mg/L of each PFAA. This near tripling of carbohydrate content coupled to micro and macroscopic visualization of cells grown with PFAAs provides strong evidence for enhanced EPS production, which may lead to increased biofilm formation in subsurface systems.

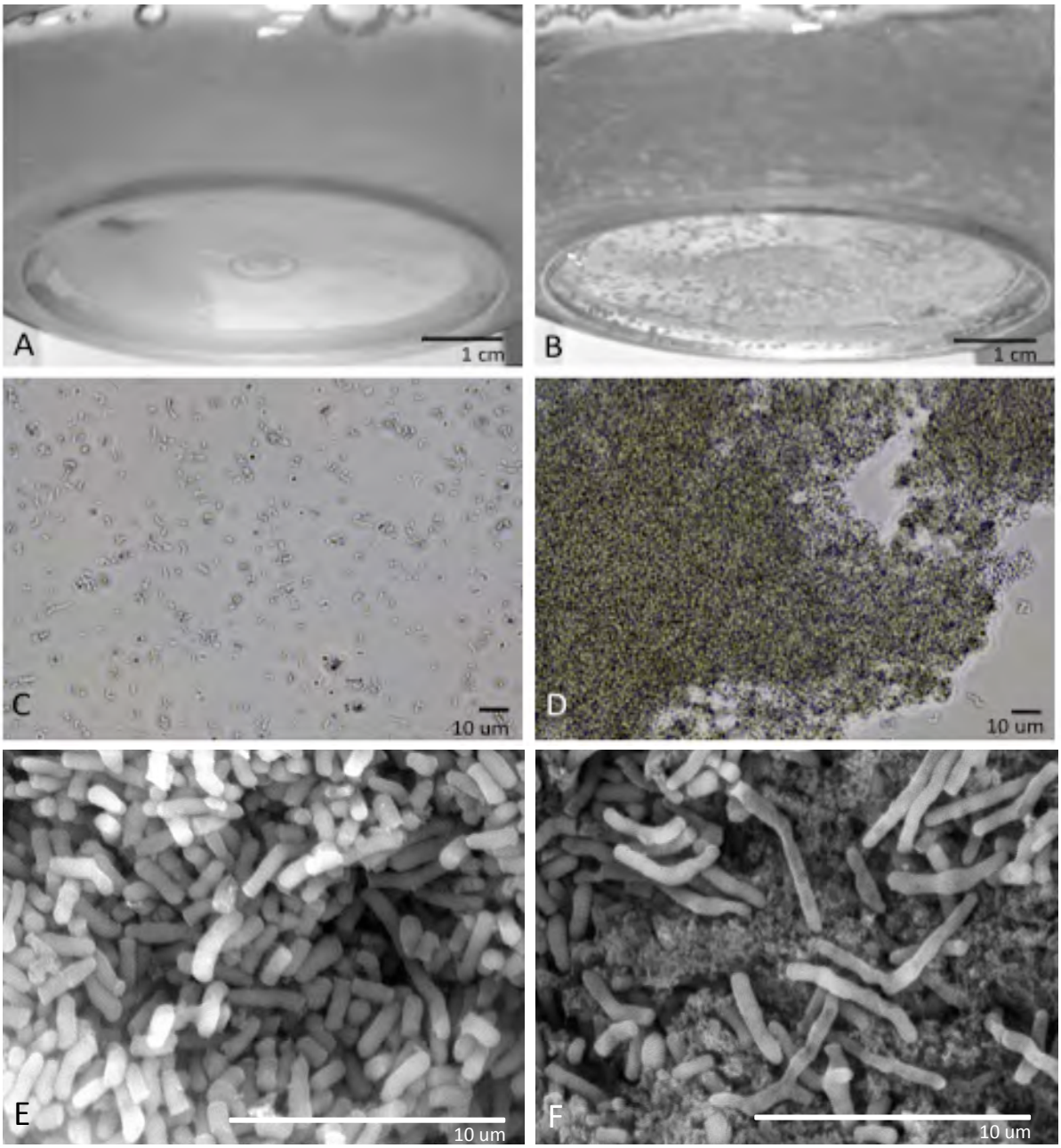

Figure 4-9. Large flocs are visible when *R. jostii* RHA1 is grown in the presence of PFAAs (right column); without PFAAs, the microbes are evenly distributed in solution (left column). **A.** Photograph of the bottom of a representative 1 L bottle used for growth without PFAAs and (**B**) with PFAAs. **C**. Light microscopy images of a representative sample without PFAAs (n=25) and (**D)** with PFAAs (n=32). **E**. SEM images capture cells as lighter, similarly sized, rod-shaped articles without PFAAs (n=15). **F**. More dehydrated EPS (gray background slurry) is captured via SEM in images of systems with PFAAs (n=28).

To further extrapolate the relevance of this axenic bacterial response, increased flocculation was also observed in soil-derived communities enriched in LB media and exposed to PFAAs. Increased floc counts, as well as larger floc areas, were observed under these conditions as compared to control communities grown without PFAAs (**Figure 4-10**). The capability of microorganisms to produce EPS is widely observed. The presence of PFAAs and the associated toxicological effects on microbial populations may encourage increased EPS formation as a stress response or through environmental changes (Stewart and Franklin, 2008). Microbial flocculation in the presence of surfactant-like molecules, such as PFAAs, may be counterintuitive if the flocculation is merely a physical process, however EPS production and subsequent flocculation may be protecting and isolating microcolonies so that they may continue to grow and reproduce (Sivan *et al.*, 2006; De Philippis and Vincenzini, 1998).

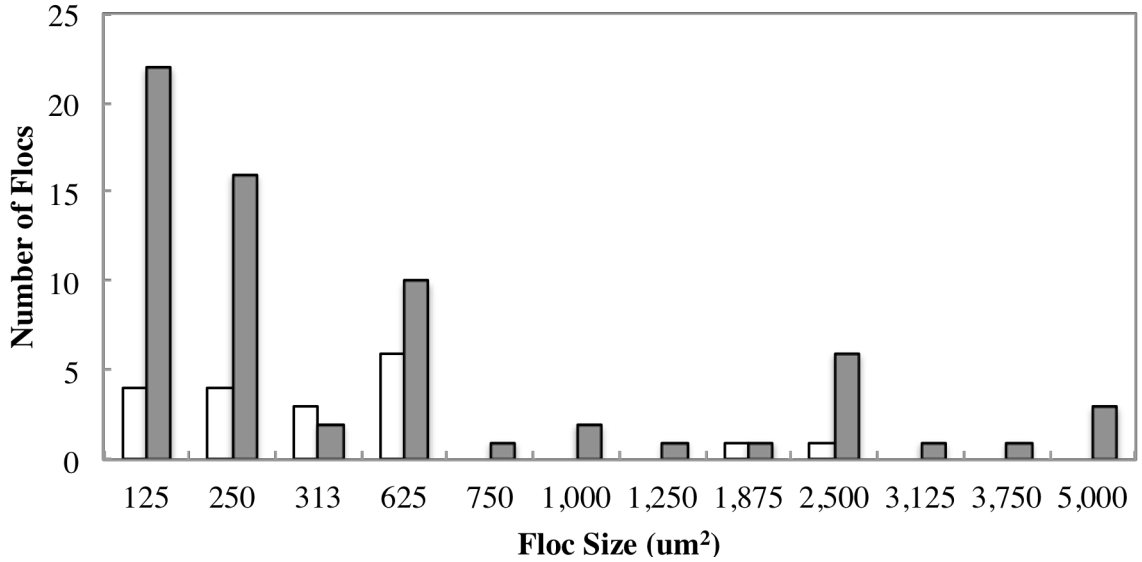

Figure 4-10. More flocs are observed in soil-derived communities grown in the presence of 110 mg/L total PFAAs (gray) than in those grown in the absence of PFAAs (white). The largest observed flocs also occurred when soil-derived communities were grown in the presence of 110 mg/L total PFAAs.

4.2.3.3 Expression of Stress Genes

Species of *Rhodococcus* have been shown to produce EPS (Perry *et al.*, 2007) as a potentially protective stress response under a variety of conditions including exposure to toxins and desiccation (LeBlanc *et al.*, 2008), carbon and nitrogen starvation (Sanin *et al.*, 2003), as well as to facilitate adhesion to polyethylene and subsequent three-dimensional microcolony formation (Sivan *et al.*, 2006; De Philippis and Vincenzini, 1998) Specifically, the production of EPS can act as a barrier between the cells and the dry environment under desiccation stress (LeBlanc *et al.*, 2008), or as a protective layer between the cells and toxins in solution including antibacterial agents and surfactants (De Philippis and Vincenzini, 1998). External stressors, such as changes in ionic strength, have even been applied to cultures in order to induce EPS production (Gong *et al.*, 2009). Alternatively, the unique chemical properties of PFAAs, particularly the ability to form micelles, may result in microbial aggregation independent of bacterial processes.

To test whether EPS production occurs in tandem with a stress response in the presence of PFAAs, the utilization of strain RHA1 with its large metabolic potential and annotated genome enables us to target for specific genes that correlate to cellular stress responses and regulation in order to better mechanistically explore this phenomenon (Goncalves *et al.*, 2006). This method does not necessarily prove that EPS production is a result of stress, or even that a stress response occurs as a function of cellular flocculation, instead we are assessing the variety of cellular responses that may occur upon exposure to PFAAs and are further exploring this interaction. To achieve this, quantification of stress-related genes within RHA1 using RT-qPCR was performed.

Table 4-4. Increased transcription of stress-associated genes

Gene	Fold Change	P	
		Student's t-test	REST[a]
sigF3	1.8	0.01	0.01
prmA	3.0	0.01	0.05

[a] Bustin *et al.*, 2009

The *prmA* gene is a part of the propane monooxygenase operon, and has been observed to be upregulated during solvent exposure and starvation conditions, potentially as a part of a general stress response (LeBlanc *et al.*, 2008; Patrauchan *et al.*, 2012). Similarly, s*igF3* is a gene encoding a sigma factor, and has been linked to desiccation, heat, and osmotic stress and is potentially part of a regulatory stress network (LeBlanc *et al.*, 2008; Ekpanyaskun 2006). Both genes are found in the chromosome of the RHA1 genome (McLeod *et al.*, 2006). Upregulation of either or both of these genes would imply activation of a stress response to an environmental variable. When RHA1 was grown with 110 mg/L total PFAAs (+PFAA), there was a two- to three-fold upregulation of both genes of interest ($p \leq 0.05$) over cells grown without PFAAs (-PFAA) (**Table 4-4**). Similar upregulation trends of statistical significance were also observed for cells grown in nutrient rich media (LB broth) and can be seen in **Table 4-5**.

Table 4-5. Fold change and statistical significance for LB grown and minimal media grown cells

Gene	Media	Fold Change	P	
			Student's t-test	REST
prmA	Minimal	3.0	0.01	0.05
sigF3	Minimal	1.8	0.01	0.01
prmA	LB	n/a	0.04	n/a
sigF3	LB	1.9	0.01	0.03

Although increased expression of these genes can be correlated to a stress response, the particular stress trigger as a result of PFAA exposure (such as nutrient limitation, environmental toxicity, or even flocculation behavior itself) is yet unknown. Whether stress conditions occur in a mixed culture or even *in situ* has not been evaluated, however considering the observation of increased flocculation in soil-derived cultures as previously discussed, microbial stress effects in PFAA source zones may be likely.

4.2.4 Environmental Implications

Ideally, subsurface zones contaminated with hydrocarbons will undergo some degree of biodegradation even in the absence of active engineering practices (Deeb *et al.*, 2002; Patterrson *et al.*, 1993). Due to the co-occurrence of hydrocarbons and PFAAs *in situ*, the continued hydrocarbon bioremediation in the presence of PFAAs is a widespread concern (Moody and

Field, 1999; Moody and Field, 2000; Moody *et al.*, 2003). The effects of PFAAs on microorganisms has not yet been studied, as compared to the effects on macroorganisms. For example, an average of 50 ng/mL of PFOA (one of the 11 analytes tested in our work) has been detected in human populations exposed to fluorinated surfactants (Freberg *et al.*, 2010). Rats have been shown to break down precursor compounds into PFOS (Xu *et al.*, 2004), bioaccumulation factors for PFAA uptake into radish, celery, tomato, and sugar snap pea crops have been calculated (Blaine *et al.*, 2014), and primates express decreased body weight and increased liver weight upon exposure to PFOS (Seacat 2002). The body of knowledge regarding human and environmental interactions with previously undetected poly and perfluoroalkyl substances is continually growing (Rotander *et al.*, 2015), and may eventually provide more accurate field and biologically-associated levels of exposure. If microorganisms are detrimentally impacted by PFAA exposure, we may see environmental effects of concern that could include inhibition of co-contaminant degradation (Hug *et al.*, 2012), shifts in carbon cycling, or changes in subsurface chemical properties such as pH or metal mobility (Stewart and Franklin, 2008; Templeton *et al.*, 2009). Although these laboratory based systems are not necessarily representative of every subsurface environment, the comparison of PFAA-containing cultures to those without can provide us with insights regarding the effects of PFAAs while controlling and monitoring variables such as temperature, microbial community effects, and contaminant mass balances. The laboratory work described herein could complement and support future research investigating anaerobic systems, mixed communities, and/or dynamic systems.

While the presence of PFAAs did not appear to alter metabolic traits relating to toluene bioremediation potential or net biomass growth of *R. jostii* strain RHA1, cells grown in the presence of high concentrations of PFAAs (≥22 mg/L total PFAAs) exhibited enhanced EPS formation and subsequent flocculation. Stress-related genes are also upregulated 2- to 3-fold over the cells grown without PFAAs. Multiple lines of evidence support that aggregation of RHA1 results from a biological response rather than only physicochemical interactions:

1. flocculation was not observed when harvested cells were exposed to media containing PFAAs as in the toluene biodegradation experiments;
2. observed flocs eventually break apart during stationary phase without a change in PFAA concentration;
3. flocculation is coupled to an increase in EPS production; and
4. the upregulation of stress-related genes implies that a biological response is occurring.

The ability to enhance flocculation is most often used in wastewater treatment trains as a part of the activated sludge process (Li and Yang, 2007). Flocculation has also been implemented in the biofuels industry, and can be seen in natural processes in both oceanic and freshwater systems (Templeton *et al.*, 2009). Flocculation can be encouraged by exposure to surfactants, such as sodium dodecyl sulfate (SDS), which can change the surface hydrophobicity of the cells (Marchesi *et al.*, 1994; Turner and Xu, 2008). Although PFAAs exhibit surfactant-like properties and can often be co-located with non-fluorinated surfactants (Guelfo and Higgins, 2013), the

effects of PFAAs on cellular flocculation and subsequent EPS production had not previously been evaluated.

Increased EPS production *in situ* may have a variety of impacts, including biofouling or clogging, which may result in the ensuing formation of preferential subsurface pathways, accelerating the transport of both co-contaminants and PFAAs (Kao *et al.*, 2001; Pintelon *et al.*, 2012; Kalin 2004). Alternatively, decreases in permeability due to biofilm formation may result in retarded transport of PFAAs or co-contaminants, especially considering the preferential PFAA sorption to organic carbon (Guelfo and Higgins, 2013; Cusack *et al.*, 1990). Regarding the sorptive properties of PFAAs, this enhanced biofilm formation may increase cellular exposure to aqueous PFAAs or co-contaminants (Kalin 2004; Monkawa 2006) or it may decrease PFAA contact with soil particles (Cao *et al.*, 2011).

Continued research assessing additional microorganisms of interest as well as increasingly environmentally relevant assemblages can be conducted to verify *in situ* impacts of PFAAs. Collectively, these results suggest that the effects of PFAA exposure may be of less concern for co-contaminant biodegradation than for other processes in environmental systems. In particular, enhanced biofilm formation and increased microbial stress responses could impact physical subsurface transport, contaminant sorption, and perhaps even microbial community structure.

4.3 Perfluoroalkyl acids inhibit reductive dechlorination of trichloroethene by repressing *Dehalococcoides* (*Task 3b*)

4.3.1 Background

PFASs are contaminants of emerging concern found throughout the environment (Key *et al.*, 1997). PFASs are used in a diverse range of industrial, consumer, and commercial applications including pesticides, non-stick coatings, and in fire-fighting foams (Key *et al.*, 1997; USEPA 2012; Moody and Field, 2000). These compounds are environmentally recalcitrant, exhibit toxicity effects in primates and microbiota, and can bioaccumulate (Moody *et al.*, 2002; Higgins *et al.*, 2007; Blaine *et al.*, 2014; Weathers *et al.*, 2015; Seacat 2002). The prevalent use and environmental longevity, coupled with improvements in quantification, have led to widespread environmental detection in groundwater, surface water, soil, and air, as well as detection in humans, wildlife, and food crops (Blaine *et al.*, 2014; Martin *et al.*, 2004; Higgins *et al.*, 2005; Rotander *et al.*, 2015). The U.S. Environmental Protection Agency has set provisional drinking water health advisories for two common PFASs: 0.4 µg/L for PFOA and 0.2 µg/L for PFOS (USEPA 2009).

PFAAs, a subset of PFASs, are present in and can arise from components of AFFF used for fuel fire suppression (Moody and Field, 1999). Use of AFFF for military firefighter training has led to the introduction of PFAAs into groundwater in sites that are often contaminated with chlorinated solvents (Moody and Field, 2000; McGuire *et al.* 2014; Guelfo and Higgins, 2013; McKenzie *et al.*, 2016) such as TCE and its toxic daughter products cis-dichloroethene (cDCE) and vinyl chloride (VC; Scheutz *et al.*, 2014). ERD is a bioremediation process for chlorinated solvents in which an electron donor, such as lactate (biostimulation), or potentially a known

microbial consortium containing *Dehalococcoides* (bioaugmentation) is supplied (Scheutz *et al.*, 2014). Members of the genus *Dehalococcoides* are known to completely degrade PCE and TCE to ethene, thus limiting the potential for toxic accumulation of vinyl chloride (Maymo-Gatell *et al.*, 1997). *Dehalococcoides* have been incorporated into ERD consortia in laboratory settings (Maymo-Gatell *et al.*, 1997; Holmes *et al.*, 2006; Hug *et al.*, 2012) and are often found in aquifers wherein complete PCE and TCE dechlorination has been observed (Yang and Zeyer, 2003; Hendrickson *et al.*, 2002). It is yet unknown how PFAAs may impact microbial communities relevant to chlorinated solvent bioremediation. While biodegradation of PFAAs is not expected (USEPA 2012), there are concerns regarding potential adverse effects from PFAA exposure on subsurface microbial communities and co-contaminant degradability (Key *et al.*, 1997). Biodegradation of another commonly co-located contaminant, toluene, was not impacted in pure culture studies, however the presence of PFAAs did correlate to increased formation of extracellular polysaccharides and enhanced transcription of stress-related genes (Weather *et al.*, 2015). Consequently, unanticipated impacts on PFAA or chlorinated solvent fate and transport in groundwater sources are possible, ranging from effects on co-contaminant degradation and microbial processes, to changes in sorptive properties of PFAAs as a result of biostimulation or bioaugmentation.

The objective of this study (*Task 3b*) was to assess potential impacts of these nontraditional contaminants, PFAAs, on reductive dechlorination of TCE. This was accomplished by querying for suppression of reductive dechlorination activity by a *Dehalococcoides*-containing methanogenic mixed community cultivated in the presence of varied concentrations of PFAAs. In parallel, we contrasted the community structure and putative functionality of these microcosms to understand ecological shifts and metabolic redundancy within this consortium that could be attributed to PFAA presence. Insights from the ecological profiles were then used to challenge an axenic culture of *Dehalococcoides* with PFAAs to understand the direct impact on this bacterial genus. Results revealed suppression of *Dehalococcoides* growth and reductive dechlorination rates in both pure culture and mixed assemblages.

4.3.2 Materials and Methods

4.3.2.1 PFAA preparation and aqueous analysis

Purity corrected stock solutions of an eleven-analyte mixture were prepared as described elsewhere (Weathers *et al.*, 2015; Guelfo and Higgins, 2013). PFAA salts (Sigma Aldrich) were suspended in a 70/30 (v/v) methanol/water solution. Water used in this study was generated with a Milli-Q system (Millipore). Unless otherwise specified, each mixture contained PFBA, perfluoropentanoate, PFHxA, PFHpA, PFOA, PFNA, PFDA, PFUnA, PFBS, PFHxS, and PFOS. These compounds represent a range of carbon chain lengths and are commonly found at AFFF-impacted sites (Key *et al.*, 1997; Moody and Field, 1999; McGuire *et al.*, 2014). Empty culture bottles were spiked with the PFAA mixture while in an anaerobic chamber (90% nitrogen, 5% hydrogen, 5% carbon dioxide) and the methanol was evaporated as described elsewhere (Weathers *et al.*, 2015). Final PFAA concentrations were verified using liquid chromatography tandem mass spectroscopy with stable-isotope surrogate standards (Wellington Laboratories). Aqueous samples were centrifuged to remove particulates, sampled, and diluted as appropriate.

A SCIEX 3200 mass spectrometer (MDS Sciex) was utilized with MultiQuant for quantitation to verify PFAA recovery (Weathers *et al.*, 2015).

4.3.2.2 Cellular preparation

Anaerobic experiments were inoculated with a *Dehalococcoides*-containing methanogenic mixed culture that was maintained in a stock bottle amended with exogenous cobalamin co-factors, such as vitamin B_{12}, to enable TCE dechlorination (Hug *et al.*, 2012; Men *et al.*, 2013). This stable and robust culture maintained in Berkeley, CA was derived from TCE-contaminated groundwater (Men *et al.*, 2013). The *Dehalococcoides* strains in this culture are most similar to *Dehalococcoides mccartyi* strain 195 (Men *et al.*, 2013). The described culture ferments lactate to produce hydrogen and acetate, the necessary electron donor and carbon source for *Dehalococcoides*. Pure culture experiments using *Dehalococcoides mccartyi* strain 195 were maintained under similar conditions as the mixed culture, but were amended with acetate and hydrogen instead of lactate (Maymo-Gatell *et al.*, 1997).

4.3.2.3 Reductive dechlorination with the mixed culture

Batch systems containing TCE, lactate, and a PFAA mixture were designed to evaluate microbial degradation rates. ERD experiments contained triplicate sets of 22, 66, or 110 mg/L total PFAAs added to sterile 60 mL serum bottles as well as 0 mg/L controls spiked with non-PFAA containing 70/30 v/v methanol/water. These concentrations were chosen to reflect what may be observed near a PFAA source zone (Moody and Field, 2000; 110 mg/L total at 10 mg/L each of 11 analytes) and to determine if there is a PFAA concentration threshold wherein biological effects are not observed. Following PFAA addition and methanol evaporation described in the prior section, bottles were sealed with butyl rubber stoppers. Next, 48.5 mL of an autoclaved mineral salts medium (He *et al.*, 2007) containing 20 mM lactate as electron donor and 100 µg/L vitamin B_{12} was added to stoppered bottles with a sterile syringe. During media addition, an exhaust needle was inserted into the stopper to avoid bottle pressurization, while low flow rates were used to minimize PFAA volatilization and flushing. After media addition, the headspace was gently flushed with N_2/CO_2 (90:10) to remove residual hydrogen and oxygen. Each bottle was then amended with approximately 20 µmoles of TCE (Sigma Aldrich, 99.9%) and allowed to sit for at least 24 hours to facilitate TCE and PFAA equilibration. At time zero, the bottles were inoculated with 3% (v/v) of the previously-grown methanogenic mixed community stock culture and incubated in the dark at 34ºC for the duration of the experiment. All bottles were inverted several times at each sampling point to promote PFAA mixing. Abiotic controls devoid of microorganisms were prepared for the parallel pure-culture experiment. After TCE dechlorination profiles were generated, the bottles were sampled for phylogenetic sequencing and verification of PFAA concentrations.

4.3.2.4 Dechlorination measurements

Chloroethenes, ethene, and methane were measured by injecting 100 µL of culture headspace into an Agilent 7890A gas chromatograph equipped with a flame ionization detector and 30 m x 0.32 mm J&W capillary column (Agilent Technologies). Hydrogen concentrations were measured by injecting diluted headspace samples into a gas chromatograph fitted with a

reductive gas detector (Trace Analytical). Between 50 and 300 µL of culture headspace was withdrawn for each hydrogen measurement and diluted in 17 mL glass vials purged with N_2 to generate concentrations within the linear calibration range of the instrument. The total volume of extracted headspace was tracked throughout the incubation to ensure that the same approximate volume was removed from all bottles (1.5 to 1.9 mL). Initial TCE dechlorination rates were determined by obtaining the slope of a time-course regression through the linear portion of the degradation curve (days 1 through 4) after accounting for loss as a function of time generated from the abiotic control. Production rates for cDCE, VC, and ethene were also tabulated during the linear portion of the generation curve for each sample.

4.3.2.5 Phylogenetic sequencing

Every sample containing the methanogenic mixed culture was extracted after dechlorination profiles were complete (~8 days). DNA was extracted with the PowerSoil DNA Isolation Kit (MO BIO Laboratories, Inc.). Extracted DNA was quantified with a Qubit 2.0 Fluorometer and dsDNA HS Assay Kit (Life Technologies). Each sample was amplified using a TC-412 Thermocycler (TECHNE) with 2 µL DNA template, 2 µL each forward and reverse primers at 10 µM each, 6.5 µL PCR grade water, and 12 µL Phusion 2× MasterMix (New England BioLabs, Inc.). Dual-indexed primers (515F and 805R) target the V4 region of the 16s rRNA gene (Integrated DNA Technologies) and are described in the SI along with the amplification protocol. Select samples were run via gel electrophoresis to confirm amplicons of a desired length of roughly 300 base pairs. Samples were purified and normalized with the SequalPrep Normalization Kit (Invitrogen) according to the manufacturer's protocol and pooled into a 2 mL RNAse and DNAse free sterile microcentrifuge tube. Pooled samples were concentrated with µltra-.05 30K Centrifugal Filter Devices (Amicon) according to the provided protocol. Pooled samples were quantified using the Qubit Fluorometer as described above and diluted and re-quantified if necessary to normalize concentrations. Half of the final pooled sample volume was archived at -80°C with the balance sent for MiSeq sequencing using the V2 250 Cycle Paired-End kit at BioFrontiers Institute (Boulder, CO).

Sequence post-processing was performed with MacQIIME version 1.9.0 (Caporaso *et al.*, 2010) with operational taxpnomic unit (OUT) picking and chimera screening using Usearch61(Edgar 2010; Edgar *et al.*, 2011) and alignment with PyNAST (Caporaso *et al.*, 2010; DeSantis *et al.*, 2006). Taxonomy was assigned with Greengenes reference database version 12_10 (McDonald *et al.*, 2012) using RDP Classifier 2.2 (Wang *et al.*, 2007). FastTree 2.1.3 was used to generate the phylogenetic tree (Price *et al.*, 2010) and was further manipulated in FigTree (Rambaut 2015). Weighted, non-rarefied beta diversity was visualized with EMPeror (Vázquez-Baeza *et al.*, 2013) and adonis and ANOSIM test statistics were calculated using compare categories (Fierer *et al.*, 2010). Samples were filtered so the minimum total observed fraction per OTU was 0.001. Taxa were summarized such that the OTU identifier with the greatest total abundance was retained: if the lowest classification for multiple OTU identifiers resulted in the same taxonomic assignment, the specific OTU identifier with the greatest total abundance was retained. The abundance of the resulting merged OTU reflects the sum of each OTU with the same taxonomic lineage. Differential abundances were calculated with the DeSeq2 package; the adjusted p values are reported herein (Love *et al.*, 2014). The relative abundances represent the average ± standard

deviation between the three experimental replicates per condition. Reporting of results and analysis within this work reflects the lowest identified taxonomic level of each OTU.

Functionality was assigned based on the class level information for the non-dechlorinating members of the consortium according to the comparative metagenomics study performed by Hug *et al.* (2012) The methanogenic mixed culture used herein is similar to the ANAS culture maintained in Berkeley, California described in Hug *et al.* (2012; Holmes *et al.*, 2006) which also uses lactate as an electron donor (Holmes *et al.*, 2006; Richardson *et al.*, 2002). The functions discussed by Hug *et al.* (2012) have been applied to the culture within this study. Sequence data have been submitted to the National Center for Biotechnology Information Sequence Read Archive database (accession numbers pending). Post-processing scripts can be found in **Appendix B**.

4.3.3 Results and Discussion

4.3.3.1 Effect of PFAAs on reductive dechlorination by a mixed culture

Batch microbial incubations across a range of PFAA concentrations revealed that TCE dechlorination was severely inhibited when the methanogenic mixed culture was grown in the presence of 110 mg/L PFAA (**Figure 4-11**). This corresponded with reduced cDCE production as well as limited VC and ethene production. Inhibition effects on TCE dechlorination were also observed at 66 mg/L manifested by a decrease in dechlorination rates of TCE as compared to the case without PFAAs ($p<0.01$), along with a decrease in cDCE, VC, and ethene production rates (**Table 4-6**). Dechlorination of TCE, production and dechlorination of cDCE and VC, and production of ethene occurred similarly between cases with no PFAAs and those with 22 mg/L. Analogous inhibitory behavior has also been observed in the presence of select AFFF formulations containing a range of PFASs (Harding-Marjanovic *et al.*, submitted). The eleven-component PFAA mixture appeared to exert this selective pressure; systems with equivalent concentrations of only perfluoroalkyl sulfonates were not affected (Harding-Marjanovic *et al.*, submitted).

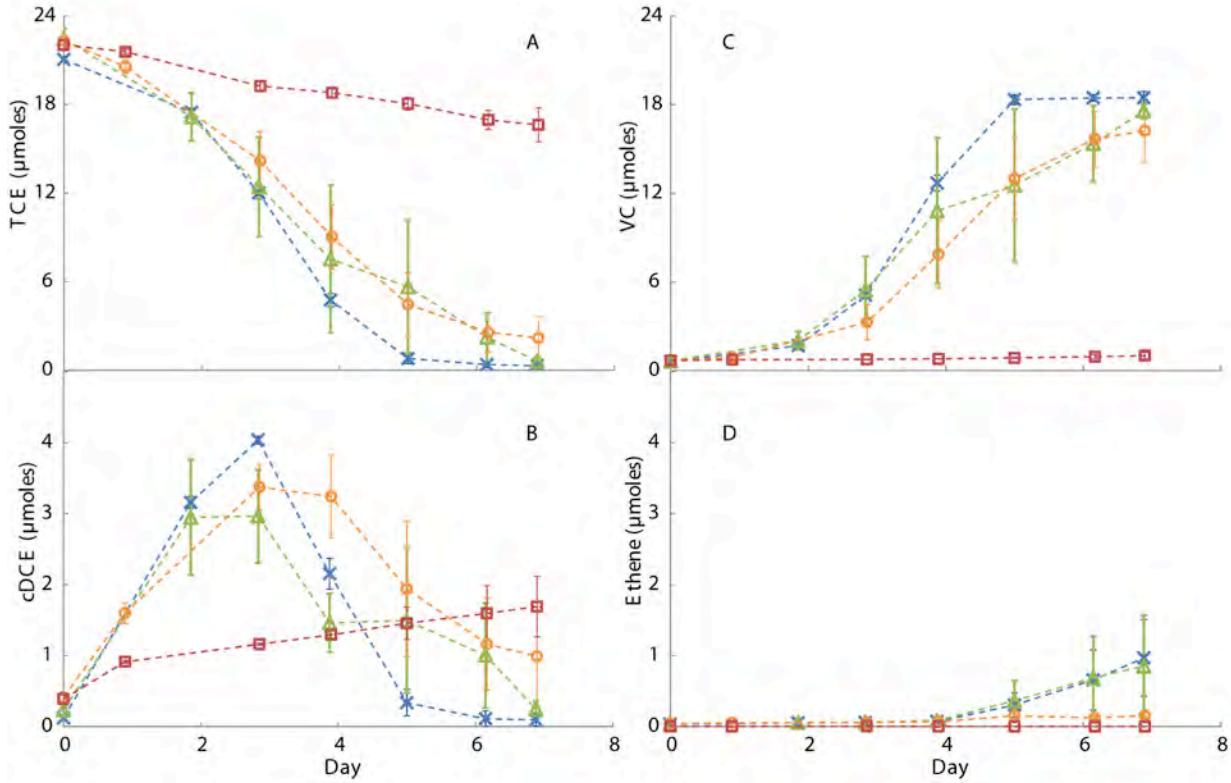

Figure 4-11. Reductive dechlorination by the mixed culture is inhibited by 110 mg/L total PFAAs (red squares) with slower rates of dechlorination for 66 mg/L total PFAAs (orange circles), while 22 mg/L total PFAAs (green triangles) is not significantly different from no PFAAs (blue x's) ($p > 0.2$ for each sampling time and compound). **A.** TCE profiles; **B.** cDCE; **C.** VC; and **D.** ethene. Error bars represent the standard error of triplicate incubations.

Table 4-6. Dechlorination (-) and production (+) rates by the mixed culture

	Rates (µmol/day)*			
	TCE	**cDCE**	**VC**	**Ethene**
No PFAAs	-5.8 ± 0.2	+1.4 ± 0.0	+5.5 ± 0.2	+0.3 ± 0.3
22 mg/L	-4.3 ± 2.9	+1.5 ± 0.7	+3.5 ± 2.7	+0.3 ± 0.4
66 mg/L	-3.3 ± 1.0	+1.0 ± 0.2	+4.5 ± 1.3	+0.0 ± 0.1
110 mg/L	-0.5 ± 0.1	+0.1 ± 0.1	+0.1 ± 0.1	0.0 ± 0.0

*Values represent triplicate averages ± standard deviation

4.3.3.2 Effects of PFAA exposure on community structure

To understand how the eleven-component PFAA mixture herein affected the dechlorination process, relative abundance, community dynamics, and putative functionalities were explored via next-generation sequencing. Phylogenetic sequencing of the methanogenic assemblage resulted in 17 total OTUs after filtering to 0.1% as described in Methods and Materials (**Figure 4-12**). This core microbiome was observed regardless of PFAA concentration; however, the relative abundance of select taxonomic units varied with increasing PFAA exposure.

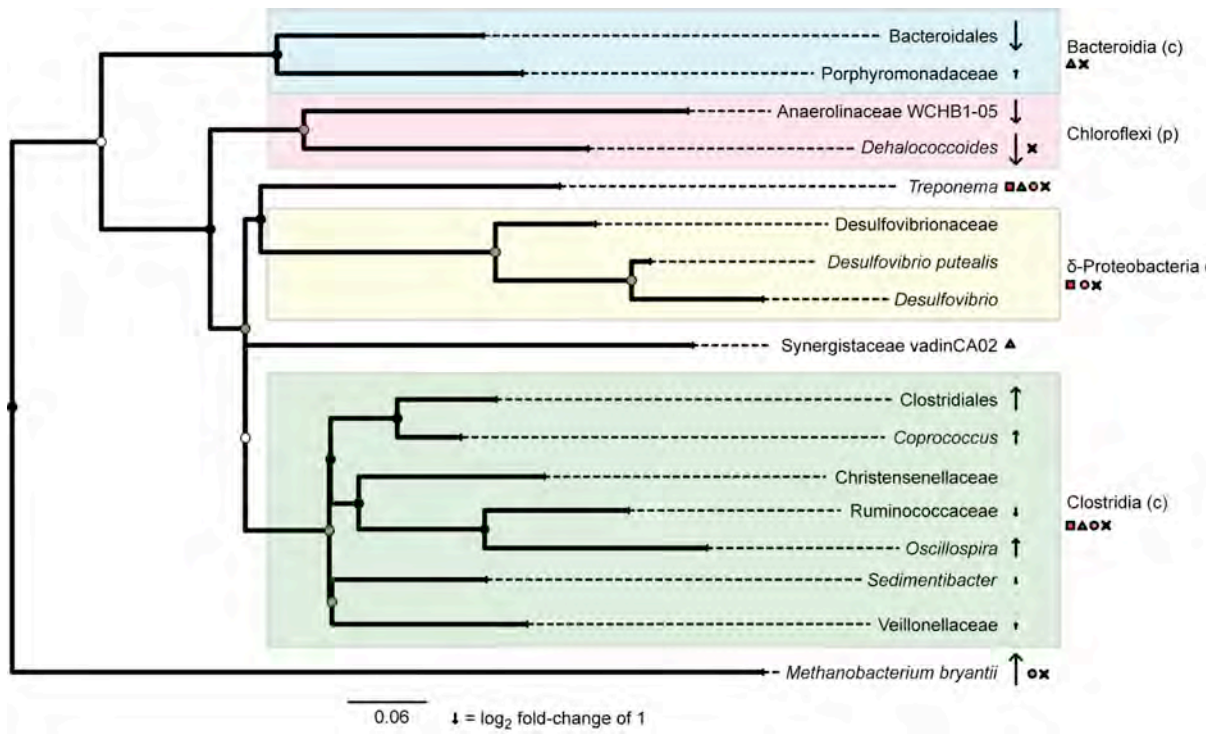

Figure 4-12. The phylogenetic tree of the unique OTUs depicts trends for putative function while changes in abundance upon exposure to PFAAs does not correlate with phylogeny. Arrows represent the $\log_2$ fold-change in abundance between no PFAAs and 110 mg/L PFAAs with arrow size correlating to the magnitude of the $\log_2$ fold-change. An upward pointing arrow represents an increase in abundance when grown with PFFAs, downward represents a decrease in abundance when grown with PFAAs. Putative functions within the community are annotated as methionine synthesis (red squares), fermenters (green triangles), corrinoid synthesis (orange circles), and oxygen scavenging (blue x's). Nodes represent FastTree local bootstrap values: (black circles) for values between 80-100%, (grey circles) for values between 50-80%, and (open circles) for values less than 50%.

The functions and taxonomy described herein reflect what is typically observed in dechlorinating methanogenic mixed-cultures (Hug *et al.*, 2012; Men *et al.*, 2013) and are thus extrapolated to this particular system. These functions are hypothetical, as data are being compared to a similar culture that is cultivated in semi-batch (versus batch) and likely contains a different strain of *Dehalococcoides* than the methanogenic mixed-culture used herein (Holmes *et al.*, 2006; Men *et al.*, 2013). This comparison is useful for assigning putative functionality considering the overall taxonomic similarities between the two analogous cultures.

This mixed-culture is fermentative and methanogenic. The general pathway of reductive dechlorination within this community begins with conversion of lactate, the electron donor, to hydrogen by a set of fermenters (Freeborn *et al.*, 2005). In this study, fermentation has been putatively assigned to eleven OTUs including members from the classes of Bacteroidia (Cupples *et al.*, 2003) and Clostridia and single members from Spirochaetes and Synergistia (**Figure 4-12**; Hug *et al.*, 2012; Sakamoto 2014). The hydrogen can then be used by *Methanobacterium bryantii* to produce methane or to complex with chlorine as it is removed from the electron acceptors (TCE, cDCE, or VC), by *Dehalococcoides*, eventually producing ethene (Hug *et al.*, 2012; Men *et al.*, 2013). Most of the remaining OTUs in this culture, along with those found within Clostridia and Spirochaetes, can be functionally assigned to a combination of methionine or corrinoid synthesizers (two functions *Dehalococcoides* lacks), or can fulfill the niche of oxygen scavengers (Hug *et al.*, 2012). These hypothesized interactions only address functionality as it relates to *Dehalococcoides* vitality; it is likely that additional processes are occurring within the system, however they are not included in this analysis. This general community composition is similar to what has been described elsewhere for reductive dechlorinating cultures sustained on lactate, which includes orders such as Clostridiales, Bacteroidales, and Spirochaetales, along with δ-proteobacteria, *Dehalococcoides*, and Archaeal methanogens (Hug *et al.*, 2012; Richardson *et al.*, 2002; Freeborn *et al.*, 2005).

The presence of PFAAs at varied concentrations tended to shift the relative abundance of many of these organisms. Analysis of beta diversity depicted two distinct groups: the samples with 110 mg/L total PFAAs clustered independently from the 0, 22, and 66 mg/L samples (**Figure 4-13**). This is also observed statistically; both adonis and ANOSIM metrics exhibit statistical significance (p=0.013 and p=0.011, respectively) when the samples are grouped by concentration. The diversity of samples grown with 66 mg/L PFAAs is not significantly different from 22 mg/L or those without PFAAs, despite a reduction in dechlorination rate as discussed previously. TCE dechlorination rates in both the 22 and 66 mg/L samples is, however, well correlated to the relative abundance of *Dehalococcoides* in each sample, with Pearson correlation coefficients of -0.72 and -0.91 respectively. This correlation further supports that *Dehalococcoides* abundance is a driving factor for both differences in community structure and inhibition of TCE dechlorination upon PFAA exposure.

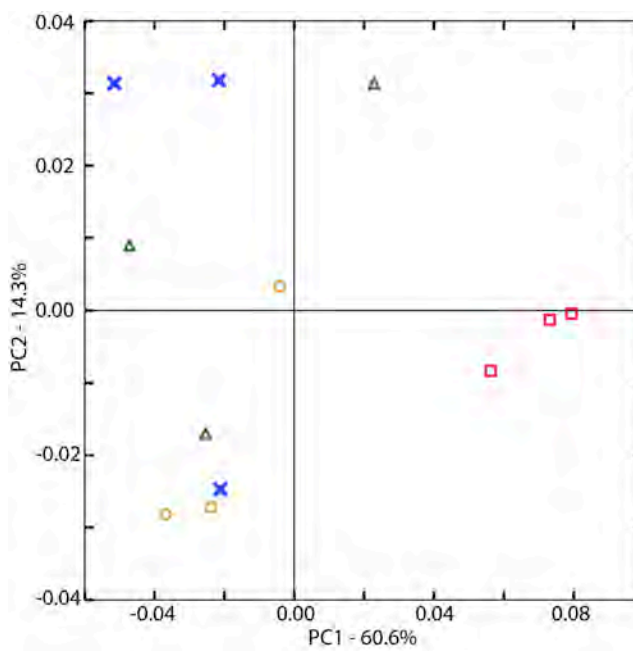

Figure 4-13. Principle component analysis of weighted non-rarefied taxon abundance shows distinct clustering of cultures grown in the presence of 110 mg/L PFAAs (red squares) on an axis that explains 60.6% of the variability. The rest of the cultures, grown either in the presence of 22 mg/L (green triangles), 66 mg/L (orange circles), or without PFAAs (blue x's) do not exhibit any significant clustering between samples.

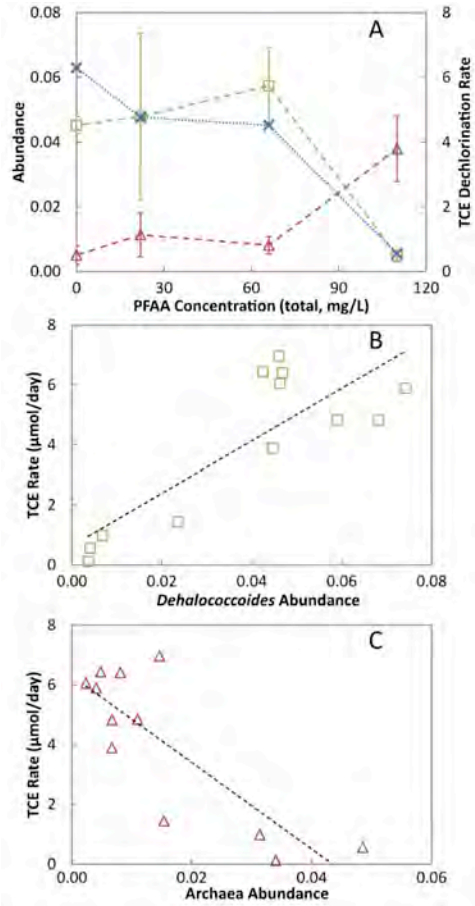

Figure 4-14. Abundances of *Dehalococcoides* (green squares) and *Methanobacterium bryantii* (red triangles) exhibit correlations with PFAA concentration (blue x's; Panel **A**). TCE dechlorination rates also correlate with *Dehalococcoides* abundance (Panel **B;** R_2 = 0.68) and with Archaea abundance (Panel **C**) (R_2 = 0.68).

The most extreme shift in community structure occurred when comparing samples without PFAAs and those grown in the presence of 110 mg/L total PFAAs. Samples that effectively dechlorinated TCE without PFAAs had an average abundance of 4.5% ± 0.2% of *Dehalococcoides*, compared to an average abundance of 0.5% ± 0.2% for samples grown in the presence of 110 mg/L total PFAAs. This is an 8.4 fold decrease in abundance ($p<0.01$) for communities grown in the presence of 110 mg/L PFAAs. An inverse shift in the relative abundance of methanogenic Archaea was also observed (**Figure 4-12**): without PFAAs the *Methanobacterium bryantii* abundance was 0.5% ± 0.3% versus 3.8% ± 0.9% with 110 mg/L PFAAs resulting in an 8.5 fold increase ($p<0.01$). This relationship is expected; *Dehalococcoides* and methanogens actively compete for the available hydrogen to either produce HCl through the dechlorination reaction or to produce methane, respectively (Hug *et al.*, 2012; Men *et al.*, 2013). The relative abundance of *Dehalococcoides* and *Methanobacterium bryantii* correlate well with TCE dechlorination rates (R^2 = 0.68 for both comparisons) as seen in **Figure 4-14**.

Although the inverse correlation between *Dehalococcoides* and Archaea is anticipated in light of the interplay between TCE reduction and methane consumption (Men *et al.*, 2013), our understanding of shifts and corresponding relationships between non-dechlorinating members of the community is limited. A consistent trend was observed in all members of δ-proteobacteria: no significant change in relative abundance was observed upon exposure to PFAAs. Members of this class (such as an unspecified *Desulfovibrionaceae* and *Desulfovibrio* sp.) are hypothesized to scavenge oxygen and synthesize corrinoid cofactors necessary for *Dehalococcoides* (Hug *et al.*, 2012; Men et al, 2012). Members of δ-proteobacteria also encode hydrogenases necessary for the conversion of hydrogen cations to H_2 along with the ability to produce exogenous methionine. Reductive dechlorination by *Dehalococcoides* irreversibly loses functionality upon exposure to oxygen, thus *Dehalococcoides* may rely on oxygen scavenging organisms, such as δ-proteobacteria, within the mixed community (Hug *et al.*, 2012). Another OTU that was not affected by PFAA presence was *Treponema*, a genus known for corrinoid and methionine synthesis, oxygen scavenging, and the ability to ferment lactate to produce H_2 (**Figure 4-12**; Hug *et al.*, 2012). As these organisms are

not significantly impacted by PFAA presence, they are likely not contributing to the inhibition of *Dehalococcoides* vitality and activity.

Conversely, eleven OTUs exhibited statistically different abundances ($p<0.05$) when grown in the presence of 110 mg/L PFAAs. To understand the potential effects of PFAAs on putative functions within the methanogenic mixed culture, we will focus on the scenario wherein the largest shifts in relative abundance occurred: between samples without PFAAs and those with 110 mg/L PFAAs, although similar trends were observed when comparing between 22 mg/L, 66 mg/L, and 110 mg/L (**Table 4-7**). Taxa that may be responsible for corrinoid synthesis and oxygen scavenging exhibited varied responses to PFAA presence, thus the inhibition of *Dehalococcoides* is not definitively connected to repression of organisms capable of corrinoid or methionine synthesis, or to oxygen scavenging within the community. For example, we hypothesize that members of the order Clostridiales are fermenters (Biddle *et al.*, 2013), and can synthesize methionine within this system (Hug *et al.*, 2012). Many of these OTUs were enhanced in the presence of 110 mg/L PFAAs: an unspecified Clostridiales increased by a fold-change of 4.7*, Coprococcus* increased by 2.4-fold*, Oscillospira* was enhanced 3.4-fold*,* and Veillonellaceae increased with a fold-change of 1.5. Others capable of fulfilling these niches were inhibited at 110 mg/L PFAAs: *Sedimentibacter* decreased 1.5-fold, and an unspecified Ruminococcaceae decreased 1.7-fold*.* Christensenellaceae, another Clostridiales*,* was not significantly impacted by PFAA presence at all. The reason some members of Clostridiales are enhanced while others are repressed or unaffected is yet to be understood.

Similarly, two OTUs in the order Bacteroidales*,* which contribute to fermentation and potentially methionine synthesis, were observed (Hug *et al.*, 2012; Bergey and Holt, 1994): one unidentified Bacteroidales was repressed in the presence of 110 mg/L PFAAs by a fold-change of 7.1, while Porphyromonadaceae was enhanced 1.8-fold. Also repressed at 110 mg/L was WCHB1-05 in the family Anaerolinaceae, which decreased by a fold change of 4.8. This OTU was the most closely related to *Dehalococcoides* as a member of the phylum Chloroflexi. Fold changes and statistical significance for each OTU and concentration comparison can be viewed in **Table 4-7**. This exercise demonstrates that the selective pressures as a result of PFAA presence are highly variable; in general, enhancement and repression do not trend with putative functionality or with phylogeny.

Table 4-7. Fold Changes and Statistical Significance (grey highlighted values p<0.05)

OTU	No PFAAs vs 110 mg/L		No PFAAs vs 22 mg/L		No PFAAs vs 66 mg/L		22 mg/L vs 66 mg/L		22 mg/L vs 110 mg/L		66 mg/L vs 110 mg/L	
	log_2 Fold-Change	p (adj)	log_2 Fold-Change	p (adj)	log_2 Fold-Change	p (adj)	log_2 Fold-Change	p (adj)	log_2 Fold-Change	p (adj)	log_2 Fold-Change	p (adj)
Methanobacterium bryantii	3.1	0.000	0.8	0.572	0.5	0.574	-0.6	0.896	1.7	0.019	2.4	0.000
Bacteroidales	-2.8	0.009	-0.2	0.942	-1.9	NA	-2.4	0.022	-2.3	0.026	0.6	0.351
Porphyromonadaceae	0.7	0.004	0.3	0.812	0.3	0.574	0.1	0.896	0.3	0.291	0.3	0.457
WCHB1-05	-2.3	0.000	-0.5	0.677	-0.3	0.713	0.2	0.896	NA	NA	-1.8	0.046
Dehalococcoides	-3.1	0.000	0.1	0.942	0.1	0.761	0.1	0.896	-3.3	0.000	-3.3	0.000
Clostridiales	2.2	0.000	0.8	0.572	0.0	0.996	-1.2	0.850	0.5	0.545	2.1	0.001
Sedimentibacter	-0.6	0.009	-0.1	0.942	-0.3	0.574	-0.1	0.896	-0.6	0.023	-0.4	0.285
Christensenellaceae	-5.2	NA	0.1	NA	0.1	NA	-0.2	NA	-6.4	NA	-4.3	NA
Coprococcus	1.3	0.026	NA	NA	0.5	0.703	2.6	0.046	3.6	0.006	0.1	0.872
Ruminococcaceae	-0.7	0.044	0.3	0.715	0.4	0.574	0.3	0.896	-1.0	0.082	-1.3	0.018
Oscillospira	1.8	0.000	0.8	0.572	0.8	0.392	-0.1	0.896	0.5	0.538	0.6	0.441
Veillonellaceae	0.5	0.006	-0.2	0.677	-0.1	0.761	0.1	0.896	0.6	0.006	0.5	0.175
Desulfovibrionaceae	-0.1	0.751	0.0	0.942	-0.2	0.703	-0.1	0.896	-0.2	0.082	0.0	0.872
Desulfovibrio putealis	0.5	0.169	-0.1	0.942	0.0	0.996	0.2	0.896	0.5	0.538	0.4	0.457
Desulfovibrionaceae - other	-0.7	0.679	0.1	0.942	-0.3	0.761	-0.5	0.896	-1.1	0.538	-0.5	0.700
Treponema	0.0	0.729	0.0	0.942	-0.2	0.574	-0.1	0.896	-0.1	0.538	0.1	0.849
vadinCA02	0.0	0.935	-0.2	0.942	0.2	0.846	0.6	0.896	0.4	0.731	-0.3	0.704
Unassigned	-4.3	NA	0.1	NA	0.0	NA	-0.5	NA	-5.3	NA	NA	NA

4.3.3.3 Reductive dechlorination of axenic Dehalococcoides

As the previously described experiments were performed with mixed cultures, it is impossible to determine whether *Dehalococcoides* was directly affected by PFAAs, or if another subset of the community upon which *Dehalococcoides* is dependent was affected. For example, it is not clear whether *Methanobacterium* excels in the presence of PFAAs or if *Methanobacterium* fills the niche resulting from *Dehalococcoides* inhibition. To understand whether *Dehalococcoides* is directly affected by PFAA exposure, the TCE dechlorination experiment was repeated with *Dehalococcoides* in pure culture. With *Dehalococcoides mccartyi* strain 195 maintained axenically, the inhibitory effects of PFAAs on TCE dechlorination behavior was similar to that of the more complex methanogenic community (**Figure 4-15**). The rates of production and dechlorination of each solvent with *Dehalococcoides* in pure culture further illustrate increasing degrees of inhibition with increasing PFAA content (**Table 4-8**).

Table 4-8. Dechlorination (-) and production (+) rates by axenic *Dehalococcoides*

	Rates (µmol/day)*			
	TCE (day 3-6)	**cDCE (day 1-6)**	**VC (day 5-10)**	**Ethene (day 0-10)**
No PFAAs	-2.5 ± 0.2	+1.3 ± 0.1	+0.8 ± 0.1	0.0 ± 0.0
22 mg/L	-2.1 ± 0.6	+1.1 ± 0.1	+0.7 ± 0.1	0.0 ± 0.0
66 mg/L	-1.2 ± 0.4	+0.5 ± 0.1	+0.6 ± 0.3	0.0 ± 0.0
110 mg/L	-0.6 ± 0.2	0.0 ± 0.0	0.0 ± 0.0	0.0 ± 0.0
Abiotic	-0.4 ± 0.1	0.0 ± 0.0	0.0 ± 0.0	0.0 ± 0.0

*Values represent triplicate averages ± standard deviation

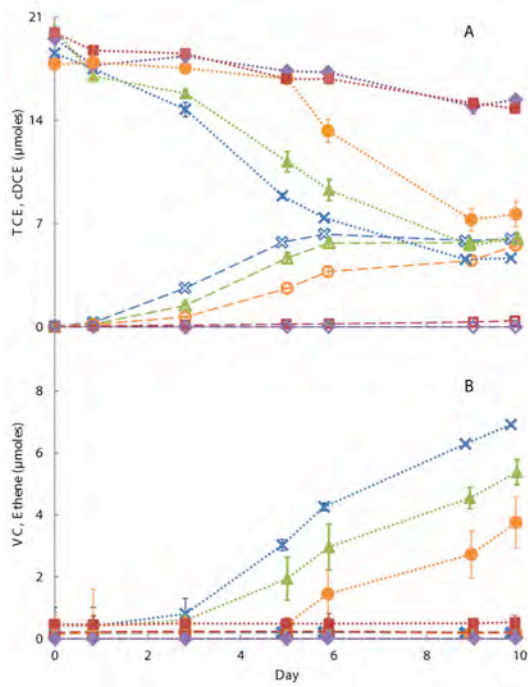

Figure 4-15. Dechlorination by *D. mccartyi* strain 195 in the presence of PFAAs. Panel **A** shows TCE profiles with the solids symbols and cDCE with the open symbols. Panel **B** shows VC (solid) and ethene (open). Inhibition of dechlorination is observed with 110 mg/L total PFAAs (red squares) and behaves similarly to the abiotic control (purple diamonds). Slower rates of dechlorination and production were observed for 66 mg/L total PFAAs (orange circles) with mild inhibition at 22 mg/L total PFAAs (green triangles) compared to no PFAAs (blue x's). Error bars represent the standard error of triplicate incubations.

Pronounced inhibition was observed at 110 mg/L with a significant reduction in TCE dechlorination rates for this concentration as compared to dechlorination rates devoid of PFAAs ($p<0.01$) (**Table 4-8**, **Figure 4-15**). Correspondingly, minimal cDCE and VC production occurred with 110 mg/L. Ethene generation was not observed above the background from inoculation carry-over in any of the treatments, which may be explained by the inefficiency of *Dehalococcoides* in pure culture (He *et al.*, 2007), coupled with TCE presence across these incubations. The dechlorination of TCE is more energetically favorable than that of VC, therefore significant generation and subsequent dechlorination of VC is not expected to occur if TCE remains in the system (Aulenta *et al.*, 2008). TCE dechlorination rates with 66 mg/L PFAAs were also significantly inhibited when contrasted with systems without

PFAAs ($p<0.01$). A delayed rate of cDCE and VC production was observed at 66 mg/L, although rates of VC production were similar between 66 mg/L and the case without PFAAs. At 22 mg/L total PFAAs, the average TCE dechlorination rate was lower than the system lacking PFAAs, yet the inhibition of the rate was not statistically significant (**Figure 4-15**). Correspondingly, both cDCE and VC production rates were slightly retarded at 22 mg/L, although the difference did not maintain statistical significance.

4.3.4 Environmental Implications

Understanding reductive dechlorination in the presence of PFAAs is of environmental concern due to the common co-location of PFAAs and chlorinated solvents, and the reliance on microbiological processes for chlorinated solvent attenuation. Concentrations up to 7 mg/L for PFOA in groundwater have been measured; a choice of 10 mg/L of each analyte as investigated here may be representative of a source zone or subsurface worst-case scenario (Moody and Field, 2000), especially considering increases in environmental detection and measurement sensitivity of a variety of PFASs (Rotander *et al.*, 2015). Additionally, increased PFAA sorption in the presence of NAPLs has been observed, particularly at higher PFAA concentrations (Guelfo and Higgins, 2013; McKenzie *et al.*, 2016). This may result in an accumulation of PFAAs where TCE is present, even outside of source zones. It is also known that PFAA precursors found in AFFF may generate additional PFAAs in groundwater over time (Houtz *et al.*, 2013). As the depth of knowledge regarding the concentration and distribution of PFAAs is continually growing, this is a current approximation of what may be observed near a source zone *in situ*. Based on the results from this study, it is clear that dechlorination of TCE is significantly inhibited both within the dechlorinating mixed community and with *Dehalococcoides* in pure culture at these high concentrations reflective of PFAA source zones or areas of NAPL co-contamination. Phylogenetic investigations revealed that the presence of PFAAs at high concentrations directly impacts *Dehalococcoides'* relative abundance and has a varied effect on the composition of the methanogenic mixed community.

It has been observed elsewhere that dechlorinating communities provided with acetate, lactate, or methanol as electron donors appear to be phylogenetically distinct from one another. These different communities, however, still exhibit conserved metabolic pathways, particularly for methionine and corrinoid synthesis, fermentation, and oxygen scavenging (Hug *et al.*, 2012). This implies that although community shifts may occur in the presence of PFAAs, the machinery required to facilitate *Dehalococcoides* growth and dechlorination may still be provided, suggesting that there exists a degree of functional redundancy within the methanogenic mixed culture. Exploring the putative functions of the mixed methanogenic communities may not necessarily provide the single key to the mechanisms behind the repression of *Dehalococcoides*; however, this is an important step in understanding the effects of PFAAs on environmentally relevant systems. To understand whether particular processes or functions are affected by PFAA presence, additional exploration such as proteomics or functional metagenomics may be utilized to understand the impacts of PFAA exposure.

The parallel observations of impacts on reductive dechlorination by *Dehalococcoides* both axenically and in community incubations confirm that source-level concentrations of PFAAs will

have a direct impact on *Dehalococcoides.* However, due to the variation in community responses, it is difficult to ascertain the mechanisms affecting the repression of *Dehalococcoides*. This repression could potentially be attributed to a stress response (Weathers *et al.*, 2015) or inhibition of vitamin B_{12} uptake (Hug *et al.*, 2012; He *et al.*, 2007). For example, vitamin B_{12}, in the form of cyanocobalamin, is a required enzymatic cofactor for reductive dehalogenases (Men *et al.*, 2013), and contains both a cyano group and 5'6'-dimethylbenzimidazole as the lower ligand (Yan *et al.*, 2013). *Dehalococcoides* growth can be hindered by changing the type of lower ligand (Men *et al.*, 2013; He *et al.*, 2007); one might hypothesize that if PFAAs chemically interact with this lower ligand, it may be converted to a form that is unusable for *Dehalococcoides*. While we do not expect or observe any defluorination, there is evidence of potential physicochemical interactions between PFAAs and vitamin B_{12}, though the coordination is not well understood (Ochoa-Herrera *et al.*, 2008). At 110 mg/L PFAAs, there are four orders of magnitude more PFAAs present ($3x10^{-4}$ mol/L) than vitamin B_{12} amendments ($7x10^{-8}$ mol/L) which could result in a deficit for use by *Dehalococcoides* (He *et al.*, 2007; Yan *et al.*, 2013). Future work to examine the effects of increasing vitamin B_{12} dosage in the presence of high concentrations of PFAAs or the quantification of cobalamin lower ligand moieties could help elucidate this potential interaction and explore its relevance to subsurface settings.

In summary, this study addresses the impacts of PFAAs on the enhanced reductive dechlorination of TCE and a community responsible for that process. PFAAs and TCE are environmental pollutants, the former is recalcitrant and not easily remediated; the latter is often treated with bioremediation via reductive dechlorination. Interestingly, high concentrations, similar to what may be found near a PFAA source zone, significantly inhibit TCE dechlorination by directly repressing *Dehalococcoides.* Because of *Dehalococcoides'* role in reductive dechlorination, suppression of *Dehalococcoides* growth may result in an accumulation of VC, especially if other dechlorinators that are not capable of attenuating this carcinogen, such as *Geobacter*, are active and unaffected (Hug *et al.*, 2012). In sites that are co-contaminated with both chlorinated solvents and PFAAs, biostimulation or bioaugmentation to enhance reductive dechlorination processes may not be the most suitable option for solvent remediation. Additionally, if ERD is the current cleanup strategy for chlorinated solvents and is observed to be ineffective, the presence of coexisting PFAAs may be the cause of inhibition. These results underscore the need for complete site investigation, monitoring, and exploration to ensure continued chlorinated solvent bioremediation in locations that may contain PFAAs.

4.4 Impacts of ISCO on PFAA Sorption in Batch Systems (*Task 3c*)

4.4.1 Background

At remediation sites where *in situ* chemical oxidation is utilized as the technology for remediation of hydrocarbons or chlorinated solvents, the resulting changes in environmental conditions caused by ISCO could alter fate and transport behavior of PFAAs. Bench-scale batch experiments were designed to mimic these environmental conditions and determine if there are any changes in sorption behavior of PFAAs. Common chemical oxidants, potassium permanganate ($KMnO_4$) and sodium persulfate (NaS_2O_8), were initially chosen due to their wide use and contrasting reaction mechanisms. TCE was chosen as the co-contaminant in the batch

experiments. Two additional batch experiments with $KMnO_4$ examine the sorption behavior without TCE and in an aqueous only environment. It was expected that sorption would likely decrease during ISCO due to loss of organic material and this is being examined in these four experiments.

4.4.2 Materials and Methods

4.4.2.1 Materials

Native spiking solutions (and stable isotope surrogates) contained standards of PFBA, PFPeA, PFHxA, PFHpA, PFOA, PFNA, PFDA, PFBS, PFHxS, and PFOS, prepared as in *Task 2* (**Table 2-1**). Analytical standards were purchased from Wellington Laboratories. Stock solutions of these analytes and the surrogate standards were prepared in a 70/30 (v/v) methanol/aqueous ammonium hydroxide (0.01%) solution. Soil A was purchased from Agvise Laboratories and sieved to 2mm. Artificial ground water (AGW) was prepared as per *Task 1* and *Task 2*. High purity $KMnO_4$, $Na_2S_2O_8$, iron(II) chloride, citric acid, TCE, sulfuric acid, ferrous ammonium sulfate and ammonium thiocyanate were utilized in the batch experiments. Optimal grade methanol along with acid optima grade methanol (1% acetic acid) and basic optima grade methanol (1% ammonium hydroxide) were used to quench the oxidation reactions. Last, 60 mL glass centrifuge tubes were used to be inert to the oxidation reactions and TCE in the system.

4.4.2.2 Experimental Conditions

The batch experiments were set up with sacrificial reactors and sampling points at 0 day (a pre-oxidation), 1 day, 7 days, and 28 days. For experiments using $KMnO_4$ and $Na_2S_2O_8$, the batch reactors containing soils had 15 grams of soils, 50 mL of AGW (with 1 g/L sodium azide to eliminate any biological activity) and 2.5 µg/L of the native PFAA mixture spiked into the aqueous phase. Reactors without soil contained 58 mL of AGW and 2.5 µg/L of the native PFAA mixture. Reactors with a co-contaminant contained 1 mL of TCE. Prior to the addition of oxidants, reactors were equilibrated for 10 days with the loamy sand, AGW, and native PFAA mixture. After this 10-day equilibration period, the reactors were spun in a centrifuge and a 1350 µL of aliquot aqueous sample was removed from each reactor and prepped for LC-MS/MS analysis. The aliquot of 1350 µL was replaced with fresh AGW, which was assumed to lead to minimal change in aqueous concentrations in the reactors. Each oxidant was then added at 10 g/L to the appropriate reactors (Siegrist *et al.*, 2011), and reactors with $Na_2S_2O_8$ were also activated with activation agents in 10:5:1 molar ratio of persulfate/iron II/chelate [citric acid] (Liang, 2004).

After addition of the oxidants, reactors were opened every 15-30 minutes for 4 hours to let the gases escape. The reactors were vortexed and placed sideways on a shaker table. After 24-hours, the first set of sacrificial reactors were sampled using the following sampling process. The reactors were centrifuged for 20 minutes at 1200 RCF, and the pH of each reactor was measured. Samples for analysis were prepared by placing 810 µL of aqueous solution from the reactor and into a microcentrifuge tube with 810 µL of methanol to quench any further reaction of the oxidant. This quenching methanol composition was dependent on the pH of the aqueous phase: a pH reading of 1-4 used basic methanol, 4.1-10 used methanol and higher than 10.1 used acidic

methanol. Lastly, 180 µL of the 2ng/mL surrogate solution were added to the microcentrifuge tubes and vortexed for 10 seconds. Following sample preparation in the microcentrifuge tube, all samples were microcentrifuged for 30 minutes at 1330 rpm. The centrifuged samples were then placed in a 2 mL auto-sampler vial for analysis by LC-MS/MS.

The $KMnO_4$ concentration in the appropriate reactors was determined by a plate reader spectrometer. A 200 µL aliquot from each reactor was placed in triplicate in the plate reader and compared to a calibration curve. The absorbance for $KMnO_4$ was read at a wavelength 530nm. Reactor samples with $Na_2S_2O_8$ underwent additional preparation to determine oxidant concentration by the plate reader spectrometer. The absorbance was read at a wavelength of 450 nm after sample preparation. A 100 µL aliquot of reactor solution was added to a 20 mL polypropylene tube. To this, 900 µL of de-ionized (DI) water, 10 mL of 2.5 N sulfuric acid and 100 µL of 0.4 N ferrous ammonium sulfate solution were added to each polypropylene tube. The solution was vortexed for 10 seconds then reacted for 40 minutes. After 40 minutes 200 µL of 0.6 N ammonium thiocyanate was added (Huang, 2002). Lastly, a 200 µL of the new solution was measured for absorbance on the plate reader. LC-MS/MS analysis for PFAAs was conducted using methods reported in *Tasks 1* and *Tasks 2*.

4.4.3 Results and Discussion

4.4.3.1 PFAA Sorption

Results of *Task 3*c single-point K_d measurements were used to confirm previously observed PFAA trends and to compare to *Task 2* observations (**Table 4-9**). All *Task 3c* single-point K_d (L/kg) values were calculated from measured soil (C_s, mg/kg) and aqueous phase (C_w, mg/L) concentrations as follows:

$$K_d = C_s / C_w \qquad \text{(eqn. 4-1)}$$

Task 2 batch equilibrium isotherm results were used in *Task 3c* as a basis of comparison for the impacts of remedial agents on batch equilibrium systems as well as to check the consistency of single-point K_d measurements where *Task 3c* conditions mirrored those used in *Task 2*. For comparison to *Task 2* sorption results, two sets of concentration-specific K_d values were calculated using the Freundlich sorption coefficient (K_f) and n values measured in *Task 2* isotherms in soil A (**Appendix A-1**). The first utilized K_f and *n* values measured in soil A and the second utilized isotherm parameters measured in soil A amended with TCE (*Task 2*). Concentration-specific K_d factors were calculated using equation 4-1, where C_s was determined from C_w values measured in *Task 3c* as follows:

$$C_s = K_f C_w^n \qquad \text{(eqn. 4-2)}$$

In general, PFAA sorption in *Task 3c* was chain length dependent for long-chain (≥C6) compounds. PFBA, PFPeA, and PFHxA exhibited the same notable behavior observed in *Task 2*. Sorption of PFBA was similar to that of PFHpA or PFOA, decreased from PFBA to PFHxA, and then followed the chain-length dependent trend observed in *Task 2*. Generally, K_d values measured in soil A+TCE were not statistically different in *Tasks 2* and *3c*, though minor

exceptions occurred for PFPeA and PFOA, where *Task 3c* values were statistically lower than those from *Task 2*.

Table 4-9. Single-point K_d values from *Task 3* batch chemical oxidant tests as compared to *Task 2* results

Analyte	Task 2				Task 3									
	Log K_d		Log K_d + TCE		Log K_d + TCE		Log K_d + MnO_4		Log K_d + $S_2O_8^-$		Log K_d + MnO_4 + TCE		Log K_d + $S_2O_8^-$ + TCE	
	(L/kg)	±	(L/kg)	±	(L/kg)	±	(L/kg)	±	(L/kg)	±	(L/kg)	±	(L/kg)	±
PFBA	-0.10	0.12	0.08	0.25	-0.15	0.15	0.23	0.09	0.11	0.05	-0.04	0.11	0.04	0.10
PFPeA	-0.53	0.09	0.10	0.09	-0.26	0.07	-0.54	0.07	-0.55	0.05	-0.44	0.10	-0.34	0.02
PFHxA	-0.71	0.16	-0.64	0.19	-0.41	0.20	-0.28	0.10	-0.08	0.11	-0.04	0.05	-0.31	0.11
PFHpA	-0.32	0.09	-0.57	0.09	-0.41	0.11	-0.01	0.05	-0.02	0.02	-0.41	0.05	0.02	0.03
PFOA	-0.05	0.13	0.12	0.12	-0.29	0.09	-0.19	0.02	0.51	0.06	-0.33	0.05	0.55	0.10
PFNA	0.47	0.13	0.35	0.56	0.26	0.13	0.29	0.29	1.25	0.27	0.40	0.04	1.26	0.06
PFDA	1.03	0.03	0.80	1.27	0.32	0.26	-0.08	0.06	1.56	0.22	0.42	0.08	1.48	0.15
PFBS	-0.02	0.07	-0.18	0.10	-0.24	0.07	-0.19	0.06	-0.17	0.03	-0.35	0.05	-0.17	0.07
PFHxS	0.11	0.13	-0.15	0.09	-0.20	0.06	-0.26	0.04	0.26	0.02	-0.24	0.05	-0.24	0.05
PFOS	0.94	0.08	0.49	1.53	0.81	0.10	0.12	0.01	1.81	0.09	0.88	0.06	0.88	0.06

4.4.3.2 Impact of Permanganate

The impacts of oxidant on PFAA sorption were measured in soil A and soil A+TCE in systems with $KMnO_4$. Sorption in each system was measured at 1, 7, and 14 days to determine changes with time and 14-day results from each type of system were compared. There was no statistical difference in K_d values with time measured in the presence of $KMnO_4$ in either soil A or soil A+TCE (**Figure 4-16**). In general, <1% of oxidant remained in solution by 1 day indicating that oxidant was mostly spent in advance of the first K_d measurement in the time series and no further changes were occurring in the system. Similarly, pH stayed consistent in soil A and soil A+TCE through the duration of the time series. Constant K_d measurements are consistent with the stable f_{oc} and pH of the systems.

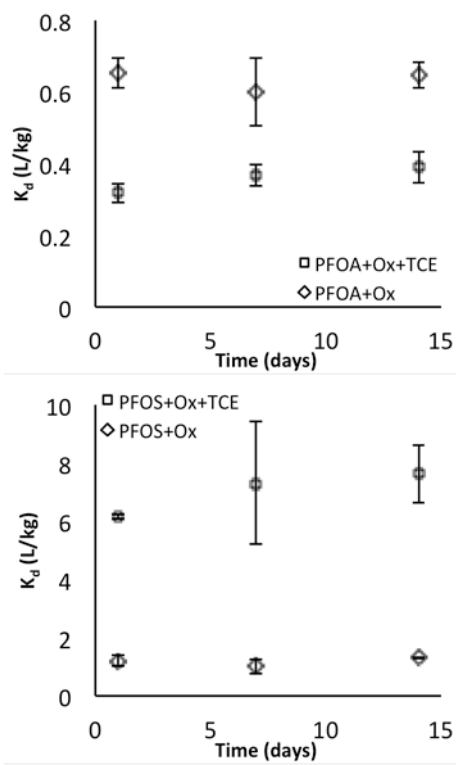

Figure 4-16. Trends in PFOA and PFOS K_d values with time after $KMnO_4$ addition to systems with (squares) and without (diamonds) TCE.

The addition of $KMnO_4$ appeared to have a chain-length dependent impact on sorption of compounds to soil A compared to systems where no $KMnO_4$ was present. Increases in K_d were measured for PFBA and PFHxA, K_d was unchanged for PFPeA, PFHPA, PFDA, PFBS, and PFHxS, and decreases in sorption were observed for PFDA, PFBS, PFHxS, and PFOS (**Figure 4-17**). In soil A+TCE, no changes occurred to sorption with the addition of $KMnO_4$,

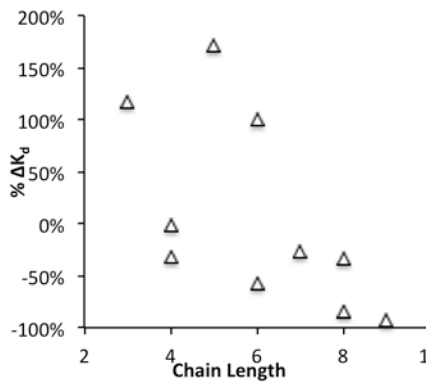

Figure 4-17. The percent change in K_d values between systems with no MnO_4 and 10 g/L $KMnO_4$ vs. PFAA chain length in soil A.

with the exception of an increase measured for PFHxA. The addition of $KMnO_4$ has the potential to destroy or change the physical characteristics of the organic matter in soil A (Siegrist *et al.*, 2011). Previous work has found that f_{oc} was reduced up to 63% in media treated with ~10 g/L of $KMnO_4$, with reductions of 20-25% being more typical (Siegrist *et al.,* 2011). If a simple reduction in f_{oc} was the primary factor impacting PFAA sorption with $KMnO_4$ addition, K_d factors would be expected to decrease by an equal magnitude for all compounds. Deposition of MnO_2 may either block or provide sorption sites. It is also possible that $KMnO_4$ preferentially targets some organic matter functional groups over others (Siegrist *et al.,* 2011). For example, if the most hydrophobic functional groups were targeted, then the greatest impacts to sorption might occur for the longest chain length PFAAs, as was observed here. It is unclear what may have caused increases in sorption of smaller PFAAs. Previous work has observed increases in K_d in systems treated with $KMnO_4$, though causes of the increase were unclear (Siegrist *et al.,* 2011). As noted in *Task 2*, there may be a subset of organic matter sites only accessible to short-chain PFAAs. It is possible that $KMnO_4$ addition increases the relative number or accessibility of such sites, though additional organic matter characterization would be required to determine this with certainty.

4.4.3.3 Impacts of Persulfate

The impacts of oxidant on PFAA sorption were measured in soil A and soil A+TCE in systems with $Na_2S_2O_8$. Sorption in each system was measured at 1, 7, and 14 days to determine changes with time and 14-day results from each type of system (PFAA, PFAA+ $Na_2S_2O_8$, PFAA+ $Na_2S_2O_8$+TCE) were compared. There was no statistical difference in K_d values measured with time in the presence of $Na_2S_2O_8$ in either soil A or soil A+TCE (**Figure 4-18**). Residual oxidant was much higher (40%±12%) in systems with $Na_2S_2O_8$ vs. $KMnO_4$, but it still remained consistent with time. Similarly, pH was much lower in $Na_2S_2O_8$ systems (2.56±0.15) vs. $KMnO_4$ for both soil A and soil A+TCE, but this value remained constant through the duration of the experiment. Impacts of lower pH will be discussed below, but stable residual oxidant amounts and solution pH are consistent with constant K_d values throughout the 14-day time period.

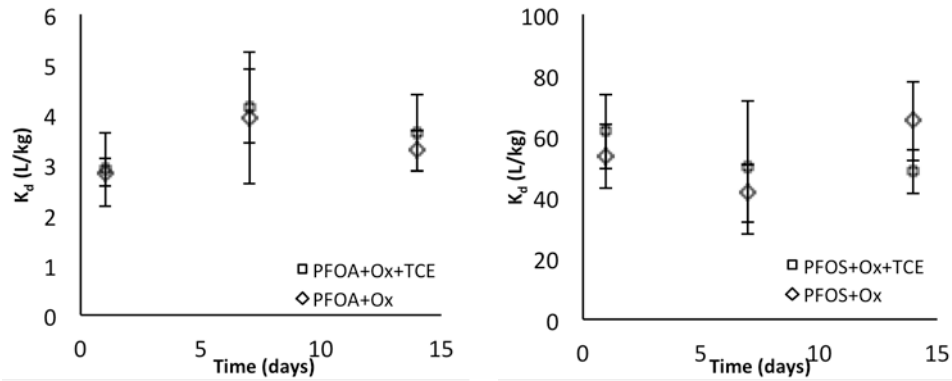

Figure 4-18. Trends in PFOA and PFOS K_d values with time after $Na_2S_2O_8$ addition to systems with (squares) and without (diamonds) TCE.

The addition of $Na_2S_2O_8$ caused chain length dependent trends in K_d in both soil A and soil A+TCE compared to systems where no oxidant was present. In general, increases in sorption were larger for longer chain length compounds in both soil A and soil A+TCE (**Figure 4-19**). Increases in sorption of PFHpA, PFOA, PFNA, and PFDA occurred in soil A and soil A+TCE as well as PFBA, PFHxA, and PFOS in soil A. No statistically significant changes to sorption of PFPeA or PFHxS occurred with $Na_2S_2O_8$ addition to either soil A or soil A+TCE as well as PFBS and PFOS in soil A+TCE. Previous work has shown that $[Na^+]$ does not impact PFAA sorption (Higgins and Luthy, 2006). However, addition of $Na_2S_2O_8$ caused significant decreases in batch reactor solution pH. Throughout the 14-day sampling period, systems had a pH<3 as compared to pH 5-7 for systems with no oxidant or with $KMnO_4$. A decrease in pH may impact sorption of PFAAs in two ways. There is debate in the literature regarding the pK_a of PFAAs, but there is general agreement that the values will be low (e.g. pK_a<3.5; Burns *et al.,* 2008, Goss, 2008). The lower the pH of a system, the higher the percentage of PFAAs present in the neutral form, potentially leading to an increase in sorption through van der Waals (e.g. hydrophobic) effects. Sorbent surface charge may also change with pH leading to a reduction in electrostatic repulsion between negatively charged PFAAs and negatively charged organic matter (Higgins and Luthy, 2007). At the observed pH, it is possible that both of these factors are leading to an increase in sorption when $Na_2S_2O_8$ is present.

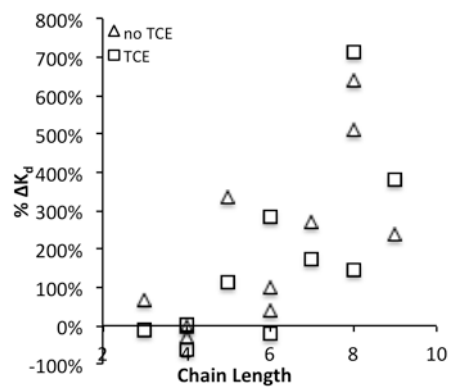

Figure 4-19. The percent change in K_d values between systems with no $S_2O_8^-$ and 10 g/L $S_2O_8^-$ vs. PFAA chain length in soil A (triangles) and soil A+TCE (squares).

These relationships can be used to try and predict changes in K_d with changing pH using *Task 2* K_d values measured in the absence of oxidant (**Figure 4-20**). The magnitude of increase in sorption measured in this study is close to the value predicted for PFNA using previous work. Increases to sorption of PFDA and PFOS are less than what would be predicted; however, previous studies only included sorption at pH ≈ 6-7.5. It is unclear whether these relationships would extend to lower pH values. In addition, predicted values account solely for changes in pH whereas it is possible that the $Na_2S_2O_8$ has other impacts to the system such as a reduction in f_{oc}, and resulting lowering of K_d as noted for systems with $KMnO_4$. If changes in pH and changes in f_{oc} were occurring simultaneously, sorption may increase to a lesser degree than would be predicted based on pH changes alone. Finally, the observed changes in sorption with $Na_2S_2O_8$ addition were chain-length dependent. Due to the limited number of PFAAs included in previous studies of the impact of pH on sorption, it is unclear whether pH impacts are chain-length dependent or whether this trend is the result of the additive effects of pH and other mechanisms such as changes in f_{oc}. Additional studies of solution chemistry impacts to PFAA sorption would be required to determine with certainty.

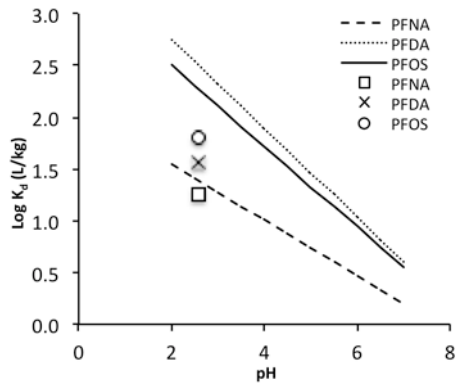

Figure 4-20. Predicted changes (lines) in log K_d with pH along with measured log K_d values (symbols) at pH ≈ 2.6 for PFNA, PFDA, and PFOS.

4.4.3.4 Data Considerations and Conclusions

All K_d values presented herein are calculated from measured soil and aqueous PFAA concentrations; however, there were some challenges in QA/QC of these data. Internal standard recovery in both the solid and aqueous phase samples were low (<50%) in many instances. Additionally, control experiments (aqueous phase only) showed recoveries of <10% of PFAA mass in the aqueous phase, which is atypical of PFAA loss to vial as shown in experiments from *Task 2*. Finally, a mass balance of PFAA recovery between the aqueous phase, solid phase, and loss to vial was low for many samples. These considerations led to the conclusion that additional efforts related to examining the impact of ISCO on the sorption of PFAAs to solid phases would best be evaluated in flow-through (i.e., column) conditions. Thus, project effort was shifted to *Task 4*.

5. FLOW-THROUGH TRANSPORT AND REMEDIATION EXPERIMENTS

5.1 Introduction (*Task 4*)

To build off the results of *Task 2* and *Task 3*, bench-scale flow-through experiments were conducted using 1-D columns. Flow through experiments enabled the integration of various equilibrium processes into a more realistic groundwater-flow scenarios. The intent was to examine the validity of employing PFAA-transport data obtained from batch experiments for simulating behavior in a model groundwater system during ambient conditions or those imposed during remediation. Specifically, flow-through experiments were designed to address the following subtasks:

Task 4a: PFAA Transport under Unaltered Conditions. One-dimensional flow-through column experiments were conducted to confirm and explore findings from *Task 2*. These experiments evaluated the transport of PFAAs under unaltered conditions. Though initial plans indicated that these experiments would also examine the impact of co-contaminants (e.g., NAPL) on PFAA transport, these NAPL experiments were incorporated into *Task 4c* (below).

Task 4b: PFAA Transport during Enhanced and Natural Bioattenuation of COCs. Flow-through column systems were designed to mimic relevant bioremediation conditions.

Task 4c: PFAA Transport during ISCO Treatment of NAPLs. One-dimensional flow-through column experiments were conducted to confirm and explore findings from *Task 2* and *Task 3*. These experiments evaluated the transport of PFAAs under unaltered conditions both in the presence and absence of NAPL, but also with and without the application of ISCO.

5.2 Relevant Advective Transport Theory

The advection-dispersion equation (ADE) describing solute transport with one-dimensional flow in a homogeneous, isotropic media where the solute undergoes ideal sorption is as follows:

$$R\frac{\partial C}{\partial P} = \frac{1}{P}\frac{\partial^2 C}{\partial X^2} = \frac{\partial C}{\partial X} \qquad \text{(eqn. 5-1)}$$

$$P = vL/D \qquad \text{(eqn. 5-2)}$$

$$X = x/L \qquad \text{(eqn. 5-3)}$$

$$p = vt/L \qquad \text{(eqn. 5-4)}$$

where C is the aqueous solute concentration, t is time, P is the Peclet number, x is distance, v is the pore water velocity, D is the dispersion coefficient, and L is the column length (Fetter, 1999). Other processes including transformation and degradation, often represented in this equation, are

not expected to play a role in PFAA transport. Analytical solutions to this equation are particularly useful when evaluating breakthrough curves (BTCs) of conservative solutes (R=1) to obtain values for the Peclet number evaluating hydrodynamic properties of a column. When solute transport is influenced by nonideal sorption, resulting from factors such as rate-limited sorption, different parameters must be evaluated in order to describe contaminant transport. In such instances, sorption may be represented by a two-stage approach that includes a solute fraction that sorbs quickly and reaches instantaneous equilibrium and a fraction that undergoes slow uptake (Cameron and Klute, 1977; Lee *et al.,* 1988; Brusseau *et al.*, 1989):

$$S_T = S_1 + S_2 = FK_dC + (1-F)K_dC \qquad \text{(eqn. 5-5)}$$

where F is fraction of solute that undergoes instantaneous sorption and K_d is the soil-water partitioning constant (Brusseau *et al.*, 1989). The nondimensional ADE that governs transport of solutes undergoing two-site sorption may be written as follows:

$$\frac{\partial C^*}{\partial p} + (\beta R - 1)C^* \frac{\partial C^*}{\partial p} + (1-\beta)R\frac{\partial S^*}{\partial p} = \frac{1}{P}\frac{\partial^2 C}{\partial X^2} - \frac{\partial C^*}{\partial X} \qquad \text{(eqn. 5-6)}$$

$$(1-\beta)R\frac{\partial S^*}{\partial p} = \omega(C^* - S^*) \qquad \text{(eqn. 5-7)}$$

where the following dimensionless parameters may be defined:

$$C^* = C/C_0 \qquad \text{(eqn. 5-8)}$$

$$S^* = S_1/(1-F)K_dC_0 \qquad \text{(eqn. 5-9)}$$

$$R = 1 + (\rho_b/\theta)K_dC_0 \qquad \text{(eqn. 5-10)}$$

$$\beta = [1 + (\rho_b/\theta)FK_dC_0]/R \qquad \text{(eqn. 5-11)}$$

$$\omega = [k(1-\beta)RL/v] \qquad \text{(eqn. 5-12)}$$

where k is the mass transfer rate coefficient (Lee *et al.,* 1988; Brusseau *et al.*, 1989).

Processes impacting column contaminant transport are often determined by inspecting the shapes of BTCs, but it can be difficult to distinguish between the various factors influencing transport (e.g. diffusion, physical nonequilibrium, rate-limited sorption). Flow interruption experiments are useful in distinguishing among rate-limited processes. Contaminant pulses are input until C* approaches one, flow is discontinued for a period of time, after which flow is resumed. Changes that occur in C* while flow is discontinued can help distinguish between various processes that may be occurring. If a nonreactive tracer is used and a drop in C* occurs during flow interruption, this indicates heterogeneity or physical nonequilibrium in the column. There are portions of the column in which slow- or no-flow conditions exist, and when flow is interrupted, diffusion of the nonreactive tracer into the slow- or no-flow portions occurs, reducing C*

(Brusseau *et al.*, 1989). In these preliminary studies for *Task 4a*, flow interruption experiments with a nonreactive tracer were used to ensure that such conditions did not impact compound transport in the columns.

When physical heterogeneities are not present, a drop in C* of a reactive compound during flow interruption indicates transformation or rate-limited sorption. In the case of PFAAs where transformation will not occur, the latter is of primary concern. The drop in C* occurs because sorption of the compound continues during flow interruption (Brusseau *et al.*, 1989). Not only can this method be used to determine what processes are occurring, but it can provide more reliable measurements of the *k* values associated with rate-limited processes. Flow interruption experiments can be used to measure values of *k* for various PFAA and in solid phases with varying organic carbon content (f_{oc}) to determine how compound structure and sorbent properties may impact sorption kinetics.

5.3 Transport Potential of Perfluoroalkyl Acids (PFAAs) at AFFF-impacted Sites: Column Experiments and Modeling (*Task 4a*)

5.3.1 Background

Under equilibrium conditions, PFAA transport potential is expected to decrease with increasing chain length with important exceptions for short chain (≤ 6 CF_2) PFAAs (Guelfo and Higgins, 2013). Similar qualitative trends were observed in experiments that studied the leaching behavior of PFAAs from soil in flow through column experiments (Gellrich *et al.,* 2012). Results of these studies may be used to make initial qualitative predictions of PFAA transport in an advective scenario; however behavior may differ if equilibrium conditions do not apply. In addition, the extent to which previous equilibrium studies can quantitatively predict PFAA transport is unknown.

In ideal transport, sorption is presumed to be instantaneous under the assumption that it occurs at much faster rates than the residence time of groundwater (Brusseau 1994). However, sorption and desorption can be rate-limited (Brusseau 1994). Various mechanisms have been proposed to explain this behavior, including interactions with organic matter (Sander and Lu, 2006). Rate-limited transport is sometimes characterized by early breakthrough and/or tailing of compounds in column breakthrough curves (BTCs; Brusseau, 1992). When rate-limited sorption occurs, contaminant plumes can have lower peak concentrations but persist for longer periods above a regulatory limit. Thus, understanding the kinetic nature of sorption is important for enhancing our conceptual models of real sites, and possible also for modeling transport and making plume predictions. Flow interruption column experiments, wherein flow through a column is stopped for a period of time (to allow conditions to progress towards sorbate-sorbent equilibrium) and then resumed, are useful in making a definitive determination of rate-limited sorption (Brusseau, 1994). Flow interruption experiments are also often conducted at high pore-water velocities to experimentally exaggerate any kinetic effects. If aqueous concentrations decrease during the stop flow period, this can indicate physical or chemical nonequilibrium. Bromide tracer tests are used to verify the absence of physical nonequilibrium in the column, such that drops in concentration of the compound of interest should confirm ongoing (e.g. rate-limited) sorption.

The objective of this work was to further the understanding of transport behavior of perfluoroalkyl carboxylates (PFCAs) and perfluoroalkyl sulfonic acids (PFSAs) in groundwater by investigating advective transport in 1-dimensional (1-D) column experiments. We conducted continuous flow column experiments at environmentally relevant pore-water velocities to determine if previously measured batch equilibrium data could be used to accurately describe PFAA transport. Flow interruption experiments were completed at higher pore water velocities to determine if rate-limited sorption influenced PFAA transport. Results of flow interruption and continuous flow experiments were used to determine mass transfer coefficients describing rate-limited transport. Lastly, the results of this study were used in combination with mathematical modeling to explore the implications of the experimental studies to transport and remediation of PFAAs under realistic site conditions.

5.3.2 Experimental Methods and Approach

5.3.2.1 Materials

Calibration standards of PFBA, PFPeA, PFHxA, PFHpA, PFOA, PFNA, PFDA, PFBS, PFHxS, and PFOS, as well as stable-isotope surrogate standards (**Table 5-1**) were purchased from Wellington Laboratories (Guelph, Ontario, Canada). Spiking solutions for all experiments were prepared from standards of PFCAs and PFSAs purchased from Sigma-Aldrich (St. Louis, MO). Stock solutions of calibration standards, spiking standards (purity-corrected), and surrogate standards were prepared in a 70/30 (v/v) methanol/aqueous solution. Unless otherwise noted, all experiments utilized a spiking solution containing all 10 PFAAs. Potassium bromide was used as a nonreactive tracer. Unless otherwise specified, all other chemicals were of reagent grade and were purchased from Thermo Fisher Scientific (Waltham, MA), Mallinckrodt Pharmaceuticals (St. Louis, MO), or Sigma-Aldrich.

Table 5-1. PFAAs and surrogate standards

Analyte	Molecular Weight	Tail Length[a]	Surrogate Standard
PFBA	213.03	3	[$^{13}C_4$] PFBA
PFPeA	263.04	4	[$^{13}C_3$] PFPeA
PFHxA	313.05	5	[$^{13}C_2$] PFHxA
PFHpA	363.05	6	[$^{13}C_4$] PFHpA
PFOA	413.06	7	[$^{13}C_4$] PFOA
PFNA	463.07	8	[$^{13}C_5$] PFNA
PFDA	513.08	9	[$^{13}C_2$] PFDA
PFBS	299.09	4	[$^{18}O_2$] PFHxS
PFHxS	399.11	6	[$^{18}O_2$] PFHxS
PFOS	499.12	8	[$^{13}C_4$] PFOS

[a]Length of fluorocarbon tail

Solid phases used in this study were selected to represent a variety of geochemical and physical characteristics (**Table 3-2**). Loamy Sand 1 (A) and Loam (B) were purchased from Agvise Laboratories (Benson, MN) and have been used by the authors in previous batch equilibrium sorption studies (Guelfo and Higgins 2013). Loamy Sand 2 (C) from an alluvial aquifer (Rifle, CO) was also used. Lastly, this study included a silica sand (0.297 to 0.420 mm; 40/50) (Accusands, Unimin Corp., Ottawa, MN) which had been previously characterized (Smits *et al.,* 2009). Soils A and B were air dried and sieved (2mm) prior to use in columns. Column aqueous phase for all experiments was artificial groundwater (AGW; deionized water with ions typically found in groundwater; **Table 3-3**) utilized in previous studies (Guelfo and Higgins 2013).

5.3.2.2 Column Design

All column experiments were conducted in 2.5 X 15 cm (No. 42400-2515) and 2.5 X 5 cm (No. 420400-2505) Kontes ® glass chromatography columns (Kimble Chase, Vineland, NJ) with a fritted, glass bed support in the influent end of the column. Columns were packed in 1-cm increments. Each increment was vortexed and tamped to establish uniform column properties. Glass wool and 1-mm glass beads were used as additional bed support at each end of the column to stabilize column packing material and establish uniform influent distribution across the bed during column operation. Following packing, columns were saturated with CO_2 to remove residual air and subsequently saturated with AGW in up-flow mode. Column bulk density and porosity were determined gravimetrically (**Table 5-2**). Columns were attached to an Ismatec ® high-accuracy peristaltic pump (IDEX Health and Science, Oak Harbor, WA). All columns were operated in up-flow mode and column influent/effluent samples were collected from 3-way valves installed at each end of the column.

Table 5-2. Summary of PFAA experimental conditions

Column	Packing Material	Column Length (cm)	Darcy Velocity (cm/min)	Pore Water Velocity (cm/min)	Bulk Density (g/cm^3)	Porosity	Longitudinal Dispersivity (cm)[a]	Experiment Type
1	Soil A	5	0.031	0.053	0.99	0.58	0.543	Continuous flow
2	Soil B	5	0.020	0.032	0.76	0.63	0.162	Continuous flow
3	Soil C	5	0.020	0.045	1.34	0.45	0.078	Continuous flow
4	40/50	5	0.031	0.067	1.45	0.46	0.067	Continuous flow
5	Soil A	15	0.286	0.476	0.99	0.60	0.325	Flow interruption
6	Soil C	15	0.286	0.697	1.44	0.41	0.192	Flow interruption
7	40/50	15	0.286	0.664	1.42	0.43	0.272	Flow interruption

[a] Determined from nonreactive tracer tests.

5.3.2.3 Bromide Tracer Tests

Prior to initiation of PFAA flow through experiments, nonreactive bromide (Br^-) tracer tests were completed to determine hydrodynamic transport conditions (**Table 5-2**) in all columns and confirm the absence of physical nonequilibrium in flow interruption columns. Br- was measured with a Cole-Parmer (Vernon Hills, IL) Br- combination electrode connected to a Thermo Orion 420 A+ pH/mV/ORP meter (Thermo Fisher Scientific). Bromide breakthrough curves were fit as described below. Br^- solutions were prepared in AGW and injected into columns until relative concentrations (C/C_0) of the effluent reached unity. In some cases, Br- tests were conducted at higher pore water velocities (**Table 5-2**) than subsequent PFAA experiments, as hydrodynamic properties should be independent of flow rate. For low flow experiments, columns were subsequently flushed with

AGW until Br^- concentrations returned to background levels. For flow interruption experiments, flow was discontinued for a period of 24 hours (**Table 5-3**) to determine if C/C_0 would change during the stop flow period, indicative of physical nonequilibrium. Following flow interruption,

Table 5-3. Design of flow interruption experiments

Experimental Step	Br-	PFAA
Initial pulse	to C/C_0=1	to C/C_0=1
Stop flow period	24 hrs	36 hrs
Post interruption pulse	to C/C_0=1	to C/C_0=1
AGW flush	to C/C_0=0	to C/C_0=0

Br^- input was continued for approximately one pore volume, after which columns were flushed with AGW to reach background Br^- levels (**Table 5-3**). Following the completion of all column experiments, Br^- tests were repeated to ensure that column properties remained consistent throughout the duration of the experiments.

5.3.2.4 PFAA Column Tests

Two types of column experiments were utilized in this study to investigate PFAA transport. Continuous flow column experiments (columns 1-4) were utilized to study PFAA transport under environmentally relevant groundwater flow conditions. Flow interruption experiments (columns 5-7) were used to determine the impact of rate-limited sorption on PFAA transport. Higher flows were used for these experiments to maximize the possibility of observing a measureable result under the assumption that measured rate constants would apply generally, as observed in other flow interruption studies (Brusseau *et al.,* 1989). Column influent consisted of a PFAA mixture (each PFAA at a nominal concentration of 5 µg/L) prepared in AGW. Depending on the porous media type, a pulse of 19-37 pore volumes of spiked AGW was injected at Darcy velocities of 0.02-0.031 cm/min (**Table 5-2**) into columns 1-4 for continuous flow experiments. Pulses of 18-23 pore volumes of spiked AGW were injected into columns 5-7 at a Darcy velocity of 0.29 cm/min (**Table 5-2**) after which flow was stopped for a period of 36 hrs. Following the flow interruption period, an additional 3-4 pore volumes of spiked AGW were injected into columns. Injection volumes for all experiments were selected to ensure that the entire suite of PFAAs reached effluent C/C_0 values of one. Following injection of spiked AGW, all columns were then flushed with AGW until PFAA concentrations returned to background (**Table 5-3**). To ensure that the hydrodynamic properties were not altered during PFAA experiments, Br- tracer tests were repeated after the completion of column experiments and resulting BTCs fitted using parameters obtained in the initial tracer tests to ensure that these parameters still described transport within the column (**Figure 5-1**). Method of moments analysis was used to calculate mass recovery of all Br- and PFAA BTCs (**Table 5-4**).

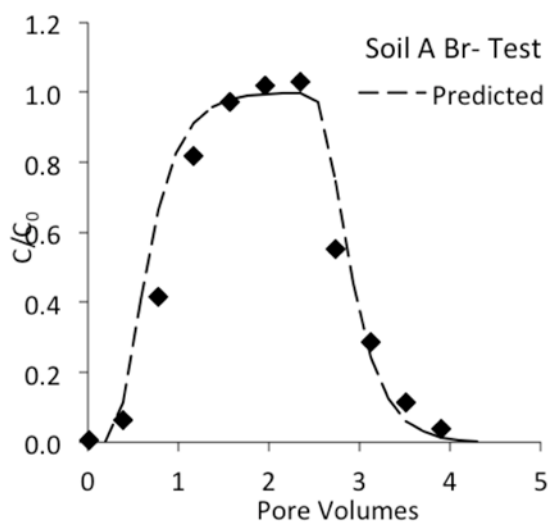

Figure 5-1. Measured Br- tracer test data in Column 1 following completion of low flow column experiments. Predicted breakthrough was generated using hydrodynamic properties measured in the column prior to the low-flow experiments. Agreement between predicted and measured data demonstrates that column hydrodynamic properties did not change during the course of the experiments.

Table 5-4. Mass recoveries from PFAA column experiments

Analyte	Column 1	Column 2	Column 3	Column 4	Column 5	Column 6	Column 7
PFBA	105%	102%	100%	97%	110%	101%	101%
PFPeA	106%	98%	105%	102%	113%	103%	107%
PFHxA	101%	105%	96%	104%	109%	105%	94%
PFHpA	103%	103%	94%	107%	107%	98%	99%
PFOA	95%	105%	95%	104%	112%	110%	102%
PFNA	95%	98%	92%	104%	108%	101%	93%
PFDA	92%	66%	97%	106%	108%	97%	92%
PFBS	99%	103%	99%	105%	107%	94%	97%
PFHxS	103%	96%	105%	102%	109%	98%	96%
PFOS	92%	78%	105%	100%	109%	94%	100%

5.3.2.5 Sample Preparation and Analysis

Column influent and effluent samples were collected manually in 2.0 mL polypropylene, microcentrifuge tubes. Tubes were weighed prior to and after sample collection to determine the exact volume of sample collected. An additional aliquot of isopropanol was then added to comprise 9% of the aqueous volume in the tube. Prior to sample preparation, samples were centrifuged (AccuSpin Micro 17, Thermo Fisher Scientific) at 17,000 RCF for 30 minutes. An aliquot of sample was then used to prepare a 1500 µL final sample for analysis in an autosampler vial. Autosampler vials contained 1350 µL of column effluent and 150 µL of 70/30 containing 0.3 ng surrogate standard (**Table 5-1**). Samples were analyzed directly via a MDS Sciex Applied Biosystems 3200 TM mass spectrometer (MDS Sciex, Ontario) LC-MS/MS, using methods modified from previous studies (Sepulvado *et al.*, 2011; Guelfo and Higgins, 2013; Higgins *et al.*, 2005). The LC-MS/MS was used to monitor two transitions for each analyte. Quantitation was performed using Analyst software (AB Sciex, Farmingham, MA). Limits of quantitation were analyte, matrix, and run-dependent but were approximately 2-9 ng/L. All values reported are corrected for recovery of surrogate standards, which were generally greater than 60% for all samples and matrices.

5.3.2.6 Equilibrium PFAA Sorption

A range of equilibrium sorption coefficients ($K_{deq,}$ L/kg) for Soils A and B were calculated based on Freundlich sorption coefficients (K_f) and linearity values (n) collected in previous work that utilized the same soils (**Table 5-5**) (Guelfo and Higgins 2013). The range of aqueous concentrations (C_w, mg/L) detected in each column was used to predict solid phase concentrations (C_s, mg/kg) as follows:

$$C_s = K_f C_w^n \qquad \text{(eqn. 5-13)}$$

Resulting C_s values and measured C_w values were used to calculate concentration-specific K_{deq} values as follows:

$$K_{deq} = \frac{C_s}{C_w} \qquad \text{(eqn. 5-14)}$$

Table 5-5. Summary of equilibrium and column Kd values (Guelfo and Higgins 2013)

Analyte	Soil A			Soil B			Soil C[a]			40/50		
	Log K_{deq} Low	Log K_{deq} High	Log K_{dcol}	Log K_{deq} Low	Log K_{deq} High	Log K_{dcol}	Log K_{deq} Low	Log K_{deq} High	Log K_{dcol}	Log K_{deq} Low	Log K_{deq} High	Log K_{dcol}
PFBA	-0.36	0.26	-0.23	0.34	1.17	-3.11	-0.21	0.21	-4.35	-0.71	M. Bal	-0.22
PFPeA	-0.68	-0.41	-0.50	-0.46	-0.41	-5.18	-0.45	-0.56	-4.33	-0.98	-0.86	-0.21
PFHxA	-0.73	-0.60	-0.47	-0.37	0.06	-4.36	-0.59		-4.66	-1.04	-0.79	-0.20
PFHpA	-0.39	-0.10	-0.20	0.06	0.47	-4.43	-0.46		-3.25	-0.61	M. Bal	-0.20
PFOA	-0.15	0.15	-0.31	0.52	0.83	-1.17	-0.52		-3.54	-0.68	M. Bal	-0.21
PFNA	0.29	0.72	-0.13	1.03	1.44	0.10	-0.25	-0.36	-1.39	-0.94	-0.63	-0.22
PFDA	0.96	1.65	0.5	1.80	2.35	0.94	0.12	0.17	-0.56	-0.42	-0.32	-0.23
PFBS	-0.19	0.33	-0.54	0.29	0.72	-5.31	-0.30	0.05	-5.88	-0.62	-0.45	-0.05
PFHxS	-0.06	0.54	-0.49	0.72	1.40	-0.46	-0.28	-0.03	-3.82	-0.58	-0.45	-0.05
PFOS	0.65	1.36	0.4	1.50	2.01	0.64	0.13	0.46	-0.66	-0.31	-0.16	-0.21

K_{deq}=equilibrium K_d values. K_{dcol}=column K_d values.
[a] In some cases for Soil C, PFAA mass over recovery prevented use of the isotherm to calculate a range of applicable K_{deq} values so a single K_{deq} value was used. Italicized K_{dcol} values PFAAs for which transport can be described by the equilibrium assumption. K_{dcol} error values are summarized in **Table 5-6.**

Table 5-6. K_{dcol} values and associated errors

Analyte	Soil A		Soil B		Soil C	
	Log K_{dcol}	±	Log K_{dcol}	±	Log K_{dcol}	±
PFBA	3.90	0.59	<0.001	0.01	<0.001	0.004
PFPeA	0.31	0.10	<0.001	0.13	<0.001	0.005
PFHxA	0.34	0.05	<0.001	0.004	<0.001	0.002
PFHpA	0.63	0.08	<0.001	0.01	<0.001	0.01
PFOA	0.49	0.07	0.07	0.02	<0.001	0.01
PFNA	0.74	0.05	1.26	0.04	0.04	0.01
PFDA	2.9	0.28	8.78	0.37	0.27	0.02
PFBS	0.29	0.04	<0.001	<0.001	<0.001	<0.001
PFHxS	0.32	0.04	0.35	0.09	<0.001	0.003
PFOS	2.4	0.11	4.38	0.22	0.22	0.03

K_{dcol}=column K_d values.

Studies measuring PFAA sorption to Soil C and 40/50 sand were not available, so limited 3-point sorption isotherms (initial C_w of 0.5-50 µg/L) were completed using methods outlined in

previous work (Guelfo and Higgins 2013). PFAA isotherms were fit with the Freundlich isotherm to obtain K_f and n values (**Table 5-7**). For the majority of PFAAs, a range of applicable K_{deq} values was calculated based on the range of C_w detected in the columns as described for Soils A and B. However, mass balance issues prevented the use of the full isotherms for some PFAAs (**Table 5-7**). As in previous studies, PFAA mass recoveries in the solid and aqueous phases as well as loss to the vial were utilized to complete mass balances in all batch reactors. In some cases, unacceptable mass balances of PFAAs occurred due to over recovery in the lowest isotherm point. When this occurred, the low point was excluded from the isotherm and an average of the values from the remaining two points on the isotherm was used as a single K_{deq} value for that analyte.

Table 5-7. Soil C and 40/50 sand isotherm results

Analyte	Log Soil C K_f (mg/kg)(mg/L)$^{-n}$	Soil C n	Soil C PFAA Recovery (%)	Log 40/50 K_f (mg/kg)(mg/L)$^{-n}$	40/50 n	40/50 PFAA Recovery (%)
PFBA	-0.76	0.80	110%	-2.13	0.28	141%
PFPeA	-0.23	1.09	104%	-0.12	1.28	113%
PFHxA	-0.52	1.02	139%	-0.34	1.16	128%
PFHpA	-0.47	1.00	158%	-0.81	0.88	145%
PFOA	-0.42	1.04	146%	-0.28	1.23	138%
PFNA	-0.10	1.05	103%	-0.25	1.14	107%
PFDA	-0.05	0.94	92%	-0.08	1.08	100%
PFBS	-0.68	0.84	111%	-0.76	0.94	112%
PFHxS	-0.62	0.86	109%	-0.73	0.94	108%
PFOS	-0.24	0.85	105%	-0.45	0.95	98%

Grey font indicates poor mass balance, so isotherm results were not used and K_{deq} was represented by an average of the two highest isotherm points for which individual mass balances were suitable.

5.3.2.7 Data Analysis

Breakthrough curves (concentration vs. time) for Br^- and PFAAs were fit with a numerical solution to the ADE using HYDRUS-1D (Simunek *et al.,* 2013). Longitudinal dispersivities (**Table 5-2**) were determined from inverse fits of Br^- tracer tests and utilized when modeling breakthrough of PFAAs. HYDRUS 1-D was used in both inverse and forward modeling of PFAA transport. Column sorption coefficients (K_{dcol}, L/kg) were obtained by inverse fits of PFAA breakthrough curves using an equilibrium sorption assumption and were compared to K_{deq} values.

Flow interruption BTCs that exhibited rate-limited sorptive behavior were fit with a two-site sorption model that assumes sorption sites can be divided into two fractions, and which is incorporated into the ADE (Van Genuchten and Wagenet, 1989). C_s is assumed to be a combination of solid phase concentrations on type 1 sites (C_s^e, mg/kg), to which sorption is assumed to be instantaneous, and type 2 sites (C_s^k, mg/kg) to which sorption is assumed to be time dependent. For type-1 and type-2 sites respectively:

$$C_s^e = fC_s = fK_dC_w \quad \text{(eqn. 5-15)}$$

$$C_s^k = (1-f)C_s = (1-f)K_dC_w \quad \text{(eqn. 5-16)}$$

where f is the fraction of sorption sites assumed to be at equilibrium with the solute. The sorption rate for type-1 sites is assumed to be linear and instantaneous and can be described as follows:

$$\frac{\partial C_s^e}{\partial t} = f\frac{\partial C_s}{\partial t} \quad \text{(eqn. 5-17)}$$

Sorption onto type-2 sites is assumed to be a first order rate process:

$$\frac{\partial C_s^k}{\partial t} = k\left[(1-f)K_dC_w - C_s^k\right] \quad \text{(eqn. 5-18)}$$

where k is the first order rate constant (min^{-1}). Continuous flow BTCs were also fit with the two-site model in some instances to facilitate a comparison of kinetic parameters at different flow velocities. In addition, the kinetic parameters from flow interruption experiments and the two-site model were used in an effort to predict continuous flow BTCs. The only difference in the application of this model to flow interruption vs. continuous flow data is that HYDRUS-1D modeling of flow interruption data incorporated a time period during which no advective processes occurred.

5.3.2.8 Contaminated Aquifer Simulations

To test the importance of rate-limited sorption in a remediation scenario, we simulated water extraction (pump and treat) from a PFOS-contaminated aquifer using HYDRUS-2D (Simunek and Van Genuchten). The aquifer scenario was simplified and hypothetical, but transport and operational parameters were based on those from an actual site (**Table 5-8**) (McGuire *et al.*, 2014). The simulated aquifer was assumed to be radially symmetric with a 15 m radius, which is representative of well spacing at existing AFFF-impacted sites (McGuire *et al.*, 2014), and 10 m thick. A pumping well yielding 136.27 m^3/day (25 gallons per minute) was set at the center of the aquifer, whereas a constant 20 m hydraulic head was imposed at the outer aquifer boundary. The simulated aquifer contained 50 µg/L of dissolved PFOS, which was initially in equilibrium with the sorbed phase. These concentrations are consistent with PFOS field measurements at an impacted facility (McGuire *et al.*, 2014). During pumping, PFOS concentrations at the "well" were recorded, analogous to well-head measurements at a field site, and compared to the PFOS provisional health advisory level of 0.2 µg/L. New water entering the domain was assumed to be

Table 5-8. Aquifer simulation conditions

Parameter	Value
Aquifer diameter (m)	30
Aquifer thickness (m)	10
Porosity	0.45
Pumping rate (m^3/day)	136.3
Bulk Density (g/cm^3)	1.5
Longitudinal dispersivity (m)	0.1
Base Case K_d (L/kg)	3
f_{oc}	0.004
Initial [PFOS] (µg/L)	50
Base case f	0.21
k (min^{-1})	9.5×10^{-7}

PFOS-free. Simulations were generated using both a linear equilibrium sorption assumption and two-site, rate-limited sorption scenarios as described above.

5.3.3 Results and Discussion

5.3.3.1 Qualitative Trend in PFAA Advective Transport

Equilibrium studies of PFAA sorption indicate that transport potential should be chain-length dependent for longer chain (≥C6) PFAAs (Guelfo and Higgins 2013). Over all, chain-length dependent trends were observed in all continuous flow column experiments, with the largest PFAAs (such as PFDA) showing the greatest retardation, but the trend was somewhat unclear for PFHxA, PFHpA, and PFOA (**Table 5-5**, **Figure 5-2**). Breakthrough of these compounds was

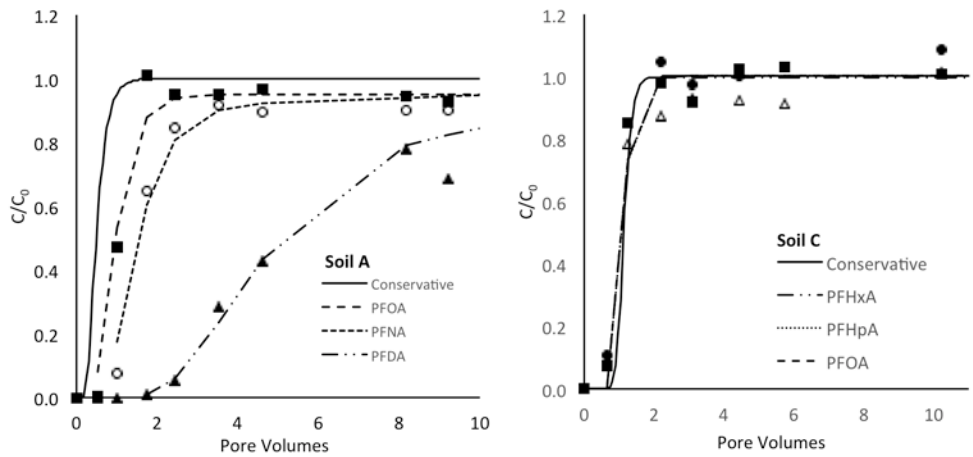

Figure 5-2. Breakthrough of PFOA (solid squares), PFNA (open circles), and PFDA (solid triangles) in Soil A (f_{oc}=0.017) and PFHxA (closed circles), PFHpA (open triangles), and PFOA (solid squares) in Soil C (f_{oc}=0.0017). The conservative (solid line) case represents a compound with no sorption (i.e., bromide), and dashed lines are model fits of the whole breakthrough curve though only the approach to C/C_0 =1 is shown so that chain-length dependent behavior can be seen.

sometimes simultaneous, implying that nonequilbrium conditions may influence transport. In batch equilibrium studies, short-chain PFAAs (<C6) did not follow chain-length dependent trends in Soils A or B, indicating that other factors such as steric and ion exchange effects may play a role in their sorption (Guelfo and Higgins 2013). Similar exceptions were observed in Soils A and B during column studies (**Table 5-5**). Equilibrium studies also indicate that PFAA transport potential should decrease with increasing porous media f_{oc} for long-chain PFAAs (Guelfo and Higgins 2013). Breakthrough curves of PFNA, PFDA, and PFOS in Soils A-C showed breakthrough that was dependent on f_{oc} (**Table 5-5**, **Figure 5-3**). Smaller compounds did not show a trend with f_{oc}, which might be another indication of nonequilibrium transport, as discussed below.

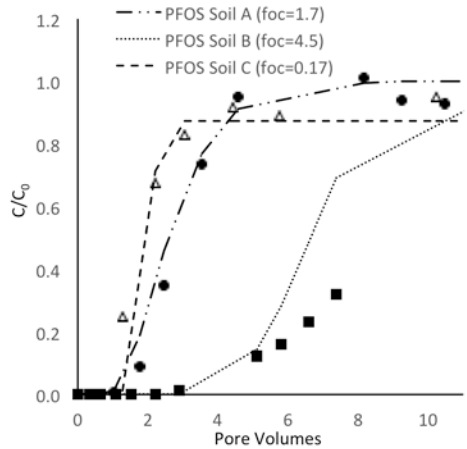

Figure 5-3. Breakthrough of PFOS in Soil A (solid circles), Soil B (solid squares), and Soil C (open triangles). Dashed lines are model fits of the whole breakthrough curve though only the approach to C/C_0 is displayed to enable observation of f_{oc} -dependent behavior.

5.3.3.2 Evaluation of Equilibrium Transport

K_{deq} were compared to K_{dcol} to determine if equilibrium conditions describe 1-D PFAA advective transport (**Table 5-5**). In Soil A, PFBA, PFPeA, PFHxA, and PFHpA K_{dcol} values were within or very near the range of K_{deq} values expected based on aqueous concentrations measured in the column, and 1-D transport of these analytes was adequately predicted by an equilibrium assumption (e.g. PFBA, **Figure 5-4a**). K_{dcol} values of the remaining PFAAs were smaller than K_{deq}, resulting in early breakthrough and tailing relative to equilibrium conditions (e.g. PFOS, **Figure 5-4a**). Similarly, in Soils B and C, all K_{dcol} values were smaller than K_{deq} values. In some cases, K_{dcol} values in these porous media were not statistically different from zero. In Soils A through C, low K_{dcol} values are likely indicative of nonequilibrium transport conditions that cannot be adequately described by assuming equilibrium transport. In 40/50 sand, K_{dcol} values were very similar for all PFAAs and higher than $K_{deq.}$ The reason for these slightly elevated K_{dcol} values is unclear, but K_{deq} values also adequately reflect PFAA transport in 40/50 sand (**Figure 5-4b**). Therefore equilibrium transport may be assumed valid for PFAAs in this porous media.

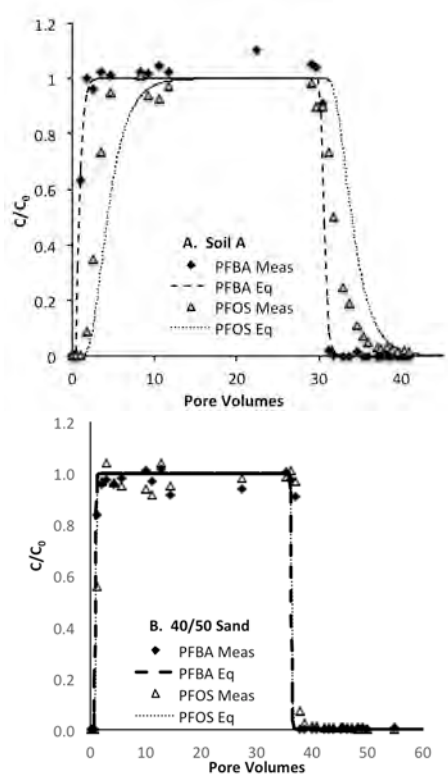

Figure 5-4. Predicted equilibrium transport and measured breakthrough of PFBA and PFOS in a.) Soil A and b.) 40/50 sand.

Results of the continuous flow experiments show evidence of nonideal transport, which may be caused by several factors including nonlinear and rate-limited sorption (Brusseau 1994). In this study, nonlinear sorption has been addressed by use of concentration-specific K_{deq} values that account for isotherm nonlinearity. Rate-limited sorption can have various impacts on BTCs including early breakthrough and tailing (Brusseau 1994) as was observed for compounds where $K_{deq} > K_{dcol}$ (**Figure 5-4a**). To investigate the potential for rate-limited sorption, continuous flow BTCs for which $K_{deq} > K_{dcol}$ were fit in HYDRUS 1-D with the two-site sorption model to obtain the kinetic parameters f and k. These values reflect the fraction of sites (f) that reach instantaneous equilibrium and the mass transfer coefficient (k) (**Equation 3-6**). These parameters were obtained by inputting K_{deq} values into the model scenario and obtaining HYDRUS 1-D fits for f and k (**Table 5-9**). Values of k ranged from 1.0 X 10^{-8} min^{-1} (PFOA, Soil C) to 4.12 X 10^{-4} min^{-1} (PFHpA, Soil C).

Table 5-9. Summary of f and k values measured in this study

Anaylte	Soil A (f_{oc} = 0.017)				Soil B (f_{oc} = 0.045)		Soil C (f_{oc} = 0.0017)			
	FI f	FI k	CF f	CF k	CF f	CF k	FI f	FI k	CF f	CF k
PFBA	N/A	N/A	N/A	N/A	<0.001	2.9	0.101	8.9	0.004	3200
PFPeA	N/A	N/A	N/A	N/A	<0.001	32	0.128	98	0.016	3100
PFHxA	N/A	N/A	N/A	N/A	0.029	1700	0.355	50	0.016	3100
PFHpA	N/A	N/A	N/A	N/A	0.004	30	0.138	150	0.008	4100
PFOA	<0.001	210	0.713	890	0.021	0.3	0.140	1.7	0.100	0.1
PFNA	0.090	340	0.370	2200	0.118	87	0.249	170	0.061	1300
PFDA	0.150	170	0.291	1800	0.136	47	0.300	6.1	0.183	2600
PFBS	<0.001	160	0.445	1700	<0.001	0.5	0.107	960	0.014	16
PFHxS	<0.001	74	0.500	100	0.067	0.9	0.134	480	0.018	47
PFOS	0.214	95	0.528	1800	0.153	307	0.173	185	0.042	1800

FI=Flow interruption. CF= Continuous flow. k in units of x 10^{-7} min^{-1}

5.3.3.3 Flow Interruption Experiments

In the present study, flow interruption experiments were completed with Soils A, C, and 40/50 sand to investigate the impact of rate-limited sorption on advective PFAA transport. Continuous flow experiments suggested rate-limited sorption for Soils A, and C, but flow interruption experiments allow for verification of this process. Prior to initiation of PFAA tests, flow interruption experiments were completed with Br- to ensure physical nonequilibrium (resulting from diffusive mass transfer between mobile and immobile regions) was not evident within the columns (Brusseau *et al.,* 1989). Physical nonequilibrium was not observed in any of the flow interruption Br- experiments (**Figure 5-5**); therefore any concentration drops observed in subsequent PFAA flow interruption experiments should be solely due to rate-limited sorption.

Decreases in PFAA concentrations during the stop flow period were observed for PFOA, PFNA, PFDA, PFBS, PFHxS, and PFOS in Soil A and PFNA, PFDA, and PFOS in Soil C (e.g. PFOS, **Figure 5-6**), indicating that rate-limited sorption impacted transport of these compounds during flow interruption experiments, as suggested by low K_{dcol} values, early breakthrough, and tailing observed in continuous flow column experiments. A comparison of K_{deq} and K_{dcol} values

suggests that rate-limited sorption also impacts PFBA, PFPeA, PFHxA, PFHpA, and PFOA in Soil C and that a drop in concentration should have occurred during the stop flow period, but the drops were not observed. It is possible that drops in the concentrations of these compounds were small and were therefore masked by the inherent scatter in the data.

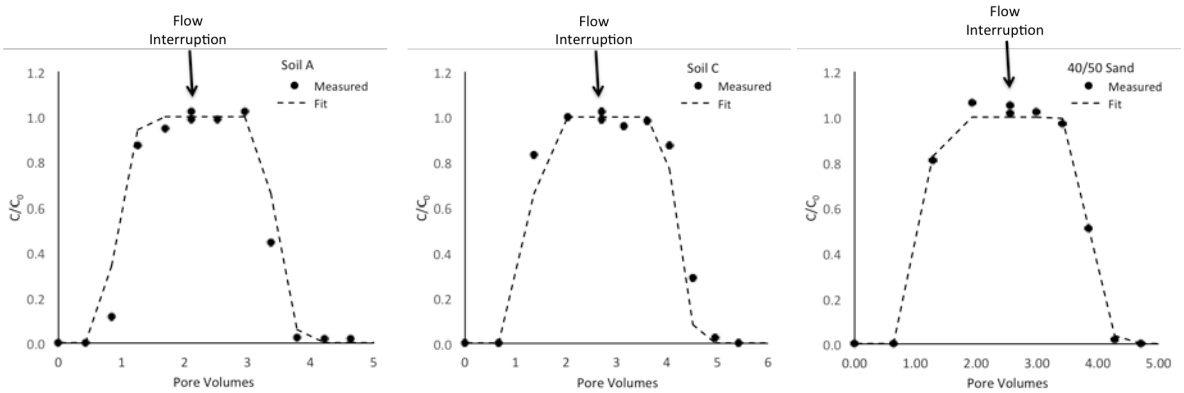

Figure 5-5. Flow interruption Br- tracer tests for Soil A, Soil C, and 40/50 sand.

Continuous flow column data indicated that PFAAs were likely in equilibrium with 40/50 sand. The flow interruption period had no impact on PFAA concentrations in the 40/50 sand nor was there any evidence of tailing in this experiment, both of which are consistent with equilibrium conditions. As with continuous flow data for the sand, flow interruption data for 40/50 sand were fit with an equilibrium assumption to ensure that K_{dcol} were greater than or equal to $K_{deq,}$ as would be consistent with equilibrium conditions (**Figure 5-4**). Equilibrium model fits to 40/50 flow interruption data yielded K_{dcol} values greater than or equal to K_{deq} values for all PFAAs, confirming equilibrium transport even at high pore water velocities (**Table 5-10**).

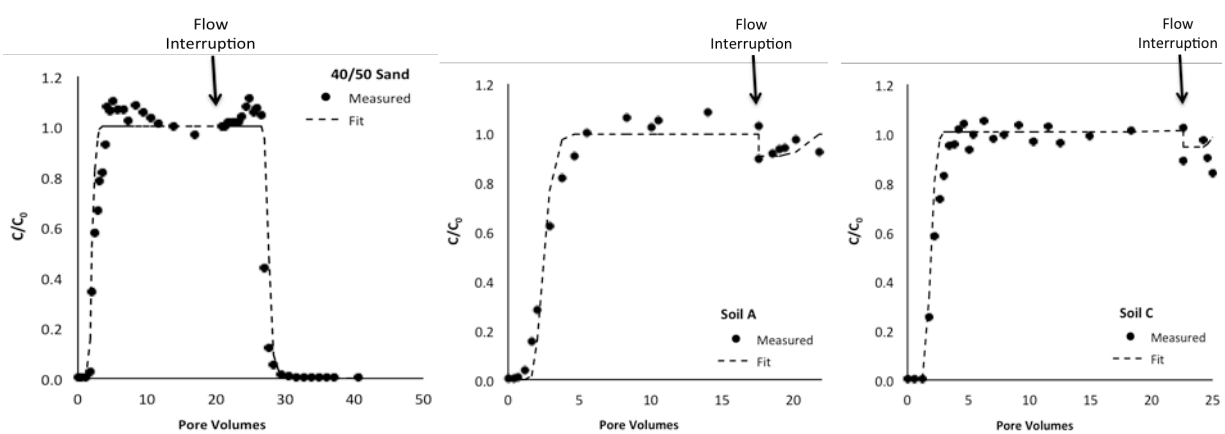

Figure 5-6. Flow interruption data and model fits for PFOS in 40/50 sand, Soil A, and Soil C. Model fits for Soils A and C were obtained using a two-site transport model whereas 40/50 model fits were obtained using the equilibrium assumption.

In addition to qualitatively confirming the influence of rate-limited sorption, another benefit of flow interruption experiments is that changes in C_w during the stop flow period can be modeled using inverse methods to parameterize the f and k values associated with the process. Ideally these kinetic parameters can then be applied to experiments conducted at lower pore water velocities (Brusseau *et al.,* 1989). Where measurable reductions in C/C_0 occurred, BTCs for flow interruption experiments in Soils A and C (Columns 5 and 6) were modeled as in continuous flow experiments by using K_{deq} in the two-site sorption transport model to obtain values for f (fraction of equilibrium sorption sites) and k (first order sorption rate) (**Figure 5-6**, **Table 5-9**). Because $K_{dcol} < K_{deq}$ for PFBA, PFPeA, PFHxA, PFHpA, and PFOA in Soil C, flow interruption BTCs for these compounds were also fit with the two-site model, even though drops in C/C_0 were not apparent. Model fits to BTCs of flow interruption data for Soils A and C would not converge on a solution that adequately captured both the drop in C/C_0 during the stop flow period and tailing of compounds. Because tailing may be impacted by experimental factors such as increased compound exposure time to the porous media during the stop flow period, the elution portion of these BTCs was removed from inverse modeling efforts, and fits focused on obtaining f and k from drops in C/C_0 during flow interruption (**Figure 5-6**). Values for k ranged from 1.74×10^{-7} min^{-1} (PFOA, Soil C) to 9.60×10^{-5} min^{-1} (PFBS, Soil C).

Table 5-10. K_{dcol} values measured in 40/50 flow interruption columns.

Analyte	FI Log K_{dcol}
PFBA	-0.89
PFPeA	-0.88
PFHxA	-0.90
PFHpA	-0.85
PFOA	-0.88
PFNA	-0.70
PFDA	-0.38
PFBS	-0.89
PFHxS	-0.85
PFOS	-0.50

FI =Flow interruption

5.3.3.4 Continuous Flow vs. Flow Interruption Kinetic Parameters

Two sets of the kinetic parameters (k and f) were generated in this study as a result of model fits to both continuous flow and flow interruption experiments (**Table 5-9**). Because the parameter sets were different between analytes, soil types, and velocities, the kinetic parameters were studied to determine if there were trends with PFAA chain length, f_{oc}, and pore water velocity. Results from Soil B and C low-flow experiments and Soil A flow interruption experiments suggest that the fraction of equilibrium sites (f) increases with increasing chain length (**Figure 5-7**), though the trend did not apply to all soil types at all pore water velocities. Similar trends have been reported for other organic compounds in previous work, wherein values for f were noted to increase with increasing octanol-water partitioning coefficient (K_{ow}) for various organic compounds (Brusseau *et al.,* 1991a). Values of f also increased with decreasing pore water velocity in Soil A (**Table 5-9**, **Table 5-11**) implying that the fraction of each PFAA at equilibrium with the solid phase is a function of the hydraulic residence time in some solid phases. This is consistent with the assumption of some

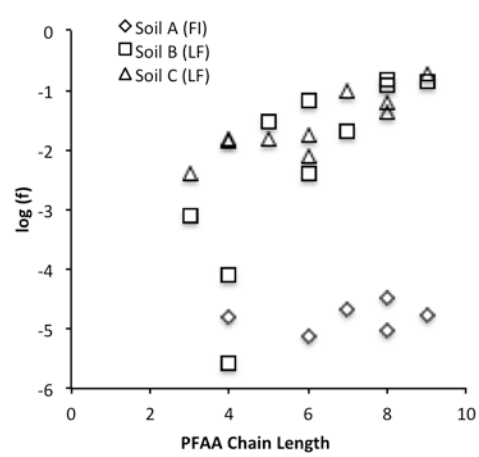

Figure 5-7. Trends in f with PFAA fluoroalkyl tail length. FI = Flow Interruption. LF = Low Flow. Only data for those cases where f displayed a trend with chain length are shown.

models that the validity of equilibrium transport is directly related to pore water velocity (Brusseau, 1992). Because this did not occur in all porous media, it is possible that the velocity-dependence of f is related to the f_{oc} of the solid phase.

Table 5-11. Summary of f values in Soil A

Analyte	FI f[1]	LF f[2]	LF +FI f[3]
PFOA	4.77E-05	7.13E-01	7.06E-01
PFNA	8.93E-02	3.70E-01	3.88E-01
PFDA	1.41E-01	2.91E-01	3.22E-01
PFBS	3.91E-05	4.45E-01	4.51E-01
PFHxS	4.47E-03	5.00E-01	3.62E-01
PFOS	2.29E-01	5.28E-01	5.41E-01

[1] f values obtained by fitting 2-site sorption model to flow interruption data.
[2] f values obtained by fitting 2-site sorption model to low flow data.
[3] f values obtained with flow.

No trends were observed between first order rate constant (k) and PFAA chain length. Values of k did vary systematically with porous media f_{oc}, tending to decrease overall with increasing organic matter content in continuous flow experiments. It should be noted that although there was an overall decrease, there was some uncertainty in the trend regarding Soil C (f_{oc} of 0.0017; **Table 5-9, Figure 5-8**). Trends of decreasing rates with increased organic matter have also been recorded previously in the literature for other organic compounds (Brusseau *et al.* 1991b). Additional discussion of the mechanisms potentially responsible for these trends is presented below.

One of the objectives of this study was to identify kinetic parameters that can be applied to various PFAA transport scenarios. Because two sets of values were generated for continuous flow and flow interruption data, it is necessary to consider if and when one set is more appropriate than the other. An advantage of flow interruption experiments is that it determines kinetic parameters based on a stop flow period during which any additional effects of advective transport are removed and the only process occurring is sorption. This potentially allows for more sensitive and accurate determination of k values (Brusseau *et al.,* 1989), indicating that flow interruption parameters may be more robust than those determined from continuous flow experiments. If so, and assuming that k is independent of flow, results of flow interruption experiments should be applicable results at other pore water velocities.

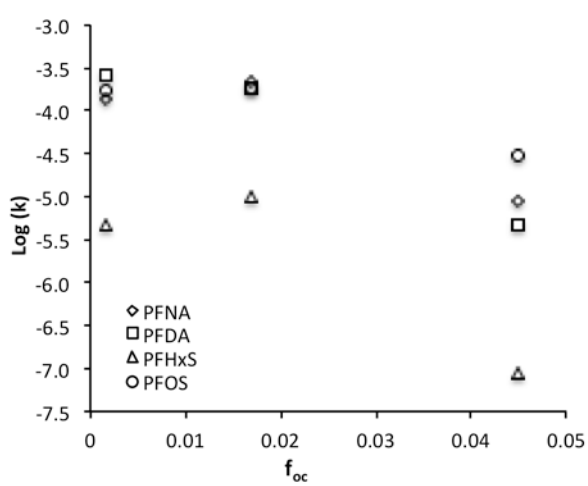

Figure 5-8. Trends in k with solid phase f_{oc}.

To evaluate this, flow interruption f and k values were used to forward model the continuous flow experiments for Soils A and C to determine if they could adequately predict PFAA transport at lower pore water velocities. Model fits were compared to those obtained by fitting the continuous flow data with the two-site sorption model. In Soil A, flow interruption f and k values predicted earlier breakthrough and did not match tailing in continuous flow experiments as compared to measured data (**Figure 5-9a**). However, k values were able to predict continuous flow BTCs when f was allowed to be a fitted parameter (**Figure 5-9b**).

The model fit obtained with this method was comparable to that obtained by fitting both f and k parameters to continuous flow data (**Figure 5-9c**). This would imply that the fraction of type 1 sites in Soil A is dependent on velocity. Alternatively, it is also possible that k varies with velocity. Values of f obtained using the flow interruption k and when both f and k are fitted parameters are very similar even though corresponding k values vary sometimes by an order of magnitude or more (**Table 5-9**, **Table 5-11**).

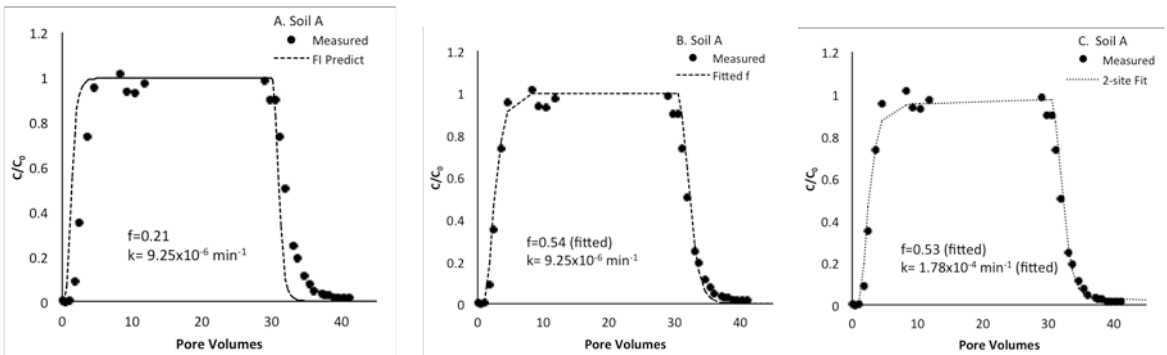

Figure 5-9. Measured continuous flow PFOS BTC in Soil A with predicted BTC a.) using flow interruption (FI Predict) f and k to forward model measured values, b.) with flow interruption k value and fitted f (Fitted f), and c.) with two-site sorption transport model fit (two-site Fit) to obtain f and k values from continuous flow data. Root mean square errors (RMSE) are 0.06 and 0.07 for panels b and c respectively.

Kinetic parameters from flow-interruption experiments were also used to forward model low-flow experiments in Soil C. In this porous media, flow interruption f and k values were able to adequately predict breakthrough in continuous flow experiments and fits were comparable to those obtained when continuous flow data were fit with the two-site sorption model to obtain f and k (**Figure 5-10**). Though model fits are comparable, values of f and k varied in a nonsystematic way between the two scenarios. Factors that may impact f and k are discussed further below.

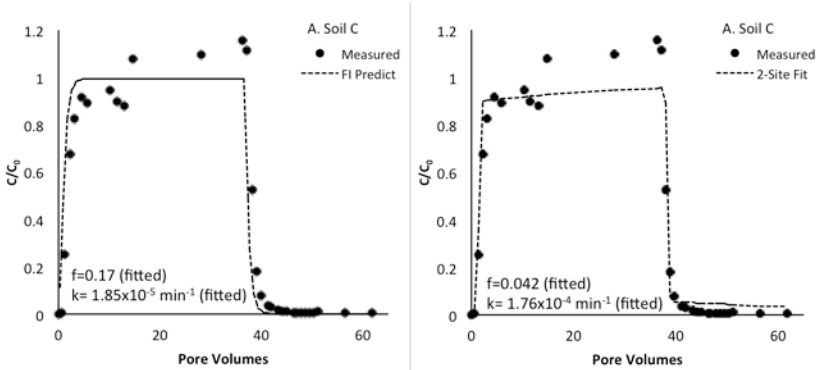

Figure 5-10. Measured continuous flow PFOS BTC in Soil C with predicted BTC a.) using flow interruption (FI Predict) f and k to forward model measured values and b.) with 2-site sorption transport model fit (2-site Fit) to obtain f and k values from continuous flow data.

5.3.3.5 Factors Impacting PFAA Mass Transfer

Rate-limited behavior in contaminant transport is generally attributed to processes related to diffusive mass transfer, specifically intraparticle diffusion and intrasorbent diffusion (Brusseau *et al.,* 1991b; Pignatello and Xing, 1996). Intraparticle diffusion is related to aqueous molecular diffusion within microporous particles diffusion (Brusseau *et al.,* 1991b; Pignatello and Xing, 1996). Pore surfaces may or may not be organic matter. Diffusion is slowed because of interactions with the pore surfaces, pore tortuosity, pore diameter, and dead end pores (Brusseau *et al.,* 1991b; Pignatello and Xing, 1996). If pores are small enough, diffusion may be further hindered by enhanced interactions with opposing pore walls. Intrasorbent diffusion occurs through the organic matter matrix as the rate-limiting step (Brusseau *et al.,* 1991b; Pignatello and Xing, 1996). Rate constants measured in this study decreased with increasing organic carbon content, indicating that intraparticle diffusion into the organic matter matrix is likely at least partially responsible for the rate-limited behavior of these compounds in porous media containing organic carbon.

In Soil A, values of f in continuous flow experiments were found to increase with increasing chain length. Previous studies have noted a similar trend and hypothesized that this effect is due to steric hindrance that occurs with increasing molecular size (Brusseau *et al.,* 1991b). That is, as molecules become larger, a smaller subset of sorption sites are accessible and the probability increases that a higher fraction of sites will be available for equilibrium, instantaneous sorption (Brusseau *et al.,* 1991b). Values of f in Soil A were also shown to increase with decreasing pore water velocity. As mentioned previously, many models assume an inverse relationship between pore water velocity and the validity of the equilibrium assumption (Brusseau, 1992), implying that as hydraulic residence times increase, the degree of nonequilibrium will decrease. As f increases, early breakthrough will decrease, and this shift can be observed when looking at the breakthrough of PFAAs in continuous flow vs. flow interruption experiments (**Figure 5-11**). Because of the stop flow period in flow interruption experiments, the experimental design of the continuous flow vs. the flow interruption scenarios was different. However, when considering only the breakthrough side of the BTCs, the experimental conditions were the same except for the water velocity. The observed shift in breakthrough confirms trends of f with pore water velocity.

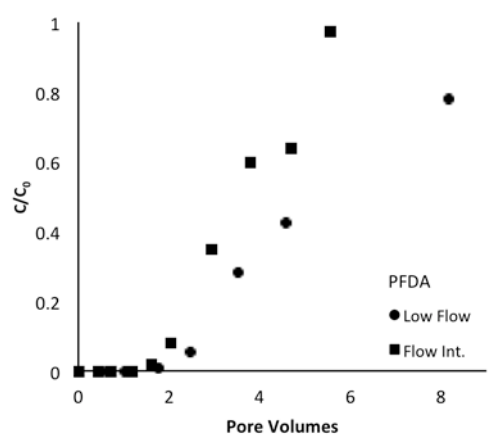

Figure 5-11. Breakthrough of PFDA in Soil A for low flow and flow interruption experiments.

In Soil A, values of k also varied between continuous flow and flow interruption experiments. As mentioned, k values measured under stop flow conditions are considered to be more robust, but a discussion of why values may have appeared to vary with experimental conditions is valuable. For either intraparticle or intrasorbent diffusion, first order rate coefficients may depend on factors such as molecular diffusion coefficients for the sorbate/sorbent pair, molecular shape, and

diffusion path length (Brusseau *et al.,* 1991b). As long as these factors do not vary with pore water velocity, k should be invariant between continuous flow and flow interruption experiments. Though k is often presumed not to vary with pore water velocity, some research has shown that k does vary with pore water velocity, with k values decreasing with decreasing pore water velocity (Brusseau, 1992). This is potentially due to changes in diffusion coefficients or diffusion path lengths, including increased turbulence and mixing at the soil-water interface during higher flows (Brusseau, 1992). In this study values of k were higher at lower pore water velocity. If k were variable with hydraulic residence time, the opposite trend would be expected, so observed trends of k are not attributed to differing flow rates.

In addition, multiple parameter sets were capable of fitting continuous flow data. Measured data were fitted using flow interruption k values and allowing f to be a fitted parameter or by fitting both f and k in continuous flow data. Values of f did not vary much, but resulting k values were different, indicating a degree of uncertainty in the mass transfer coefficient. This may be due to scatter and failure to capture the full tailing effect in continuous flow BTCs. To further investigate this, parameter sets that yielded good fits to continuous flow data (f with flow interruption k values and f with continuous flow k values) were utilized to generate BTCs for the conditions applicable to continuous flow experiments in Soil A (**Figure 5-12a**). Forward modeling using these parameters yields similar BTCs, with a slight differences in the approach to a C/C_0 of one and in the tailing. The differences in these curves support the idea that less scatter in the initial breakthrough and additional capture of tailing trends would reduce uncertainty in estimates of k.

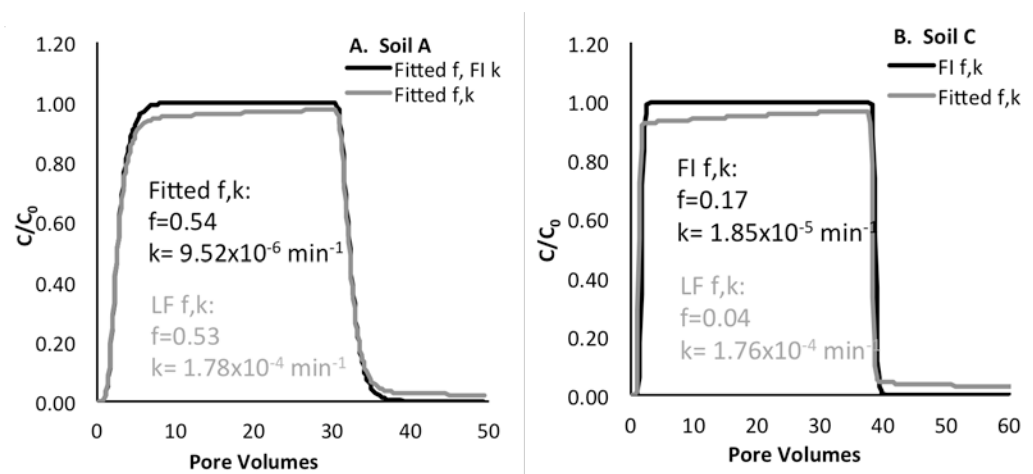

Figure 5-12. Forward modeling of BTCs in a.) Soil A using kinetic parameters obtained with flow interruption k values and f as a fitted parameter (Fitted f, FI k) and kinetic parameters from low flow experiments (LF f, k) and b.) Soil C using parameters from flow interruption (FI f, k) and low flow (LF f, k) experiments.

Similar to Soil A, values of f in Soil C were sometimes found to increase with increasing chain length. However, there were no systematic differences in either f or k values with pore water velocity for Soil C. Similar to Soil A, multiple parameter sets were capable of producing similar fits to continuous flow BTCs. In the case of Soil C, flow interruption f and k values could be

used to generate a fit to continuous flow data, as opposed to having to generate f as a fitted parameter as in the case of Soil A. Additionally, a fit could be obtained by letting f and k both be fitted values (as with Soil A). The f and k values from these two sets of parameters were not similar (**Table 5-9**). No changes in early PFAA breakthrough occurred between flow interruption and continuous flow data, confirming that f should not change with velocity for this soil. Because changes in f with velocity are likely a steric effect related to diffusion into the organic matter, it is possible that the lower organic matter content of Soil C is insufficient to yield any related changes in the fraction of equilibrium sorption sites. As in Soil A, kinetic parameter sets yielding good fits to Soil C continuous flow data were used to generate BTCs to try and determine the source of uncertainty in k values (**Figure 5-12b**). Continuous flow parameters yielded a slightly slower approach to $C/C_0 = 1$ and tailing at a higher concentration, again suggesting that scatter in the data and capturing of tailing data may have led to uncertainty in the kinetic parameters.

5.3.3.6 Implications for PFAA Remediation

Groundwater modeling efforts require an estimation of contaminant retardation in the subsurface. Such estimates are often made utilizing K_d measurements from batch equilibrium studies. The results of this study show that use of equilibrium K_d values may be appropriate when predicting transport of some PFAAs in some porous media. Regardless of the uncertainty surrounding f and k values, flow interruption experiments confirm that rate-limited processes also apply, particularly for longer-chain PFAAs and in porous media with appreciable organic carbon content. A failure to consider rate-limited processes can have implications in both risk assessment and remediation scenarios, because it may impact factors such as bioavailability and estimates of remedial effectiveness (Pignatello and Xing, 1996). An illustrative example of this importance is demonstrated by considering a simple pump and treat scenario for the remediation of PFOS. Although in situ treatments are largely considered favorable over ex situ methods, to date, no in situ methods have been found that are effective in the treatment of PFOS. Therefore pump and treat may be one of the only viable options for mitigating transport of subsurface PFAA plumes. In addition, because of the strong sorption of PFOS relative to other PFAAs, it is useful to consider the potential impacts of rate-limited sorption on PFOS transport.

A radially symmetric pump and treat scenario for water extraction of a PFOS-contaminated aquifer was simulated with conditions representative of a typical AFFF-impacted site (**Table 5-8**) (McGuire *et al.*, 2014). The effect of rate-limited sorption on PFOS removal was evaluated by considering multiple equilibrium and rate-limited scenarios. Initial transport parameters for these scenarios were $K_{deq} = 3$ L/kg based on field K_d values from an impacted facility (McGuire *et al.*, 2014). PFOS flow interruption kinetic parameters from Soil A (**Table 5-9**) were used as a 'base case' for evaluating rate-limited transport. Because of the uncertainty surrounding k values and the potential for f to vary with pore water velocity, we evaluated the sensitivity of the rate-limited model results to parameters K_{deq}, f and k by increasing or decreasing the value of each parameter by a factor of two compared to the base case. These combinations of parameters were used to compare pumping times required to reach PFOS levels below the provisional health advisory level of 0.2 µg/L from an original concentration of 50 µg/L. Pumping was continued for 90 days after concentrations declined to the regulatory limit of 0.2 µg/L .

In the equilibrium scenario, PFOS reached concentrations less than 0.2 µg/L after 654 days compared to the base case rate-limited scenario, which took 1033 days (58% longer) (**Figure 5-13a**). Once pumping was discontinued, PFOS levels rebounded in the base case rate limited scenario but to levels below 0.2 µg/L. In rate-limited scenarios, when parameters were varied by a factor of two, the remediation times changed. The shortest time to remediation occurred at low K_{deq}, high k, and high f ("rate limited short") and the longest time occurred at high K_{deq}, low k, and low f ("rate limited long"; **Figure 5-13a**). Rebound concentrations exceeded the provisional health advisory level of 0.2 µg/L in the "rate-limited long" scenario, demonstrating that under certain conditions, rebound may become a factor in trying to maintain PFOS concentrations below particular levels after pump-and-treat efforts are ceased.

The sensitivity analysis for K_{deq}, f, and k showed that estimates of time for remediation are most heavily influenced by changes to K_{deq} and k (**Figure 5-13b**). Interestingly, the model was not that sensitive to changes in f. Thus, even though f was shown to vary with pore water velocity in column experiments, elucidation of the exact values may not be crucial to estimating PFAA transport. The sensitivity of the model to K_{deq} should be easy to address in modeling scenarios with published PFAA K_{oc} values, given that the porous media f_{oc} is known.

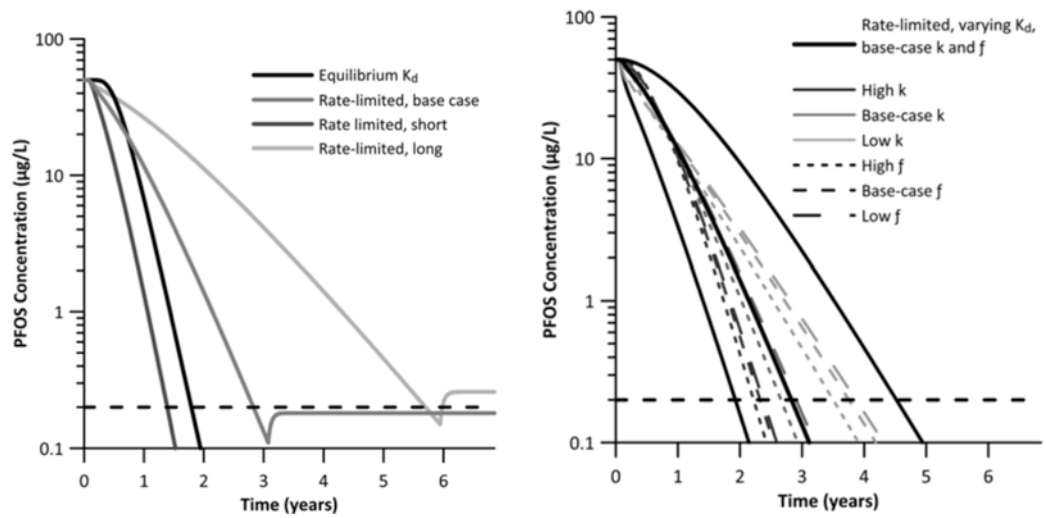

Figure 5-13. Results of PFOS pump and treat simulation showing a.) time for remediation under equilibrium, base case, and extreme scenarios and b.) results of a sensitivity analysis for f and k parameters.

The sensitivity of the model to values of k emphasizes the importance of additional examination of the factors impacting k, in particular the relationship with solid phase organic matter. Regardless of the uncertainty surrounding first order mass transfer rate coefficients, these results illustrate the potential importance of considering non-equilibrium sorption in calculations of treatment costs and timeline estimates for site-closures.

5.3.4 Conclusions

Studies of PFAA transport potential under equilibrium conditions have provided valuable information that can be extended to advective transport including equilibrium sorption values

and qualitative trends. The current study demonstrated decreasing mobility with increasing chain length for long chain PFAAs, and an overall trend of decreasing mobility with increasing f_{oc}. This study also confirmed the results of previous studies that showed anomalous sorptive behavior for short chain PFAAs. Continuous flow column studies in 40/50 sand demonstrated that an equilibrium sorption assumption is valid for predicting porous media with little or no organic carbon content, but results from Soils A-C showed nonequilibrium transport. Flow interruption experiments confirmed that this behavior was caused by rate-limited sorption. Both continuous flow and flow-interruption experiments were fit with a two-site sorption model yielding two sets of kinetic parameters. In general, because flow interruption parameters were based on experiments that measured rate-limited behavior in the absence of an advective component, k values from this data set were considered more robust. Additionally, these k values were capable of predicting continuous flow BTCs when coupled with an appropriate value of f. In the case of Soil C, f values did not appear to vary between continuous flow and flow interruption experiments; however, in Soil A, f values were a function of pore water velocity.

Application of flow interruption kinetic parameters to a pump and treat simulation demonstrated the importance of considering rate-limited PFAA transport behavior. Though f values may vary with pore water velocity, a sensitivity analysis demonstrated that this may not be a crucial factor when considering long-term transport. Models were much more sensitive to changes in k, illustrating the importance of having a valid k value for PFAA modeling efforts. Additional research may be needed to better understand how the slow fraction and mass transfer coefficients are impacted by velocity and/or vary with other factors such as concentration or sorption hysteresis. However, this study shows that equilibrium conditions will not adequately predict PFAA transport under certain conditions, and that a complete understanding of the transport of these compounds will involve additional studies of their behavior under advective conditions.

5.4 PFAA Transport with Active Microbial Communities (*Task 4b*)

5.4.1 Background

To address *Task 4b*, the fate and transport of PFAAs in the presence of active microbial communities was investigated. The results of *Task 3a* (**Section 4.2**), in which microbial communities responded to PFAAs by producing EPS (Weathers *et al.*, 2015) suggested that additional sorptive capacity for the solid phase could be produced by microorganisms when PFAAs are presence. This EPS may result in PFAA retardation in situ and/or changes in subsurface flow parameters. The objective of this subtask was thus to examine the extent to which active microbial communities would impact PFAA retardation in one-dimensional column experiments.

5.4.2 Materials and Methods

Fourteen 2.8cm x 8cm (diameter x length) polypropylene and glass columns (Kimble-Chase) were wet-packed and tamped with low-organic carbon sediment (Loamy Sand 2; **Table 3-2**) in a manner similar to those described in **Section 5.3** above. These columns were then biostimulated with 10 mg/L glucose and exposed to PFAA concentrations of 11, 55, or 110 mg/L total of 11 distinct analytes (spiked into AGW; **Table 2-3**) for approximately 200 pore volumes (~85 days)

at 6 cm^3/hr. Columns were initially flushed for at least 3 pore volumes before introduction of a bromide tracer to establish baseline measurements of pore water velocity. Each concentration of PFAA was assigned to columns in triplicate, including a control devoid of PFAA amendment. Two columns inactivated with 1 g/L sodium azide served as further controls for microbial growth. Breakthrough and tailing of each analyte was measured and subsequently modeled with HYDRUS-1D to explore sorption coefficients over time for microbially active columns and to establish the effects of biostimulation on PFAA transport.

The five different experimental systems were:

A. Biostimulated columns (in triplicate) without PFAAs, termed "-PFAA";
B. Duplicate inactivated columns with sodium azide as described elsewhere22 and 110 mg/L total PFAAs (10 mg/L of 11 different PFAA analytes) termed "-Bio";
C. Biostimulated columns (in triplicate) with 110 mg/L total PFAAs, termed "110";
D. Biostimulated columns (in triplicate) with 55 mg/L total PFAAs (5 mg/L each of 11 analytes), titled "55"; and
E. Biostimulated columns (in triplicate) with 11 mg/L total PFAAs (1 mg/L each of 11 analytes), defined as "11".

The upper limit of PFAA concentrations were chosen based on source-zone concentrations observed in situ (Moody and Field, 2000). This is also where microbial effects on EPS formation (as discussed in **Section 4.2**) and community succession within laboratory batch systems (**Section 4.3**) have been documented (Weathers *et al.*, 2015; Weathers *et al.*, 2016). The lower level, 11 mg/L total PFAAs, is the highest concentration at which EPS production was not consistently observed (Weathers *et al.*, 2015).

Upon completion of the initial 90 g/L bromide tracer, biostimulated columns were amended with roughly 10 pore volumes of local, turf-grass derived Luria-Bertani microbial enrichments resuspended in 1:4 v:v Luria-Bertani broth to AGW. After this inoculation period, AGW was amended with 10 mg/L glucose to continue biostimulation. Glucose amendments were calculated stoichiometrically such that if all glucose was utilized, residual oxygen would remain in the system, ideally maintaining an aerobic community. PFAAs at the desired concentration were also added to the AGW after evaporation.

Aqueous PFAA samples were sampled from each column upon introduction of PFAAs to capture the contaminant front of the breakthrough curve. After approximately 80 pore volumes (~27 days), another bromide tracer test was implemented to examine changes in advective transport that could result from microbial colonization or other experimental variables. To accompany the non-reactive breakthrough, falling-head permeability was also measured. After tailing of the bromide tracers (~37 days), one column from each of the 110, 55, 11, and –PFAA sets was removed for solid-phase PFAA extraction, protein, EPS, and ATP extraction and quantification. This dataset represents the microbial characteristics that may occur upon uninterrupted PFAA exposure in the subsurface. At this time, the PFAAs were no longer added to the influent. Aqueous PFAA samples collected at this point during the experiment were thus

intended to describe the tailing behavior of the PFAA pulse. Flushing with AGW continued for approximately 90 pore volumes (~ day 70), until a third and final bromide tracer test was conducted. Each column was then removed and archived.

5.4.3 Results

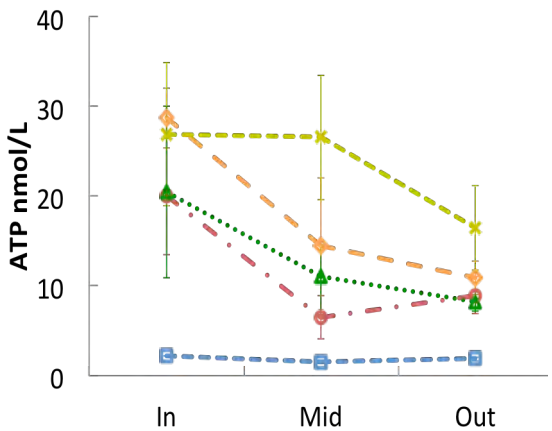

Figure 5-14. Microbial activity as measured by ATP is greater for the biostimulated columns than for the inactivated system (blue squares). Activity is greatest at the inlet for all biostimulated conditions and least at the outlet. There is no significant difference in activity between 110 mg/L total PFAAs (red circles), 55 mg/L total PFAAs (orange triangles), 11 mg/L total PFAAs (yellow x's), and for the system without PFAAs (green triangles).

Samples for aqueous and solid-associated PFAAs were quantified with LC-MS/MS according to previously published methods (Guelfo and Higgins, 2013). ATP was also quantified immediately after extraction as per Velten *et al.* (2007). Respiration as surrogate for microbial activity in the inlet, middle, and effluent end of the columns was approximated by ATP concentration immediately after the columns were taken offline. **Figure 5-14** shows that the activity in biostimulated columns was greater than the inactivated columns, and that activity is greatest at the inlet. This is expected considering the increased availability of nutrients at the front end of the column. These data were developed from duplicate measurements for each extraction, with two samples extracted for ATP per column location. Unfortunately, ATP was only quantified for one –Bio column due to contamination of the second –Bio column. As measured by this ATP assay, no significant activity differences were observed as a function of PFAA exposure, with the exception of the middle portion of the 11 column where activity appears to be stimulated.

Permeability was also quantified via falling-head tests at the point of longest PFAA exposure (~37 days). Results are shown in **Figure 5-15**, and demonstrate that, as expected, there was a reduction in permeability as a result of stimulated microbial activity. Additionally, the reduction in permeability is greatest for the systems amended with 110 mg/L total PFAAs vs. the system without PFAAs (no overlap in average ± standard deviations), which may be a result of biofilm formation. Such behavior is consistent with that the stimulation of EPS production as discussed in Weathers *et al.* (2015).

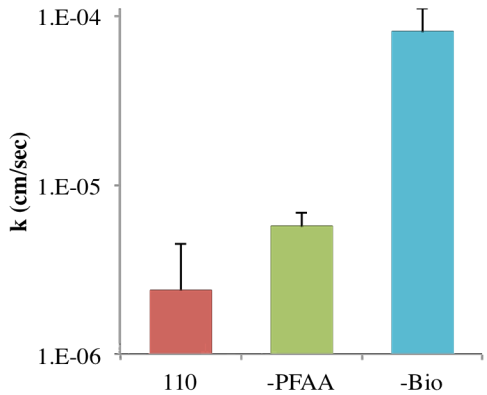

Figure 5-15. Permeability decreases upon microbial stimulation (110, -PFAA) compared to –Bio, and is further reduced in the system with 110 mg/L total PFAAs.

Modeling of bromide tracers using HYDRUS-1D was used to verify the calculated porosity from packing and to estimate the change in modeled longitudinal dispersivity (αL). Dispersivity, as fit by HYDRUS-1D and assuming constant porosity, can be used to reflect spreading as a potential result from microbial colonization of the pore spaces. **Figure 5-16** shows an increase in this fitted parameter as a function of time for biostimulated systems regardless of PFAA exposure. Average modeled dispersivities for each column are represented in **Figure 5-16**; error bars represent the standard error of the model fits.

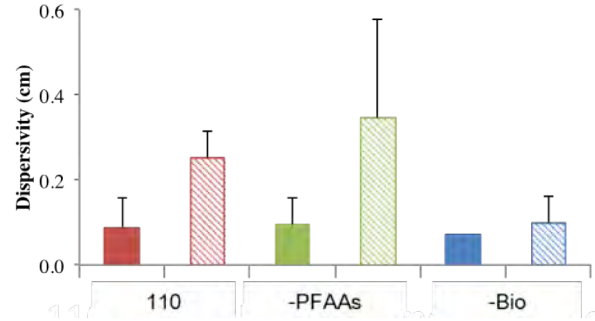

Figure 5-16. Dispersivity of the non-reactive tracer increases for biostimulated systems over time. Solid bars represent the initial dispersivities before inoculation or PFAA exposure, hashed bars are the dispersivities at the peak of PFAA exposure.

All applicable PFAA influent, effluent, and solid-associated samples were analyzed by LC-MS/MS. This report documents the front of the PFOA and PFHxS breakthroughs as representatives of the complete dataset that has been modeled by HYDRUS-1D. The model input includes PFAA data from each column exposed to a particular condition. The model fits are shown in **Figure 5-17**. It is evident that the best fit for the case with PFAAs includes a larger dispersivity. A distribution coefficient, K_d, is also modeled by HYDRUS-1D. From K_d, the retardation factor, R, can be calculated using **Equation 5-19**:

$$R = 1 + \frac{\rho_b}{n} K_d \qquad \text{(eqn. 5-19)}$$

where ρ_b is the bulk density of the soil (initially estimated at 1.85 g/cm3), and *n* is the porosity as fit by the initial non-reactive bromide breakthrough. A retardation factor of 1 implies no retardation: increases in sorption will increase the retardation factor. **Table 5-12** summarizes the porosity, distribution coefficient, retardation factor, and dispersivity for PFOA and PFHxS in the –Bio and 110 mg/L columns. Modeled fits agree with the findings from the non-reactive tracers, namely that the fit parameter of longitudinal dispersivity is greater after exposure to biostimulation and 110 mg/L PFAAs than for the case without active biomass for both PFOA and PFHxS. The retardation factor is also greater in the presence of active biomass. Breakthrough and tailing data for the remaining column sets for select representative compounds are shown in **Figure 5-18.**

Table 5-12. Modeled parameters for PFOA and PFHxS in the –Bio and 110 mg/L systems

	n	PFOA			PFHxS		
		K_d	R	αL	Kd	R	αL
-Bio	0.41	0.0005	1.002	0.147	0.031	1.14	0.252
110 mg/L	0.39	0.056	1.27	0.518	0.062	1.30	0.537

An assessment of these results shows the potential for novel findings for in situ applications of PFAA transport. Biomass appears to be affecting PFAA transport by increasing spreading behavior and enhancing retardation, at least for concentrations relevant to PFAA source-zones.

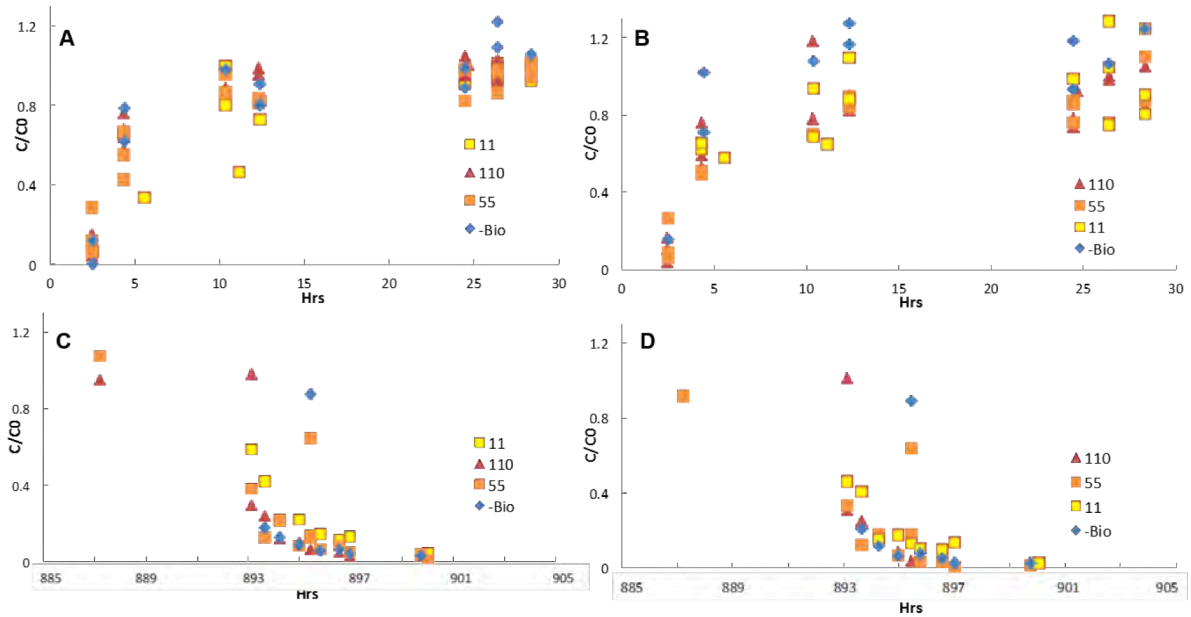

Figure 5-18. The breakthrough (**A, B**) of PFHxS and PFOA, respectively in biostimulated columns with varying levels of PFAAs (11, 55, 110) as compared to non-stimulated columns (-Bio). Also shown is the tailing behavior observed for PFHxS (**C**) and PFOA (**D**) in these columns.

5.4.4 Conclusions

In brief, these data suggest that continued biological activity will occur even when exposed to high concentrations of PFAAs (110 mg/L total). Activity was sufficiently repressed in the inactivated columns, while activity in the other columns generally decreased as a function of distance from the inlet. Upon comparison of permeability between the –PFAA, -Bio, and 110 mg/L PFAA scenarios, it is evident that the permeability is reduced in the presence of active microbiological communities. Columns with 110 mg/L PFAAs exhibited the greatest reduction in permeability. This may be a result of increased biofilm formation as a stress response activated upon PFAA exposure as observed previously (Weathers *et al.*, 2015). This same trend is also expressed as an increase in dispersivity in the microbially active columns. These results suggest that PFAAs do not inhibit bulk microbial activity, but may enhance biofilm formation thus reducing permeability, providing extra sorption sites and potentially impacting PFAA retardation.

5.5 Effects of chemical oxidants on PFAA transport in columns (*Task 4c*)

5.5.1 Background

PFASs are a diverse set of anionic, cationic, and zwitterionic organofluorine surfactants. PFASs exhibit unique physical and chemical properties including hydrophobicity and oleophobicity, and

a subset of PFASs, the PFAAs, also exhibit extreme stability with respect to thermal, chemical, and biological degradation ((Moody and Field, 2000; Prevedouros *et al.*, 2006; Backe *et al.*, 2013; D'Agostino *et al.*, 2014). PFASs have been widely used in a variety of industrial and consumer applications for over 50 years, and are now found throughout the world in variety of biological and environmental matrices (Prevedouros *et al.*, 2006; Lau *et al.*, 2007). PFAAs include perfluoroalkyl carboxylates (PFCAs; $F\text{-}(CF_2)_n\text{-}COO^-$) and perfluoroalkyl sulfonates (PFSAs; $F\text{-}(CF_2)_n\text{-}SO_4^-$), both of which are primarily anionic at environmentally relevant pH values (e.g., pH 4-9). PFAAs also exhibit low volatility, high water solubility, are considered proteinophillic, and the longer chain length compounds (i.e., carbon chain lenth≥8) have been demonstrated to bioaccumulate and possibly biomagnify (Prevedouros *et al.*, 2006; Conder *et al.*, 2008). While human epidemiologic PFAS studies have been mostly inconclusive, animal studies have frequently found dose dependent hepatic, reproductive, developmental, immunicological, and hormonal effects (Lau *et al.*, 2007; Steenland *et al.*, 2010; Lindstrom *et al.*, 2011). Drinking water provisional health advisories have been developed for PFOA and perfluoroocatane sulfonate (PFOS) by the U.S. Environmental Protection Agency (USEPA 2009).

AFFFs are employed by municipalities, industry, and the military to extinguish liquid fuel fires (Moody and Field, 2000). Many AFFF formulations have included PFASs (and in some cases, PFAAs), in addition to other hydrocarbon surfactants and solvents (Moody and Field, 2000; Place *et al.*, 2012). Repeated historic use at firefighter training areas has resulted in groundwater and porous media contamination, with PFAA groundwater concentrations reaching low mg/L levels and often co-occurring with hydrocarbons and chlorinated solvents (Moody and Field, 2000; Backe *et al.*, 2013; Moody and Field, 1999, McGuire *et al*., 2014). While the body of knowledge regarding PFAA fate and transport in surface waters and engineered treatment works is growing (e.g., as reviewed in by Ahrens, 2011), comparatively little research has been conducted to understand PFAA fate and transport in the subsurface, particularly under conditions representative of remediation technology applications.

ISCO is a mature remediation strategy that has been applied to clean up soil and groundwater contaminated by chlorinated solvents and hydrocarbons (Siegrist *et al.*, 2011). Recent laboratory-scale batch research has also tested chemical oxidative decomposition of PFAAs with varying amounts of success depending on oxidant type, activation method, solution chemistry, and reaction conditions (Hori *et al.*, 2004; Hori *et al.*, 2005; Lee *et al.*, 2009; Wang *et al.*, 2008; Lee *et al.*, 2010; Lee *et al.*, 2012a; Lee *et al*., 2012b; Liu *et al.*, 2012a; Liu *et al.*, 2012b; Mitchell *et al.*, 2013). However, exogenous energy sources (UV light, elevated temperatures) and reaction conditions (pure oxygen atmosphere), that would not be applicable for *in situ* treatment, have often been employed to enhance PFAA decomposition. ISCO has been observed to result in altered geochemical conditions (Siegrist *et al.*, 2011), and while there is a limited body of knowledge pertaining to PFAA transport as affected by geochemical conditions (Higgins *et al.*, 2006; Tang *et al.*, 2010; Guelfo and Higgins, 2013), to the best of our knowledge, no data on the effects of chemical oxidants on PFAA fate and transport in porous media have been collected.

The overall objective of this study was to investigate PFAA fate and transport in porous media as affected by ISCO. The specific objectives included: 1) evaluating the ability of environmentally-

relevant ISCO applications to degrade PFAAs; 2) examining changes to PFAA transport as impacted during oxidant application; and 3) determining the impacts of post-ISCO altered geochemistry on PFAA transport. The research objectives were investigated primarily using 1-dimensional columns and a six-phase approach to represent pre-oxidation, during-oxidation, and post-oxidation effects on PFAA fate and transport.

5.5.2 Experimental Methods and Approach

5.5.2.1 Experimental design

The experimental design included six phases (three days/phase amounting to ~35 pore volume/phase; **Figure 5-19**) to enable evaluation of environmentally relevant PFAA fate and transport through saturated porous media in an unoxidized system (phase i), during chemical oxidant application (phase ii and iii), and a post oxidation (phases iv, v, and vi). Source water was artificial groundwater (AGW), PFAA-containing AGW (PFAA-AGW; nominally 2 µg/L each PFAA), or oxidant-containing PFAA-AGW (oxidant-PFAA-AGW); see **Table 5-13** for details. Four oxidant treatments were tested: control (no oxidant), permanganate (8.4 mM MnO_4^- from $KMnO_4$), activated persulfate (52.1 mM $S_2O8_2^{2-}$ from $Na_2S_2O_8$ activated with 26.0 mM $FeCl_2$ and 5.2 mM $C_6H_8O_7$; Liang *et al.*, 2004), and catalyzed hydrogen peroxide (CHP; 49.0 mM H_2O_2 catalyzed with 0.5 mM $FeSO_4$). Each of the four treatments was tested in duplicate (i.e., two columns).

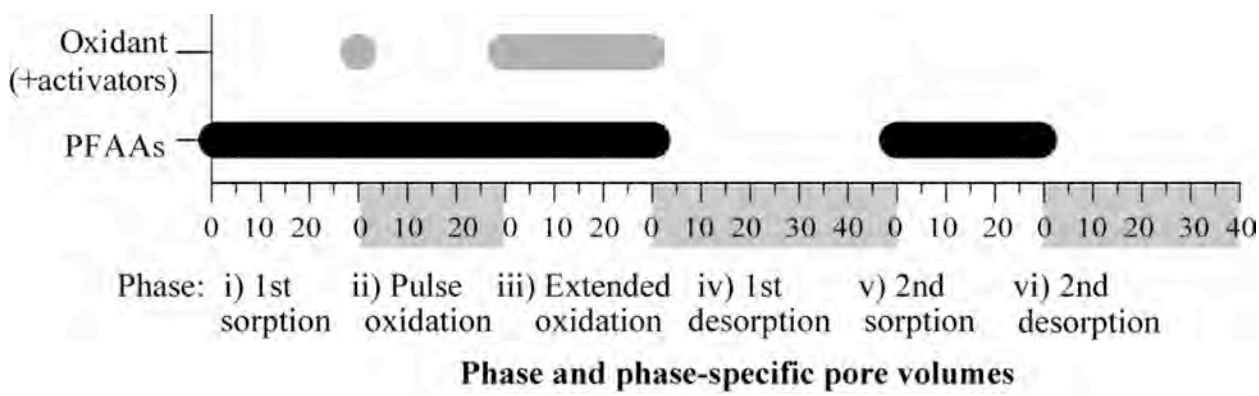

Figure 5-19. Six phrase experimental design where artificial groundwater (AGW) is continually provided and amended with PFAAs (PFAA-AGW; black) and oxidants (gray) as specified.

5.5.2.2 Materials

Well-characterized and PFAA-free loamy sand porous media (purchased from Agvise), which had been previously used in PFAA sorption studies (e.g., Guelfo and Higgins, 2013), was sieved (2 mm) and air-dried for use in all experiments. The loamy sand had a pH of 6.1, was 81% sand,

Table 5-13. Influent water quality parameters for provided influent waters

Source water	Components	Influent pH	Ionic strength	Salinity (‰)	Fe (mM)
Artificial groundwater (AGW)	Millipore water + 0.01 mM MnSO4 + 1.27 mM Na2SO4 + 1.93 mM NaCl + 0.48 mM NaHCO3	7.5	0.0056	0.33	0.0
PFAA-AGW	AGW + 2 µg/L each PFAA	7.5	0.0056	0.33	0.0
Activated persulfate	PFAA-AGW + 52.1 mM Na2S2O8 + 26.0 mM FeCl2 + 5.2 mM C6H8O7	1.9	0.2633	17.03	26.0
Permanganate	PFAA-AGW + 8.4 mM KMnO4	7.8	0.0140	1.66	0.0
Catalyzed hydrogen peroxide	PFAA-AGW + 14.7 mM H2O2 + 0.5 mM FeSO4	3.4	0.0076	0.91	0.5

10% silt, 9% clay, and had moderate organic matter content (f_{oc}=0.0089) that possibly exceeds typical aquifer organic matter content, but enables observable transport effects; **Table 5-14** contains additional characterization data. The loamy sand porous media was purchased from and principally characterized by Agvise prior to use in the experiments. Agvise analysis included soil pH (water), textural class (hydrometer method), dry bulk density (disturbed), cation exchange capacity, cations (K, Ca, Mg, Na, H via base saturation data), and Fe and Al (via citrate-bicarbonate-dithionite extractable). Porous media organic content (foc) was determined by TestAmerica Laboratories (USEPA WS-846 Method 9060A). Deionized water (Millipore, 18 Ω), Optima methanol (Fisher), and ACS reagent grade or better oxidant and activator reagents were used. AGW contained 0.01 mM $MnSO_4$, 1.27 mM Na_2SO_4, 1.93 mM NaCl, and 0.48 mM $NaHCO_3$ in deionized water (Guelfo and Higgins, 2013; **Table 5-13**). The investigated PFAA suite included: PFBA, PFPeA, PFHxA, PFHpA, PFOA, PFNA, PFDA, PFUnA, PFBS, PFHxS, and PFOS. Both anionic and neutral PFAAs may have been present due to the range of pH conditions that occurred, however the PFAAs will consistently be referred to using the listed abbreviations. PFAA native standards and mass-labeled surrogates were purchased from Wellington laboratories and were used for quantitation, while PFAA salts, for use in the experiments, were purchased from Sigma Aldrich.

Table 5-14. Loamy sand characteristics

pH	6.1
foc (%)	0.885
Sand (%)	81
Silt (%)	1
Clay (%)	9
Bulk density (disturbed; g/mL)	1.13
Cation exchange capacity (meq/100 g)	11.6
K (mg/kg)	319
Ca (mg/kg)	1084
Mg (mg/kg)	171
Na (mg/kg)	11
H (mg/kg)	33
Fe (mg/kg)	2210
Al (mg/kg)	930

5.5.2.3 Column packing and characterization

Glass columns (25 mm ID x 80 mm length; Kontes FlexColumn Economy) were dry-packed, CO_2 flushed, and AGW saturated. They were dry-packed using sonication and tamping to consolidate the porous media; glass beads and glass wool were included at both ends as additional support to ensure uniform flow distribution. Gravimetric analysis during the column packing procedure was used to determine porosity, pore volume, dry- and wet-bulk density, as shown in **Table 5-15**. Columns were packed, up-flow CO_2 flushed (2 minutes, ~5 psi backpressure), and then up-flow saturated with artificial groundwater (AGW; **Table 5-13**) for three to five pore volumes. For each column, hydrodynamic transport conditions were characterized via conservative tracer breakthrough curves (100 mg Br^-/L from KBr). For each individual column, Br^- mass recovery was calculated via method of moments and breakthrough curves were inversely modeled in HYDRUS 1-D (Šimůnek *et al.*, 2008) to fit a numerical solution to the advective-dispersive equation. The fit dispersivities were overlapping across all columns (95% confidence interval), so a single model was fit to all of the columns breakthrough curve data, and the estimated dispersivity (0.48 ± 0.06 across all columns) was used in PFAA inverse modeling. Packed column characterization results are shown in **Table 5-15**. Saturated media hydrodynamic transport characterization via bromide conservative tracer breakthrough curves and HYDRUS 1-D inverse modeling (Šimůnek *et al.*, 2008; **Table 5-15**) confirmed columns' statistical similarities. HYDRUS 1-D was selected to cover more complex modeling formulations of the project's other components. The eight columns' estimated longitudinal dispersivity (D_L = 0.48 ± 0.06 cm) and porosity (0.48 ± 0.06) were used in PFAA inverse modeling; the average linear velocity was 83.4 ± 3.7 cm/d.

Table 5-15. Packed loamy sand characteristics

Parameter	Mean	Standard deviation
Loamy sand foc (n=2) [a]	0.0089	0.0016
Soil height (cm; n=8) [b]	6.73	0.20
Porosity (n=8) [b]	0.40	0.15
Porous media pore volume (mL; n=8) [b, c]	15.49	0.71
Average linear velocity (cm/day; n=8) [b]	83.41	3.67
Dispersivity (cm; all column fit simultaneously) [d]	0.48	0.06

[a] CO2 evolution analysis
[b] gravimetric analysis conducted during column packing
[c] affected by soil mass and packing
[d] HYDRUS 1-D analysis

5.5.2.4 Column experiments, sample collection, and supporting batch experiments

Column experiments were conducted at room temperature in ambient light for 18-20 days as follows: i) 1st sorption (PFAA- AGW), ii) pulse oxidation (1 pore volume of oxidant-PFAA-AGW followed by PFAA-AGW), iii) extended oxidation (oxidant-PFAA-AGW for the entire phase), iv) 1st desorption (AGW), v) 2nd sorption (PFAA-AGW), and vi) 2nd desorption (AGW). The pulse oxidant phase (phase ii) was included to determine if there was an immediate and measurable response to the chemical oxidant application, and the extended oxidation phase (phase iii) was included as a remediation-relevant scenario.

The experimental setup included source water (AGW, PFAA-AGW, or oxidant-PFAA-AGW; **Table 5-13**) being continuously stirred with a stir bar, a high-precision multi-channel Ismatic peristaltic pump, an influent three-way valve, a packed column, and an effluent three-way valve (**Figure 5-20**). Replicate columns drew from the same source water. PFAA-AGW and oxidant-PFAA-AGW were created by spiking in a PFAA stock solution (7.5 mg/L of each PFAA in 70/30 (v/v) methanol/aqueous), where the stock solution was created from PFAA salts (Sigma Aldrich); the working solution contained 2 µg/L of each PFAA. In the case of activated persulfate and catalyzed hydrogen peroxide (CHP), the peristaltic pump provided oxidant and a syringe pump provided concentrated stock activator or catalyst that were mixed in an intermediate vessel (~0.5 hr residence time) and then supplied to the column. Influent samples were collected once/day from two columns (i.e., two samples/day), and sampled columns rotated on a schedule. Effluent sample times were selected to capture the PFAA suite breakthrough, with more intensive sampling at the beginning of a phase. For each phase, 18-27 effluents samples were collected from each column. A subset of collected samples, typically ~60% of collected samples, was analyzed by LC/MS/MS; unanalyzed samples were archived and analyzed as needed to provide a more complete profile.

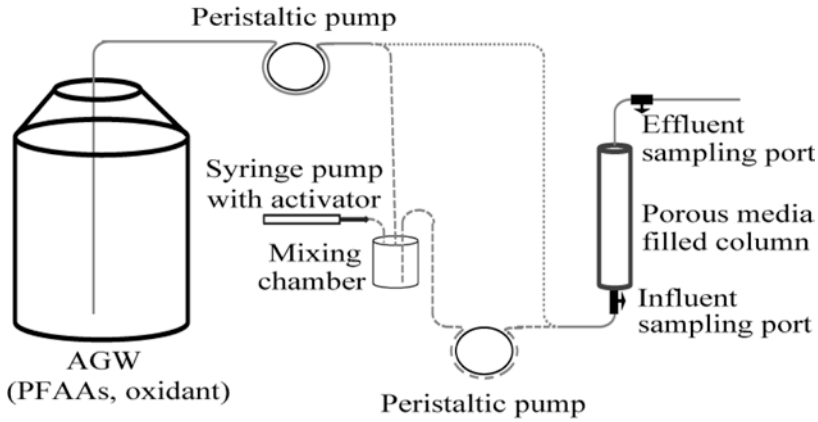

Figure 5-20. Experimental setup, including differential fluid flow paths for different applications where flow paths are as follows: solid-lined paths are used by all fluids; dashed-lined paths are used during activated persulfate and catalyzed hydrogen peroxide application; and dotted-lined paths are used for all other applications.

Column effluent samples were collected as follows: PFAA samples (18-27 samples/column·phase) which were quenched with methanol within 1 h (1:1 sample:methanol), pH samples (6-7 samples/column·phase), total organic carbon samples (TOC; 3 samples/column·phase), and metals samples (3 samples/column·phase). At the conclusion of the experiment, PFAA-AGW was supplied to the columns for five days to achieve complete breakthrough; the porous media columns were then stored in the dark at 6°C, and subsequently dissected for porous media organic carbon content (2 samples/column; TestAmerica via CO_2 evolution per USEPA WS-846 Method 9060A) and sorbed PFAA concentrations (3 samples/column; methanolic extraction per Guelfo and Higgins, 2013). Batch studies, to assess spike recovery and aqueous chemistry influences via pH adjustment and Fe amendments, were performed according to Guelfo and Higgins (2013) and are detailed in previously in this report.

To help inform the results of the column studies, limited batch studies were conducted, per Guelfo and Higgins (2013), to assess spike recovery and the influence of ISCO-relevant altered geochemistry on PFAA sorption. In vials, 15 g of soils were combined with AGW and PFAA stock; the PFAA working concentration was 2 µg/L for each PFAA. Spike recovery experiments

were conducted in glass vials, and the soil had been incubated on the shaker table for 10 days with PFAA-free oxidant-AGW prior to the addition of PFAAs. A full-factorial experimental design was employed to understand the effect of pH (2.1, 3.1, 3.7, and 5.4) and cation concentration (0, 0.25, 2.5, and 25 mM Fe amendments). Geochemistry batch experiments were conducted in plastic vials and were amended with iron (from $FeCl_2$) as appropriate, and pH adjusted (HCl or NaOH) as appropriate; no pre-incubation was needed. PFAA-containing batch systems were placed on a shaker table for 14 days, after which time, were centrifuged and the liquid was decanted off.

In the case of spike recovery and Fe-pH batch samples, the 15 g soil sample was extracted in its entirety. In the case of post-experiment soil extractions, a 2 g wet weight subsample was extracted. Soil samples were amended with isotopically-labeled surrogate; concentrations reflect surrogate recovery corrections. Basic methanol (1% NH4OH) was added to the soil sample, heated (45°C) and sonicated for 1 h, agitated on a shaker table at room temperature for 2 h, and then solids and liquids were separated by centrifugation (1467 Gs for 20 min). The extract was decanted into a glass scint vial and saved for further processing. The soil sample was then basic methanol extracted two additional time (three times total), and decanted extracts were pooled. The extract was evaporated to dryness in a heated water bath (50°C) under a continuous nitrogen stream and the residue was reconstituted in acidic methanol (1% C2H4O2). The reconstituted extract was transfer to a microcentrifuge tube that contained 20-40 mg ENVI-Carb (Supelco). The suspension was vortexed for 30 s and subsequently separated via centrifugation (17,000 Gs, 30 min). An aliquot of clean reconstituted extract was processed for analysis and another aliquot was archived. An aliquot of the aqueous chemistry batch study supernatant was analyzed by inductively coupled plasma atomic emission spectroscopy (ICP-AES) and the cumulative polyvalent cation concentration (ΣM^{++}) was the molar sum of Al, As, B, Ba, Ce, Ca, Cd, Co, Cr, Cu, Fe, Mg, Mn, Ni, Pb, Si, Sr, V, Zn, Sn, Mo, Sb, and Ti.

For all batch systems, both aqueous and extracted porous media were analyzed for PFAAs, which allowed for the direct calculation of partitioning coefficient values (K_d and K_{oc}). Spike recovery data were generally 100 ± 30%.

5.5.2.5 Analytical procedures

PFAA analysis was accomplished using LC-MS/MS (ABSciex 3200 detailed previous in this report) operated in negative electrospray ionization mode. Methanol-quenched PFAA samples were pH neutralized as needed (target pH 5-9). Samples were centrifuged, an aliquot was removed, and amended with mass-labeled surrogates (200 ng/L). Isotope dilution was used for LC/MS/MS analysis of PFAAs; PFAA transitions, surrogates, and limits of quantitation (LOQs) are shown in **Table 5-16**. Methanol-quenched PFAA samples were pH neutralized as needed (target pH 5-9). Samples were centrifuged (13,000 Gs for 20 min), an aliquot was removed, and amended with mass-labeled surrogates (200 ng/L). A 1 mL methanol-quenched, isotope-diluted sample was injected onto a 50 mm x 4.6 mm 3 µm particle size Gemini C18 column (Phenomonex). The mobile phase was 10 mM $NH_4C_2H_3O_2$ aqueous and methanol gradient that was pumped through an isolator column. Column effluent samples were analyzed in the order collected to minimize sharp changes in sequential samples' concentrations. Quantitation, based

on isotope dilution, was performed using Analyst software (ABSciex); surrogate recovery was generally >30% and reported PFAA concentrations reflect surrogate recovery corrections. Two transitions were monitored for each analyte, where the primary transition was used for quantification and the secondary for confirmation of unexpected results. Continuous calibration verification samples were included every 20 samples and blanks were included every six samples; analytical variability was generally <10% and carry over was minimal. Generally, PFAA concentrations in the effluents from replicate columns revealed RSDs that were ≤25%. The limits of quantitation (LOQs) were analyte, matrix, and run dependent, but were generally 10-80 ng/L for quenched aqueous samples and 0.02-0.6 ng/g for extracted porous media samples. TOC samples were preserved with H_3PO_4 and analyzed with a Shimadzu TOC-L analyzer, pH samples were immediately analyzed (Denver Instrument 215 with a Thermo gel-filled electrode), and metals samples were preserved with HNO_3 and analyzed via ICP-AES.

Table 5-16. PFAA analytes with associated transitions, surrogates, and LOQs.

Analyte (chain length)	MRM transitions		Mass labeled surrogate	Average LOQ [a]	
	Primary	Secondary		Aqueous (ng/L)	Porous media (ng/kg)
PFBA (3)	168.90	89.00	PFBA	13	13
PFPeA (4)	219.00	68.70	PFPeA	11	11
PFHxA (5)	269.00	118.70	PFHxA	15	11
PFHpA (6)	319.10	168.96	PFHpA	13	15
PFOA (7)	369.00	168.80	PFOA	34	13
PFNA (8)	418.80	218.90	PFNA	14	3
PFDA (9)	468.80	219.10	PFDA	19	34
PFUdA (10)	518.79	269.79	PFUdA	13	14
PFBS (4)	98.91	79.85	PFHxS	24	3
PFHxS (6)	99.00	79.80	PFHxS	13	3
PFOS (8)	99.10	80.00	PFOS	68	13

[a] LOQs established based on the following criteria: S:N>30; peak area>2x max blanks; estimated standard concentration within 30% of actual standard concentration

5.5.2.6 PFAA data analysis

HYDRUS 1-D was employed to inversely fit the PFAA effluent profiles (measured effluent concentration/measured influent concentration). PFAA sorption coefficients were estimated for each experimental phase separately (i.e., phase i, iv, v, and vi) to elucidate changes in the PFAA-porous media interaction. As all columns were similar (**Table 5-15**), replicate columns' PFAA breakthrough data were combined for modeling, such that phase i PFAA breakthrough models included data from eight columns, while all other PFAA HYDRUS models were fit based on the data from the duplicate columns. Data points <LOQ were included in the inverse modeling, using the Analyst estimated concentration, as they were temporally consistent with expectations. HYDRUS-fit distribution coefficient estimates ($K_{d,fit}$) were converted into retardation factors (R_{fit}; **Equation 5-20**).

$$R_{fit} = 1 + \frac{\rho_b}{\theta} \cdot K_{d,fit} \qquad \text{(eqn. 5-20)}$$

Where dry bulk density (ρ_b) and porosity (θ) were gravimetrically determined during packing.

Partitioning coefficients were calculated based on post-experiment extracted porous media, including a correction for the pore water PFAA concentrations (**Equation 5-21**).

$$K_d = \frac{C_s}{C_w} = \frac{(m_{extracted} - C_w \cdot V_{pore}) / m_{sed}}{C_w} \qquad \text{(eqn. 5-21)}$$

Where C_s and C_w are the respective PFAA solid (ng/kg) and aqueous (ng/L) concentrations, $m_{extracted}$ is the PFAA mass extracted from the post-experiments column porous media sub-sample (m_{sed}), and V_{pore} is the volume of pore water that was included in the porous media sub-sample extraction (gravimetrically determined). For inclusion, C_s and C_w must be quantifiable (i.e., >LOQ). In select cases, the pore water-corrected porous media concentration (C_s) was less than zero, and no distribution coefficient values are reported. Calculated K_d and measured porous media organic carbon content (f_{oc}) values were used to calculate porous media organic carbon-water partitioning coefficient (K_{oc}) as follows (**Equation 5-22**):

$$K_{oc} = \frac{K_d}{f_{oc}} \qquad \text{(eqn. 5-22)}$$

The aqueous chemistry batch experiment results were statistically analyzed, for each PFAA, to elucidate cation concentration and pH effects on PFAA distribution coefficients. The cumulative polyvalent cation concentration (molar sum of ICP-AES measured cations which was predominantly comprised of Ca, Mg, Fe; indicated as log ΣM^{++}), was found to be a better model predictor than was iron concentration. The employed statistical model was as follows (**Equation 5-23**):

$$\log(K_{d,i}) = \beta_{0,i} + \beta_{1,i} \cdot pH + \beta_{2,i} \cdot \log(\Sigma M^{++}) + \beta_{3,i} \cdot pH \cdot \log(\Sigma M^{++}) \qquad \text{(eqn. 5-23)}$$

where R software was used to determine the parameter estimates (e.g., $\beta_{1,i}$) for PFAA i. For each PFAA, this model was refined by removing independent variables that were not statistically significant for estimating log $K_{d,i}$ (α=0.05).

5.5.3 Results and Discussion

5.5.3.1 PFAA transport through unoxidized porous media

A representative profile of PFAA column effluent levels is provided in **Figure 5-21** (concentrations are averaged for duplicate columns).

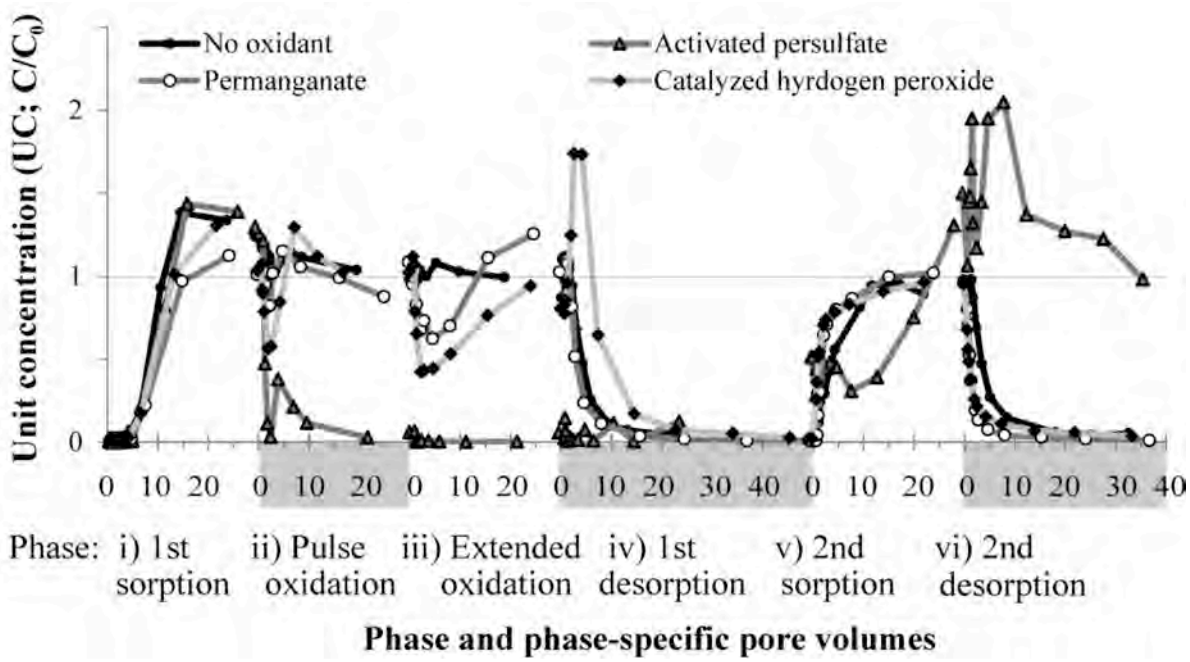

Figure 5-21. Column PFOS effluent profiles (total experiment duration was 18-20 days), where the source waters are shown in **Figure 5-19** and detailed in **Table 5-13**. Each profile represents the average of two columns' effluent concentrations (i.e., 138 - 153 effluent samples/profile), where replicate columns effluent profiles RSD<25%. TOC and pH effluent profiles are shown in **Figure 5-23 and Figure 5-24.**

To establish a PFAA transport baseline, PFAA breakthrough was observed in porous media prior to oxidant application. An example of measured PFAA unit concentrations (C/C_0) and the associated HYDRUS fitted breakthrough curves are shown in **Figure 5-22A**; the estimated retardation factors for the PFAA suite are shown in **Figure 5-22B**. PFAAs of chain length six and longer displayed increased retardation with increasing chain length; there was a 0.62 log K_d increase for each additional CF_2 moiety (similar to batch study data of 0.45 to 0.6 $\Delta\log K_d/\Delta CF_2$; Higgins *et al.*, 2006; G uelfo and Higgins, 2013). In previous batch studies, shorter chain length compounds were found to be more sorbing than the chain length dependent trend would predict (Guelfo and Higgins, 2013). In this study, PFCAs of chain length five and shorter generally had retardation factor estimates that included unity (i.e., no retardation, resulting in relatively rapid travel time through the column), though PFBA was slightly retarded, providing further evidence of a potential steric effect on short-chain PFAA sorption. PFSAs sorbed more than PFCAs of equivalent chain length, though the difference was slightly larger than measured in earlier studies (Δ0.49 log K_d herein vs. 0.23 in Higgins and Luthy, 2006).

Effluent pH and TOC were monitored throughout the six phase experiment. Effluent pH and TOC values are shown in **Figure 5-23** and **Figure 5-24**. TOC was also measured in the persulfate effluent water, however column duplicate variability was high, possibly due to the citric acid-containing activator and insufficient pre-column mixing to ensure homogeneous application. Due to the high variability, activated persulfate effluent TOC values are not shown (**Figure 5-24**). For persulfate-exposed columns, post-experiment porous media organic content was statistically the same as the source material.

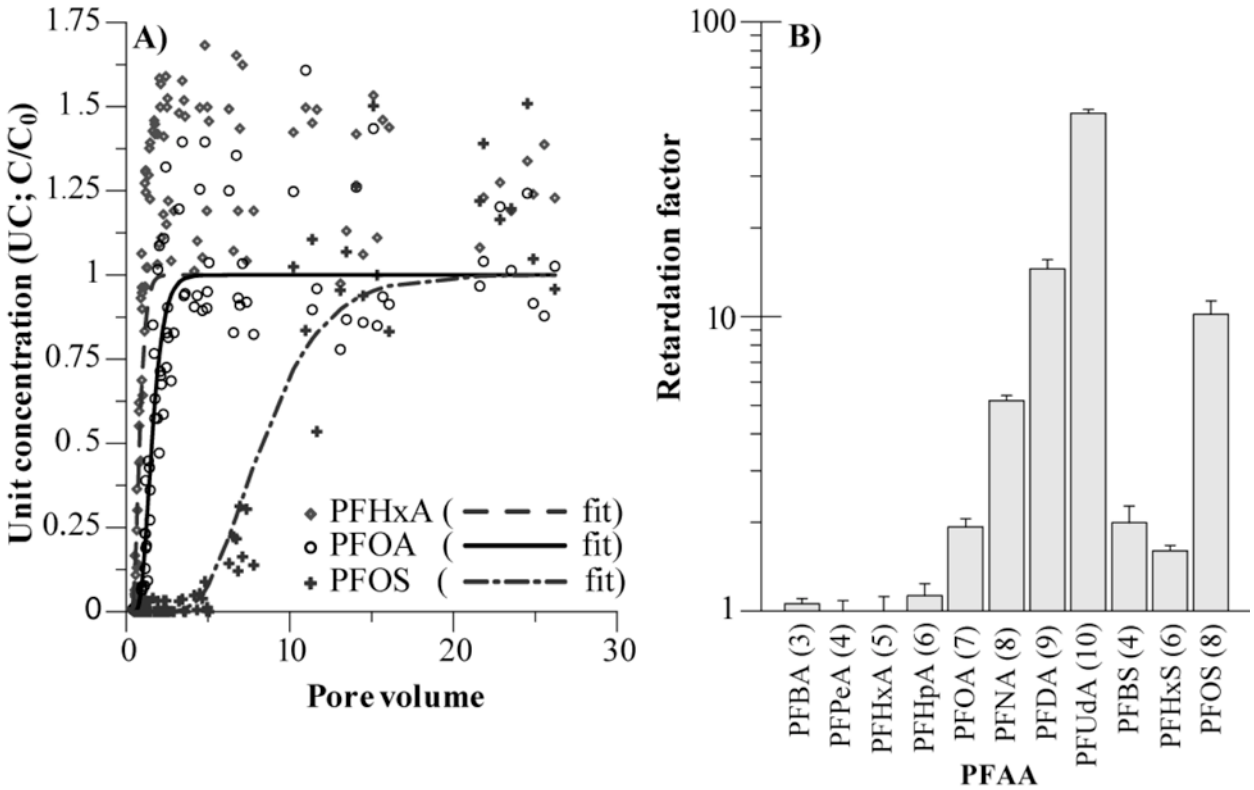

Figure 5-22. PFAA phase i breakthrough in porous media systems; columns' (n=8) data are fit with one HYRDUS model. A) select PFAA column effluent measured concentrations and associated HYRUS fits. B) Retardation factors estimates for the PFAA suite.

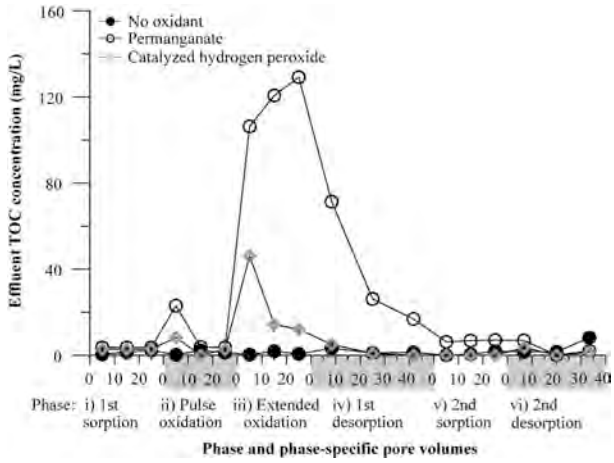

Figure 5-23. TOC effluent profile.

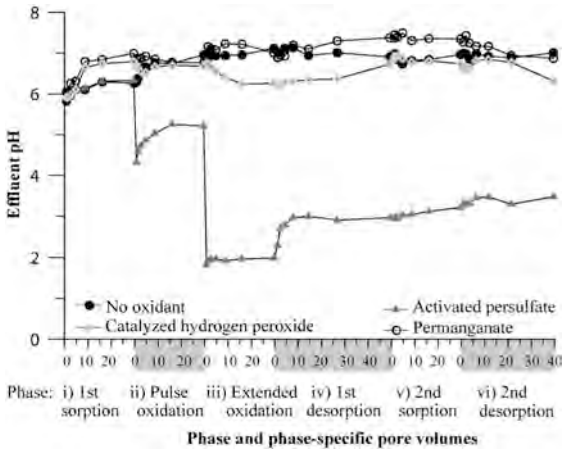

Figure 5-24. pH effluent profile.

5.5.3.2 PFAA fate during ISCO application to the porous media

To determine if PFAAs were being degraded under the ISCO conditions tested, PFAA mass recoveries were determined and analyses were conducted for potential transformation products. PFAA mass recoveries over the course of the experiment, shown in **Table 5-17**, were calculated

on two bases: 1) phases i – iv; and 2) phases i – vi. Data analysis focused on the phase i – iv mass balance calculations, however, some effluent profiles (e.g., longer chain length compounds exposed to persulfate) suggested incomplete desorption after oxidant application, which warranted mass balance calculations based on phases i-vi. For the columns not subjected to ISCO, 87-127% recovery was observed (**Table 5-17**), where experimental and analytical error likely contributed to the observed slight over- and under-recoveries. Similar recoveries were observed for the ISCO columns, with the notable exception of the longer chain-length compounds. These compounds, particularly in persulfate-oxidized systems, exhibited substantial under-recoveries which were at least partially explained by incomplete desorption during the final phase of the experiment (e.g., **Figure 5-21**).

Table 5-17. Calculated PFAA mass recovery values for duplicate columns (%; mean ± standard deviation for phases i-iv, unless otherwise indicated)

PFAA (chain length)	No oxidant	Activated persulfate	Permanganate	Catalyzed hydrogen peroxide
PFBA (3)	96 ± 1	82 ± 3	95 ± 0	97 ± 2
PFPeA (4)	127 ± 4	113 ± 14	82 ± 2	91 ± 6
PFHxA (5)	125 ± 7	140 ± 20	112 ± 3	102 ± 6
PFHpA (6)	112 ± 5	130 ± 17	91 ± 2	92 ± 0
PFOA (7)	118 ± 3	97 ± 2	88 ± 1	86 ± 3
PFNA (8)	91 ± 3	94 ± 4 [a, b]	100 ± 2	96 ± 4
PFDA (9)	102 ± 0	79 ± 5 [a, b]	79 ± 2	84 ± 11
PFUdA (10)	87 ± 3 [a, b]	8 ± 0 [a, b]	86 ± 1 [a]	73 ± 6 [a, b]
PFBS (4)	56 ± 2 [c]	53 ± 8 [c]	80 ± 8	95 ± 7
PFHxS (6)	92 ± 4	114 ± 11	94 ± 5	96 ± 6
PFOS (8)	108 ± 7	88 ± 5 [a, b]	97 ± 3	100 ± 6

[a] Mass recovery based on phase i-vi, due to phase iv concentrations not reaching C/C0~0
[b] Phase vi final C/C0 ≥ 0.1 (i.e., PFAA remaining in soil); incomplete mass recovery expected
[c] Incomplete PFBS mass recoveries are expected (e.g., ~50%), as phase i-iv plateaus were C/C0 ~0.5

As PFAA persulfate oxidation mechanisms have typically included a stepwise reduction in PFAA chain length (i.e., loss of a CF_2 moiety; Hori *et al.*, 2005; Lee *et al.*, 2009; Lee *et al.*, 2010; Lee *et al.*, 2012a; Lee *et al.*, 2012b; Liu *et al.*, 2012a), one could expect under-recovery of PFUdA and over-recovery of shorter chain-length PFCAs if oxidative decomposition was occurring (e.g., Hori *et al.*, 2005); a detailed review of previous PFAA-chemical oxidant findings is included in below. Slight over-recoveries were observed for some shorter chain length PFCAs, though this was also observed to a lesser extent in no oxidant control columns (**Table 5-17**). Perfluoropropanoate (PFPrA, $F\text{-}(CF_2)_2\text{-}COO^-$) was not included in the spiking mixture and would be the stepwise decomposition product. PFPrA analysis was selectively undertaken for the extended persulfate oxidation samples, and PFPrA was not detected.

A moderate amount of experimental work has been previously conducted to assess chemical oxidants potential for PFAA decomposition and defluorination. Studies have largely focused on persulfate and PFOA, though the experimental conditions have often not been ISCO-relevant. Generally, higher persulfate concentrations, exogenous energy, iron activation, and acidic

conditions (favoring the formation of sulfate radicals over hydroxyl radicals)[4] resulted in increased PFCA degradation rates, though departures from stated trends were observed and attributed to various self-quenching mechanisms (Hori *et al.*, 2005; Wang *et al.*, 2008; Lee *et al.*, 2009; Lee *et al.*, 2010; Lee *et al.*, 2012a; Lee *et al.*, 2012b; Liu *et al.*, 2012); elevated Cl^- was also observed to decrease PFOA decomposition rates, likely due to radical scavenging (Lee *et al.*, 2010). In the present study, activate persulfate solutions contained 54 mM chloride. Chloride scavenging may result in decreased PFAA oxidation by activated persulfate, but, based on the results of Lee *et al.* (2010), PFAA oxidation should only be inhibited 25% or less due to the chloride present in the system. The agreed upon persulfate-PFCA reaction mechanism is decarboxylation resulting in an unstable alcohol, which then undergoes HF elimination and hydrolysis resulting in PFCA with a chain length of n-1, such that a stepwise chain length reduction occurs and can ultimately result in complete mineralization and the formation of F^- and CO_2 (Hori *et al.*, 2005; Lee *et al.*, 2009; Lee *et al.*, 2010; Lee *et al.*, 2012a; Lee *et al.*, 2012b; Liu *et al.*, 2012). Several studies have been able to entirely account for fluorine and carbon via mass balance (Hori *et al.*, 2005; Lee *et al.*, 2012a; Lee *et al.*, 2012b; Hori *et al.*, 2004). Lee *et al.* (2012) fit a second order rate law to persulfate decomposition of PFOA in the dark at environmentally relevant temperatures, which would result in a PFOA decomposition rate of 0.018 M^{-1} h^{-1} in this study if the influent concentrations and 21°C are assumed (i.e., $t_{1/2}$~200 h, or ~22% PFOA decomposition during the three day phase iii extended oxidation).

Lee *et al.* (2012) did not include an iron activator. However, at room temperature, PFOA decomposition by persulfate has generally been found to be minimal, and the addition of iron (zero valent iron or Fe^{2+}) does not increase PFOA decomposition rates (Lee *et al.*, 2009; Lee *et al.*, 2010; Lee *et al.*, 2012; Liu *et al.*, 2012). Slow PFOS decomposition by permanganate has been observed (k ~ 0.0003 h^{-1} for 100 µg/L PFOS, 1 mg/L $KMnO_4$, pH=7.2, and T=65°C), where increased temperature, increased permanganate concentrations, and acidic conditions were generally found to result in faster PFOS decomposition (Liu *et al.*, 2012). Liu *et al.* (2012) also suggested that permanganate attacks the C-C and C-S bonds, suggesting the resulting formation of shorter chain length PFSA homologues or alternate PFASs. Iron catalyzed hydrogen peroxide, via the formation of superoxide, has also been demonstrated to show promise for the degradation and defluorination of PFOA (Mitchell *et al.*, 2013).

Phase specific effluent profile qualitative scoring and mass recovery calculations were conducted for phase ii and iii for each PFAA. Qualitative scoring criterion, examples, and results are shown in **Table 5-18** and **Table 5-19** for phase ii and phase iii, respectively, and mass recoveries are shown in **Table 5-20** for phase ii and phase iii.

Table 5-18. PFAA pulse oxidation (phase ii) effluent profile qualitative scoring results, indicating the effect on PFAA fate and transport due to changes in aqueous and porous media quality

PFAA (chain length)	No oxidant	Activated persulfate	Permanganate	Catalyzed hydrogen peroxide
PFBA (3)	0	1	0	0
PFPeA (4)	0	1	0	0
PFHxA (5)	0	1	0	0
PFHpA (6)	0	2	0	0
PFOA (7)	0	2	0	1
PFNA (8)	0	3	0	1
PFDA (9)	0	3	1	1
PFUdA (10)	0	3	1	1
PFBS (4)	0	1	0	0
PFHxS (6)	0	2	0	1
PFOS (8)	0	3	1	1
Qualitative scoring			**Figure 5-21** phase ii example	Phase ii mass recovery
0 ≡ no effect, small disturbances			No oxidant	100.2 ± 9.9%
1 ≡ small reduction, recovers quickly			Permanganate	99 ±12.5%
2 ≡ large reduction, C/C0 ~ 0, recovers gradually			Not shown	92.8 ± 25%
3 ≡ large enduring reduction, C/C0~0, incompletely recover			Persulfate	18.6 ± 6.6%

Table 5-19. PFAA extended oxidation (phase iii) effluent profile qualitative scoring results

PFAA (chain length)	No Oxidant	Activated persulfate	Permanganate	Catalyzed hydrogen peroxide
PFBA (3)	0	1	0	0
PFPeA (4)	0	2	2	0
PFHxA (5)	0	1	0	0
PFHpA (6)	0	1	2 (0) [a]	0
PFOA (7)	0	1	2 (0) [a]	1
PFNA (8)	0	1	1	1
PFDA (9)	0	3	1	1
PFUdA (10)	0	3	1	2
PFBS (4)	0	1	2	0
PFHxS (6)	0	1	0	0
PFOS (8)	0	3	1	1
Qualitative scoring			**Figure 5-21** phase iii example	Phase iii mass recovery
0 ≡ no effect, small disturbances but no generally trend			No oxidant	99.9 ± 9.4%
1 ≡ brief reduction and recovery to C/C0=1; recovery typically occurs promptly			Permanganate	78.1 ± 24.0%
2 ≡ reduction and plateau, where steady state concentration is C/C0<1			CHP	63.5 ± 16.5%
3 ≡ remain at C/C0~0 from entire phase 3			Persulfate	4.5 ± 3.3%

[a] Plateau or dip occurs between 0.8≤ C/C0 ≤1, which could be due to analytical error

Table 5-20. PFAA pulse oxidation mass recovery values.

PFAA (chain length)	No oxidant	Activated persulfate	Permanganate	Catalyzed hydrogen peroxide
phase ii				
PFBA (3)	92	92	97	99
PFPeA (4)	125	118	91	96
PFHxA (5)	119	123	110	100
PFHpA (6)	108	118	95	94
PFOA (7)	110	68	93	86
PFNA (8)	87	26	102	96
PFDA (9)	105	15	91	86
PFBS (4)	55 a	51 a	89	101
PFHxS (6)	90	93	95	96
PFOS (8)	106	15	99	102
phase iii				
PFBA (3)	94	60	90	97
PFPeA (4)	118	75	71	93
PFHxA (5)	111	125	112	98
PFHpA (6)	103	92	85	91
PFOA (7)	114	50	81	83
PFNA (8)	90	39	96	81
PFDA (9)	109	7	73	45
PFUdA (10)	101	6	73	39
PFBS (4)	57 [a]	56 [a]	69	103
PFHxS (6)	85	99	92	97
PFOS (8)	100	1	101	75

[a] PFBS breakthrough curve plateaued C/C0 ~ 0.5; this is likely due to the use of an unmatched surrogate (i.e., PFHxS); persulfate contrasts to the control should be valid

Stepwise reduction in PFAA chain length due to oxidation has been previously observed, therefore, given the PFAA spiking suite, PFUdA and PFOS, for which there would be no sources, are the PFAAs most likely to reveal oxidative decomposition. The PFUdA effluent profile is shown in **Figure 5-25**. Under-recoveries were observed for some longer chain length PFAAs, particularly those exposed to persulfate. For example, following the persulfate pulse application, near zero effluent PFUdA concentrations were observed for the remainder of the experiment (~15 days, as shown in **Figure 5-25**), which resulted in substantial PFUdA under-recovery (8%).

Taken together, these data suggest that little to no oxidative decomposition of PFAAs was occurring, and that the under-recoveries, particularly of PFUdA and PFOS in the persulfate columns, were primarily the result of unexpectedly slow desorption (and thus premature cessation of column sampling). In fact, following the pulse persulfate application (phase ii), effluent PFUdA concentrations remained near zero for the remainder of the experiment (**Figure 5-25**). This included near zero PFUdA concentrations for the second sorption and desorption phases (phases v and vi), for which complete breakthrough was observed for shorter chain length PFAAs.

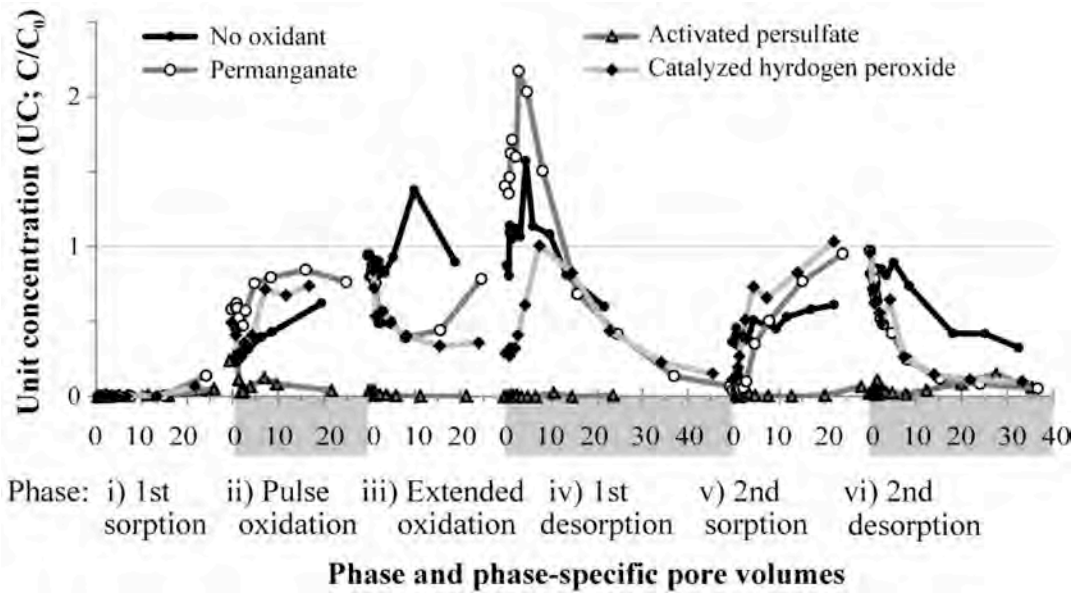

Figure 5-25. PFUdA effluent profile.

PFUdA forward modeling was conducted to determine if aqueous chemistry changes were likely responsible for observed effluent profiles, specifically the near-zero effluent concentrations observed in persulfate-exposed columns. Results of the aqueous chemistry batch studies (as shown in **Figure 5-25**) were used to predict, using the statistical software R, the soil water distribution coefficient for extended oxidation (phase iii) aqueous chemistry conditions. K_d values were converted to retardation factors (**Equation 5-20**), and then PFUdA effluent profiles were forward modeled in CXTFIT. CXTFIT models were produced for the phase iii estimate and the prediction interval values. Model estimates are shown in **Figure 5-26A**, and the persulfate prediction interval is shown in **Figure 5-26B**.

To more thoroughly assess PFAA oxidative transformations, pentafluoropropanoic acid (PFPrA) were further investigated, as it was not included in the spiking solution and is likely to be produced if PFAA decomposition is occurring via a stepwise reduction in CF_2 moieties. PFPrA was not included in the routine quantitative analysis. Instead, qualitative analysis of PFPrA was undertaken via orthogonal liquid chromatography (Backe *et al.*, 2013) with an Ab Sciex 5600 quadrupole time-of-flight mass spectrometer (QTOF). PFPrA stock solutions were analyzed to determine chromatographic retention times and to produce characteristic fragmentation patterns. Then two phase iii (extended oxidation) samples from the persulfate systems were analyzed. For each sample, PFPrA was monitored based accurate mass, retention time, and fragmentation. PFPrA peaks were not detected, which suggests that stepwise decomposition was not occurring the columns to which persulfate was applied.

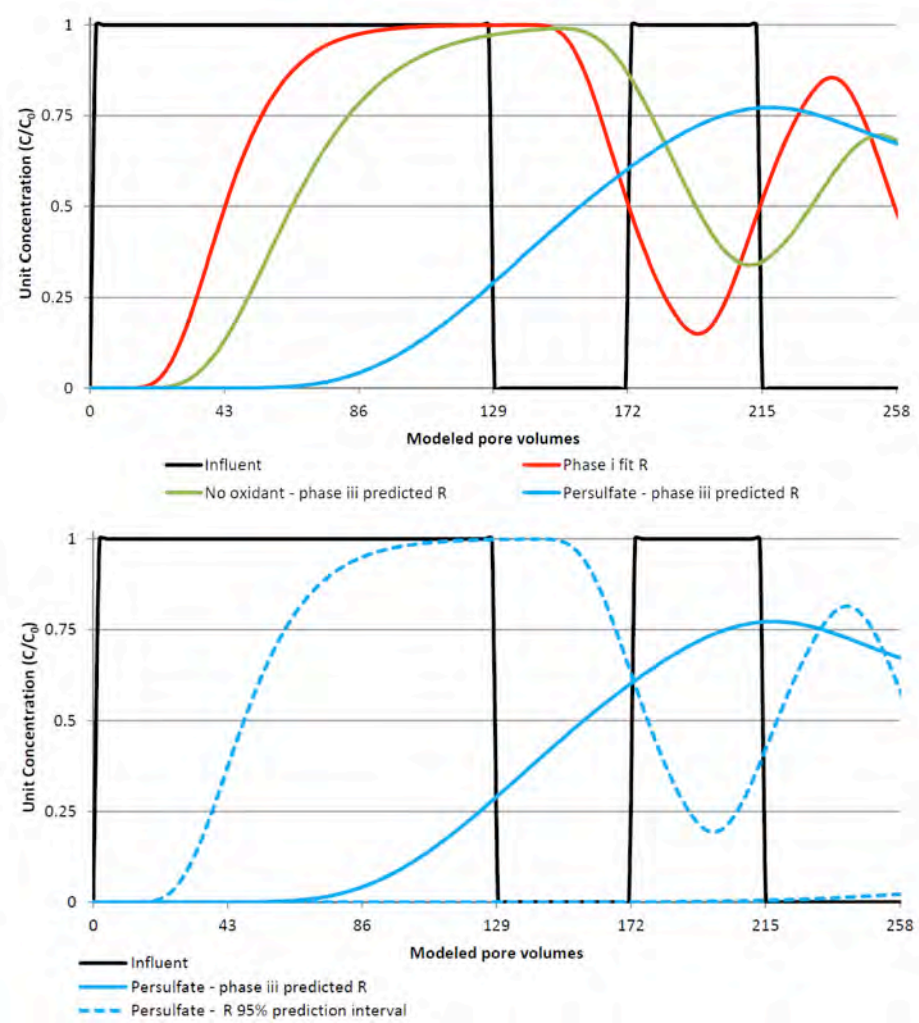

Figure 5-26. PFUdA effluent profile Modeled PFUdA effluent profiles as affected by aqueous chemistry for (A) estimate from the batch data-based statistical model (**Table 5-21**), and (B) persulfate exposed column prediction interval. "Phase i fit R" is based on the fit retardation factor (i.e., R = 49 for measured data), while phase iii estimates and predictions were produced based on the effluent water quality parameters and the PFUdA statistical model.

Water quality changes in the persulfate-exposed column are likely to substantially retard PFUdA breakthrough (e.g., extended oxidation (phase iii) PFUdA retardation factors were 76 and 178 for the no oxidant reference and persulfate-exposed systems, respectively, based on aqueous chemistry changes). The persulfate-exposed forward model estimate did include substantial breakthrough ($C/C_o \sim 0.75$; **Figure 5-26A**), but the 95% upper prediction interval resulted in near-zero effluent concentrations for the duration of the experiment (**Figure 5-26B**). Taken together, it is possible that water quality changes could be solely responsible for the near-zero PFUdA effluent concentration in the persulfate-exposed column, but it is more likely that there are other factors, such as altered geochemistry within the porous media, influencing PFUdA sorption and thus transport. While PFOS was fully recovered in the CHP columns, PFUdA was

slightly under-recovered, which could be attributable to incomplete desorption or analytical error. Given the lack of evidence of shorter chain length PFCA formation in the CHP columns, this suggests sample variability contributed to the lower PFUdA recovery, at least in the case of the CHP columns.

ISCO may have limited effectiveness for the oxidation of PFAAs in porous media, as its *in situ* nature results in lower temperatures (as compared to bench experiments), a general absence of exogenous energy sources, and likely presence of abundant scavenging species. The presence of competitive reducing agents such as soil organic matter (SOM) or scavengers such as chloride (Cl^-) are likely responsible, at least in part, for the differences observed between this study compared with previous single-phase studies in which PFAA decomposition was observed (Hori *et al.*, 2004; Hori *et al.*, 2005; Lee *et al.*, 2009; Wang *et al.*, 2008; Lee *et al.*, 2010; Lee *et al.*, 2012a; Lee *et al.*, 2012b; Liu *et al.*, 2012a; Liu *et al.*, 2012b; Mitchell *et al.*, 2013).

5.5.3.3 Aqueous chemistry effects on PFAA sorption

To better understand the implications of ISCO-relevant water quality changes on PFAA sorption, potential pH and cation effects were tested in batch systems with subsequent statistical analysis. The statistical model parameter estimates (i.e., $\beta_{1,i}$ and $\beta_{2,i}$ for PFAA i from the statistical model (**Equation 5-23**) are shown in **Figure 5-27C**. The cumulative polyvalent cation concentration reflects measured aqueous concentrations, however those values may change with porous media character.

Final PFAA partitioning distribution (Log K_d) statistical models, which generally included log cumulative polyvalent cations and pH, are provided in **Table 5-21**. Sorption generally increased with increasing polyvalent cation concentration and with decreasing pH values, which is consistent with electrostatic interactions resulting from changes in the SOM. Cumulative polyvalent cation concentration, as affected by pH and iron

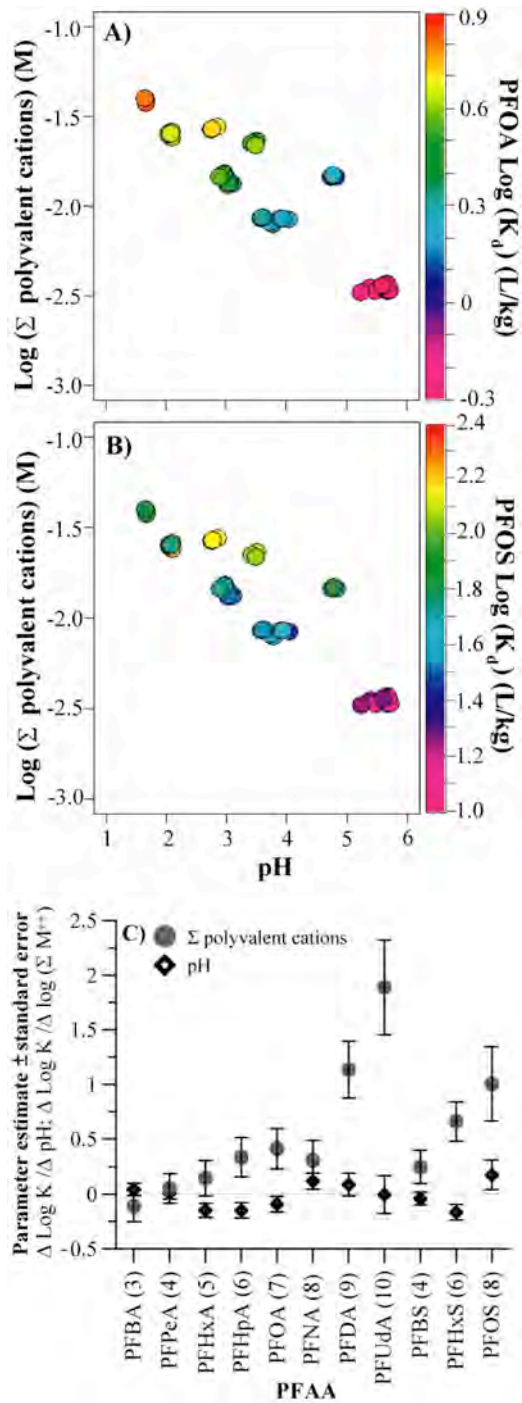

Figure 5-27. The effects of an oxidized system on PFAA transport. Phase i and phase v sorption breakthrough curve retardation factors are contrasted for the PFAA suite.

amendment level, generally had a greater effect and was more significant than was pH (i.e., larger estimate value and lower p-value). The cumulative aqueous polyvalent cation concentration parameter estimate increased with increasing chain length (at α=0.05, β_2 was significant for PFAAs of chain length six and longer), which suggests that polyvalent cations may be affecting hydrophobic interactions. Higgins and Luthy (2006) observed similarly increased PFAA sorption to surface water sediments in the presence of divalent calcium (0.36 log K_{oc}/log [Ca] for chain length seven and longer).

Table 5-21. Final statistical model estimates for the effects of water quality on PFAA distribution coefficients; based on batch system measured aqueous and extracted sediment concentrations

PFFA (chain length)	Final Statistical Model	
	Description	**Equation**
PFBA (3)	Intercept	Log K_d = -0.05
PFPeA (4)	Cations	Log K_d = 0.43 + 0.23 Log(Σ Me^{++})
PFHxA (5)	pH	Log K_d = 0.67 - 0.11 pH
PFHpA (6)	pH and cations	Log K_d = 1.11 - 0.13 pH + 0.31 Log(Σ Me^{++})
PFOA (7)	pH and cations	Log K_d = 1.88 - 0.14 pH + 0.52 Log(Σ Me^{++})
PFNA (8)	pH and cations, and interactions	Log K_d = 1.80 + 0.12 pH + 0.31 Log(Σ Me^{++}) + 0.09 pH * Log(Σ Me^{++})
PFDA (9)	pH and cations	Log K_d = 3.02 + 0.10 pH + 1.10 Log(Σ Me^{++})
PFUdA (10)	pH and cations	Log K_d = 3.76 + 0.24 pH + 1.34 Log(Σ Me^{++})
PFBS (4)	Cations	Log K_d = 0.50 + 0.30 Log(Σ Me^{++})
PFHxS (6)	pH and cations	Log K_d = 1.82 - 0.10 pH + 0.51 Log(Σ Me^{++})
PFOS (8)	Cations	Log K_d = 3.27 + 0.85 Log(Σ Me^{++})

Parameter estimates for pH were generally lower than for cumulative polyvalent cation concentration, which is consistent with Higgins and Luthy (2007). Previous studies have examined aqueous chemistry effects on PFAA sorption (Higgins and Luthy, 2006; Tang *et al.*, 2010), however this is the first report of chain length-dependent effects. Previous research on organic compounds demonstrated substantially increased K_{oc} values for the neutral species as compared to the anionic species (e.g., 7-60 fold with a sigmoidal curve shape; Tülp *et al.*, 2009). This study's statistical model accurately fit the data across the tested pH range (pH ~1.9-5.4; i.e., no obvious heteroscedasticity), which suggests that the PFAA's acid dissociation constant was not approached; this is consistent with PFOA pK_a~0, as estimated by Goss (2008a, 2008b). The results of the batch studies suggest that aqueous chemistry changes are at least partially responsible for the observed effluent profiles.

5.5.3.4 Effects of oxidant species and altered geochemistry on PFAA transport

ISCO application did impact PFAA transport, as decreased PFAA effluent concentrations were observed in both the pulse and extended oxidation phases (**Figure 5-21**). In light of the evidence suggesting PFAAs are not being degraded, the observed decreases in effluent concentrations can be likely ascribed to increased sorption. These increases could be due to either temporary changes in aqueous chemistry (including the presence of radical species and changes in pH or dissolved polyvalent cation concentrations) or permanent changes to the porous media quality (including altered SOM, changes to porous media surface charge, or formation of new solid or

gaseous phases). Phase-specific effluent profile qualitative scoring and mass recovery calculations were conducted for phase ii and iii for each PFAA and the results are included in **Table 5-18, Table 5-19, and Table 5-20.** Responses to oxidant application were PFAA and oxidant specific, but the three oxidants each produced immediate and measurable reductions in effluent PFAA concentrations in response to the oxidant pulse (phase ii) and extended oxidation (phase iii), and effluent concentration reductions were observed within 1-1.5 pore volumes of oxidant application (i.e., advective travel time through the column). The relative impact of the oxidants was generally of the order: activated persulfate >> catalyzed hydrogen peroxide ≥ permanganate ≥ no oxidant. Moreover, effects were generally greater for longer chain PFAAs; for persulfate-exposed longer chain length PFAAs (PFDA, PFUdA, and PFOS), C/C_0 remained near zero throughout the extended oxidation.

Application of chemical oxidants resulted in changes in the source and column effluent water quality (**Table 5-13**, **Figure 5-23,** and **Figure 5-24**); changes to the porous media quality were indicated, where organic matter is commonly believed to be the dominant sorbing phase (Prevedouros *et al.*, 2006; Higgins and Luthy, 2006; Higgins and Luthy, 2007; Guelfo and Higgins, 2013). Appreciable elevated effluent OM concentrations were observed when permanganate was applied (~120 mg/L TOC), and to a lesser extent for CHP (~20 mg/L TOC). Activated persulfate-exposed columns' effluent TOC concentrations varied widely, therefore these data are not reported. However activated persulfate exposed columns had statistically similar porous media organic matter content (f_{oc}) as the no oxidant columns (α=0.05), based on post-experiment analysis. Immediately following oxidant application, noteworthy PFAA effluent concentration increases were generally not observed for any of the treatments, indicating that sorbing site reduction, due to SOM destruction, alteration, or exportation, was not a dominant mechanism governing PFAA transport changes during ISCO. Application of activated persulfate resulted in the largest changes to PFAA transport, and also the greatest source and effluent water quality changes, including pH reductions, elevated iron concentrations, and elevated solution ionic strength (**Table 5-13**).

5.5.3.5 Effects of oxidized porous media on PFAA transport

The porous media had oxidant applied for 73.85 h, which likely resulted in an altered porous media matrix. The effects of an oxidized system on PFAA transport was explored with two approaches: 1) column transport retardation factors (phases iv-vi), exemplified by **Figure 5-28** contrasting pre-oxidant (phase i) and post-oxidant transport (phase v; contrasts with phase iv and vi are shown in **Figure 5-29** and **Figure 5-30**), and 2) post-experiment extracted porous media-derived distribution coefficients (**Figure 5-31**). Transport changes were observed between phase i and phase v, even for columns that were not exposed to oxidant at any time. Potential causes of the observed acceleration include: alterations in column hydrology (e.g., short-circuiting within the column), changes in aqueous chemistry, a system-wide loss of sorption sites (e.g., OM desorption and exportation), site occupation (e.g., irreversible PFAA-OM binding), or site alteration (e.g., OM migration into porous media pores). Column short-circuiting is unlikely as not all PFAAs eluted at the same time and duplicate columns performed similarly.

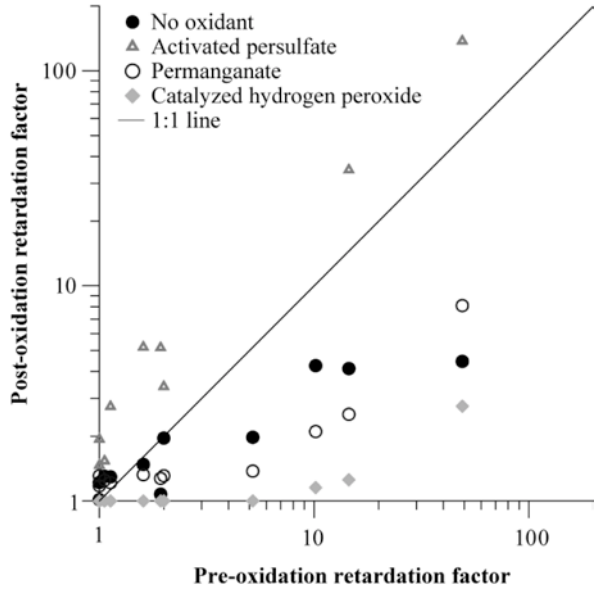

Figure 5-28. The effects of an oxidized system on PFAA transport. Phase i and phase v sorption breakthrough curve retardation factors are contrasted for the PFAA suite.

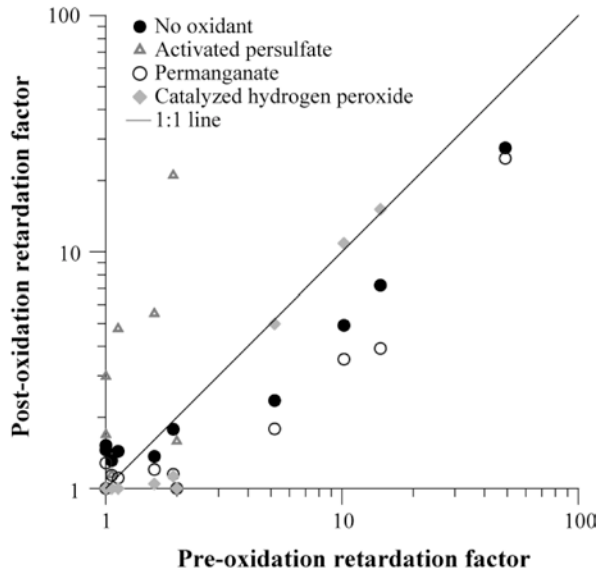

Figure 5-29. Phase i/iv retardation factor contrasts.

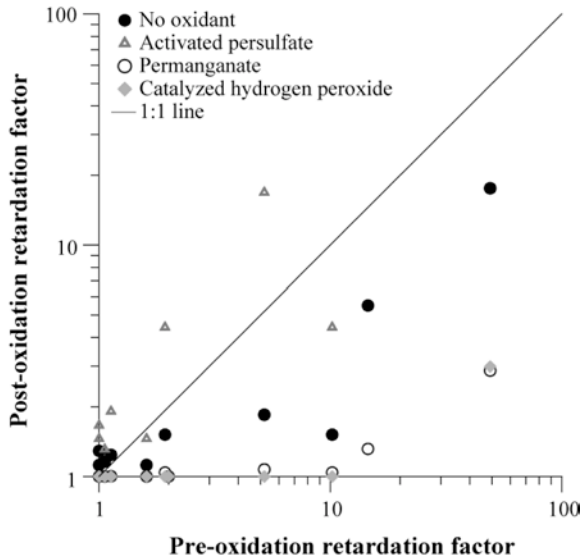

Figure 5-30. Phase i/vi retardation factor contrasts.

Changes in aqueous chemistry possibly contributed to accelerated breakthrough. Changes in aqueous chemistry over the course of the six experimental phases was generally moderate for no oxidant, permanganate-exposed, and CHP-exposed systems and remained circumneutral throughout the experiment; by contrast, activated persulfate systems were quite acidic post-oxidation (i.e., pH~3) and substantially elevated cumulative polyvalent cation concentrations were observed during oxidant application. To better understand the potential implications of the

aqueous chemistry on all systems, the results of the batch experiments' statistical analysis were used to account for changes as shown in **Equation 5-24**:

$$\log K_{d,i-set} = \log K_{d,i-obs} - \beta_{1,i} \cdot \left(pH_{obs} - pH_{set}\right) - \beta_{2,i} \cdot \left(\log \Sigma M^{++}{}_{obs} - \log \Sigma M^{++}{}_{set}\right) \quad \text{(eqn. 5-24)}$$

where $K_{d,i\text{-set}}$ is the estimated K_d value for an assumed reference condition (pH_{set}=7 and log $\Sigma M^{++}{}_{set}$ =-3 M) $\beta_{1,i}$ and $\beta_{2,i}$ are parameter estimates for PFAA i from the statistical analysis, and $K_{d,i\text{-obs}}$ is the PFAA i's HYDRUS fit distribution coefficient for the experimental system's observed aqueous chemistry (pH_{obs} and log $\Sigma M^{++}{}_{obs}$). However, using this approach to account for the effect of pH differences did not resolve the accelerated transport in the no oxidant reference case; due to the greater pH difference, moderated K_d adjustment were calculated for persulfate-exposed systems.

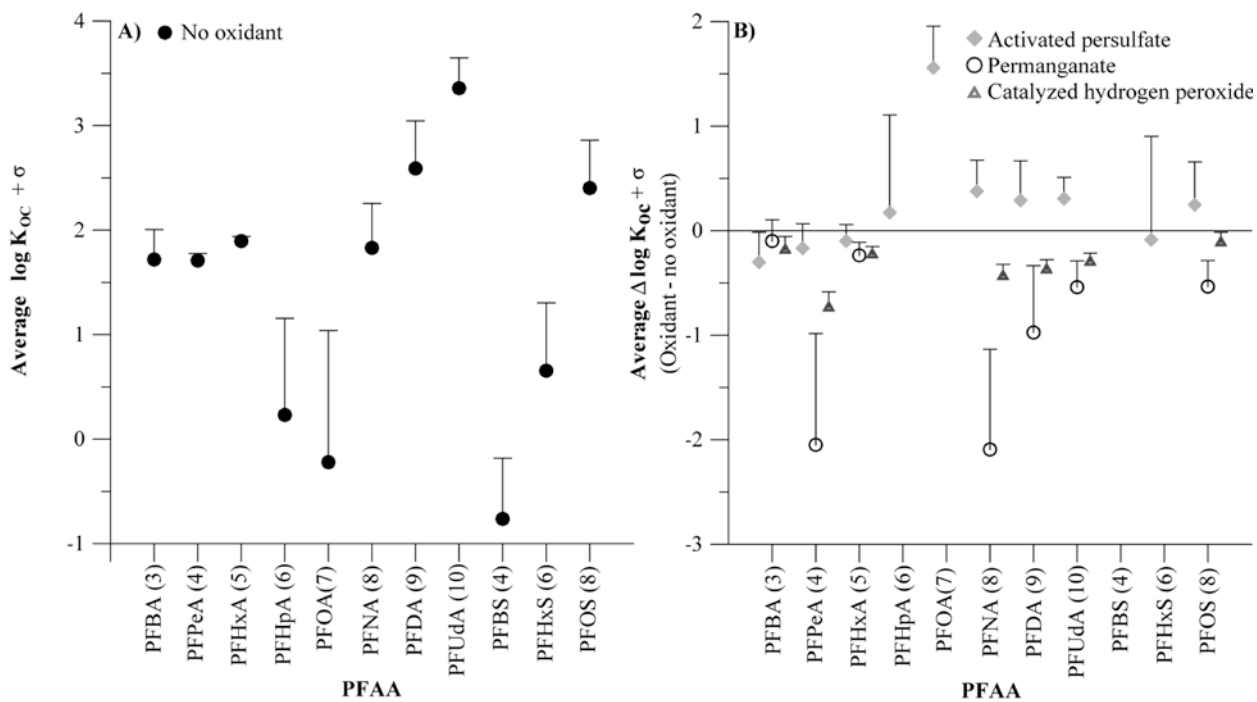

Figure 5-31. Post-experiment column porous media calculated K_{oc} distribution coefficients when: A) no oxidant was used, and B) the change in K_{oc} due to exposure to an oxidant ($K_{oc(oxidant)}$ - $K_{oc(no\ oxidant)}$). Sorbed concentrations were corrected to account for pore water concentrations, which in some cases resulted in negative calculated sorbed mass; K_{oc} values are not shown for negative calculated sorbed mass.

For the no oxidant control system, significant loss of SOM was not observed, either via effluent TOC analysis or post-experiment f_{oc} analysis (~7.6% SOM loss based on f_{oc}). While irreversible binding to SOM is generally not considered to be applicable for PFAA, Pan *et al.* (2009) observed substantial sorption-desorption hysterysis which was interpreted as an indication of irreversible binding. Finally, OM rearrangement into pore space or reductions in OM accessibility (Higgins and Luthy, 2007) could potentially explain the expedited breakthrough in the absence of ISCO application.

Retardation breakthrough contrasts were prepared for phase iv and vi, shown in **Figure 5-29** and **Figure 5-30**. The trends are generally consistent among the post-oxidation phases, however in permanganate-exposed and CHP-exposes systems, retardation factors decreased as time progressed (i.e., retardation factor rank order was typically phase iv > phase v > phase vi). No temporal trends were observed for the no oxidant control systems phase iv – vi retardation factors. This suggests that porous media quality was continuing to change post-exposure to permanganate or CHP, which could be explained by temporal changes in the amount of accessible organic matter (i.e., reduction in F_{access} value).

Columns that were never exposed to any oxidant (i.e., no oxidant systems) exhibited accelerated PFAA breakthrough (i.e., R_{fit} rank order phase v<phase i). However, this is most likely due to site alteration (e.g., OM migration into porous media pores). OM rearrangement into pore space would likely impact OM accessibility which would be particularly relevant for a partial penetration (i.e., not absorption) mechanism (e.g., F_{access} reduction; Higgins and Luthy, 2007).

PFAA transport in persulfate oxidized systems was more retarded than the no oxidant controls. The persulfate oxidation resulted in highly altered behavior in response to both the pulse and extended oxidations, and due to the atypical behavior, post-oxidation retardation factors could not be fit for the full PFAA suite. During activated persulfate application, the pH was depressed and the polyvalent cation concentration increased, which likely contributed to increased sorption. However, upon cessation of activated persulfate application, the pH remained depressed but the aqueous polyvalent cation concentration recovered to near pre-oxidant application concentrations, therefore water quality changes were not fully responsible for the changes in PFAA retardation (**Figure 5-32**), implying that changes to the porous media occurred during persulfate application. The increased sorption to persulfate exposed porous media was confirmed with post-experiment porous media extraction (**Figure 5-31**).

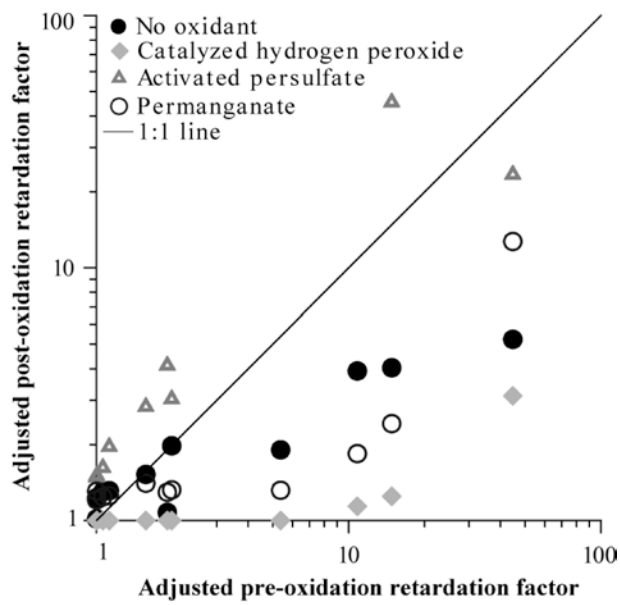

Figure 5-32. Phase i – phase v retardation factors, for which log cumulative polyvalent cation concentration and pH effects are accounted; all samples retardation factors is calculated for pH 7 water containing log (Σ M++)=-3.

Both CHP and permanganate appeared to accelerate the breakthrough of PFAAs, generally in advance of the no oxidant systems (**Figure 5-28**). Permanganate caused all PFAAs of chain length less than eight to breakthrough essentially simultaneously. SOM exportation (~30% reduction based on f_{oc}) likely contributed to the accelerated breakthroughs. However, post-experiment porous media extraction indicated that permanganate-exposed PFAAs had lower K_{oc}

values than did the no oxidant porous media (α=0.05, controlling for chain length and head group effects; **Figure 5-31**), which suggests that there were changes to porous media quality such as preferentially oxidation of aliphatic SOM (Siegrist *et al.*, 2011). PFAA transport in CHP-exposed systems was further accelerated when compared to permanganate-impacted systems (**Figure 5-28**), however CHP-exposed breakthrough curves were not well fit with equilibrium assumptions. Minimal SOM was exported (~6% SOM reduction based on f_{oc}). Post-experiment porous media extraction revealed that the K_{oc} values for CHP-exposed systems were more similar to no oxidant systems than to the permanganate-exposed systems K_{oc} values (**Figure 5-31**), which further suggests that rate limited sorption is important for CHP-exposed systems. Similar to the phase i breakthrough and previous work, extracted porous media K_{oc} values (**Figure 5-31**; analogous K_d data shown in **Figure 5-33**) followed a linear chain length dependent trend for PFAAs of chain length seven and longer, while shorter chain length compounds were more sorbtive than the chain length trend would predict. K_{oc} values were generally permanganate < CHP < no oxidant < persulfate.

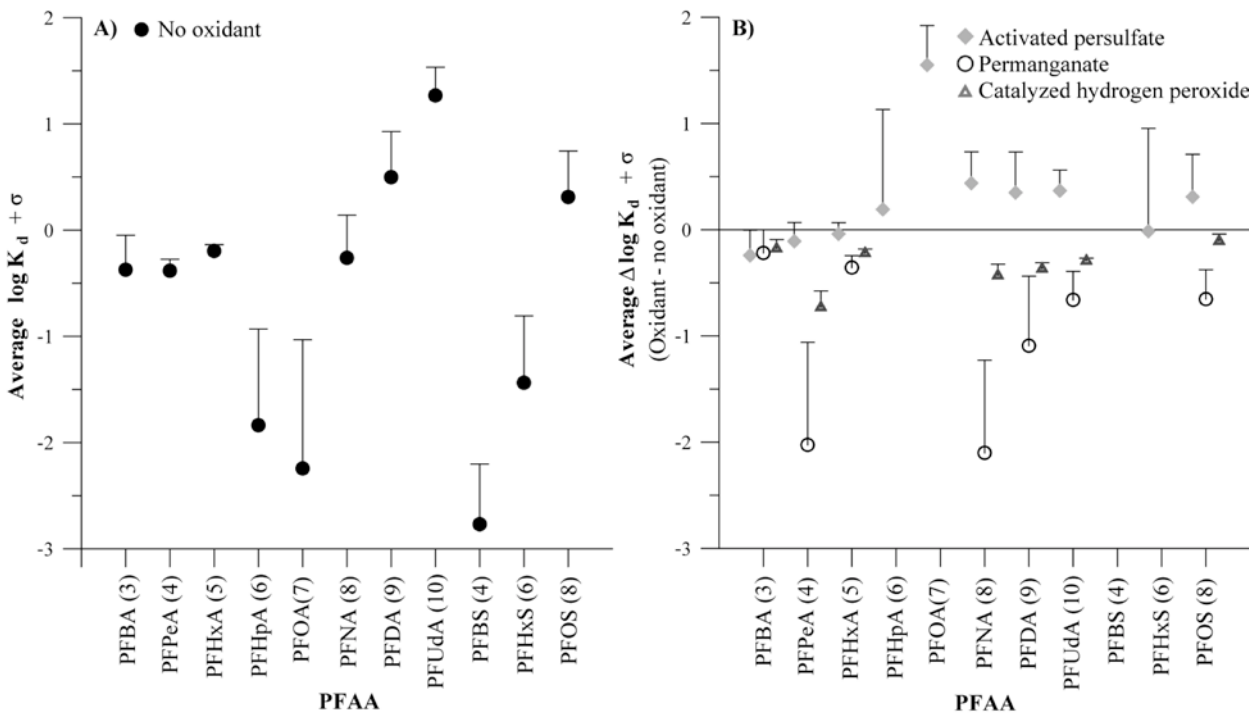

Figure 5-33. Post-experiment column porous media calculated K_d distribution coefficients when: A) no oxidant was used, and B) the change in K_d due to exposure to an oxidant (Log K_d(oxidant) – Log K_d(no oxidant)). Sorbed concentrations were corrected to account for pore water concentrations, which in some cases resulted in negative calculated sorbed mass; K_d values are not shown for negative calculated sorbed mass.

5.5.4 Conclusions

Based on the findings of this research, ISCO using activated persulfate, permanganate, or CHP, does not appear viable for remediation of PFAA-contaminated porous media, at least as currently practiced. However, PFAA transport was observed to be influenced by ISCO application, demonstrating that remedial strategies at sites containing PFAAs with other contaminants need to

be carefully planned and evaluated prior to full-scale remediation. The current study and previous research have demonstrated that PFAA sorption is impacted by a myriad of parameters including co-contaminants, mineralogy, SOM quantity and quality, pH, aqueous polyvalent cation concentration, and PFAA characteristics (head group and chain length). Each of these parameters influences PFAA transport through un-remediated porous media. Furthermore, site characteristics and remediation-induced changes in aqueous and geochemistry, including the presence of conventional co-contaminants (e.g., non-aqueous phase liquids; Guelfo and Higgins, 2013; Pan *et al.*, 2009), may affect PFAA transport and are likely to have implications for PFAA plume management.

In the present research, activated persulfate resulted in decreased PFAA mobility, while permanganate and CHP increased PFAA mobility. Bearing in mind that aqueous and geochemical changes are likely site specific, ISCO could potentially enhance other PFAA remediation strategies that rely on contaminant m obility. For example, CHP or permanganate-based ISCO might be used to accelerate PFAA transport and recovery during pump-and-treat remediation efforts. By contrast, activated persulfate could be applied as a PFAA containment strategy. Larger scale and longer term research is advised to better understand this enhanced or decreased mobility potential; longer term research may also provide evidence of as-of-yet undemonstrated slow oxidative PFAA decomposition in porous media.

Finally, future research and field testing should evaluate a broader suite of PFASs. Much of the previous research on PFAA sorption and oxidant decomposition has focused only on PFOA or PFOS, and there is a paucity of data on the other PFAAs. Distinguishable head group and chain length differences exist, which do not always follow linear trends, and further research on a larger suite of PFAAs is needed, particularly in light of the manufacturing shift toward shorter chain length PFAAs. Additionally, a variety of PFASs, beyond the legacy PFAAs investigated in this study, have been identified or indicated in AFFF formulations and at AFFF-impacted sites (Backe *et al.*, 2013; D'Agostino *et al.*, 2014; Place *et al.*, 2012; Houtz *et al.*, 2013). Field data suggests that these compounds can decompose to form PFAAs in the environment (McGuire *et al.*, 2014; Houtz *et al.*, 2013). Generally, the PFAA precursors are expected to be less mobile, however application of chemical oxidants may result in accelerated decomposition to PFAAs which are comparatively more mobile.

5.6 The influence of a non-aqueous phase liquid (NAPL) and chemical oxidant application on perfluoroalkyl acid (PFAA) fate and transport (*Task 4c*)

5.6.1 Background

For over fifty years, PFASs have been used in a wide variety of industrial and consumer product applications (Ahrens, 2011). PFAAs are a subclass of PFASs that are comprised of varying length perfluorinated carbon chains with a carboxylic (i.e., perfluorocarboxylic acids; PFCAs, F-$(CF_2)_x$-COO^-) or sulfonate head group (i.e., perfluoroalkyl sulfonates; PFSAs, F-$(CF_2)_x$-SO_3^-) and PFAAs have received the most attention due to their thermal, chemical, and biological stability, resulting in environmental persistence (Prevedouros *et al.*, 2006; Ahrens, 2011). PFAAs

are hydrophobic and oleophobic surfactants that are anionic and highly water soluble at environmentally relevant pH values (Prevedouros *et al.*, 2006; Lau *et al.*, 2007; Conder *et al.*, 2008; Steenland *et al.*, 2010; Lindstrom *et al.*, 2011). In animal studies, longer chain length PFAAs (eight carbon chain length and greater) have been found to bioaccumulate and potentially biomagnify, and dose-dependent toxicities have been observed in some studies (Lau *et al.*, 2007; Conder *et al.*, 2008). PFAA human toxicity concerns exist (Lau *et al.*, 2007; Steenland *et al.*, 2010; Lindstrom *et al.*, 2011) and drinking water provisional health advisories (PHA) have been issued in the U.S. for two PFAAs (perfluorooctanoic acid (PFOA) and PFOS (USEPA 2009).

AFFF, employed for extinguishing liquid fuel fires, can include PFASs. The repeated use of AFFF at historic firefighter training areas has been associated with substantially elevated PFAS subsurface concentrations (e.g., concentrations that exceed the PHA values by orders of magnitude; Moody and Field, 1999; Moody and Field, 2000; Backe *et al.*, 2013; McGuire *et al.*, 2014). Furthermore, co-contaminants including fuel chemicals, chlorinated solvents, and hydrocarbon surfactants have been detected at AFFF-impacted sites (Moody and Field, 1999; Moody and Field, 2000; Backe *et al.*, 2013; McGuire *et al.*, 2014), some of which may be present as non-aqueous phase liquids (NAPLs). Batch studies have demonstrated that NAPLs and surfactants impact PFAA equilibrium sorption (Pan *et al.*, 2009; Guelfo and Higgins, 2013), though these effects have not, to date, been investigated during flow-through conditions with porous media.

ISCO is a relatively mature remediation technology that has been applied to clean up soil and groundwater contaminated by chlorinated solvents and hydrocarbons (Siegrist *et al.*, 2011). Laboratory studies have demonstrated that chemical oxidants can effectively transform PFAAs in purely aqueous systems, though transformation rates are highly variable and dependent on oxidant species, exogenous energy sources, and water quality (Hori *et al.*, 2004; Hori *et al.*, 2005; Wang *et al.*, 2008; Lee *et al.*, 2009; Lee *et al.*, 2010; Lee *et al.*, 2012a; Lee *et al.*, 2012b; Liu *et al.*, 2012a; Liu *et al.*, 2012b). However, chemical oxidant treatment of porous media contaminated by PFAAs revealed they were not effectively transformed, but rather that their transport was substantially altered in response to oxidant treatment (McKenzie *et al.*, 2015). Oxidant application can result in changes to water quality and porous media geochemistry, which are known to impact PFAA sorption (Higgins and Luthy, 2006; Higgins and Luthy, 2007; Tang *et al.*, 2010; Guelfo and Higgins, 2013; McKenzie *et al.*, 2015), therefore PFAA mobility changes in response to oxidant treatment are not surprising.

Groundwater containing NAPL is a complex three-phase system (i.e., water, porous media, and NAPL), and there are a variety of potential interactions that can occur, both prior to and during oxidant treatment. The research reported in this paper was conducted to understand how chemical oxidant treatment in porous media of NAPL contaminants such as TCE could affect PFAA fate and transport. This research was carried out as an extension to McKenzie *et al.* (2015) and was accomplished using 1-D saturated porous media columns, conducted over 18-20 days, through six experimental phases that captured: pre-oxidant conditions (phase i), during-oxidant treatment (phases ii and iii), and post-oxidant conditions (phases iv-vi). The specific objectives of this research were to use environmentally relevant conditions to understand how chemical

oxidant treatment of TCE NAPL-contaminated groundwater can impact PFAA fate and transport during oxidant treatment (persulfate activated with $FeCl_2$ and citric acid, permanganate, and catalyzed hydrogen peroxide) and PFAA mobility after oxidant treatment. This paper describes the results of this research and compares the findings to those obtained using matched TCE-free columns as presented in McKenzie *et al.* (2015).

5.6.2 Materials and Methods

5.6.2.1 Experimental design

TCE NAPL was applied to the 1-D columns prior to the start of the experiment. The experimental design included six phases, shown in **Figure 5-34**. Using this approach, the effect of TCE on PFAA fate and transport in saturated porous media was evaluated in an unoxidized column (phase i), during oxidant treatment (phases ii and iii), and in a column that had been treated with a chemical oxidant (phases iv, v, and vi). Two oxidant-treatment phases – pulse

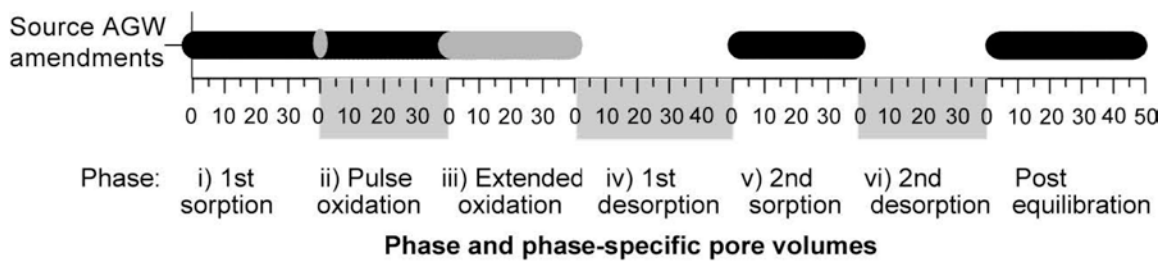

Figure 5-34. Overall experimental design of 1-D column study for which AGW was continuously supplied for the 18-20 day experiments, and amended with PFAAs (black; i.e., PFAA-AGW) or oxidant + PFAAs (gray; i.e., oxidant-PFAA-AGW), as appropriate. Effluent samples were collected for the analysis of 11 PFAAs (67-77 analyses/column), pH (42-51 analyses/column), aqueous TCE (18 analyses/column), and metals (18 analyses/column); a detailed sample collection timeline is shown in **Figure 5-35**. Following the conclusion of phase vi, the columns were re-equilibrated with PFAA-AGW (five days) and then dissected for sorbed PFAA and porous media organic carbon content (f_{oc}) analyses.

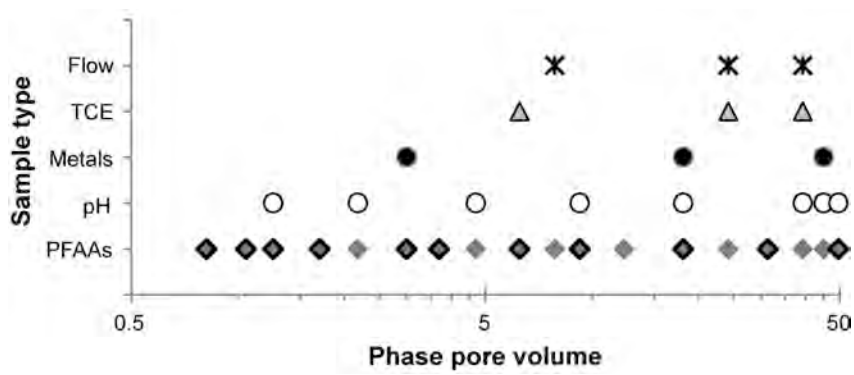

Figure 5-35. Approximate column effluent sampling time points for PFAAs, pH, metals, TCE, and flow (note the log scale on the x-axis). For PFAAs, more samples were collected than analyzed; all collected PFAA samples are shown (gray diamonds) and PFAA samples that were analyzed are outlined in black. Similar sampling timelines were applied to each experimental phase.

(phase ii) and extended (phase iii) – were included to explore potential impacts of shorter- and longer-term chemical oxidant treatment such as would occur during ISCO application.

Each phase lasted three to five days (~50 pore volumes/phase). The influent source water was artificial groundwater (AGW), AGW amended with PFAAs (PFAA-AGW), or AGW containing PFAAs and an oxidant (oxidant-PFAA-AGW). The experimental setup is shown in **Figure 5-36**. At the conclusion of the final experimental phase (phase vi), PFAA-AGW was provided for five additional days to re-equilibrate the porous media with PFAA-AGW. The columns were subsequently dissected to directly measure porous media organic content (f_{oc}) and sorbed PFAAs. This experimental design allowed for the assessment of PFAA fate and transport through saturated porous media as impacted by TCE, chemical oxidants, and any interaction between them.

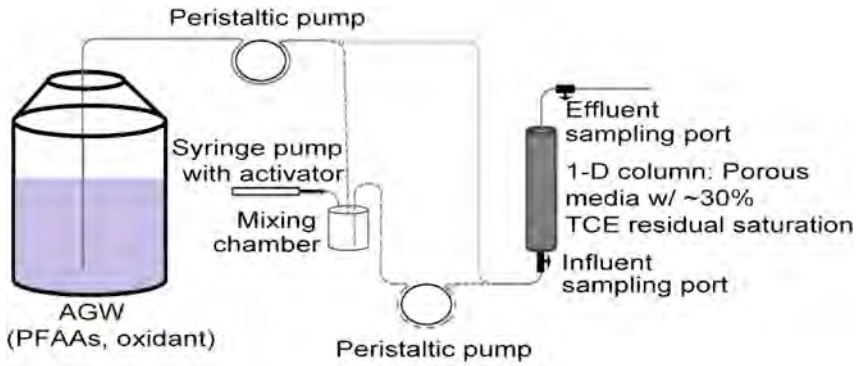

Figure 5-36. Schematic of experimental setup for 1-D column testing of TCE-applied saturated porous media. Fluid flows were as follows: all fluid was carried through solid lines; persulfate and CHP containing PFAA-AGW were carried in the dashed lines; and AGW, PFAA-AGW, and permanganate-PFAA-AGW were carried through the dotted lines.

Experimental design, materials, and methods are largely identical to those detailed in McKenzie *et al.* (2015). A general overview is provided herein and differences are highlighted. Persulfate, permanganate, and catalyzed hydrogen peroxide were the tested oxidants (i.e., "oxidant-treated columns"), which were compared to columns that were never treated with any oxidant (i.e., "no oxidant reference"); each of the four treatments was tested with duplicate 1-D columns packed with a loamy sand soil (described below). Results from the current study are labeled as "TCE-applied" columns (data from eight TCE-applied columns) and are contrasted with those presented in McKenzie *et al.* (2015), which are labeled "TCE-free" columns (data from eight TCE-free columns with the same oxidant conditions). Columns are considered "matched" if the only experimental design difference is the application of TCE prior to the start of the experiment. Treatment averages are expressed as mean ± standard deviation, statistical results are expressed as estimates ± standard error, and HYDRUS 1-D modeling results are expressed as model estimates ± the limits of the 95% confidence interval.

5.6.2.2 Materials

AGW contained $MnSO_4$, Na_2SO_4, and NaCl, which were reagent grade or better, was created using 18 MΩ water (Guelfo and Higgins, 2013; **Table 5-22**). Persulfate, permanganate, catalyzed hydrogen peroxide (CHP), and stabilized TCE were all ACS grade or better. PFAA salts, purchased from Sigma Aldrich, were used to create a PFAA stock in 70/30 methanol/water (v/v; Optima methanol). When amended with 2 µg/L PFAA (nominal; PFAA-AGW), the PFAA suite included: PFBA, perfluoropentanoate (PFPeA), PFHxA, PFHpA, PFOA, PFNA, PFDA,

PFUnA, perfluorobutanesulfonate (PFBS), perfluorohexanesulfonate (PFHxS), and perfluorooctanesulfonate (PFOS). The composition of the AGW amended with an oxidant and nominal 2 µg/L PFAA (oxidant-PFAA-AGW) is also shown in **Table 5-22.** Due to the range of pH conditions encountered, both anionic and neutral PFAA forms may have been present; however the above listed abbreviations will be consistently used. For quantification purposes, high purity native and mass-labeled PFAAs were purchased from Wellington.

Table 5-22. Composition of source waters (adapted from McKenzie *et al.*, 2015)

Source water	Components	Influent pH	Ionic strength	Salinity (‰)	Fe (mM)
Artificial groundwater (AGW)	Millipore water + 0.01 mM $MnSO_4$ + 1.27 mM Na_2SO_4 + 1.93 mM NaCl + 0.48 mM $NaHCO_3$	7.5	0.0056	0.33	0.0
PFAA-AGW	AGW + 2µg/L each PFAA	7.5	0.0056	0.33	0.0
Persulfate	PFAA-AGW + 52.1 mM $Na_2S_2O_8$ + 26.0 mM $FeCl_2$ + 5.2 mM $C_6H_8O_7$	1.9	0.2633	17.03	26.0
Permanganate	PFAA-AGW + 8.4 mM $KMnO_4$	7.8	0.0140	1.66	0.0
Catalyzed hydrogen peroxide	PFAA-AGW + 14.7 mM H_2O_2 + 0.5 mM $FeSO_4$	3.4	0.0076	0.91	0.5

Loamy sand (purchased from Agvise; Northwood, ND), which was well characterized (**Table 5-23**; by Agvise) and tested to be PFAA-free (at Colorado School of Mines; unpublished data), was dried, sieved (2 mm), and used for all experiments. The loamy sand was 81% sand, 9% clay, 10% silt, had a pH of 6.1, and had moderate organic matter content (f_{oc}=0.0089). The organic matter content was higher than that of some aquifer sediments, but is consistent with previous work (Guelfo and Higgins, 2013; McKenzie *et al.*, 2015) and therefor enables direct comparisons between TCE-applied and TCE-free columns.

Table 5-23. Porous media and TCE characteristics

Loamy sand	
pH	6.1
foc (%)	0.885
Sand (%)	81
Silt (%)	1
Clay (%)	9
K (mg/kg)	319
Ca (mg/kg)	1084
Mg (mg/kg)	171
Na (mg/kg)	11
H (mg/kg)	33
Fe (mg/kg)	2210
Al (mg/kg)	930
Phase density (g/mL)	2.47
Trichloroethylene (TCE)	
Density (g/mL)	1.46
Measured solubility (mg/L)	1392

5.6.2.3 Column packing, characterization, and TCE application

Loamy sand was dry packed in 2.5 cm ID x 8 cm glass columns (Kontes FlexColumn Economy) and the porous media was consolidated via sonication and tamping. Columns were dry packed using sonication and tamping to achieve appropriate consolidation. Dry bulk density (ρ_{db}; **Equation 5-25**), wet bulk density (ρ_{wb}; **Equation 5-26**), water filled-porosity (θ_w; **Equation 5-27**) were determined gravimetrically, as follows:

$$\rho_{db} = \frac{m_{sed}}{h_{sed} \cdot \pi \cdot r_{col}^2} \qquad \text{(eqn. 5-25)}$$

$$\rho_{wb} = \frac{m_{sed} + m_{porewater}}{h_{sed} \cdot \pi \cdot r_{col}^2} \qquad \text{(eqn. 5-26)}$$

$$\theta_w = \frac{m_{porewater} / \rho_{water}}{h_{sed} \cdot \pi \cdot r_{col}^2} \qquad \text{(eqn. 5-27)}$$

where m_{sed} is the mass of sediment dry packed into the column, $m_{pore\ water}$ is the mass of water in the pores with the density ρ_{water}, h_{sed} is the estimated height of the packed soil (estimated based on the difference between the total column height at the estimated glass bead height), r_{col} is the manufacturer-stated column radius, and ρ_m is the particle density determined, using a volumetric flask via Archimedes' principle, to be 2.47 g/cm^3. Packed column characteristics are shown in **Table 5-24**.

The packed columns were upflow flushed with CO_2 and then upflow saturated with three to five pore volumes of AGW. TCE was then immediately applied through the influent port using the "inject-withdraw" method as described in Petri *et al.* (Petri *et al.*, 2008). TCE application was accomplished via the "inject-withdraw" method described in Petri 08. TCE was loaded into a glass syringe that was connected to the column influent port via a three way valve. The column had been previously saturated with AGW. Tubing was connected to the effluent port, and the tubing end was submerged in an AGW-filled water bath at a constant head. The column was held in a vertical orientation, and the TCE was up-flow applied at a constant velocity using a syringe pump (the "inject" phase) until TCE was dripping out of the effluent tubing line. Maintaining the same column orientation and tubing configuration, a vacuum was created by manually pulling the syringe plunger out to slowly draw AGW back through the column (the "withdraw" phase); this was continued until AGW was observed coming into the glass syringe. Residual TCE NAPL saturation (S_N) was calculated as follows (**Equation 5-28**, **Equation 5-29**):

$$S_N = \frac{m_{TCEcolumn} - m_{watercolumn}}{\rho_{TCE} - \rho_{water}} \qquad \text{(eqn. 5-28)}$$

$$S_w = 1 - S_N \qquad \text{(eqn. 5-29)}$$

where $m_{TCE\ column}$ is the mass of the column after TCE had been applied using the inject-withdraw method, $m_{water\ column}$ is the mass of the AGW saturated column (i.e., just prior to starting the TCE inject-withdraw application), ρ_{TCE} is the density of TCE, and ρ_{water} is the density of water.

Due to the number of experimental conditions, two rounds of testing were required. The first round included the no oxidant reference and persulfate conditions; TCE residual saturation was 17.3 ± 1.7%. The second experimental round included permanganate and catalyzed hydrogen peroxide treatments, and TCE residual saturation was determined to be 40.3 ± 3.6%. The difference between the TCE residual saturation values between the two experimental rounds is likely due to differences in manual withdraw speed; however, column pore volumes were calculated separately for each column to reflect individual column packing the flow characteristics which accounted for TCE residual saturation.

The overall residual TCE saturation (S_N) was 29±12%. At the beginning of phase i, the porous media contained 6.6 ± 2.7 g TCE, and replicate columns' TCE mass relative standard deviation was <15%. Dry bulk density (ρ_b), water-filled porosity (θ_w), and TCE residual saturation (S_N) were gravimetrically determined. Bromide tracer breakthrough tests were used to characterize the columns' hydrodynamic transport properties and the breakthrough curve data was then inversely fit using HYRDRUS 1-D (Šimůnek *et al.*, 2008). Packed column characterization results are shown in **Table 5-24**. The longitudinal dispersivities were statistically similar for the columns (D_L = 0.48 ± 0.06 cm). Water filled porosities (θ_w) within the packed columns varied somewhat, due to differences in NAPL residual saturation (S_N), so column-specific θ_w values were used in PFAA inverse modeling. The initial average linear velocity, calculated based on column-specific porosity and flow rate, was 120 ± 27 cm/d.

Table 5-24. Porous media packed column characteristics

Parameter	Mean	Standard deviation
Soil height (cm; n=8) [a]	6.59	0.13
Soil mass (g; n=8) [a]	47.56	0.42
Porosity (prior to TCE application; n=8) [a]	0.45	0.01
Residual TCE saturation (%; n=8) [a]	28.87	12.60
Porous media pore volume (mL at start of phase i; n=8) [a, b]	11.30	2.30
Average linear velocity (cm/day; n=8) [a]	120.43	26.75
Longitudinal dispersivity (cm; all column fit simultaneously) [c]	0.48	0.06

[a] gravimetric analysis conducted during column packing
[b] affected by soil mass, packing, and TCE application
[c] HYDRUS 1-D analysis

5.6.2.4 Column experiments and sample collection

The saturated porous media 1-D column experiments were conducted in vertical up-flow mode at room temperature in ambient light. Influent source water composition is shown in **Table 5-22**; persulfate activated with $FeCl_2$ and citric acid (52.1 mM $S_2O_8^{2-}$/L from $Na_2S_2O_8$ activated with

26.0 mM $FeCl_2$ and 5.2 mM $C_6H_8O_7$), permanganate (8.4 mM MnO_4^-/L from $KMnO_4$), and CHP (49 mM H_2O_2/L catalyzed with 0.5 mM $FeSO_4$) were the tested oxidants. In this study, persulfate was activated based on the optimization work of Liang *et al.* (2004), who studied persulfate activated with $FeSO_4$ and citric acid. In the current study, persulfate activated with $FeCl_2$ and citric acid was employed and is referred to simply as "persulfate;" the use of $FeCl_2$ will be discussed later. Hydrogen peroxide was catalyzed with $FeSO_4$ and persulfate was activated with $FeCl_2$ and citric acid, which were provided as stock solutions via a syringe pump and combined with the oxidant-PFAA-AGW in an intermediate vessel with a 0.5 h residence time (**Figure 5-36**). Column influent samples were collected from a three-way valve immediately prior to the column base, and column effluent samples were collected from a three-way valve that was 10 cm downgradient from the column exit. Column effluent sampling was conducted as demonstrated in **Figure 5-35**.

Column effluent samples were collected for analysis of: pH (6-7 samples/phase), PFAAs (18-27 samples/phase), TCE (3 samples/phase), metals (3 samples/phase), and oxidants (only during oxidant treatment, until oxidant breakthrough; 10-18 samples/column). An approximate sampling schedule is shown in **Figure 5-35**. Samples collected for PFAA analysis were immediately methanol quenched (1:1 methanol:sample) and samples collected for TCE analysis were hexane extracted (20 µL effluent into 1980 µL hexane) within 1 h of collection. Column flow rates were gravimetrically measured on a daily basis. A slight decline in flow rate was observed over the course of the experiment, but this was accounted for in the column-specific pore volume calculations. Following post-experiment PFAA re-equilibration (~five days, after phase vi), the columns were stored in the dark at 6°C, and subsequently dissected to produce three samples/column (inlet, middle and outlet) for PFAA extraction and two samples/column for f_{oc} analysis (inlet and outlet).

5.6.2.5 Ancillary batch experiments

Batch experiments were conducted to further investigate PFAA sorption to TCE, and independent variables included TCE volume, pH, and iron amendments (Fe^{2+} from $FeCl_2$); soil was not included in the batch experiments. AGW and TCE were combined in glass vials with polypropylene-lined caps (nominal 40 mL), where the TCE volume was varied (0 = control, 3, or 10 mL neat TCE), and AGW was added such that the total volume was 42 mL to minimize head space (i.e., TCE plus 42, 39, or 32 mL of AGW). Four AGW pH values were tested: 2.3, 3.7, 6, 8.2 where the pH was adjusted with HCl or NaOH; the effect of 25 mM Fe from $FeCl_2$ was also tested at pH 2.3 and 3.7. PFAAs were added to each vial (up to 44.8 µL of 1.875 mg/L PFAA stock solution in 70% methanol) to achieve initial nominal aqueous concentrations of 2 µg/L of each PFAA for all treatments, and all treatments were tested in triplicate.

The 40-mL vials (containing AGW (without or with amendments), TCE (0, 3, or 10 mL), and PFAAs (2 µg/L)) were capped and placed upright on a shaker table and agitated for three days; to minimize mass-transfer limitations, the vials were vortexed daily. This experimental design allowed for consistent macroscopic TCE-water interfacial area (i.e., the cylindrical vial cross-sectional area) with variable TCE volume; microscopic differences in interfacial architecture may have been present and contributed to the variability in the results. No-TCE cases were used

as controls, and separate controls were included for each aqueous chemistry condition (i.e., pH and Fe amendment). After three days, an aliquot of the aqueous phase was removed for PFAA analysis and the pH was measured.

5.6.2.6 Analytical procedures

Porous media-associated PFAAs were extracted with basic methanol with heat, sonication, and shaking prior to analysis (Guelfo and Higgins 2013). Methanol quenched aqueous PFAA samples were pH adjusted as needed (targeted pH range between 5 and 9), centrifuged, and an aliquot was amended with mass labeled surrogate (200 ng/L working concentration). PFAAs were quantified via isotope dilution LC-MS/MS (ABSciex API 3200) operated in negative ionization mode; analytical details are included elsewhere (Higgins and Luthy, 2006; Guelfo and Higgins, 2013; McKenzie *et al.*, 2015). Surrogate recovery was generally >30% and presented results reflect surrogate recovery corrections. Based on blank and continuous calibration verification, carry over was minimal and analytical variability was generally ≤10%. The relative standard deviation among replicate columns was generally ≤25%. Limits of quantitation (LOQs) were matrix, run, and analyte dependent, but quenched aqueous samples generally had LOQs of 10-80 ng/L and extracted porous media samples were generally 0.02-0.6 ng/g. Further details can be found in McKenzie *et al.* (2015). Samples were pH analyzed within 15 minutes of collection. Aqueous samples for metal analysis were acidified (1% HNO_3) and analyzed with ICP-AES. TCE samples were hexane extracted and analyzed via GC-µECD. Porous media solids were freeze dried and organic carbon content (f_{oc}) was analyzed by TestAmerica via USEPA WS-846 Method 9060A.

Oxidant concentrations were measured spectrophotometrically using a 96-well plate containing 180 µL of solution. Samples for persulfate analysis were amended with H_2SO_4 and $(NH_4)_2Fe(SO_4)_2$, and incubated for 45 minutes; then NH_4SCN was added and the resultant solution was measured at λ=450 nm (Huang *et al.*, 2002). Permanganate was directly measured at λ=530 nm. Hydrogen peroxide was analyzed using the FOX method, requiring $FeSO_4$, H_2SO_4, D-sorbitol, and xylenol orange tetrasodium amendments and measured at λ= 530 nm (Wolff, 1994). All blanks, standards, and samples were analyzed in duplicate, and the results were averaged. For each oxidant, standards were analyzed with each sample set and samples were diluted as needed when over-saturation was encountered (i.e., above the linear range).

5.6.2.7 Data analysis

To assess potential PFAA transformations, a mass balance was calculated via method of moments. This was generally employed for phase i – phase iv. However, longer chain length PFAAs, particularly those in persulfate-treated columns, were not completely desorbed at the end of phase iv, thus necessitating a mass balance calculation for phase i – phase vi; this is further discussed in McKenzie *et al.* (2015).

Column effluent profiles were analyzed on a pore volume basis, where pore volumes were calculated individually for each of the eight columns at each PFAA sampling time point to account for initial packing, flow rate, and S_N (which was affected by TCE dissolution and TCE oxidation). TCE dissolution was calculated based on measured effluent TCE concentrations, and

TCE oxidation was estimated based on the effluent profile (i.e., residual TCE depletion suggested by minimal effluent TCE concentration or comparison to no-oxidant reference).

HYDRUS 1-D was employed to inversely fit the advection-dispersion-retardation equation to measured PFAA effluent data. Each experimental phase was fit separately, with effluent data from replicate columns (i.e., eight columns' effluent data contributed to 1st sorption fit (phase i), and two columns' data contributed to each of the post-oxidation fits (phase iv-vi)). PFAA concentrations <LOQ occurred at time points consistent with expectations and were included, at the Analyst®-estimated concentration, in HYDRUS inverse fitting. The HYDRUS-estimated solid water distribution coefficient ($K_{d,fit}$) was converted to a retardation factor (R_{fit}) using **Equation 5-30**:

$$R_{fit} = 1 + \frac{\rho_b}{\theta_w} \cdot K_{d,fit} \qquad \text{(eqn. 5-30)}$$

Post-experiment solid-water and organic carbon normalized distribution coefficients were also calculated (K_d and $K_{oc,}$ respectively), per the methods listed in McKenzie *et al.* (2015).

PFAA aqueous analysis from the TCE batch studies was used to calculate TCE distribution coefficients ($K_{i,\ TCE\text{-}w}$ for PFAA I; **Equation 5-31**). Vial losses for all TCE-containing treatments were calculated based on the aqueous concentration difference to the appropriate control (**Equation 5-31**). The effect of TCE volume, pH, and iron concentration was investigated, where each treatment was prepared in triplicate; no-TCE controls were prepared for each solution chemistry condition (relecting pH and Fe concentration) and were employed to account for vial losses in the TCE-containing treatments.

$$K_{i,TCE-w} = \frac{\left(\left(C_{i,w} \cdot V_w\right)_{control} - \left(C_{i,w} \cdot V_w\right)_{treatment}\right) / V_{TCE}}{C_{i,w}} \qquad \text{(eqn. 5-31)}$$

where $f_{i,\ x}$ is the fraction of PFAA i found in phase x (either water or TCE), $C_{i,\ x}$ is the concentration of PFAA i in phase x, and V_x is the volume of phase x.

For the column data, time-based effluent profiles were converted to pore volume-based effluent profiles, accounting for reductions in TCE NAPL volume and the formation of MnO_2 solids from permanganate application. Water-filled pore volume changes (i.e., increased due to NAPL dissolution or oxidation and decrease due to MnO_2(s) formation) were calculated for each sampling time point. Porous media TCE NAPL volume was calculated based on measured effluent TCE concentration and estimated TCE oxidation (**Equation 5-32**, **Equation 5-33**, **Equation 5-34**):

$$m_{PM,t} = m_{PM,t-1} - \Delta m_{PM,t} \qquad \text{(eqn. 5-32)}$$

$$\Delta m_{PM,t} = \Delta m_{dissolution,t} + \Delta m_{oxidation,t} \quad \text{(eqn. 5-33)}$$

$$\Delta m_{PM,t} = C_{w,t} \cdot v_t \cdot \Delta t + \Delta m_{dissolution,t} \cdot F_{oxidant} \quad \text{(eqn. 5-34)}$$

where $m_{PM,t}$ is the porous media-associated TCE mass at sampling time point t, $\Delta m_{PM,t}$ is the change thereof over time Δt (i.e., between sampling time points), which can occur due to TCE dissolution ($\Delta m_{dissolution,t}$) and TCE oxidation ($\Delta m_{oxidation,t}$). TCE dissolution was calculated based on effluent TCE concentration ($C_{w,t}$) and column flow rate (v_t), each of which were measured daily. TCE oxidation was estimated as an oxidant-specific increase over dissolution. Permanganate- and CHP-treated column's TCE effluent concentration became minimal during phase v, and it was assumed that the TCE NAPL was depleted, but that SOM-associated TCE remained in the column and provided the low effluent TCE concentrations that were observed for the remainder of the experiment. SOM-associated TCE (m_{SOM}) was calculated as follows:

$$m_{SOM} = m_{sed} \cdot C_w \cdot f_{oc} \cdot K_{oc} \quad \text{(eqn. 5-35)}$$

where m_{sed} is the sediment mass in the packed column, C_w is the aqueous TCE concentration and K_{oc} = 86 is the soil organic carbon-water partitioning coefficient for TCE. TCE reduction due to oxidation ($\Delta m_{oxidation,t}$) was estimated as a multiplier ($F_{oxidant}$) to $\Delta m_{dissolution,\ t}$. For permanganate and CHP, this was fit, such that m_{SOM} was reached at the appropriate time point in the TCE effluent profile; fit $F_{permanganate}$ = 51 and F_{CHP} = 40.5, meaning that during permanganate and CHP application, TCE was being depleted ~40-50 times faster than during non-oxidation phases (i.e., due to dissolution alone). By contrast, persulfate-treated columns effluent profile suggested that TCE NAPL remained throughout the experiment, and the TCE effluent profiles for the no oxidant reference and persulfate-treated columns were similar throughout the experiment; $F_{persulfate}$ = 1 was employed (i.e., during persulfate application $\Delta m_{PM,t}$ was twice that of the no oxidant reference columns).

Permanganate reduction results in MnO_2(s) formation when the pH is between 3.5 – 12 (Siegrist *et al.*, 2011), as it was in the current experiments. The volume of formed MnO_2 solids ($\Delta V_{MnO2,t}$) was calculated, for each sampling time point t, as follows (**Equation 5-36**):

$$\Delta V_{MnO_2(s),t} = C_{w-MnO_4} \cdot v_t \cdot \Delta t \cdot \frac{MW_{MnO_2}}{MW_{MnO_4}} \cdot \rho_{MnO_2} \quad \text{(eqn. 5-36)}$$

where $C_{w\text{-}MnO4}$ is the applied influent permanganate concentration, v_t is the column flow rate based on daily measurements, Δt is the time between sampling points, ρ_{MnO2} is the mineral phase density (5.04 g/cm^3), and MW_{MnO2} and MW_{MnO4} are the appropriate molecular weights. The amount of MnO_2 solid that was formed constituted a negligible mass and volume.

The estimated TCE NAPL and MnO_2(s) volumes were used to estimate water-filled porosity (θ_w = water volume/total volume) and dry bulk density (reflecting all potential sorping mass; i.e., $(m_{sed} + m_{PM})/(h_{sed} \bullet \pi \bullet r_{col}^2)$). The dispersivity was fixed based on conservative tracer inverse

modeling. HYDRUS 1-D fit the solid water distribution coefficient ($K_{d,fit}$), which was converted to a retardation factor (R_{fit}) using column-specific phase-averaged bulk density (ρ_b) and water-filled porosity (θ_w) as follows (**Equation 5-37**):

$$R_{fit} = 1 + \frac{\rho_b}{\theta_w} \cdot K_{d,fit} \qquad \text{(eqn. 5-37)}$$

In previous multi-phase research (water, soil, and NAPL included), the retardation factor was calculated as follows:

$$R = 1 + \frac{S_N}{1 - S_N} \cdot K_{NW} + \frac{\rho_b}{\theta_w} \cdot K_d \qquad \text{(eqn. 5-38)}$$

where K_{NW} is the NAPL-water portioning coefficient. Similarly, previous batch system research on soil-NAPL-water was conducted, and partitioning distribution coefficients were predicted based on **Equation 5-39** (Guelfo and Higgins, 2013):

$$K_d = f_{oc} \cdot K_{oc} + f_{NAPL} \cdot K_{NW} \qquad \text{(eqn. 5-39)}$$

where f_{NAPL} is the fraction of NAPL in the soil. Guelfo and Higgins (2013) found that K_{NW} was PFAA chain length dependent and, more importantly, that Eq S17 under-predicted PFAA sorption. This suggests that multiple interactions are influencing PFAA sorption. Based on these results, the current study employed the simplified **Equation 5-37**, where all sorption is included in K_d and ρ_b and θ_w reflect NAPL, formed solids, and porous media effects. This approach is simple and allows for the determination of transport effects in the 1-D column, but does not contribute to a mechanistic understanding of factors influencing PFAA retardation.

5.6.3 Results and discussion

5.6.3.1 1-D column studies water quality

Column effluent samples were collected and analyzed throughout the experiment for evaluation of water quality (**Figures 5-37** through **Figure 5-42**). Most columns maintained circumneutral pH values throughout the experiment, but the pH of the persulfate-treated columns was substantially reduced (e.g., pH 2 during extended persulfate treatment; **Figure 5-39**). Persulfate treatment also resulted in elevated effluent polyvalent cation concentration,

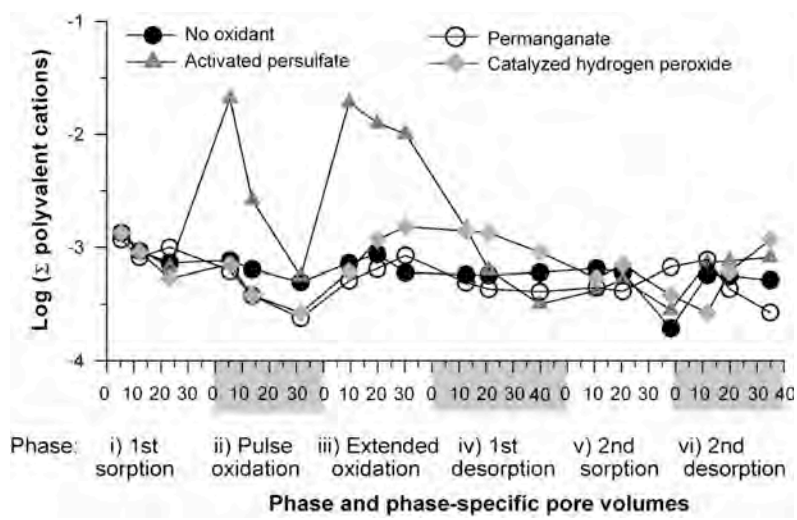

Figure 5-37. Effluent profiles for oxidant columns log cumulative molar polyvalent cation concentrations (average of duplicate columns).

likely due both to the iron activation and cations leaching from the soil due to the low pH (**Figure 5-37**). Effluent TCE concentrations were generally observed to be ~600 mg/L prior to oxidant treatment, and the permanganate- and CHP-treated columns had near zero effluent TCE concentrations during the second sorption and desorption phases (phases v and vi; **Figure 5-42**), suggesting NAPL depletion (estimated S_N and θ_w are shown in **Figure 5-43** and **Figure 5-44**, respectively). Complete oxidant breakthrough (i.e., influent and effluent oxidant concentrations were equivalent; **Figure 5-41**) was only observed in persulfate-treated columns. The experimental data enabled preparation of PFAA effluent profiles, as exemplified in **Figure 5-45** for PFOA and **Figure 5-46** for PFOS. PFAA effluent profiles were evaluated to determine the effect of oxidants on PFAA fate and transport.

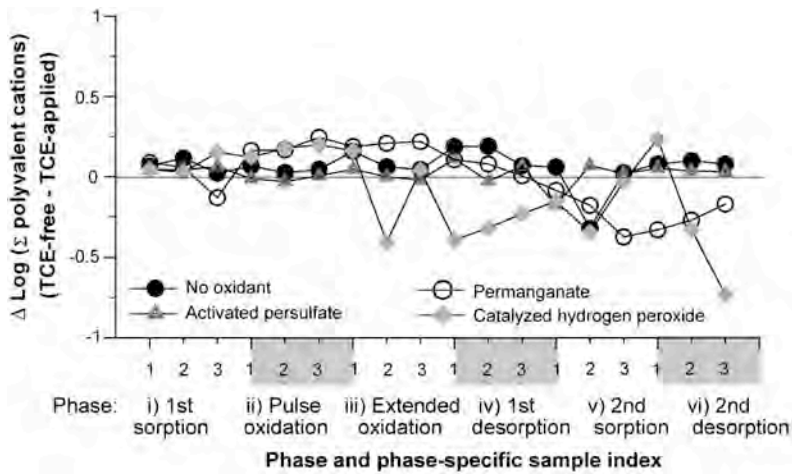

Figure 5-38. Effluent profile contrasting the log cumulative molar polyvalent cation concentration for TCE-free and TCE-applied (Δlog (Σ polyvalent cation) = log (Σ polyvalent cation)$_{TCE\text{-}free}$ - log (Σ polyvalent cation)$_{TCE\text{-}applied}$). Positive Δlog (Σ polyvalent cation) values indicate that there were more aqueous polyvalent cations in the TCE-free columns than in the TCE-applied columns. TCE-free data from McKenzie et al. (2015).

Water quality has been found to affect PFAA sorption; in the study of match TCE-free 1-D columns McKenzie *et al.* (2015) found cumulative polyvalent cation concentration and pH were generally statistically significant predictors of PFAA sorption distribution coefficients. Understanding that cumulative polyvalent cation concentration and pH likely contribute to differences in PFAA sorption, water quality differences between matched columns were calculated. Cumulative polyvalent cation concentration and differences thereof (Δ Log Σ polyvalent cation concentration) are shown in **Figure 5-37** and **Figure 5-38**, respectively, and pH and differences in pH (ΔpH) are shown in **Figure 5-39** and **Figure 5-40**, respectively.

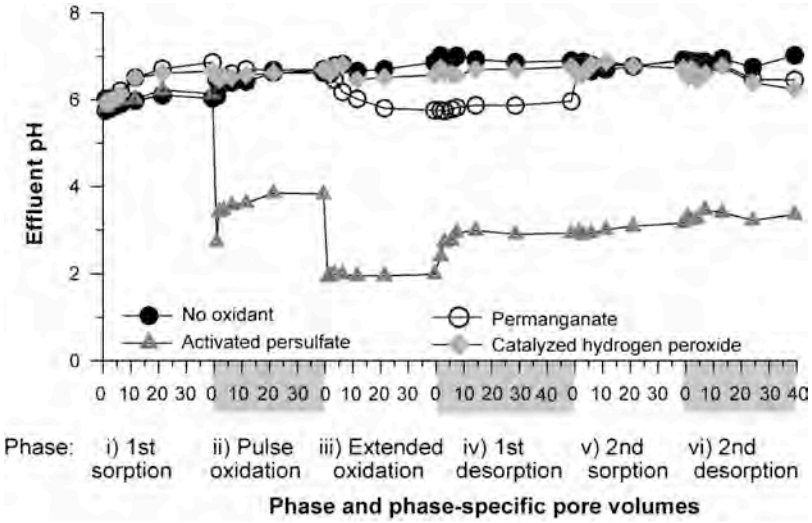

Figure 5-39. Oxidant columns' pH effluent profiles (average of duplicate columns).

Most columns maintained circumneutral pH values throughout the experiment, but persulfate-treated columns' pH was substantially reduced due to the persulfate pulse and extended oxidation applications (e.g., pH 3.5 and 2, respectively; **Figure 5-39**). Generally, persulfate application had the greatest effect on column effluent water quality and was associated with depressed pH and elevated polyvalent cation concentration. Comparing matched columns, the persulfate pulse caused a greater pH reduction in the TCE-applied columns (**Figure 5-40**), but did not cause a noteworthy difference in polyvalent cation concentration (**Figure 5-38**). Permanganate pulse and extended oxidation phases in the TCE-applied columns cause elevated polyvalent cation concentrations and depressed pH values compared to the matched columns. CHP oxidation of the TCE-applied columns resulted in slightly elevated pH and elevated polyvalent cation concentrations, compared with the matched TCE-free columns. Increased polyvalent cation concentration could be a result of altered influent water quality, namely inclusion of ferrous iron in persulfate and CHP cases, or due to in-column processes such as cation exchange or mineral dissolution. Similarly, pH changes could be due to influent water quality (e.g., influent persulfate had a pH~1.9), or due to in-column processes including inorganic byproduct evolution (e.g., CO_3^{2-} release, potentially resulting in gas evolution).

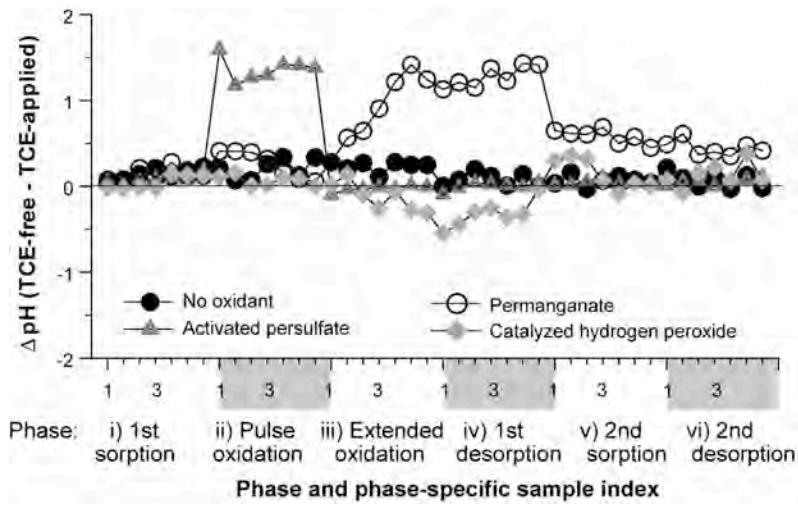

Figure 5-40. Effluent profile contrasting the pH values for TCE-free and TCE-applied ($\Delta pH = pH_{TCE\text{-}free} - pH_{TCE\text{-}applied}$). Positive ΔpH values indicate that the pH rank order was: TCE-free > TCE-applied. TCE-free data from McKenzie et al. (2015).

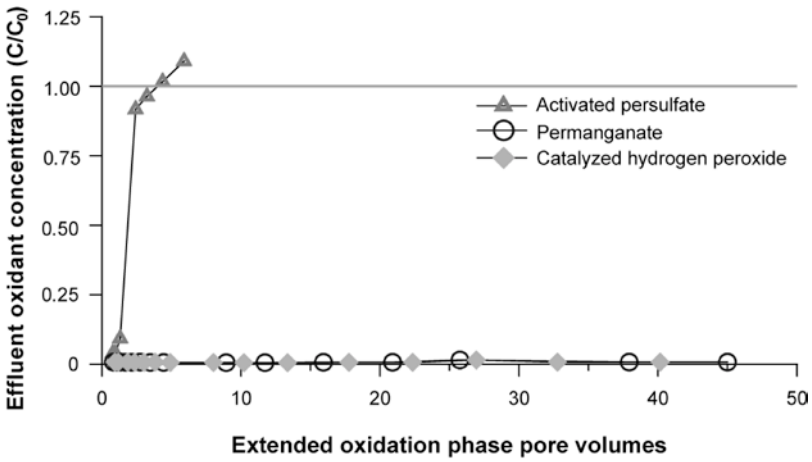

Figure 5-41. Column effluent oxidant unit concentrations during the extended oxidation phase (iii). Effluent persulfate monitoring ceased after complete breakthrough was achieved.

Column effluent was monitored for oxidants only during the pulse and extended oxidation phases (the latter shown in **Figure 5-41**). In the case of permanganate and CHP, oxidant breakthrough was not observed in response to the pulse or extended oxidant applications, which

suggests that the applied oxidant was insufficient to meet the contaminated porous media oxidant demand. By contrast, pulse persulfate application resulted in partial breakthrough and extended persulfate application resulted in complete persulfate breakthrough, in spite of TCE remaining in the column, which suggests that TCE NAPL oxidation by persulfate was slow relative to advective transport rates.

Column effluent TCE concentrations are shown in **Figure 5-42**. Moderate TCE levels were observed in the effluent of all of the columns through the first desorption phase (phase iv; >300 mg/L TCE), suggesting that NAPL was present in all columns during this phase (phase iv) and that the NAPL is potentially providing additional sorption capacity. Effluent TCE concentrations were consistently less than TCE at its solubility limit (measured to be 1392 mg/L), which suggests that there were mass transfer limitations to TCE dissolution within the columns. Effluent TCE concentrations were substantially reduced due to extended oxidant application (phase iii) for all tested oxidants, which suggests that the oxidants were proficiently oxidizing dissolved TCE. Persulfate-treated columns' effluent TCE concentration reduction was only temporary (i.e., not throughout the persulfate treatment phase), which suggests that the dissolved TCE was not fully oxidized by the persulfate treatment. This may be due, at least in part, to the use of $FeCl_2$ as an activator, where the chloride may be acting as a radical scavenger and thus reducing the TCE oxidation (e.g., Siegrist *et al.*, 2011). These columns continued to exhibit

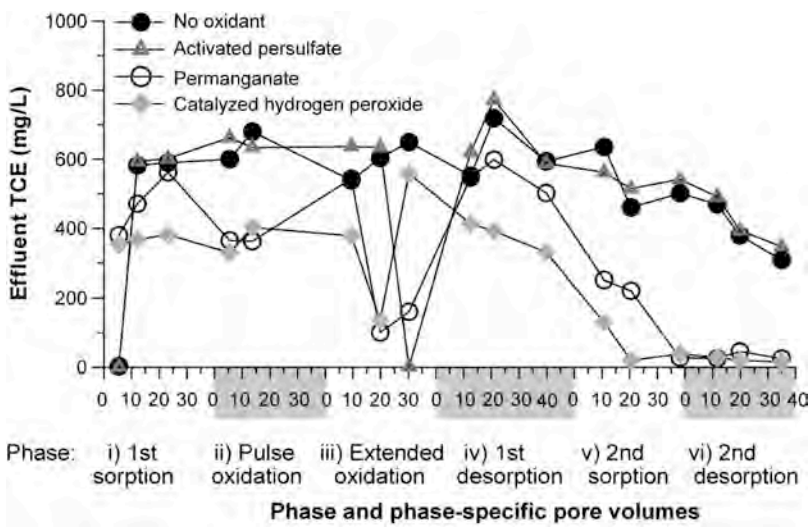

Figure 5-42. Oxidant columns' TCE concentration effluent profiles. TCE-saturated AGW solution (i.e., at solubility limit) had a measured concentration of 1392 mg TCE per L.

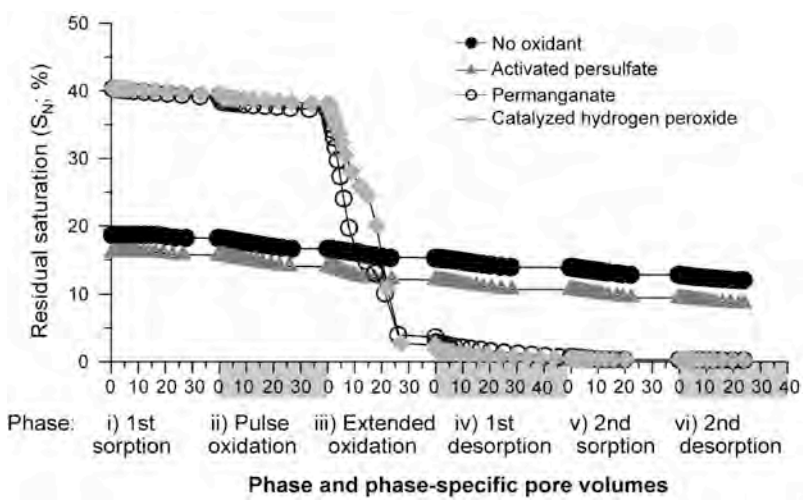

Figure 5-43. Calculated column-average TCE residual saturation for the 18-20 day experiment. TCE residual saturation was calculated for each PFAA sampling time point.

elevated column effluent TCE concentrations through the remainder of the experiment (**Figure 5-42**) in spite of complete persulfate breakthrough during the extended oxidation, which indicates that the conditions (aqueous- or geochemical conditions) or kinetics were not favorable for TCE destruction by persulfate. During the second sorption phase (phase v), TCE concentrations in the effluent from the permanganate- and CHP-treated columns was minimal (**Figure 5-42**), suggesting that column NAPL had been largely or entirely depleted.

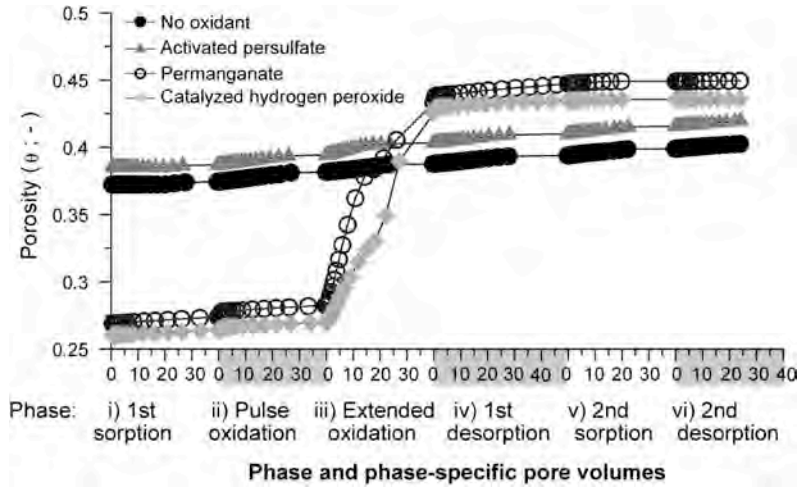

Figure 5-44. Calculated column-average porosity for the 18-20 day experiment. Column porosity was calculated for each PFAA sampling time point.

Column-average (i.e., not accounting for intra-column heterogeneities) TCE residual saturation were calculated as previous detailed, and the experiment-wide evolution of S_N is shown in **Figure 5-43**. Residual saturation depletion and solid formation (permanganate only for the formation of MnO_2 (s)) were used to calculated column-average porosity evolution, which is shown in **Figure 5-44**. It should be noted that **Figure 5-43** and **Figure 5-44** show column-average values, but that it is highly likely that in addition to the temporal differences that are displayed, spatial differences likely also existed.

TCE was expected to be preferentially depleted at the influent end of each column, due to dissolution and oxidation, which would result in spatial and temporal NAPL heterogeneities (including NAPL S_N and interfacial area). Similar spatial and temporal heterogeneities in organic carbon quality and quantity may also occur due to oxidant application. Taken together, these complexities suggest that a single, composite sorption coefficient would be the best approach to predicting PFAA transport in these mixed column columns. Column residual saturation and porosity were calculated for each sampling time point. These values represent column spatial averages and temporal averages, where the temporal average was determined by calculating the arithmetic mean of sampling time point values.

5.6.3.2 PFAA sorption by TCE

NAPL has the potential to alter sorbing characteristics of and access to soil organic matter (SOM), and provide potential new interfacial or absorptive capacity. Results from the ancillary batch experiments revealed that NAPL TCE can sorb PFAAs (no soil two-phase NAPL-AGW batch systems; results are provided in **Table 5-25** and **Table 5-26**). Based on the batch experiment results, the fraction of the PFAA that was associated with the NAPL TCE (f_{TCE}) was generally greater when more TCE was present (**Figure 5-47A**; statistic ally significant differences indicated "*"; α=0.05). If interfacial accumulation (i.e., adsorption) was the dominant process, then the TCE associated fraction (f_{TCE}) values would be the same, regardless of TCE volume, as the cross-sectional interfacial area was the same in all systems. These results suggest that PFAAs were transferred from the aqueous phase into the NAPL phase (i.e., absorption, which is also referred to as partitioning). Absorptive processes are well characterized by a TCE-water distribution coefficients (K_{TCE}). If it was only an absorptive (partitioning) process, then distribution coefficient values would be the same, regardless of TCE volume. In contrast, the aggregated TCE distribution coefficient values (log K_{TCE}) were commonly statistically equivalent for the two different TCE conditions (3 mL or 10 mL in 39 or 32 mL of AGW; **Figure 5-47B** with α=0.05), though differences in log K_{TCE} values for specific water quality conditions (i.e., pH and Fe concentration) were found to be statistically significant in some cases. Collectively, these data suggest a complex sorptive interaction between PFAAs and TCE that may include both absorption and adsorption. Both the TCE-associated fraction and the TCE distribution coefficient were observed to increase with

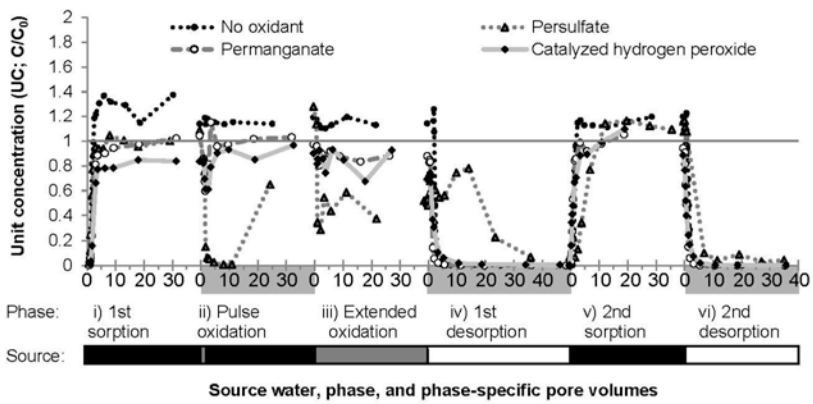

Figure 5-45. TCE-applied 1-D column PFOA effluent profiles for the six phase experiment, conducted over 18-20 days. AGW source water was continuously provided throughout the experiment duration, and AGW amendments as appropriate (shown at the bottom): no amendment (white), with PFAAs (black), or an oxidant and PFAAs (gray). Each of the presented profiles represents that average effluent unit concentrations of duplicate columns, where duplicate columns' sample RSDs were generally <25%.

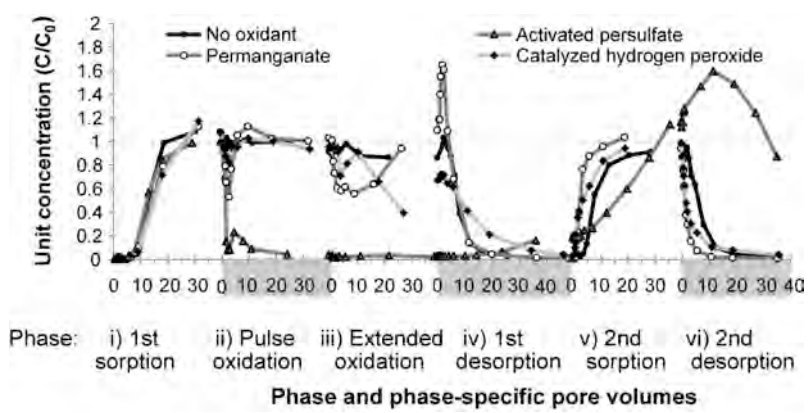

Figure 5-46. TCE-applied 1-D column PFOS effluent profile for the six phase experiment.

increasing PFAA chain length, irrespective of TCE volume (**Figure 5-47**). This suggests that hydrophobic interactions are at least partially responsible, and a 0.36 ± 0.02 log K_{TCE}/CF_2-group increase was observed for PFAAs of perfluorocarbon chain length of six carbons and longer. Guelfo and Higgins (2013) also calculated PFAA TCE-water distribution coefficients for three-phase batch systems (NAPL-soil-water), and found similar chain length trends. They also observed that shorter chain length PFCA sorption increased in the presence of TCE, but inconsistent effects were observed for medium and longer chain length PFAAs.

Table 5-25. Fraction of PFAAs that were TCE associated based on batch experiments

	f_{TCE} - average ± standard deviation			
	pH~2.3, 0 mM Fe		**pH~2.3, 25 mM Fe**	
	3 mL TCE	**10 mL TCE**	**3 mL TCE**	**10 mL TCE**
PFBA (3)	0.11 ± 0.02	0.27 ± 0.01	0.08 ± 0.08	0.26 ± 0.03
PFPeA (4)	0.09 ± 0.01	0.24 ± 0.00	0.10 ± 0.02	0.27 ± 0.03
PFHxA (5)	0.14 ± 0.03	0.28 ± 0.01	0.11 ± 0.06	0.25 ± 0.03
PFHpA (6)	0.13 ± 0.03	0.30 ± 0.01	0.11 ± 0.12	0.30 ± 0.04
PFOA (7)	0.15 ± 0.02	0.42 ± 0.01	0.10 ± 0.06	0.44 ± 0.02
PFNA (8)	0.34 ± 0.01	0.74 ± 0.01	0.26 ± 0.07	0.72 ± 0.01
PFDA (9)	0.66 ± 0.02	0.93 ± 0.00	0.57 ± 0.12	0.92 ± 0.01
PFUdA (10)	0.85 ± 0.03	0.98 ± 0.00	0.76 ± 0.13	0.97 ± 0.01
PFBS (4)	0.10 ± 0.03	0.26 ± 0.01	0.05 ± 0.05	0.18 ± 0.07
PFHxS (6)	0.07 ± 0.03	0.26 ± 0.01	0.05 ± 0.05	0.26 ± 0.06
PFOS (8)	0.16 ± 0.04	0.57 ± 0.05	0.20 ± 0.08	0.64 ± 0.04
	pH~3.7, 0 mM Fe		**pH~3.7, 25 mM Fe**	
	3 mL TCE	**10 mL TCE**	**3 mL TCE**	**10 mL TCE**
PFBA (3)	0.08 ± 0.2	0.25 ± 0.05	0.09 ± 0.02	0.24 ± 0.02
PFPeA (4)	0.06 ± 0.02	0.22 ± 0.06	0.10 ± 0.01	0.27 ± 0.03
PFHxA (5)	0.10 ± 0.03	0.26 ± 0.05	0.07 ± 0.03	0.26 ± 0.00
PFHpA (6)	0.10 ± 0.02	0.28 ± 0.04	0.09 ± 0.03	0.29 ± 0.00
PFOA (7)	0.11 ± 0.04	0.32 ± 0.03	0.12 ± 0.02	0.38 ± 0.01
PFNA (8)	0.10 ± 0.03	0.40 ± 0.02	0.11 ± 0.04	0.57 ± 0.01
PFDA (9)	0.26 ± 0.04	0.73 ± 0.03	0.31 ± 0.11	0.87 ± 0.00
PFUdA (10)	0.56 ± 0.04	0.93 ± 0.01	0.52 ± 0.16	0.96 ± 0.00
PFBS (4)	0.06 ± 0.00	0.23 ± 0.06	0.21 ± 0.06	0.47 ± 0.04
PFHxS (6)	0.04 ± 0.02	0.22 ± 0.03	0.08 ± 0.03	0.26 ± 0.06
PFOS (8)	0.16 ± 0.44	0.53 ± 0.03	0.12 ± 0.10	0.62 ± 0.03
	pH~6.0, 0 mM Fe		**pH~8.2, 0 mM Fe**	
	3 mL TCE	**10 mL TCE**	**3 mL TCE**	**10 mL TCE**
PFBA (3)	0.13 ± 0.03	0.30 ± 0.02	0.07 ± 0.04	0.28 ± 0.01
PFPeA (4)	0.08 ± 0.03	0.26 ± 0.01	0.07 ± 0.02	0.24 ± 0.01
PFHxA (5)	0.10 ± 0.01	0.26 ± 0.02	0.07 ± 0.02	0.23 ± 0.01
PFHpA (6)	0.06 ± 0.02	0.28 ± 0.02	0.13 ± 0.01	0.30 ± 0.01
PFOA (7)	0.11 ± 0.04	0.42 ± 0.11	0.11 ± 0.03	0.28 ± 0.00
PFNA (8)	0.11 ± 0.01	0.74 ± 0.25	0.14 ± 0.03	0.30 ± 0.02
PFDA (9)	0.19 ± 0.04	NA	0.39 ± 0.08	0.57 ± 0.10
PFUdA (10)	0.29 ± 0.07	NA	0.78 ± 0.05	0.87 ± 0.06
PFBS (4)	0.12 ± 0.03	0.27 ± 0.01	0.10 ± 0.00	0.27 ± 0.01
PFHxS (6)	0.12 ± 0.01	0.26 ± 0.01	0.10 ± 0.02	0.28 ± 0.02
PFOS (8)	0.11 ± 0.04	0.51 ± 0.03	0.13 ± 0.04	0.348 ± 0.05

Table 5-26. TCE-water distribution coefficients based on treatment triplicates from batch experiments.

	Log K_{TCE} - average ± standard deviation			
	pH~2.3, 0 mM Fe		**pH~2.3, 25 mM Fe**	
	3 mL TCE	**10 mL TCE**	**3 mL TCE**	**10 mL TCE**
PFBA (3)	-0.01 ± 0.07	-0.12 ± 0.04	-0.43 ± 0.64	-0.13 ± 0.05
PFPeA (4)	-0.11 ± 0.04	-0.18 ± 0.01	-0.10 ± 0.17	-0.10 ± 0.07
PFHxA (5)	0.12 ± 0.10	-0.09 ± 0.03	-0.06 ± 0.15	-0.16 ± 0.06
PFHpA (6)	0.10 ± 0.10	-0.05 ± 0.03	-0.30 ± 0.65	-0.04 ± 0.08
PFOA (7)	0.16 ± 0.05	0.17 ± 0.02	-0.18 ± 0.36	0.21 ± 0.03
PFNA (8)	0.62 ± 0.01	0.78 ± 0.03	0.41 ± 0.10	0.74 ± 0.01
PFDA (9)	1.20 ± 0.03	1.45 ± 0.02	1.00 ± 0.18	1.36 ± 0.04
PFUdA (10)	1.68 ± 0.08	1.94 ± 0.09	1.41 ± 0.26	1.83 ± 0.08
PFBS (4)	-0.02 ± 0.12	-0.14 ± 0.03	-0.21 ± 0.23	-0.36 ± 0.23
PFHxS (6)	-0.26 ± 0.22	-0.13 ± 0.02	-0.61 ± 0.42	-0.14 ± 0.14
PFOS (8)	0.18 ± 0.11	0.43 ± 0.08	0.25 ± 0.25	0.54 ± 0.07
	pH~3.7, 0 mM Fe		**pH~3.7, 25 mM Fe**	
	3 mL TCE	**10 mL TCE**	**3 mL TCE**	**10 mL TCE**
PFBA (3)	-0.11 ± 0.12	-0.15 ± 0.13	-0.08 ± 0.09	-0.18 ± 0.05
PFPeA (4)	-0.28 ± 0.13	-0.22 ± 0.15	-0.05 ± 0.08	-0.12 ± 0.06
PFHxA (5)	-0.01 ± 0.15	-0.14 ± 0.13	-0.22 ± 0.19	-0.14 ± 0.01
PFHpA (6)	-0.04 ± 0.08	-0.08 ± 0.09	-0.10 ± 0.17	-0.08 ± 0.01
PFOA (7)	0.01 ± 0.15	0.01 ± 0.07	0.04 ± 0.11	0.10 ± 0.02
PFNA (8)	-0.04 ± 0.15	0.15 ± 0.03	-0.03 ± 0.19	0.43 ± 0.01
PFDA (9)	0.47 ± 0.09	0.77 ± 0.07	0.55 ± 0.22	1.14 ± 0.02
PFUdA (10)	1.04 ± 0.06	1.48 ± 0.08	0.96 ± 0.28	1.65 ± 0.02
PFBS (4)	-0.25 ± 0.02	-0.20 ± 0.17	0.34 ± 0.15	0.26 ± 0.08
PFHxS (6)	-0.43 ± 0.22	-0.22 ± 0.09	-0.13 ± 0.18	-0.14 ± 0.15
PFOS (8)	0.20 ± 0.14	0.39 ± 0.05	-0.03 ± 0.37	0.54 ± 0.06
	pH~6.0, 0 mM Fe		**pH~8.2, 0 mM Fe**	
	3 mL TCE	**10 mL TCE**	**3 mL TCE**	**10 mL TCE**
PFBA (3)	0.06 ± 0.11	-0.03 ± 0.05	-0.22 ± 0.29	-0.09 ± 0.02
PFPeA (4)	-0.17 ± 0.22	-0.11 ± 0.04	-0.21 ± 0.10	-0.18 ± 0.02
PFHxA (5)	-0.04 ± 0.07	-0.11 ± 0.04	-0.20 ± 0.14	-0.21 ± 0.03
PFHpA (6)	-0.27 ± 0.12	-0.06 ± 0.05	0.09 ± 0.04	-0.05 ± 0.02
PFOA (7)	-0.01 ± 0.18	0.19 ± 0.21	0.01 ± 0.11	-0.08 ± 0.01
PFNA (8)	-0.01 ± 0.03	0.90 ± 0.59	0.11 ± 0.11	-0.04 ± 0.05
PFDA (9)	0.26 ± 0.12	NA	0.71 ± 0.12	0.44 ± 0.18
PFUdA (10)	0.50 ± 0.15	NA	1.47 ± 0.10	1.18 ± 0.21
PFBS (4)	0.04 ± 0.12	-0.09 ± 0.04	-0.02 ± 0.03	-0.11 ± 0.03
PFHxS (6)	0.04 ± 0.06	-0.12 ± 0.04	-0.02 ± 0.07	-0.09 ± 0.04
PFOS (8)	-0.02 ± 0.17	0.35 ± 0.03	0.06 ± 0.16	0.29 ± 0.08

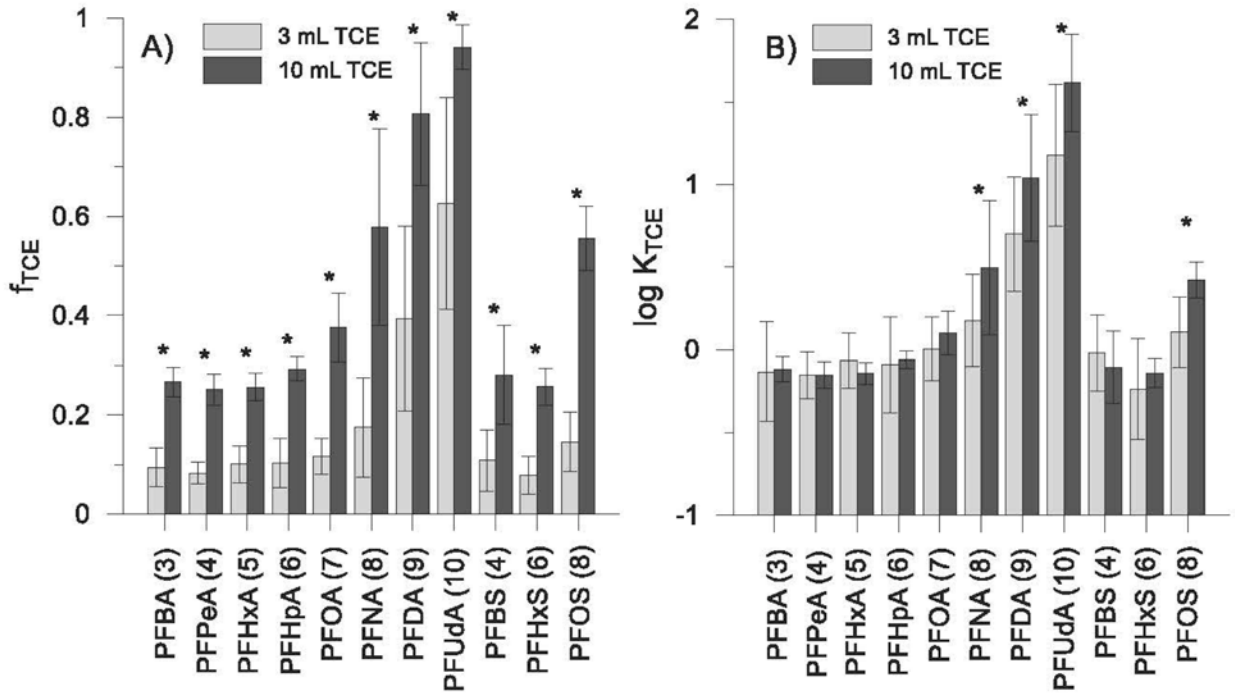

Figure 5-47. PFAA sorption to TCE based on batch experiment data, presented as: A) fraction (fTCE) of the PFAA associated with the TCE, and B) the TCE-water distribution coefficient (log KTCE). Each point is the average of triplicate measurements from six aqueous chemistry treatment conditions (pH range 2.3 – 8.2 with 0 or 25 mM Fe; total n=18), and the error bars are one standard deviation. Variability was typically less for a single treatment. The TCE volume main effect statistical significance (= 0.05) is indicated with "*", however interactions were also selectively statistically significant (not shown).

The first sorption phase of the column experiments (i; prior to oxidant treatment of the porous media columns) was also analyzed to elucidate the effects of a NAPL on PFAA transport. In addition to the NAPL effects observed in the batch systems, in the 1-D advective columns, NAPL also has the potential to reduce water-filled porosity. NAPL sorption to SOM and porosity reductions have the potential to change PFAA transport. In TCE-applied columns (SN~30%), PFAA breakthrough was generally similar to or accelerated relative to the TCE-free columns, on a temporal basis (e.g., exemplified by PFDA in **Figure 5-48A**). Sorption site occlusion and water-filled porosity reductions could contribute to faster transport due to sorption reduction and increased average linear velocity, respectively.

However, dimensionless pore volume-based profiles (to account for column-specific differences in pore volumes) suggested that PFAA transport was more strongly retarded in TCE-applied columns (PFDA example in **Figure 5-48B**; retardation factors for all PFAAs shown in **Figure 5-48C**), which suggests that PFAA sorption was enhanced in TCE-applied columns. The specific sorptive mechanism for the PFAA-TCE NAPL interactions (i.e., absorption or interfacial adsorption) could not be determined for the 1-D columns.

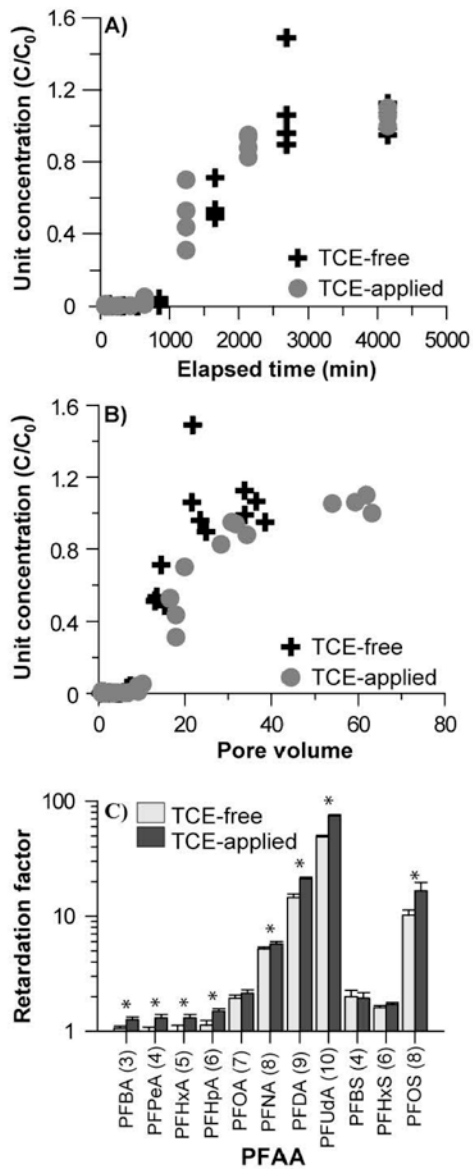

Figure 5-48. NAPL effects on PFAA transport in the first sorption phase (i; prior to oxidant treatment); PFAA data for TCE-free columns is from McKenzie et al. (2015) A) NAPL presence accelerated PFDA transport on a temporal basis; B) NAPL presence decreased PFDA transport on a pore volume basis; and C) NAPL effects on PFAA suite retardation factors (log scale), where "*" indicates statistical significance (i.e., 95% confidence intervals did not overlap).

Among TCE-applied columns, PFAA chain length and head group trends were generally consistent with those observed in TCE-free columns (McKenzie et al., 2015) and previous research. Among TCE-applied columns, sorption increased 0.58 ±0.03 log Kd per CF2 moiety (based on a statistical evaluation of PFAAs of perfluorocarbon chain length of six and longer) which is in agreement with previous studies (0.45 - 62 log Kd per CF2 moiety; Higgins and Luthy, 2006; Guelfo and Higgins, 2013; McKenzie et al., 2015); hydrophobic interactions are indicated.

In the TCE-applied columns in this study, sorption of PFCAs of perfluorocarbon chain length of six and less were statistically equivalent (overlapping 95% CI), and had $1.25<R_{fit}<1.5$. Previous research has found short chain length compounds to be more sorbing than the chain length dependent trend would predict, and that sorption increased with decreasing chain length; this was attributed to ion exchange or sorption to SOM regions that were sterically inaccessible to the larger PFAAs (Guelfo and Higgins, 2013). In TCE-applied columns, for equivalent chain length, PFSAs were found to be more strongly sorbing than the corresponding PFCA ($\Delta 0.38 \pm 0.09$ log K_d based on a statistical evaluation of PFAAs of perfluorocarbon chain length of six and longer) which is consistent with previous findings (0.23 and 0.43, in Higgins and Luthy (2006) and McKenzie et al (2015), respectively).

5.6.3.3 PFAA fate and transport during chemical oxidant treatment (phases ii and iii)

Mass balance calculations indicated either complete PFAA recovery or under-recovery associated with increased sorption (**Table 5-27**), which was similar to that of the matched TCE-free columns (McKenzie *et al.*, 2015). This is in contrast with previous research on homogenous system have demonstrated PFCA transformation through chemical oxidant treatment, particularly persulfate, which results in a step-wise chain length reduction reaction pathway (e.g., Hori *et al.*, 2005; Lee *et al.*, 2010). Perfluoropropanoate (PFPrA), a shorter chain length PFCA, would be produced in a chemical oxidation transformation pathway that proceeded in a step-wise chain length reduction fashion; its absence was confirmed in the

matched TCE-free columns (McKenzie *et al.*, 2015). Persulfate oxidation rate could have been affected by the presence of scavengers, including chloride from the $FeCl_2$ activator (George and Chovelon, 2002; Lee *et al.*, 2012). As radical scavenging may affect oxidation reactions, the levels of chloride present in the current study (~0.054 M) likely had a slight reduction in the rate of persulfate oxidation of PFAAs such as PFOA (e.g., ~20% reduction based on the results of Lee *et al.*, 2012, where a 22% reduction in the PFOA oxidation rate was observed for 0.06 M chloride). While scavenging may have affect persulfate oxidation of TCE, based on the data in this study and in the matched TCE-free columns (McKenzie *et al.*, 2015), PFAA transformations likely did not occur.

In response to persulfate treatment, strong sorption increases were observed for longer chain length PFAAs (quantitative and qualitative evaluations shown in **Table 5-28**, **Table 5-29**, **Table 5-30**, and **Table 5-31**), which was consistent with the matched TCE-free columns (shown in **Figure 5-49** and **Figure 5-50**). More in depth analyses of the general trends and previous PFAA oxidation studies can be found in McKenzie *et al.* (2015).

Table 5-27. Experiment-wide calculated PFAA suite mass recovery values for duplicate columns

PFAA (chain length)	PFAA mass recovery (%; mean ± standard deviation for phases i - iv, unless noted)			
	No oxidant reference	Persulfate	Permanganate	Catalyzed hydrogen peroxide
PFBA (3)	89 ±3	95 ± 1	95 ± 1	92 ± 2
PFPeA (4)	95 ±6	107 ± 9	82 ± 2	85 ± 0
PFHxA (5)	109 ±3	98 ± 2	112 ± 3	103 ± 4
PFHpA (6)	91 ± 2	89 ± 5	91 ± 2	95 ± 4
PFOA (7)	119 ± 3	96 ± 7	88 ± 1	86 ± 2
PFNA (8)	96 ± 1	89 ± 5 [a, b]	100 ± 2	89 ± 7
PFDA (9)	88 ± 2	58 ± 1 [a, b]	79 ± 2	79 ± 7
PFUdA (10)	80 ± 2 [a, b]	6 ± 1 [a, b]	86 ± 1 [a]	65 ± 5 [a, b]
PFBS (4)	59 ± 13 [c]	51 ±2 [c]	80 ± 8	89 ± 4
PFHxS (6)	93 ± 3	102 ± 5	94 ± 5	91 ± 2
PFOS (8)	92 ± 6	70 ± 5 [a, b]	97 ± 3	91 ± 4

[a] Mass recovery based on phase 1 - 6, due to phase 4 concentrations not reaching C/C_0~0
[b] Phase vi final $C/C_0 \geq 0.1$ (i.e., PFAA remaining in soil); incomplete mass recovery expected
[c] Incomplete PFBS mass recoveries are expected (e.g., ~50%), as phase 1 - 4 plateaus were C/C_0 ~0.5

An oxidant pulse (phase ii) was applied to determine if an immediate and measurable response occurred, and the three day extended oxidation (phase iii) was included as a more ISCO-relevant scenario. If an oxidant had no effect, the PFAA unit concentration would remain near unity (C/Co~1), however a noteworthy deviation from unity would indicate changes to PFAA fate and transport (e.g., effluent profiles in response to persulfate application for PFOA shown in **Figure 5-45** and PFOS in **Figure 5-46**). Similar to the methods detailed in McKenzie *et al.* (2015), PFAA mass recovery was calculated for the TCE-applied columns via method of moments, where the PFAA mass recovery was calculated for either phase i-iv or i-vi. The former was preferred, however for some cases, incomplete desorption at the end of the first desorption phase

(iv) was suggested by the effluent profile shape, and a mass recovery for phase i-vi was necessitated (**Table 5-27**).

Table 5-28. PFAA pulse oxidation (phase ii) effluent profile qualitative scoring results, indicating the effect on PFAA transport due to changes in aqueous and porous media quality

PFAA (chain length)	No oxidant reference	Persulfate	Permanganate	Catalyzed hydrogen peroxide
PFBA (3)	0	1	0	0
PFPeA (4)	0	1	1	0
PFHxA (5)	0	1	0	0
PFHpA (6)	0	2	1	1
PFOA (7)	0	2	1	1
PFNA (8)	0	3	1	1
PFDA (9)	0	3	1	1
PFUdA (10)	0	3	2	1
PFBS (4)	0	1	0	0
PFHxS (6)	0	2	1	1
PFOS (8)	0	3	1	0
Qualitative scoring			**Figure 5-45** phase ii example	Phase ii mass recovery
0 ≡ no effect, small disturbances			No oxidant	94.6 ± 11.1%
1 ≡ small reduction, recovers quickly			Permanganate	91.7 ±15.2%
2 ≡ large reduction, UC ~ 0, recovers gradually			Persulfate	74.1 ± 12.9%
3 ≡ large enduring reduction, UC~0, incomplete recovery			Not shown	8.9 ± 3.0%

Table 5-29. PFAA extended oxidation (phase iii) effluent profile qualitative scoring results.

PFAA (chain length)	No oxidant reference	Persulfate	Permanganate	Catalyzed hydrogen peroxide
PFBA (3)	0	2	0	0
PFPeA (4)	0	2	2	1
PFHxA (5)	0	1	0	0
PFHpA (6)	0	2	2 (0) [a]	2
PFOA (7)	0	2	2 (0) [a]	0
PFNA (8)	0	2	1	2
PFDA (9)	1 (0) [a]	3	1	2
PFUdA (10)	0	3	1	2
PFBS (4)	0	1	2	0
PFHxS (6)	0	1	0	0
PFOS (8)	0	3	1	2
Qualitative scoring			**Figure 5-45** phase iii example	Phase iii mass recovery
0 ≡ no effect, small disturbances but no general trend			No oxidant	91.5 ± 11.8%
1 ≡ brief reduction and recover to C/C_0=1; recovery typically occurs promptly			Not shown	79.4 ± 23.0%
2 ≡ reduction and plateau, where steady state concentration is C/C_0<1			Persulfate	65.3 ± 25.3%
3 ≡ remain at C/C_0~0 from entire phase 3			Not shown	4.4 ± 2.5%

[a] plateau or dip occurs between $0.8 \leq C/C_0 \leq 1$, which could be due to analytical error

Table 5-30. PFAA pulse oxidation phase (ii) mass recovery values. Low mass recoveries could be due to compound retention within the column or transformations; a holistic study-wide view indicates that transformations are generally not likely.

PFAA (chain length)	No oxidant reference	Persulfate	Permanganate	Catalyzed hydrogen peroxide
PFBA (3)	89	92	97	94
PFPeA (4)	98	105	100	93
PFHxA (5)	107	86	104	102
PFHpA (6)	93	81	100	101
PFOA (7)	116	57	100	90
PFNA (8)	90	11	101	97
PFDA (9)	92	10	88	96
PFUdA (10)	80	5	86	80
PFBS (4)	61 [a]	39 [a]	102	96
PFHxS (6)	90	73	97	87
PFOS (8)	98	11	101	96

[a] PFBS breakthrough curve plateaued $C/C_0 \sim 0.5$; this is likely due to the use of an unmatched surrogate (i.e., PFHxS)

Table 5-31. PFAA extended oxidation (phase iii) mass recovery values. Low mass recoveries could be due to phase iii initial unit concentration < 1, compound retention within the column, or transformations; a holistic study-wide view indicates that transformation are generally not likely.

PFAA (chain length)	No oxidant reference	Persulfate	Permanganate	Catalyzed hydrogen peroxide
PFBA (3)	85	95	89	91
PFPeA (4)	95	78	83	86
PFHxA (5)	96	91	108	97
PFHpA (6)	81	55	91	84
PFOA (7)	115	71	88	81
PFNA (8)	95	7	98	63
PFDA (9)	89	3	60	49
PFUdA (10)	94	7	40	54
PFBS (4)	58 [a]	65 [a]	88	89
PFHxS (6)	93	112	96	94
PFOS (8)	89	3	85	63

[a] PFBS breakthrough curve plateaued $C/C_0 \sim 0.5$; this is likely due to the use of an unmatched surrogate (i.e., PFHxS)

As discussed in McKenzie *et al.* (2015), under-recoveries were observed for longer chain length PFAAs after exposure to persulfate. However, the effluent profiles suggest that the under-recovery is due, at least in part, to premature sampling cessation prior to the complete PFAA desorption (e.g., PFOS exposed to persulfate in **Figure 5-46**). Generally, PFAA mass-recovery values were ~100%, or within the analytical error, which suggests that PFAA transformations were not occurring. Furthermore, samples from the matched columns were further chemically

analyzed using liquid chromatography quadrupole time of flight mass spectrometry (LC QTOF) to assess if perfluoropropanoate (PFPrA) was being formed. PFPrA is a PFCA with a two carbon perfluorinated chain, and would be observed if stepwise PFAA chain length reduction, such has commonly been observed (Hori *et al.*, 2005; Lee *et al.*, 2009; Lee *et al.*, 2010; Lee *et al.*, 2012a; Lee *et al.*, 2012b; Liu *et al.*, 2012a), were occurring. McKenzie *et al.* (2015) did not observe the formation of PFPrA, and this was taken as further evidence that the PFAAs were not being transformed.

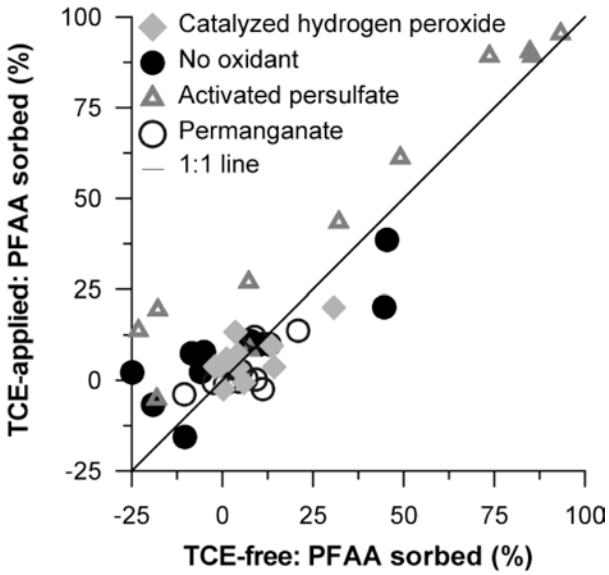

Figure 5-49. Oxidant pulse effects (phase ii) on the PFAA suite for TCE-applied and TCE-free columns. Data are expressed as PFAA percent sorbed: 100 – $m_{effluent}/m_{influent}$*100 where $m_{influent}$ and $m_{effluent}$ were calculated via method of moments.

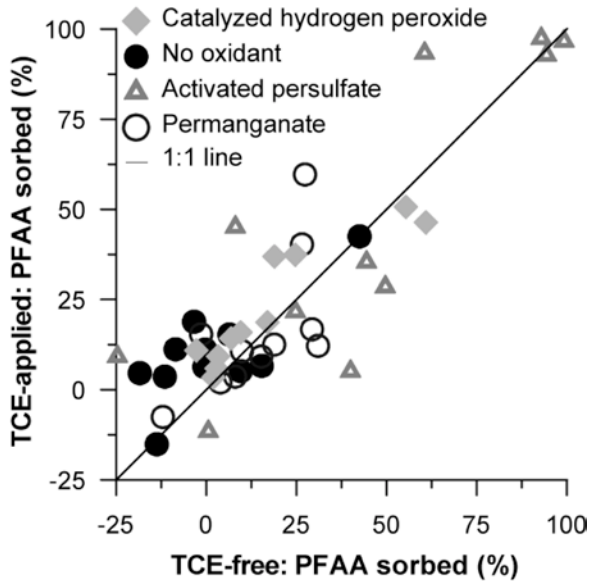

Figure 5-50. Extended oxidation effects (phase iii) on the PFAA suite, expressed as PFAA under-recovery which is calculated as follows: 100 – $m_{effluent}/m_{influent}$*100 where $m_{influent}$ and $m_{effluent}$ were calculated via method of moments. TCE-free data from McKenzie et al. (2015).

Experiment-wide TCE-applied columns' PFAA mass recovery values, which were generally near 100% (**Table 5-27**), suggest that PFAA transformation did not occur in response to the application of permanganate, persulfate, or CHP, which was also previously observed in TCE-free columns (McKenzie *et al.*, 2015). Generally, the presence of an oxidizable NAPL should reduce PFAA oxidation, as the NAPL would provide a more accessible oxidant demand.

Oxidant application could also change PFAA sorption via a variety of mechanisms, including: alterations to the NAPL volume, interfacial area, tension, and shape; exposure of previously NAPL-occluded SOM; formation of new solid or gaseous phases; and changes to aqueous chemistry. Effluent profiles showed marked PFAA effluent concentration reductions during oxidant application (e.g., **Figure 5-45**); because the data in this study do not indicate PFAA transformations occurred, this evidence suggests that substantial changes in PFAA sorption were occurring in response to oxidant application. In TCE-applied columns, both the pulse and extended oxidant applications resulted in immediate and measurable changes in PFAA effluent concentrations, where effluent concentrations were generally unaffected or were reduced

(effluent concentration plateau was unaltered at C/C_o ~1 or was reduced to less than 1, respectively). Effluent concentration increases above C/C_0~1 were generally not observed, which suggests that sorption site destruction, either by way of NAPL or SOM oxidation, was not a dominant factor influencing PFAA sorption in TCE-applied columns.

To better understand the implications of oxidant application of PFAA transport, phase ii and iii were qualitatively assessed by scoring the effluent profile (**Table 5-28** and **Table 5-29**). PFAA mass recovery values were calculated for pulse and extended oxidation phases (**Table 5-30** and **Table 5-31**). Among the test oxidants, persulfate application resulted in the greatest PFAA sorption increases. In persulfate-treated columns, greater PFAA percent sorbed values were observed for the TCE-applied columns than the matching TCE-free columns, though few other general trends could be drawn from the pulse and extended oxidation PFAA percent sorbed contrasts (**Figure 5-49** and **Figure 5-50**); analytical variability may have masked underlying mechanism-based trends.

To further assess oxidant-induced sorption increases, the experimental phase-specific PFAA percent sorbed was calculated ($100 - m_{effluent}/m_{influent}*100$, where $m_{effluent}$ was calculated via method of moments) and are shown in **Figure 5-49** and **Figure 5-50**. If little to no additional sorption occurred in response to the oxidant application, then the PFAA effluent concentration would remain at $C/C_0=1$ and the calculated PFAA percent sorbed would be near zero. Negative calculated percent sorbed values indicate that $m_{effluent}>m_{influent}$. By contrast, if there was a substantial increase in sorption in response to the oxidant application, then a noticeable reduction in the PFAA effluent concentration would o ccur (e.g., $C/C_0<<1$) and the calculated percent sorbed would be noticeably greater than 0%. The rank order of oxidants effects (i.e., the largest PFAA percent sorbed are listed first) was activate persulfate >> CHP ~ permanganate > no oxidant reference, where the greatest effect was observed for the longer chain length PFAAs. Water quality differences, in particular increased aqueous polyvalent cation concentration and decreased pH, have been associated with increased PFAA sorption (Higgins and Luthy, 2006; Higgins and Luthy, 2007; Tang *et al.*, 2010; Guelfo and Higgins, 2013; McKenzie *et al.*, 2015). Compared to the other TCE-applied columns, effluent from persulfate-treated columns had elevated cumulative polyvalent cation concentration and lowered pH (due in part to Fe and citric acid activation), and the altered water quality may be responsible, at least in part, for the increased sorption. Interestingly, pulse oxidant PFAA percent sorbed values were equal or slightly greater in the TCE-applied columns than in the matched TCE-free columns, especially for persulfate-treated columns. Sorption differences are likely due, at least in part, to differences in water quality (shown as deviations above the 1:1 line in **Figure 5-31**).

ISCO application also has the potential to cause further water quality changes, beyond those observed in the present study, which could further impact PFAA transport. ISCO-induced water quality changes include substantial pH shifts due to activation methods, or evolution of soluble inorganic byproducts (e.g., pH range from 1 to 10 in laboratory studies), and elevated dissolved metals (from oxidant impurities or due to release from the porous media; Siegrist *et al.*, 2011). Persulfate and CHP oxidative species are pH-dependent, so substantial pH shifts could alter the oxidative mechanism; additionally, acidic conditions have been demonstrated to improve PFAA

transformation rates for permanganate and persulfate. Further, evolution of inorganic byproducts, such as chloride (Cl^-) or carbonate (CO_3^{2-}), could result in oxidant scavenging, which could decrease oxidative rates (e.g., Liu *et al.*, 2012a), or could also form new radicals (e.g., $Cl^\bullet$, $Cl_2^{\bullet-}$, $HCO_3^\bullet$ or $CO_3^{\bullet-}$) resulting in different oxidation mechanisms (Siegrist *et al.*, 2011). Liu *et al.* (2012b) found that MnO_2 (s) promoted PFOS transformation in the presence of permanganate. Evolution of new solid or gaseous phases, as a result of NAPL oxidation, could provide new interfaces for PFAA accumulation.

Oxidant application can result in the generation of new phases, namely the formation of MnO_2 solids due to permanganate application, and CO_2 evolution due to the application of permanganate or CHP. While manganese dioxide solids are not expected to offer substantial binding potential, the air-water interface is known to concentration surfactants including PFAAs. Gas evolution was observed in TCE containing columns that were treated with permanganate and CHP. Gas evolution due to persulfate application is theoretically possible due to mineralization of organics, but no cases of persulfate-induced CO_2 were known to the authors of a 2011 ISCO review book (Siegrist *et al.*, 2011).

5.6.3.4 PFAA transport in oxidized porous media (phases iv – vi)

After oxidants had been consumed or advectively removed, PFAA transport in porous media could be impacted by oxidation-induced changes in aqueous and geochemical conditions. Oxidant treatment potentially changed the NAPL (volume and interfacial area), the porous media (e.g., selective SOM oxidation), or water quality (pH and the cation concentrations). To assess if there were effects on PFAA transport, the following analyses were made: 1) comparisons of the effects of different oxidants for TCE-applied columns (**Figure 5-51**); 2) examinations of temporal trends for each oxidant (**Figure 5-52**); and 3) comparisons of matched TCE-applied and TCE-free columns (**Figure 5-52**). PFAA effluent profiles, in some cases, were less well fit by the advection-dispersion-retardation equation, which assumed reversible, equilibrium sorption. Poorer fits were most commonly observed in CHP-treated columns (e.g., **Figure 5-53**), potentially due to rate-limited sorption or gas evolution, and generally for longer chain length compounds, especially in persulfate-treated columns. The mechanistic reason(s) for the relatively poorer fits for PFAA effluent profiles during the

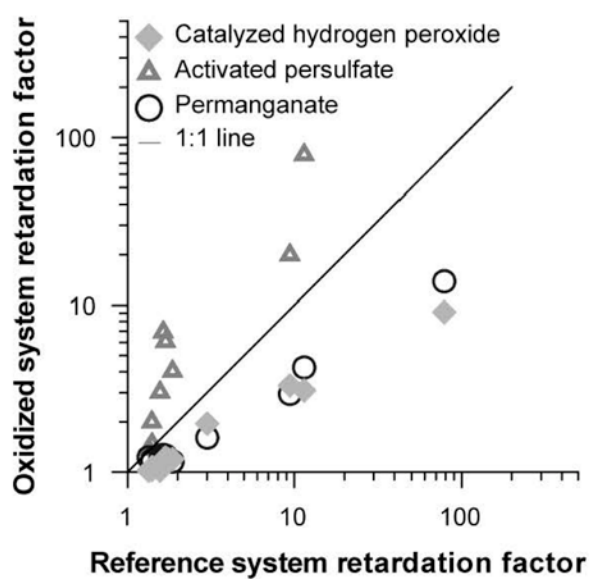

Figure 5-51. Retardation factor contrasts between oxidized columns and the no oxidant reference columns for the second sorption phase (v) in TCE-applied columns (note the log scales). All evaluated PFAAs' retardation factors are shown, save PFNA and PFUdA in persulate-treated columns, for which adequate fits could not be obtained.

oxidation phases are unknown; the estimated retardation factors are presented as fit by HYDRUS 1-D.

To understand the implications of oxidant treatment, PFAA transport in oxidized columns was compared to the PFAA transport in the no oxidant reference columns. In **Figure 5-51**, data points above the 1:1 line indicate increased PFAA retardation in oxidant-treated column compared to the no-oxidant reference column (i.e., decreased mobility); by contrast, data points below the 1:1 line suggest decreased PFAA retardation (i.e., increased mobility) in the oxidant-treated column. Among TCE-applied columns, PFAA transport in the second sorption phase (v) was fastest in CHP- and permanganate-treated columns, and slowest in persulfate-treated columns (i.e., retardation factors were typically CHP ≈ permanganate <no oxidant reference<persulfate, which was observed for both PFCAs and PFSAs; **Figure 5-51**). Potential mechanistic explanations, more fully discussed in McKenzie *et al.* (2015), are briefly summarized here: accelerated transport in permanganate-treated columns was likely due to SOM exportation and changes in geochemistry; accelerated transport in CHP-treated columns was attributed to rate-limited sorption; and retarded transport in the persulfate-treated columns was likely due to water quality and geochemical changes. Similar trends were observed for the other post-oxidation phases (first desorption (phases iv) and second desorption (phase vi); **Figure 5-54** and **Figure 5-55**). Compared to the experiment initiation (i.e., phase i), PFAA mobility in the no oxidant reference columns slightly increased over the course of the experiment (**Figure 5-56**), which was similarly observed in the matched TCE-free columns (McKenzie *et al.*, 2015).

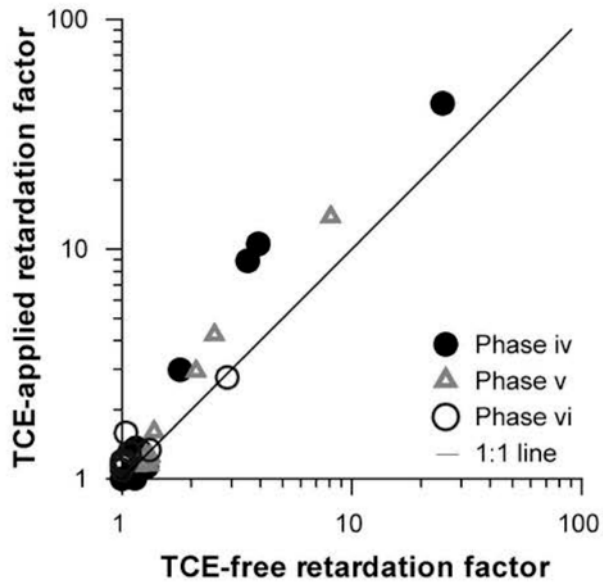

Figure 5-52. Post-permanganate treatment temporal trends for TCE-applied and TCE-free columns (McKenzie et al., 2015). PFAA transport was faster in later post-oxidation phases, and PFAA retardation factors became more similar between matched columns.

TCE-applied columns were compared to their matched TCE-free columns for each of the post-oxidation phases. For a given experimental phase, post-oxidation retardation factors were generally greater in TCE-applied columns than in TCE-free columns for both PFCAs and PFSAs in permanganate- and CHP-treated columns (e.g., **Figure 5-52**). This was likely due to water quality effects, as when compared to their matched TCE-free columns, TCE-applied permanganate- or CHP-treated columns were also observed to have either higher polyvalent cation concentrations or decreased pH. When compared to the other columns, persulfate-treated columns exhibited greater sorption of both PFCAs and PFSAs, which was also attributed to higher polyvalent cation concentrations and decreased pH as compared to the other columns. However, persulfate-treated columns' retardation factors were similar in matched TCE-free and

TCE-applied systems, as were their water quality characteristics. Generally, greater retardation of both PFCAs and PFSAs was observed across all columns when higher polyvalent cation concentrations or decreased pH values were observed, which is consistent with previously observed water quality effects (McKenzie *et al.*, 2015).

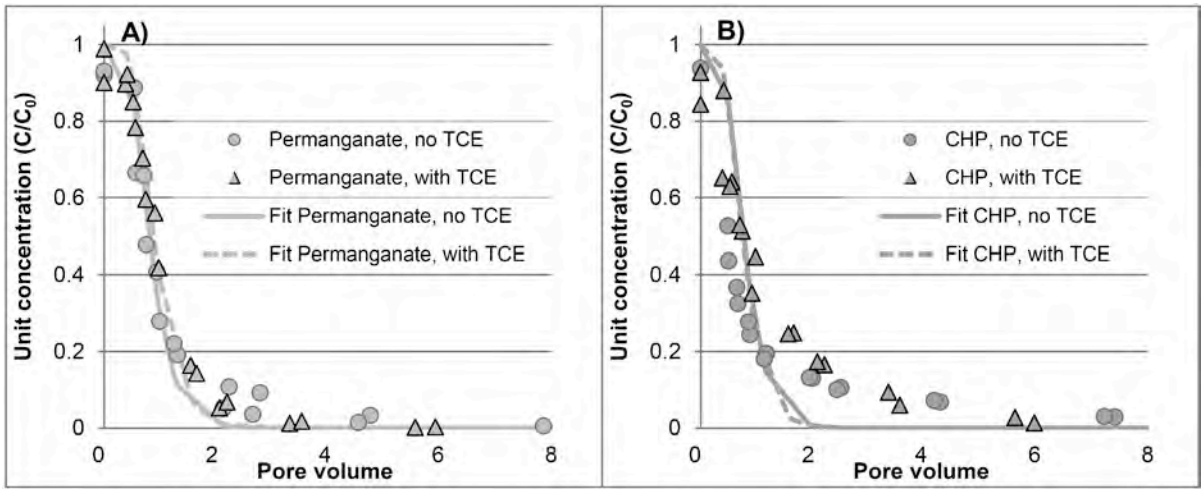

Figure 5-53. PFOA examples from second desorption (phase vi) of HYDRUS 1-D inverse modeling fits on the advection, dispersion, retardation Equation with reversible, equilibrium assumptions. A) Permanganate showing fairly good inverse fitting, and B) CHP showing less good inverse fitting.

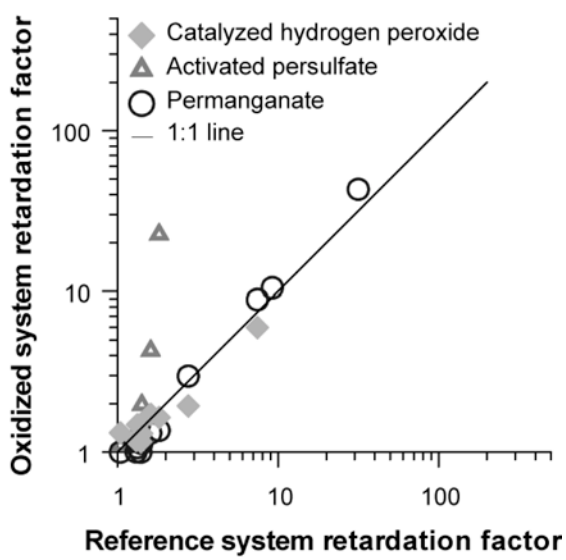

Figure 5-54. Retardation factor contrast for the first desorption phase (iv) in TCE-applied columns.

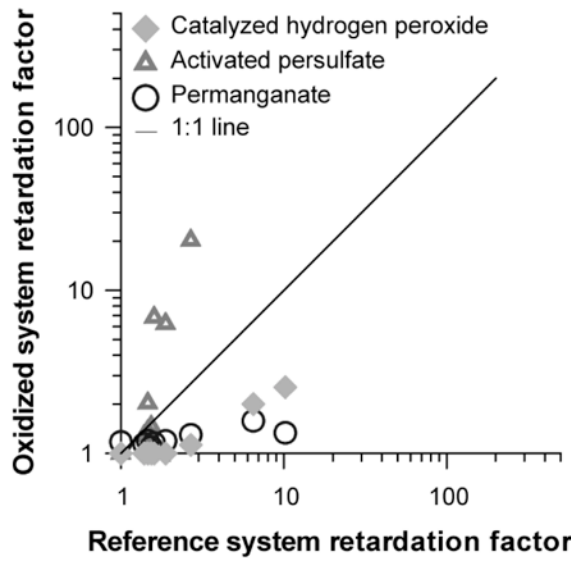

Figure 5-55. Retardation factor contrast for second desorption phase (vi) in TCE-applied columns.

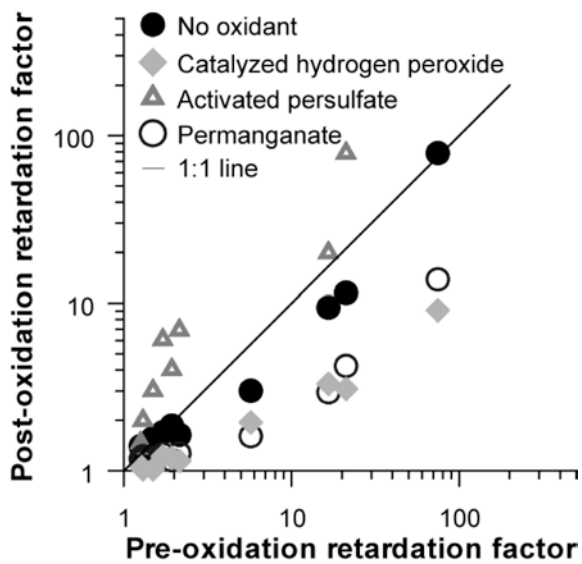

Figure 5-56. Retardation factor contrast for pre-oxidation (phase i) – post-oxidation (phase v) in TCE-applied columns (log scale).

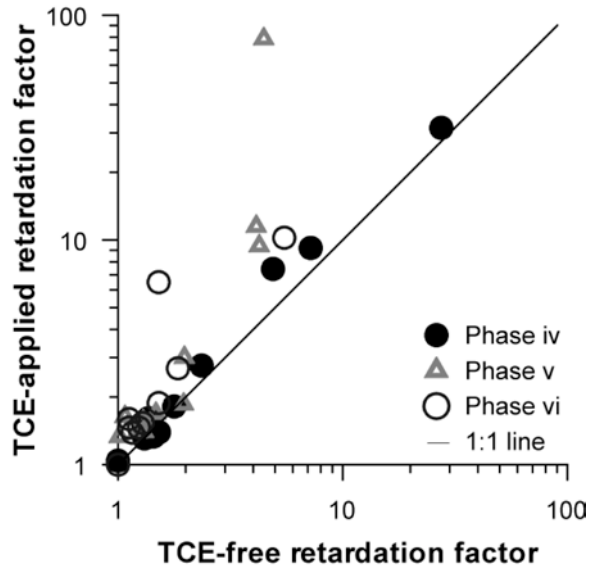

Figure 5-57. No oxidant temporal trends for TCE-applied and TCE-free columns; note that phase vi PFUdA could not be reasonably fit and are not shown.

Mobility increased in permanganate- and CHP-treated columns over time (i.e., retardation factors generally decreased with each subsequent post-oxidation phase; **Figure 5-52**, with analogous plots shown in **Figure 5-57**. **Figure 5-58**, and **Figure 5-59**). This was also observed in the TCE-free columns. Furthermore, while mobility in the first desorption phase was generally less in TCE-applied columns than in matched TCE-free columns, the matched columns became more similar over time (post-oxidation). The increasing similarity between the matched columns could be due to loss of NAPL sorbing sites.

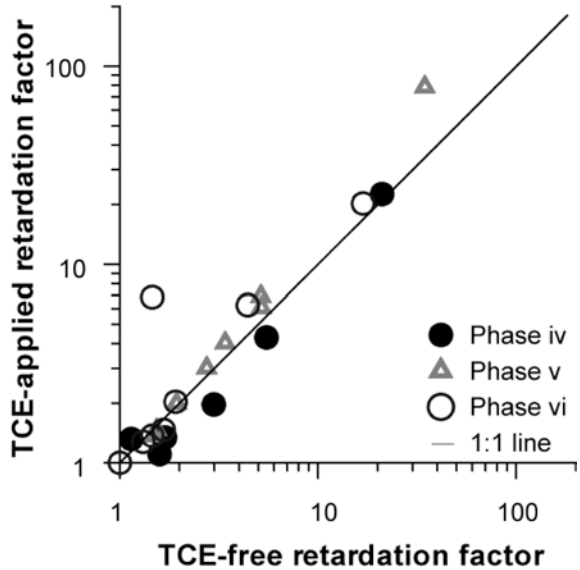

Figure 5-58. Post-persulfate treatment temporal trends for TCE-applied and TCE-free columns. Note that several PFAAs could not be reasonably fit and are not shown; temporal proximity to persulfate application (i.e., phase iv) and longer chain length compounds were most affected. TCE-free data from McKenzie et al. (2015).

In some cases, the advection-dispersion-retardation equation, assuming reversible, equilibrium sorption did not do a very good job of fitting the PFAA breakthrough in the oxidant treated columns (e.g., **Figure 5-53**); this was observed most PFAAs in persulfate-treated columns and for longer chain length PFAAs in CHP-treated columns. Potential explanations for this include rate limited sorption and gas evolution resulting in microbubbles. Poorer fits were most commonly observed in CHP-treated columns, potentially due to rate-limited sorption or gas evolution, and generally for longer chain

length compounds, especially in persulfate-treated columns.

Comparative analysis of retardation factors were conducted between the oxidized columns and the no oxidant reference columns for each of the post-oxidation phases (**Figure 5-51**, **Figure 5-54**, **Figure 5-55**). Retardation factors for persulfate-treated columns were consistently greater that the no oxidant reference retardation factors, indicating that PFAA transport was decreased. Permanganate- and CHP-treated columns had retardation factors that were similar to or less than the no oxidant reference column (first desorption and second sorption/desorption, respectively), indicating that PFAA transport was increased.

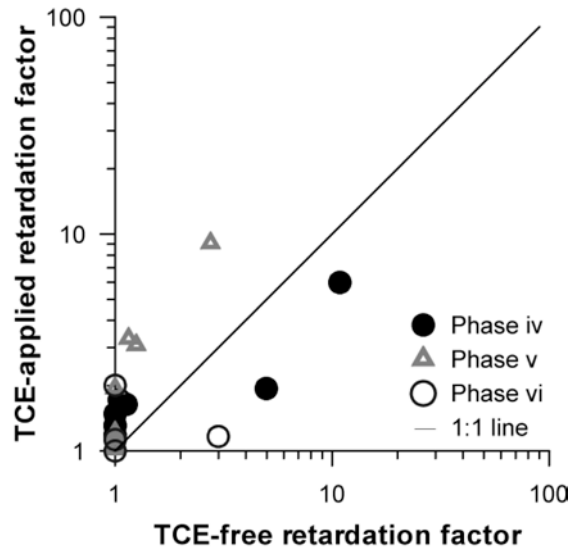

Figure 5-59. Post-CHP application temporal trends for TCE-applied and TCE-free columns. Note that reasonable fits could not always be achieved for PFDA (neither phase iv or vi) and PFUdA (phase iv). TCE-free columns are presented in McKenzie et al. (2015).

PFAA mobility changes were observed in the current no oxidant reference TCE-applied study, as they had been previously observed in the match TCE-free columns (McKenzie *et al.*, 2015). No oxidant reference columns mobility changes were less in the current TCE-applied study (i.e., in **Figure 5-56**, they are closer to the 1:1 line) than in the matched TCE-free columns. McKenzie *et al.* (2015) concluded that the observed increased PFAA mobility was most likely attributable to SOM structural changes (e.g., reductions in F_{access}); a more involved discussion in provided by McKenzie *et al.* (2015). The NAPL presence is likely to obscure some of the SOM-water interactions, which might prevent SOM structural changes. The comparatively lesser change to PFAA transport in the TCE–applied no oxidant reference column supports the F_{access} reduction hypothesis.

Temporal trends in PFAA retardation factors were also observed for permanganate- and CHP-treated columns, but less so for no oxidant reference or persulfate-treated columns. This suggests that permanganate- and CHP-treated porous media quality was continuing to change, which could be explained by temporal changes in the NAPL (e.g., reductions in NAPL volume or interfacial area) or in the amount of accessible organic matter (i.e., reduction in F_{access} value).

5.6.3.5 Post-experiment PFAA partitioning coefficients

Columns were re-equilibrated with P FAA-AGW following the cessation of sampling (conclusion of phase vi) and soil organic carbon partitioning coefficients (K_{oc}) were calculated (**Figure 5-61**). K_{oc} values should not be affected by changes in soil organic carbon content (f_{oc}; e.g., ~30% f_{oc} reduction in permanganate-treated columns), however changes to soil organic carbon quality may result in changes to observed K_{oc} values. The no oxidant reference columns' K_{oc} values displayed a chain length-dependent trend for perfluorinated tails of seven or greater, which is similar to that observed in the beginning of the experiment (based on HYDRUS fits)

and in previous batch studies (Guelfo and Higgins, 2013). The anomylously low K_{oc} values observed for PFHpA, PFOA, and PFHxS are likely due to underestimates of porous media-associated PFAA concentrations resulting from an attempt to account for sample pore water concentrations.

Also similar to this study's post-oxidation phase retardation factors, sorption generally increased in persulfate-treated columns and generally decreased in permanganate-treated columns (**Figure 5-60** and **Figure 5-61**). CHP-treated columns were similar to the no oxidant reference columns' K_{oc} values, which further suggests that rate limited sorption may be occurring in CHP-treated columns. The observed distribution coefficient values among the oxidant-treated columns were fairly similar to post-experiment matched TCE-free columns' distribution coefficient values (**Figure 5-60**).

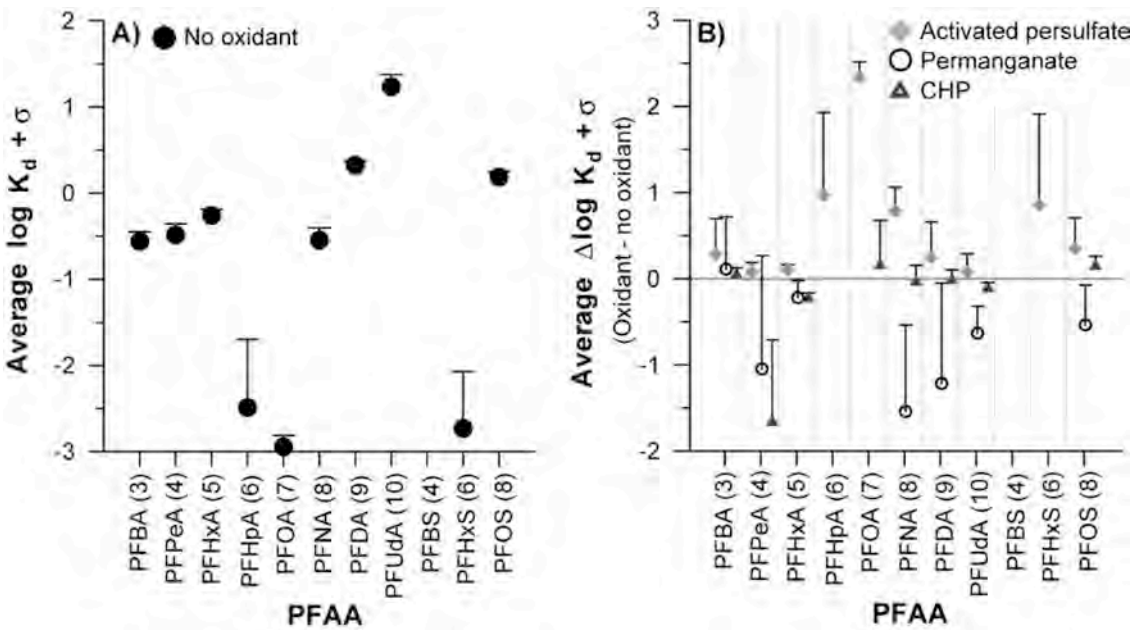

Figure 5-60. Calculated K_d distribution coefficients for post-experiment extracted porous media for: A) no oxidant columns, and B) the change in K_d due to exposure to an oxidant ($K_{d(oxidant)} - K_{d(no\ oxidant\ reference)}$). Sorbed PFAA masses were corrected to account for pore water concentrations, which resulted in negative calculated sorbed mass; in such cases, K_d values are not shown.

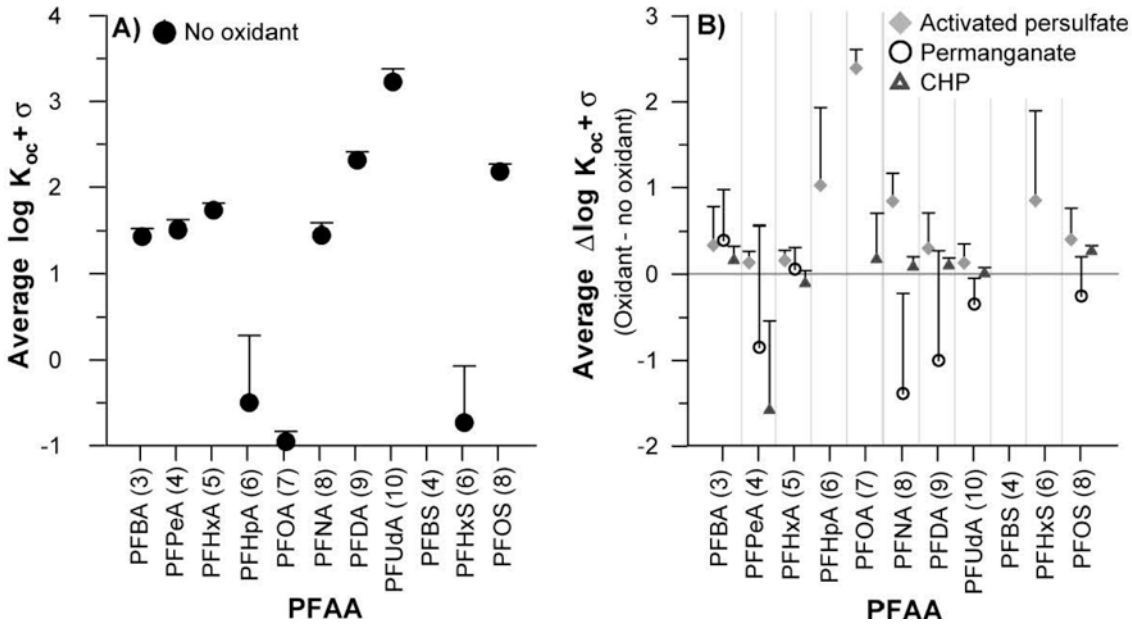

Figure 5-61. Calculated Koc distribution coefficients for post-experiment extracted porous media for: A) no oxidant reference columns, and B) the change in K_{oc} due to exposure to an oxidant ($K_{oc(oxidant)}$ - $K_{oc(no\ oxidant\ reference)}$). Sorbed PFAA masses were corrected to account for pore water concentrations, which resulted in negative calculated sorbed mass; in such cases, K_{oc} values are not shown.

5.6.4 Conclusions

Based on the results of TCE-AGW batch systems, PFAAs largely absorb into the TCE NAPL, and absorption increases with increasing PFAA chain length; interfacial accumulation may also contribute. PFAA retardation increased in TCE-applied columns, with similar chain length and head group dependent trends as have been previously observed. The data in this study suggest that chemical oxidant treatment does not result in transformation of PFAAs in TCE NAPL-contaminated porous media, but changes to PFAA sorption do occur in response to oxidant treatment. Water quality changes may be at least partially responsible for the increased sorption. PFAA mobility was increased in columns that were treated with permanganate or CHP, but was decreased in persulfate-treated columns. The PFAA mobility differences were attributed to changes in geochemistry. Finally, chemical-oxidation remediation efforts at sites where PFAAs are present with co-contaminants will likely influence the mobility of PFAAs, but the underlying mechanisms are not fully understood. More research should be conducted to elucidate this issue for chemical oxidation and also other chemically-enhanced remediation efforts.

6. DESORPTION OF PFASs FROM AFFF-IMPACTED SOIL

6.1 Introduction

In response to initial results from a companion SERDP project (ER-2128) as well as results from a field site characterization study funded by the U.S. Air Force (AFCEC BAA 689; McGuire *et al.,* 2014), an additional experimental task was added to examine the desorption of PFASs, particularly PFAAs from field-collected materials. This task employed bench and bench-scale column experiments to examine PFAA and PFAS desorption from AFFF-impacted soil under various conditions. Specific conditions evaluated included both unaltered conditions (batch and column) and desorption in the presence of chemical oxidants (column experiments).

6.2 Background

AFFFs have been used to extinguish hydrocarbon fires by the DoD at a number of sites across the country and are known to contaminate soils, groundwater, and aquifer solids with PFAAs and precursors to PFAAs at these locations (Moody *et al.,* 2003; Moody and Field, 2000; McGuire *et al.,* 2014; Backe *et al.,* 2013). These sites are highly contaminated with PFAAs, with concentrations in groundwater typically well above the provisional health advisory levels issued by the U.S. Environmental Protection Agency of 0.4 µg/L and 0.2 µg/L for PFOA and PFOS in drinking water, respectively (USEPA 2009), suggesting a need to understand the sources of PFAAs and their rates of release into groundwater. Additionally, in-depth analyses indicate that AFFF formulations contain a broad suite of chemicals which vary significantly in composition between manufacturers, formulations, and AFFF production year (Place and Field, 2012; D'Agostino and Mabury, 2014). Once released into the environment, AFFF components can undergo natural transformations that result in products which cannot necessarily be readily identified (Backe *et al.,* 2013; Dinglasan *et al.,* 2004; Plumlee *et al.,* 2009; Rhoads *et al.,* 2008; Muller *et al.,* 2011). Uncertainty in regards to chemical composition, coupled with the lack of available standards for many AFFF constituents, means that while it is possible to quantify a portion of the fluorochemicals in AFFF-contaminated samples, it is difficult to fully characterize AFFF formulations as well as formulations that have undergone changes in the environment due to degradation. Even when a broad suite of fluorochemicals (such as PFAAs and their presumed AFFF-derived precursors) are specifically measured, these chemical-specific measurements fail to fully capture the total fluorochemical load (Houtz *et al.,* 2013).

Fluorinated compounds in AFFF typically include perfluorinated chains of 3 to 10 carbons attached to non-fluorinated organic structures. The non-fluorinated portions of the molecules vary widely in structure but generally contain charged functional groups such as carboxylic acids, sulfonic acids, and amines (Place and Field, 2012). For many of these compounds, the non-fluorinated part of the molecule can be transformed in biotic or abiotic reactions which, through a number of intermediate steps, ultimately produce PFCAs and PFSAs (Dinglasan *et al.,* 2004; Plumlee *et al.,* 2009; Rhoads *et al.,* 2008; Wang *et al.,* 2011; Nguyen *et al.,* 2013; Taniyasu *et al.,* 2013) In natural systems, this conversion may be incomplete: some 20 years after cessation of AFFF-release at the Ellsworth AFB firefighter training area, high

concentrations of PFAA precursors were measured (Houtz *et al.,* 2013). Increasing concerns about the health effects of these compounds (Rosenmai *et al.,* 2013) make their environmental fate an important area of research; both PFAAs and PFAA precursors have been found in human blood samples (Lee and Mabury, 2009), and transformations of precursors has also been observed in the human body (Nilsson *et al.,* 2013).

The sorption and transport potential of PFAAs has been studied with batch and column experiments which show that these compounds are capable of subsurface transport (Higgins and Luthy, 2006; Guelfo and Higgins, 2013; Johnson *et al.,* 2007; Gellrich *et al.,* 2012; You *et al.,* 2006). Additionally, field studies have shown that PFAAs can be leached from contaminated surface soils into deeper sediment layers (Sepulvado *et al.,* 2011; Washington *et al.,* 2010), with the transport potential of PFAAs strongly dependent on the compound's perfluorinated carbon chain length and the organic carbon content of the solid phase. Evidence also suggests that equilibrium models are not sufficient to describe PFAA transport (Guelfo *et al.,* in prep.), possibly due to hysteresis effects in sorption and desorption to NOM (Pignatello 2012). To the best of our knowledge, no studies have focused on the desorption and mobility of PFAAs and/or PFAA precursors from AFFF-contaminated field materials, though studies at field contaminated sites have measured precursors in surface soils as well as in aquifer solids and groundwater, implying that PFAAs and their precursors are mobile (Moody *et al.,* 2003; McGuire *et al.,* 2014; Houtz *et al.,* 2013). Hysteresis has been observed in the adsorption and desorption or organic molecules to natural sediments (Miller and Pedit, 1992; Kan *et al.,* 1994; Weber *et al.,* 1998) which necessitates studies to specifically measure desorption of organic contaminants.

Thus, the objective of this task was to use batch and bench-scale column experiments to measure and compare desorption of PFAAs and PFAA precursors from field materials contaminated by AFFF. In batch systems, the infinite sink approach, in which the aqueous phase is regularly analyzed and replenished with clean aqueous phase, was used to quantify the desorption of AFFF-derived compounds and examine the relative mobility of PFAAs and PFAA precursors as measured by the total oxidizable precursor (TOP) assay (Houtz and Sedlak, 2012). Kinetic modeling of desorption data provided insight into the mobility of PFAA precursors relative to PFAAs and other organic contaminants. Further, limited bench-scale column experiments examined the extent to which PFAAs were mobilized from AFFF-impacted soils under advective conditions as well when exposed to chemical oxidants. Because of the widespread use of AFFF and resulting contamination of environmental media (Moody *et al.,* 2003; Moody and Field, 2000; McGuire *et al.,* 2014), developing an accurate understanding of the mobility of PFAAs and PFAA precursors in environmental materials is needed to ascertain the potential for contaminated soils and aquifer solids to serve as long term sources of PFAAs and PFAA precursors to groundwater.

6.3 Materials and Methods

6.3.1 Materials

6.3.1.1 Soils

Soil and aquifer solid samples were collected from Ellsworth AFB (South Dakota, USA) in October 2011 and August 2012 (McGuire *et al.,* 2014). Samples were homogenized on site and stored in methanol rinsed high-density polyethylene (HDPE) bottles. Solid samples were refrigerated until analysis and were sieved to less than 2 mm before use. Three surface soils (Samples A, B, and C) and two aquifer sediments (Samples D and E) from Ellsworth AFB were used in this study; they were chosen to represent a range of distances from the source zone. Surface soils were collected 0.2 - 0.3 m below ground surface (bgs), aquifer sediment were collected at the water table 3.5 - 6.0 m bgs. Firefighter training was suspended at Ellsworth in 1990, so the contaminants had been aging in the sediments for many years at the time of collection. Additional information on the extent of PFAS contamination at Ellsworth can be found in McGuire *et al.,* (2014). A sixth sample (Sample F) was collected as a composite sample during an excavation of a firefighter training area at Scott AFB (Illinois, USA). This sample was notable for the presence of hydrocarbon co-contaminants which were observed visually during methanolic extractions.

6.3.1.2 Soil and Aquifer Solid Characterization

Sample TOC was measured using USEPA method 9060A, reported on a dry weight basis. Measured TOC values are as follows: Sample A, 1.61%; Sample B, 2.97%; Sample C, 0.48%; Sample D, 0.69%; Sample E, 1.73%; Sample F, 9.80%. Insufficient sample mass was available for TOC analysis of Samples G and H. Sample pH (for Samples A-F) was measured in a 1:2 sediment: 0.01 M $CaCl_2$ suspension (Miller and Kissel, 2010). All measured pH values fell between 7.4 and 8.0 (**Table 6-1**). Due to limited quantities of some samples, texture analysis could only be conducted on Sample A (Sand, 35%; Silt, 22%; Clay, 43% (Agvise Laboratories, hydrometer method).

Table 6-1. Summary of sample characteristics

Sample	Source	TOC	pH
A	Ellsworth AFB Surface	1.61%	7.42
B	Ellsworth AFB Surface	2.97%	7.46
C	Ellsworth AFB Surface	0.48%	7.79
D	Ellsworth AFB Subsurface	0.69%	7.94
E	Ellsworth AFB Subsurface	1.73%	7.98
F	Scott AFB Composite	9.80%	7.94

6.3.1.3 Solids Extraction

Extraction of PFAAs and PFAA precursors from contaminated soils and aquifer solids followed previously published procedures (Sepulvado *et al.,* 2011). The solid phase was extracted with 99:1 (v/v) methanol/ammonium hydroxide as the extraction solvent and three rounds of extraction were performed to ensure complete removal of PFASs. PFAA precursor analysis required that solids extracts be prepared as aqueous samples (Houtz *et al.,* 2013). After an ENVI-CARB cleanup step, methanolic extracts were amended with 75 µL ammonium hydroxide (to ensure consistently high pH and minimize PFAS volatilization), evaporated to dryness, and then re-suspended in water. The ENVI-CARB cleanup does not remove PFAAs or PFAA precursors (Houtz *et al.,* 2013; Sepulvado *et al.,* 2011), and three rounds of extraction have been found to be sufficient for complete PFAA and PFAA precursor extraction (Houtz *et al.,* 2013).

6.3.1.4 Analytical Standards and Methods

Standards of PFCAs and PFSAs, as well as stable-isotope surrogate standards of PFCAs and PFSAs, were purchased from Wellington Laboratories and prepared in 70/30 (v/v) methanol/aqueous ammonium hydroxide (0.01%) solutions. Other reagent grade chemicals and solvents were purchased from Sigma Aldrich or Fisher Scientific. PFCAs studied were PFBA (x=3), PFPeA (x=4), PFHxA (x=5), PFHpA (x=6), PFOA (x=7), PFNA (x=8), and PFDA (x=9). PFSAs studied were PFBS (x=4), PFHxS (x=6), PFOS (x=8). Isotope standards for all compounds excluding PFBS were available and employed; PFHxS was used as the mass labeled internal standard for PFBS analysis.

6.3.1.5 PFAA Precursor Oxidation

Oxidative conversion of PFAA precursors into PFCAs occurs by reaction with hydroxyl radicals (·OH) which can be produced by thermolysis of persulfate ($S_2O_8^{2-}$) at pH greater than 12 (Houtz and Sedlak, 2012). Following the total oxidizable precursor (TOP) method established by Houtz and Sedak (2012) and validated for AFFF-impacted soils and groundwater by Houtz *et al.,* (2013), reconstituted (aqueous) soil or aquifer solids extracts and desorption time course aqueous supernatant samples were amended with concentrated solutions of potassium persulfate and sodium hydroxide to achieve initial reaction conditions of 150 mM sodium hydroxide and 60 mM potassium persulfate. Samples were heated for to 12 (solid phase extracts) hours at 85°C depending on the sample type. These reaction conditions have been shown to lead to complete conversion of PFAA precursors to PFCAs (Houtz and Sedlak, 2012). After heating, samples were cooled to room temperature and neutralized with concentrated HCl to a pH between 4 and 10, then diluted with methanol to a 50:50 (v/v) water:methanol ratio and refrigerated until analysis. Before analysis, samples were centrifuged to remove precipitated salts.

6.3.1.6 Analytical Methods

Samples were analyzed in a 75:25 (v/v) water:methanol mixture. Aqueous samples were further diluted 10% with a 70:30 (v/v) methanol:water aliquot containing surrogate standards. Surrogate standards were added to solid samples prior to the extraction process. All samples were analyzed on a ABSciex 3200 mass spectrometer using LC-MS/MS by methods similar to those described previously (Higgins and Luthy, 2006; Higgins *et al.,* 2005). A 50 mm x 4.6 mm Gemini C18 column was used for the LC, eluents used for LC were aqueous ammonium acetate (10mM) and ammonium acetate in methanol (10mM). Quantitation was done using Analyst software (AB SCIEX).

6.3.2 Experimental Approach

6.3.2.1 Batch Desorption Experiments

Batch desorption experiments were prepared in 50 mL polypropylene tubes. A 50 mL aliquot of uncontaminated artificial groundwater (AGW; as detailed in McKenzie *et al.,* 2015) was combined with 1 to 5 g of soil or aquifer solids, depending on the concentrations of PFCAs and PFSAs. Desorption experiments were carried out in triplicate for all materials studied. Desorption reactors were agitated on a shaker table for 23 hours then removed and centrifuged at

1860 relative centrifugal force (rcf) for 30 minutes. An aliquot of the aqueous phase was collected and frozen for later analysis and all remaining water was removed and discarded. Fresh AGW was then added to the reactor. The experiments continued for 14 days, thereby exposing soil and aquifer solid samples to approximately 0.7 L of clean AGW over two weeks. After the final aqueous sample was collected, the remaining material was extracted using the method described above to recover any compounds which did not desorb into the aqueous phase. The volume of aqueous phase removed each day was carefully tracked via gravimetric measurements to ensure that masses of PFAAs desorbed could be determined. The mass of water removed showed slight variability over the course of the experiments due to swelling in the samples, but day to day variability rarely exceeded 1%.

6.3.2.2 Batch System Modeling

Desorption data were modeled with a dual rate exponential model using Origin 9.1 Pro (OriginLab). This model allows for the division of the mass of chemical in the solid phase into fast and slow desorbing compartments (**Equation 6-1**; Cornelissen *et al.,* 1997; Chai *et al.,* 2006; Johnson *et al.,* 2001):

$$\frac{M_t}{M_0} = F_f\left(e^{-k_f * t}\right) + F_s\left(e^{-k_s * t}\right) + y_0 \qquad \text{(eqn. 6-1)}$$

where M_t is the analyte mass remaining in the solid phase at time t (day), M_0 is the initial mass of analyte in the solid phase, F_f is the fraction of analyte in the fast desorbing compartment, F_s is the fraction in the slow desorbing compartment, and k_f and k_s (day^{-1}) are the rate constants associated with the fast and slow compartments. F_s is defined as equal to 1-F_f, while y_0 represents an immobile fraction only recovered at the end of the experiment with a methanolic extraction. A kinetic model was chosen because it has been observed that equilibrium models will often over-predict the quantity of PFAAs which will leach from field contaminated samples (Sepulvado *et al.,* 2011).

6.3.2.3 Column Experiments

Similar to the column experiments described in **Section 5**, glass columns (25 mm ID x 80 mm length; Kontes FlexColumn Economy) were dry-packed with 5 of Sample A soil, with the remaining volume on the top of the column contained methanol-washed glass beads. Column experiments were conducted at room temperature in ambient light. Approximately 570 mL of artificial groundwater (AGW) was pumped into each column (at ~0.1 mL/min), and in some cases, this AGW included chemical oxidants (permanganate at 8.4 mM or persulfate at 52,1 mM, with activators and concentrations identical to those described in McKenzie *et al.,* 2015). In addition, select columns were leached with AGW for which the pH had been adjusted to 1.5 (with HCl) to mimic the lower pH conditions observed when persulfate was employed as a chemical oxidant.

Column experiments were conducted in down flow mode and were unsaturated. The appropriate source water for each experiment was provided via a peristaltic pump. Column effluent samples were collected from a three-way valve ~10 cm downstream of the column outlet approximately

every 5 min, with a total volume collected per sample of ~500 µL. Column effluent samples were quenched with methanol and/or pH adjusted (with ammonium hydroxide) when appropriate. A brief summary of the experimental conditions examined in the column desorption experiments is summarized in **Table 6-2** below. Sample A was extracted and analyzed for PFAA content as per Sepulvado *et al.,* (2011). Aqueous samples were analyzed for PFAAs as per McKenzie *et al.,* 2015.

Table 6-2. Column desorption experiment conditions examined

Soil	Column Influent	Experimental Replicate Columns
A	AGW (pH 7)	2
A	AGW (pH 1.5)	2
A	AGW + Persulfate (pH 1.5)	2
A	AGW + Permanganate (pH 7)	2

The cumulative mass desorbed for each column experiment was calculated using an area-under-the-curve approach and accounted for the variable volume eluted from each column between each sampling event.

6.4 Results and Discussion

6.4.1 Analysis of Fresh Soils and Aquifer Solids

At the time soil and aquifer solid samples were prepared for desorption experiments, three aliquots of each material were reserved for analysis without exposure to water (i.e. analyzed "fresh"). These fresh materials were extracted and the TOP assay was applied to the extracts to confirm that PFAA precursors were present in the solid samples and being successfully converted by the assay. Extraction results with and without oxidative conversions of precursors are given in **Figure 6-1**. The six samples displayed a range of PFAA concentrations and levels of PFCA production; all samples showed significant production of PFCAs upon oxidation. All samples also demonstrated little to no measurable production or destruction of PFSAs with oxidation, confirming results of previous work (Houtz and Sedlak, 2012).

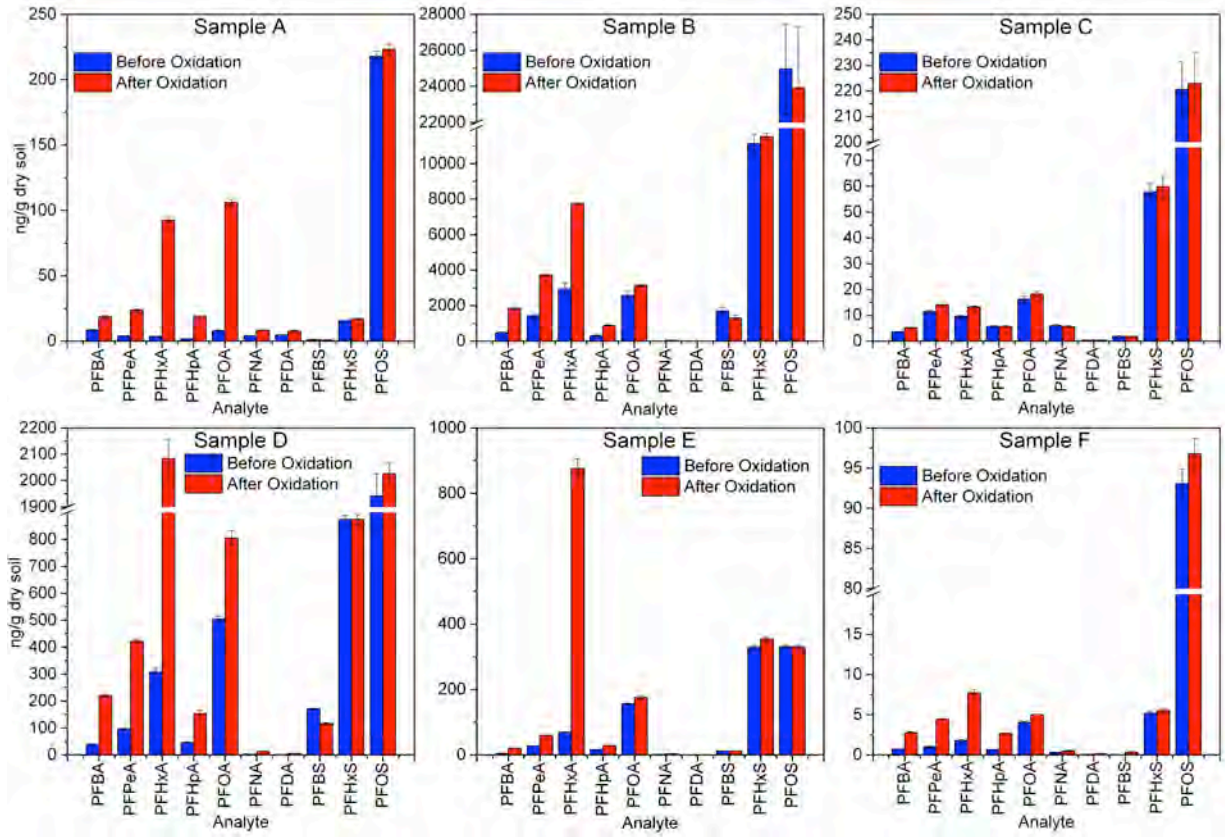

Figure 6-1. PFAA concentrations in fresh soils and aquifer solids before and after application of precursor oxidation assay. Error bars are the standard deviation of triplicate samples.

6.4.2 PFAA Desorption in Batch Systems

To quantify the precursors present in samples, the measured PFAA masses before oxidation were subtracted from measured masses after oxidation. The differences between these measured values are referenced using a Δ (e.g. ΔPFOA = PFOA after oxidation - PFOA before oxidation). PFAA masses desorbed from solids during batch experiments were calculated based on measured aqueous phase concentrations for each day of the experiment. An example of cumulative mass desorbed of a single analyte (PFOA) from a single solid is given in **Figure 6-2**. These exemplar data show that most of the PFOA present in the solid desorbed within the first two days of the experiment, but that the much larger mass of PFOA precursors desorbed over a longer period of time; measurable mass continued to be desorbed daily for the duration of the experiment.

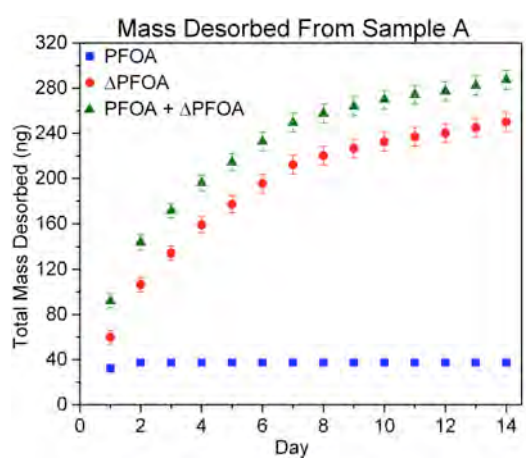

Figure 6-2. Example of the cumulative desorption of PFOA and PFOA precursors as well as their sum. Error bars are the standard deviation of triplicate samples.

The total mass recovered from the batch desorption experiments was compared to masses extracted from the solids that were not exposed to desorption experiments (**Table 6-3**). In some cases, the mass balance between these measurements was poor, especially for ΔPFCAs. Both over-recovery and under-recovery was observed. One possible explanation for poor mass balance is that the oxidation of the same set of precursors in samples of AGW versus extracts might have produced different sets of PFCAs, and as a result, some compounds will appear to be over recovered while others will be under recovered. Mass balance was also poor for unoxidized PFHxA in several samples; this issue is discussed below.

Table 6-3. Cumulative mass desorbed/mass extracted from solids used in batch experiments

	PFBA	PFPeA	PFHxA	PFHpA	PFOA	PFNA	PFDA	PFBS	PFHxS	PFOS
A	95.5%	91.3%	657.1%	111.2%	104.4%	139.1%	115.1%	119.7%	105.2%	136.6%
B	91.4%	94.2%	94.6%	85.7%	86.4%	104.8%	94.8%	76.1%	90.6%	85.6%
C	100.4%	97.2%	374.7%	105.7%	125.5%	128.1%	97.3%	128.1%	97.3%	84.5%
D	114.2%	125.5%	112.4%	95.3%	89.7%	85.6%	79.7%	60.9%	97.0%	98.7%
E	109.9%	101.1%	116.5%	87.0%	90.1%	90.2%	[a]	68.0%	90.8%	87.3%
F	84.5%	136.0%	412.8%	93.2%	87.2%	[a]	[a]	107.5%	89.8%	96.2%
ΔPFAA										
	PFBA	**PFPeA**	**PFHxA**	**PFHpA**	**PFOA**	**PFNA**	**PFDA**			
A	216.8%	61.6%	103.2%	115.0%	57.5%	32.4%	31.7%			
B	143.2%	132.3%	218.2%	154.0%	291.1%	114.9%	[a]			
C	1157.2%	324.9%	1304.0%	[a]	277.3%	[a]	[a]			
D	105.5%	120.3%	94.0%	109.7%	165.7%	56.9%	13.0%			
E	181.0%	235.3%	118.8%	117.6%	99.6%	36.5%	[a]			
F	646.0%	114.8%	398.4%	24.1%	43.3%	[a]	1707.5%			

[a] Some values excluded due to negligible PFAA measurement.

6.4.3 Modeling of Batch Systems

Modeling results for PFAAs in are presented in **Table 6-4**; modeling results for ΔPFCAs (PFAA precursors) are presented in **Table 6-5**. Compounds that desorbed quickly were modeled with only a single compartment (i.e., $F_f = 1$ and $F_s = 0$). These fast desorbing compounds included all the PFAAs before oxidation (see **Table 6-4**). For the more slowly desorbing precursor compounds, a two compartment model often provided a better fit of the data; two compartment model fits had smaller root mean square error (RMSE) values than one compartment model fits in all instances where the software was able to converge on a fit using two compartments (**Table 6-6**).

Comparisons of desorption data and model fits between the solids are shown in **Figure 6-3**. Rapid desorption of PFAAs is observed, although Samples A and F do show significantly slower desorption of PFOS than the other solids. Desorption rates of PFOA and PFHxS are similar among all six samples, but Samples A and F show a greater fraction of each analyte retained in the solid phase for the duration of the experiment. In **Figure 6-3b**, select ΔPFCA desorption data are plotted along with model fits. These data show greater variability between samples, and, as with PFAAs without oxidation, the slowest desorption was in Sample A. Greater variability between the different samples in ΔPFAA data suggests that it may be more difficult to make

predictions about PFAA precursor desorption rates than about the desorption of PFAAs themselves.

Table 6-4. Desorbed masses and fitting parameters (**Equation 6-1**) for batch samples prior to oxidation

	Sample A		Sample B		Sample C	
Analyte	**Mass Desorbed, ng**	**k_f (day^{-1})**	**Mass Desorbed, ng**	**k_f (day^{-1})**	**Mass Desorbed, ng**	**k_f (day^{-1})**
PFBA	8.06± 3.84		440 ± 7.51	4.08 ± 0.01	3.68 ± 0.18	3.23 ± 0.64
PFPeA	3.59± 1.49		1340 ± 51.1	4.53 ± 0.01	11.1 ± 0.73	2.87 ± 0.12
PFHxA	23.3 ± 1.27	0.16 ± 0.01	2770 ± 61.3	3.51 ± 0.15	36.1 ± 1.00	0.22 ± 0.03
PFHpA	2.09± 0.04		256 ± 16.5	3.99 ± 0.01	6.08 ± 0.03	3.35 ± 0.22
PFOA	8.46± 0.22	2.10 ± 0.04	2210 ± 147		20.4 ± 0.90	2.50 ± 0.02
PFNA	5.76± 0.21	1.28 ± 0.02	17.0 ± 1.15		7.79 ± 0.25	2.18 ± 0.02
PFDA	5.46± 0.19	0.60 ± 0.03	6.39 ± 0.53		0.33 ± 0.03	1.24 ± 0.06
PFBS	1.35± 0.50		1290 ± 59.2		1.63 ± 0.01	
PFHxS	16.7 ± 1.30	2.01 ± 0.09	10100 ± 475	3.61 ± 0.01	60.6 ± 1.70	2.54 ± 0.01
PFOS	299 ± 7.41	0.54 ± 0.01	21300 ± 1120	2.13 ± 0.06	272 ± 4.39	1.52 ± 0.01

	Sample D		Sample E		Sample F	
Analyte	**Mass Desorbed, ng**	**k_f (day^{-1})**	**Mass Desorbed, ng**	**k_f (day^{-1})**	**Mass Desorbed, ng**	**k_f (day^{-1})**
PFBA	49.2 ± 1.17	2.67 ± 0.08	5.98 ± 0.20	2.60 ± 0.02	0.679 ± 0.02	
PFPeA	131 ± 3.45	2.77 ± 0.02	30.0 ± 1.81		1.43 ± 0.21	
PFHxA	378 ± 18.9	2.65 ± 0.03	86.0 ± 4.13	2.12 ± 0.24	7.76 ± 0.20	0.26 ± 0.02
PFHpA	47.9 ± 4.36	2.89 ± 0.02	15.4 ± 1.20	2.77 ± 0.02	0.650 ± 0.01	
PFOA	494 ± 26.5	2.71 ± 0.02	150 ± 4.51	2.78 ± 0.01	3.70 ± 0.11	0.98 ± 0.04
PFNA	3.11 ± 0.15		2.00 ± 0.10			
PFDA	1.24 ± 0.12					
PFBS	114 ± 4.11	2.96 ± 0.02	8.56 ± 3.52	3.24 ± 0.42	0.383 ± 0.01	
PFHxS	925 ± 41.6	2.64 ± 0.02	319 ± 11.2	2.55 ± 0.05	4.88 ± 0.26	1.76 ± 0.09
PFOS	2090 ± 39.2	1.87 ± 0.01	308 ± 16.1	2.21 ± 0.01	93.6 ± 1.29	0.27 ± 0.02

Values of fitting parameters are not reported where there were insufficient data for fitting. Standard errors are values produced by the fitting software (Origin 9.1 Pro, OriginLab).

Table 6-5. Desorbed masses and fitting parameters for batch samples after oxidation (**Equation 6-1**).

Analyte	Sample A Mass Desorbed, ng	F_f	k_f (day^{-1})	k_s (day^{-1})	Sample B Mass Desorbed, ng	F_f	k_f (day^{-1})	k_s (day^{-1})
ΔPFBA	22.0 ± 4.80	1	0.18 ± 1		1940 ± 105	1	2.40 ± 0.09	
ΔPFPeA	12.3 ± 2.27	1	0.75 ± 1		3040 ± 232	1	2.71 ± 0.02	
ΔPFHxA	92.2 ± 1.62	0.27 ± 0.04	0.75 ± 0.96	0.21 ± 0.01	10500 ± 493	0.96 ± 0.01	2.67 ± 0.06	0.17 ± 0.06
ΔPFHpA	19.7 ± 0.65	0.04 ± 0.06	1.35 ± 0.90	0.23 ± 0.02	897 ± 36.1	0.90 ± 0.04	2.40 ± 0.16	0.51 ± 0.15
ΔPFOA	56.6 ± 1.79	0.07 ± 0.05	1.29 ± 1	0.22 ± 0.01	1660 ± 260	1	1.85 ± 0.04	
ΔPFNA	1.40 ± 0.35	1	0.24 ± 1		32.3 ± 7.50	1	2.09 ± 0.07	
ΔPFDA	0.973 ± 0.35	1	0.19 ± 0.07					
	Sample C				**Sample D**			
	Mass Desorbed, ng	**F_f**	**k_f (day^{-1})**	**k_s (day^{-1})**	**Mass Desorbed, ng**	**F_f**	**k_f (day^{-1})**	**k_s (day^{-1})**
ΔPFBA	17.5 ± 2.20	1	0.17 ± 0.02		207 ± 9.15	1	1.83 ± 0.08	
ΔPFPeA	8.31 ± 1.43	0.81 ± 0.19	2.35 ± 1.03	0.38 ± 0.35	429 ± 29.9	0.85 ± 0.02	2.25 ± 0.06	0.58 ± 0.05
ΔPFHxA	47.4 ± 2.73	0.86 ± 0.06	2.48 ± 0.34	0.41 ± 0.15	1820 ± 70.5	0.91 ± 0.01	1.61 ± 0.02	0.15 ± 0.02
ΔPFHpA	3.34 ± 0.40	0.50 ± 0.35	2.14 ± 2.65	0.34 ± 0.25	129 ± 8.14	0.84 ± 0.00	1.58 ± 0.08	0.13 ± 0.06
ΔPFOA	5.71 ± 0.97	0.89 ± 0.15	1.66 ± 0.37	0.31 ± 0.52	543 ± 49.6	0.57 ± 0.01	2.27 ± 0.08	0.25 ± 0.01
ΔPFNA	0.37 ± 0.33	0.51 ± 0.46	1.55 ± 2.11	0.22 ± 0.41	6.01 ± 0.52	1	1.30 ± 0.10	
ΔPFDA	0.116 ± 0.05	1	1.70 ± 0.12		0.563 ± 0.16			
	Sample E				**Sample F**			
	Mass Desorbed, ng	**F_f**	**k_f (day^{-1})**	**k_s (day^{-1})**	**Mass Desorbed, ng**	**F_f**	**k_f (day^{-1})**	**k_s (day^{-1})**
ΔPFBA	30.4 ± 1.11	0.63 ± 0.05	1.99 ± 0.32	0.16 ± 0.04	13.6 ± 0.08	1	0.33 ± 0.02	
ΔPFPeA	78.0 ± 3.85	1	2.32 ± 0.03		4.18 ± 0.32	1	1.19 ± 0.04	
ΔPFHxA	1020 ± 13.4	0.81 ± 0.02	3.17 ± 0.22	0.49 ± 0.04	24.8 ± 0.34	1	0.95 ± 0.14	
ΔPFHpA	16.0 ± 1.26	1	2.47 ± 0.03		0.506 ± 0.05			
ΔPFOA	21.0 ± 10.3	1	1.75 ± 0.08		0.447 ± 0.26	1	1.26 ± 0.16	
ΔPFNA	0.535 ± 0.11							
ΔPFDA					2.05 ± 0.38			

Values of fitting parameters are not reported where there were insufficient data for fitting. Standard errors are values produced by the fitting software (Origin 9.1 Pro, OriginLab).

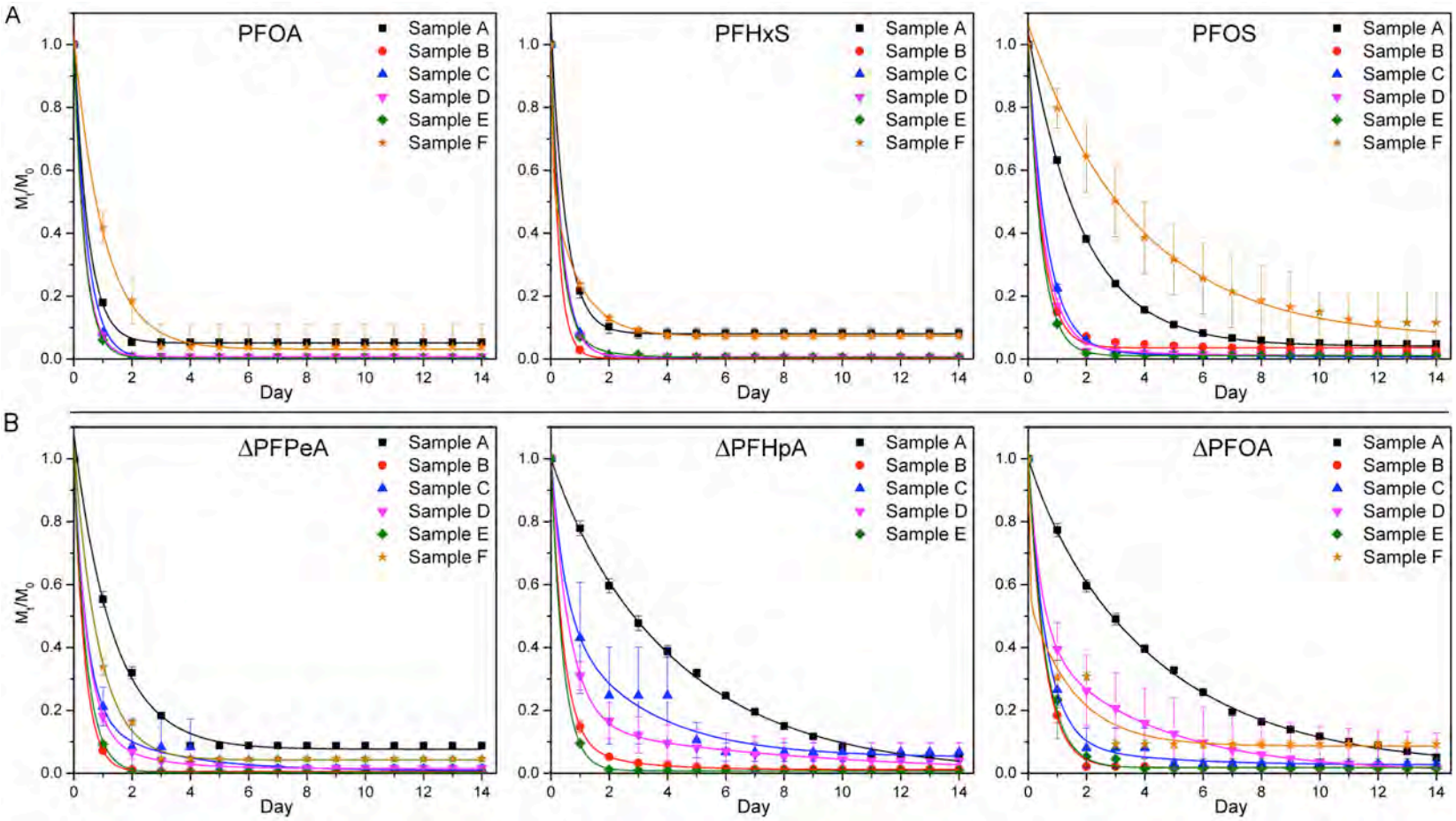

Figure 6-3. Example desorption data with corresponding model fits ($r^2 > 0.99$) plotted as solid lines. M_t/M_0 is the ratio of mass remaining in the solid phase to the total mass recovered. Error bars are standard deviations of experimental triplicates.

Modeled desorption rate constants are summarized in **Figure 6-4**. As discussed above, the two-compartment model was only necessary with the ΔPFCA data due their slower desorption as compared to samples before oxidation. Of note are the generally lower k values for many ΔPFCAs as compared to the PFCAs. When the ΔPFCA data were fit better with a two compartment model, the rate constant of the slow fraction (ks) was consistently 3 to 15 times smaller than the rate constant of the fast fraction (kf). Error bars were omitted from **Figure 6-4** to improve data visibility; all standard errors as generated by Origin 9.1 are reported in **Table 6-4** and **Table 6-5**. Standard errors were typically between 1% and 10% of reported desorption constants, indicating that the variability observed in **Figure 6-4** is noteworthy.

Table 6-6. Root mean square error of model fits

Analyte	2 Site Model	1 Site Model
Soil A, C6 Delta	3.93E-03	2.10E-02
Soil A, C7 Delta	1.61E-02	1.73E-02
Soil A, C8 Delta	1.18E-02	1.79E-02
Soil B, C6 Delta	3.39E-03	7.06E-03
Soil B, C7 Delta	5.51E-03	8.68E-03
Soil C, C5 Delta	4.55E-02	4.87E-02
Soil C, C6 Delta	1.32E-02	1.85E-02
Soil C, C7 Delta	9.03E-02	9.67E-02
Soil C, C8 Delta	3.33E-02	3.45E-02
Soil C, C9 Delta	1.50E-01	1.56E-01
Soil D, C6 Delta	3.85E-05	2.12E-03
Soil D, C7 Delta	3.30E-03	4.36E-03
Soil D, C8 Delta	5.43E-05	6.11E-03
Soil E, C4 Delta	1.67E-05	9.31E-04
Soil E, C6 Delta	1.24E-04	7.99E-03
Soil F, C6 Delta	1.34E-05	1.17E-03

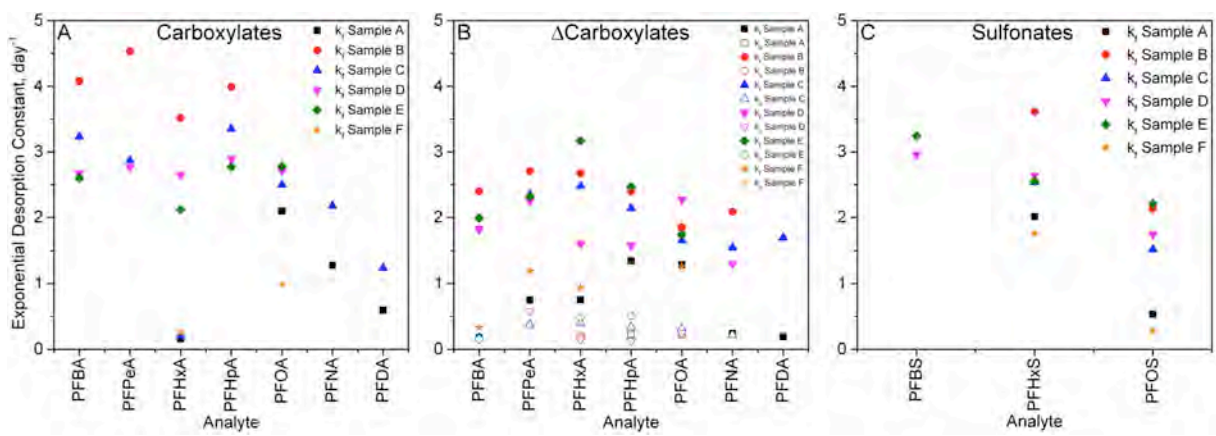

Figure 6-4. Summary of desorption rate constants (See **Equation 6-1**). Standard error values reported in **Table 6-4** and **Table 6-5**. Larger rate constants correspond to faster desorption.

6.4.3.1 Fast and Slowly Desorbing Modeled Fractions

For all PFAAs and a portion of PFAA precursors, the fraction of the compounds calculated to be in the fast desorbing fraction (F_f) was one, but approximately half of the precursors had F_f values less than one. Several studies have demonstrated relationships between F_f and the organic carbon-water partitioning coefficient (K_{oc}). For example Cornelissen *et al.,* (1997) found a strong positive correlation between log K_{oc} and log(F_s/F_f), indicating that increasing F_s from 0.1 to 0.5 increased the log K_{oc} of a compound by 1.5 log units. Another study (Chai *et al.,* 2006) was able to accurately predict K_{oc} ($K_{oc,pred}$) in soils where a large proportion of the organic contaminant is in the slow desorbing phase using literature values ($K_{oc,lit}$) with the relationship (**Equation 6-2**):

$$K_{oc,pred} = \frac{K_{oc,lit}}{F_f} \qquad \text{(eqn. 6-2)}$$

From this relationship the PFAA precursors measured in this study can be estimated to have K_{oc} values 1.04 to 25 times larger than if $F_f = 1$. Larger K_{oc} values can be related to the retardation factor (R) by **Equation 6-3** (Schwarzenbach *et al.,* 2003):

$$R = 1 + \frac{\rho_b}{\emptyset} K_{oc} f_{oc} \qquad \text{(eqn. 6-3)}$$

where ρ_b is the sediment bulk density, ø is the sediment porosity, and f_{oc} is the organic carbon content. R is a measure of a contaminant's transport relative to groundwater with larger values corresponding to decreased mobility. It is evident from **Equation 6-3** that larger K_{oc} values will result in larger R values and thus decreased transport, therefore having a fraction of PFAA precursors in a slow desorbing compartment results in an increase in the retardation of the compound.

An additional important implication of F_f values less than one is that it implies a less bioavailable fraction. Studies suggest that only the fast desorbing fraction of a compound is bioavailable (Barnier *et al.,* 2014; Cornelissen *et al.,* 2011) and that a positive correlation exists between the fast desorbing fraction and biota-sediment accumulation factors (BSAFs; You *et al.,* 2006). If natural conversion of precursors into PFAAs is primarily biologically mediated, this study suggests that slow desorbing fractions of precursors may remain untransformed in the environment.

The calculated parameters k_f and k_s vary widely in value between published studies, so they are most useful when comparing different compounds in the same soils. To this end, this study demonstrated that PFAA precursor desorption usually shows slower kinetics than PFAAs, which will result in lower mobility. Comparisons between the kinetic parameters calculated herein and published values for other organic contaminants should be viewed skeptically due to the large variations between studies. However, the finding that k_f and k_s values for PFAAs and PFAA precursors are high in the range of previously reported values suggests that these compounds are relatively mobile in the environment, and despite their slower desorption (as compared to PFAAs), PFAA precursor mobility needs to be considered when building a site remediation plan.

6.4.3.2 Chain Length Effects

Based on previous work, one would expect these data to show negative correlations between perfluoroalkyl chain length and desorption rate constants (Sepulvado *et al.,* 2011; Washington *et al.,* 2010). The PFCA and PFSA data in **Figure 6-4** (Panels A and C) generally support this expectation, with slower desorption of the longer PFAAs. Trends between desorption rate and carbon chain length are provided in **Figure 6-5**, with associated data provided in **Table 6-7**. Briefly, linear fits of modeled k_f values of PFCAs and PFSAs vs. chain length are shown in **Figure 6-5**, fitting parameters are given in **Table 6-7**. Standard errors of fitting parameters and r^2 values as calculated by the fitting software are reported where the number of fit points is greater than 2. PFCAs only show linear behavior at carbon chain lengths ≥ 6 (PFHpA); shorter chain length data points were eliminated due to their high variability and clear absence of chain-length dependent trends. The fits of Samples A, B, C, and F have similar slopes (~ -0.70) for both PFCA and PFSA data. The slopes of Samples D and E are significantly smaller, which may be related to the quality of the materials and/or their exposure to PFAAs (both samples are aquifer solids as opposed to surface soils). However, the sample size is simply too small to state conclusively that PFAA desorption from subsurface materials is significantly different than from surface soils.

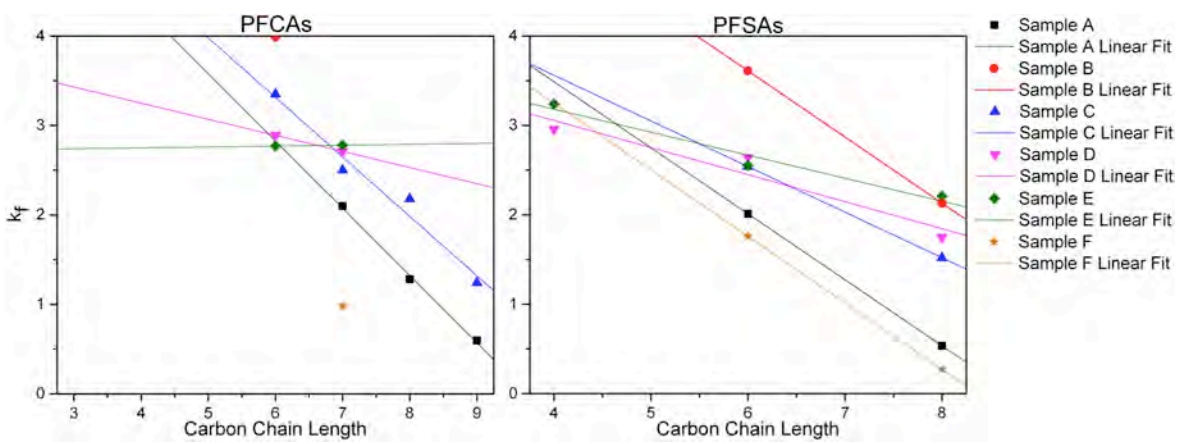

Figure 6-5. Linear fits of desorption rate constants calculated by Origin 9.1 Pro (OriginLab). Fitting parameters are reported in **Table 6-7.**

Table 6-7. Linear fitting parameters (y = mx + b) calculated by Origin 9.1 Pro (OriginLab)

	PFCAs			PFSAs		
	m	b	r^2	m	b	r^2
A	-0.75 ± 0.4	7.34 ± 0.32	0.99	-0.74	6.44	
B				-0.70	8.05	
C	-0.66 ± 0.08	7.31 ± 0.63	0.96	-0.51	5.60	
D	-0.10	3.97		-0.30 ± 0.08	4.26 ± 0.51	0.86
E	0.01	2.71		-0.26 ± 0.05	4.21 ± 0.31	0.93
F				-0.74	6.22	

For the PFCAs, the trends of slower desorption with longer carbon chain length is especially apparent in the longer chain length compounds. The apparent absence of trends with

perfluorinated carbon chain length in the ΔPFCA data (**Figure 6-4b**) is not surprising; unlike PFCAs and PFSAs, for the PFAA precursors there is not a direct correlation between the "measured" perfluorinated chain length of the compound and the size of the molecules due to considerable size variations in the non-fluorinated portions of the molecules (Place and Field, 2012; Backe *et al.,* 2013; Houtz and Sedlak, 2012). Additionally, the TOP assay can shorten the length of the perfluorinated carbon chain (Houtz and Sedlak, 2012). Consequently the perfluorinated carbon chain length of the PFCAs produced by the TOP assay are not fully representative of the size of the precursor compound that was transformed and any trends that may exist between precursor sizes and desorption rates are lost in the process of oxidation.

Table 6-4 and **Figure 6-4** show that for 3 samples, Sample A, Sample C, and Sample F, desorption of PFHxA was anomalously slow. Additionally, the desorption experiments for these three samples greatly over-recovered PFHxA as compared to the PFHxA mass measured in the samples initially (**Table 6-3**). The reason for this behavior is unknown, but a potential explanation is that precursor compounds may have been converted into PFHxA at some stage of the desorption experiment, even when the TOP assay was not applied to the samples. Thus, what appeared to be slowly desorbing PFHxA may in fact have been some slowly desorbing precursor compound, which was converted into PFHxA after desorption. Biotic transformation of precursors into PFHxA has been observed in other studies (Wang *et al.,* 2011) but it is assumed that the addition of sodium azide suppressed any microbial activity, therefore any transformations would likely be abiotic. Preliminary experiments (data not shown) indicated that sodium azide did not react with precursor compounds to form PFCAs. Photolysis of precursor compounds into PFHxA has been observed with long (>100 day) exposure to sunlight (Taniyasu *et al.,* 2013), and indirect photolysis has been shown to convert precursors into PFOA (Plumlee *et al.,* 2009; Nguyen *et al.,* 2013). It is unknown if a similar process is occurring in these experiments, as no specific precautions were taken to minimize phototransformation and experiments were conducted in ambient laboratory lighting conditions.

To the best of our knowledge, we are the first to report desorption rate constants for PFAAs and PFAA precursors, though similar desorption data have been measured for other organic contaminants, primarily chlorinated benzenes, PAHs and PCBs (Cornelissen et all, 1997; Chai *et al.,* 2006; Johnson *et al.,* 2001; Oh *et al.,* 2013; Barnier *et al.,* 2014). For example, desorption rate constants (k_f and k_s) for the PAH phenanthrene were found to vary over multiple orders of magnitude: k_f values ranged from 0.0289 to 18.7 (day^{-1}; Johnson *et al.,* 2001; Barnier *et al.,* 2014), k_s values ranged from 0.000896 to 0.148 (day^{-1}; Johnson *et al.,* 2001). These studies used Tenax® resin beads to keep the aqueous concentrations low, so direct comparisons to the data reported herein may not be entirely appropriate. Results for other organic contaminants were comparable to those of phenanthrene (Cornelissen *et al.,* 1997; Oh *et al.,* 2013; Barnier *et al.,* 2014). The k_f and k_s values measured in this study, while not anomalously high, are high in the range of values measured for other organic contaminants.

6.4.5 PFAA Desorption from Columns

6.4.5.1 Untreated Columns

As illustrated in **Figure 6-6**, the desorption of many PFAAs under ambient conditions was fairly rapid, though not complete. When flushed with AGW (at pH ~ 7), the concentration of many PFCAs in the column effluent rapidly declined (**Figure 6-6A**). Noticeably, the two longer chain length PFCAs, PFNA and PFDA, appear to desorb much more slowly than their shorter-chain analogs. However, the total mass recovered in the aqueous phase (**Table 6-8**) was far from complete. Of the PFCAs, only PFOA approached complete desorption (~75%) at pH 7 in 570 mL of AGW. It is not clear why the other PFCAs, particularly those whose desorption profiles suggest faster kinetics (**Figure 6-6A**), were not completely recovered in the aqueous phase. Given the essentially complete recoveries of these same chemicals in the same soil in batch systems (**Table 6-3**), it is likely that the low recoveries reflects low but non-quantifiable concentrations (i.e., below the limits of quantitation) in the column effluent after the first 25 mL of AGW had passed through the system: samples that were <LOQ were counted as zero contributions to the mass recovered. Future work may want to evaluate this presumably low level and prolonged release of PFCAs from AFFF-impacted soils under advective conditions.

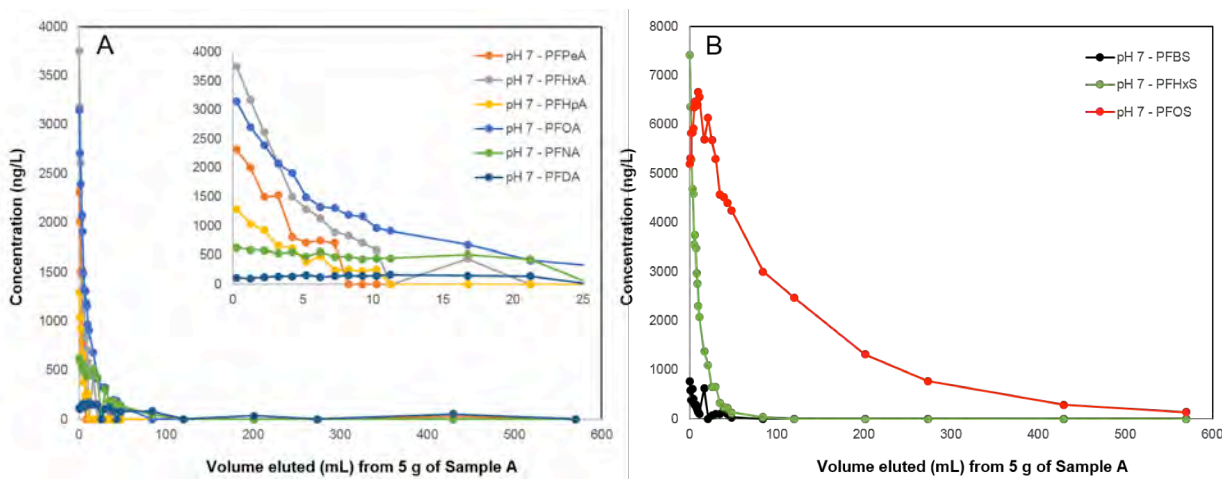

Figure 6-6. Desorption profiles of select perfluorocarboxylates (**A**) and perfluorosulfonates (**B**) from Sample A upon application of artificial groundwater (pH 7). Results presented are the averages of duplicate experimental columns. Inset in **A** provides the desorption profile for the PFCAs within the first 25 mL of applied AGW.

Table 6-8. Cumulative mass recovery (%) of PFAAs in the aqueous phase after elution of 570 mL through 5 g of Sample A under various conditions. Error values reported are the percent differences for the average mass recovered from duplicate experimental columns.

	PFPeA	PFHxA	PFHpA	PFOA	PFNA	PFDA	PFBS	PFHxS	PFOS
pH 1.5	26 ± 9	50 ± 7	32 ± 1	54 ± 3	21 ± 5	2 ± 2	51 ± 1	67 ± 0.2	34 ± 1
pH 7	37 ± 2	62 ± 13	39 ± 2	75 ± 7	81 ± 23	40 ± 6	139 ± 14	77 ± 7	80 ± 2
Permanganate	322 ± 132	808 ± 97	106 ± 30	151 ± 11	122 ± 2	10 ± 2	95 ± 17	108 ± 20	92 ± 1
Persulfate	34 ± 1	59 ± 3	37 ± 2	32 ± 4	8 ± 1	1 ± 1	44 ± 3	64 ± 0.2	29 ± 3

A much starker contrast was evident from the desorption profiles of the PFSAs (**Figure 6-6B**). The desorption profile for PFHxS was similar to the profiles of many of the PFCAs, whereas PFOS concentrations in the column effluent increased slightly within the first 10-15 mL before decreasing. Notably, the aqueous PFOS concentration only dropped below the current provisional health advisory level (200 ng/L; USEPA 2009) in the final samples collected, providing further evidence of a need to understand source zone depletion with respect to PFAAs at AFFF-impacted sites. Interestingly, the mass recovered for both PFOS and PFHxS in the aqueous was approaching completion (77% for PFHxS, 80% for PFOS). Given the stronger sorption of these compounds as compared to the PFCAs, this further supports the assertion that the low mass recoveries for the column-eluted PFCAs at pH 7 was primarily due to insufficiently sensitive analytical methods to measure the low concentrations eluting over time.

As evidenced in **Figure 6-7**, desorption of PFAAs from AFFF-impacted soil is also impacted by porewater pH. Though primarily conducted to serve as pH controls for the column leaching experiments when chemical oxidants were added to the AGW, when the AFFF-impacted soil was flushed with acidified (pH ~1.5) AGW, the desorption of PFAAs from the soil was slower (**Figure 6-7**) and generally less complete (**Table 6-8**). This was particularly evident for PFOS and PFHxS, where clear differences can be observed in the column effluent profiles (**Figure 6-7B**). For the PFCAs, the impact of pH was not as evident, though the neutral pH effluent was generally higher in concentration for PFOA (**Figure 6-7A**), at least for the first 10 mL. PFHxS behaved quite similarly, with the effluent profiles for the neutral and acidified AGW being nearly identical after the first 10 mL (**Figure 6-7B**). Cumulatively, this translated to slightly lower mass recoveries for these two PFAAs in the acidified columns as compared to the neutral pH columns (**Table 6-8**). The impact of pH was not surprising, as stronger sorption of both PFCAs and PFSAs at lower pH values has been observed previously (Higgins and Luthy, 2006).

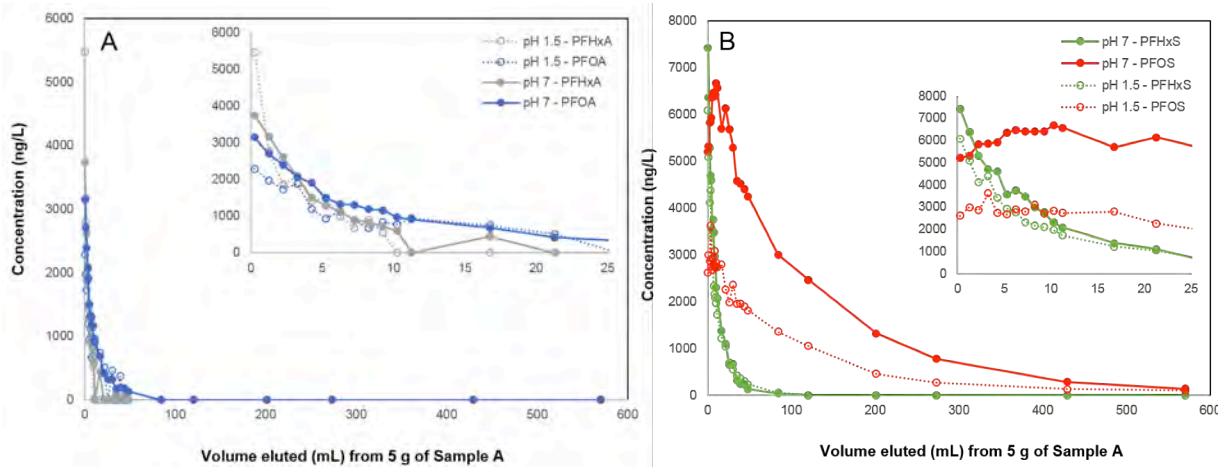

Figure 6-7. Comparison of desorption profiles of select perfluorocarboxylates (**A**) and perfluorosulfonates (**B**) from Sample A upon application of artificial groundwater at both pH 7 (solid symbols and lines) and pH 1.5 (open symbols, dashed lines). Insets provide the desorption profiles within the first 25 mL of applied AGW.

6.4.5.2 Columns Treated with Chemical Oxidants

When AFFF-impacted soil was flushed with AGW containing chemical oxidants (permanganate and persulfate), several types of interactions could impact the desorptive release of PFAAs. First, as the oxidants typically impact the aqueous chemistry (i.e., pH), the oxidants could affect the affinities of the PFAAs for the solid phases, thereby impacting their desorption. Second, if the oxidants are capable of transforming PFAA precursors to PFAAs, one might expect an increase in the PFAA release as a result of the application of a chemical oxidant. A close comparison of the effluent profiles for the columns receiving oxidants (when compared to the pH-matched controls) indicates that for PFHxS and PFOS, permanganate has a slight effect on their release from AFFF-impacted soil (as compared to the pH 7 control; **Figure 6-8, Table 6-8**). In the case of PFOS, the peak effluent concentrations are slightly shifted temporally (slightly later), and the total mass recovered was slightly higher (92% vs. 80%) than the pH-matched control though. The effect of permanganate on PFHxS release was similar, with slightly more mass recovered in the aqueous phase (108% vs. 77%) and a slightly higher concentration in the first 10 mL of column effluent. In the case of persulfate, however, persulfate generally decreased the concentration of PFHxS and PFOS in the column effluent (as compared to the pH 1.5 control), but did not have a particularly pronounced impact, as compared to the pH control, on the mass of PFHxS and PFOS recovered in the column effluent (**Table 6-8**). In short, these data suggest that while permanganate may facilitate the release of PFHxS and PFOS, persulfate appears to slow down the release of these chemicals from AFFF-impacts soil, primarily through a lowering of the porewater pH and the secondary impacts of this pH shift on the sorption of these compounds to the solid phases.

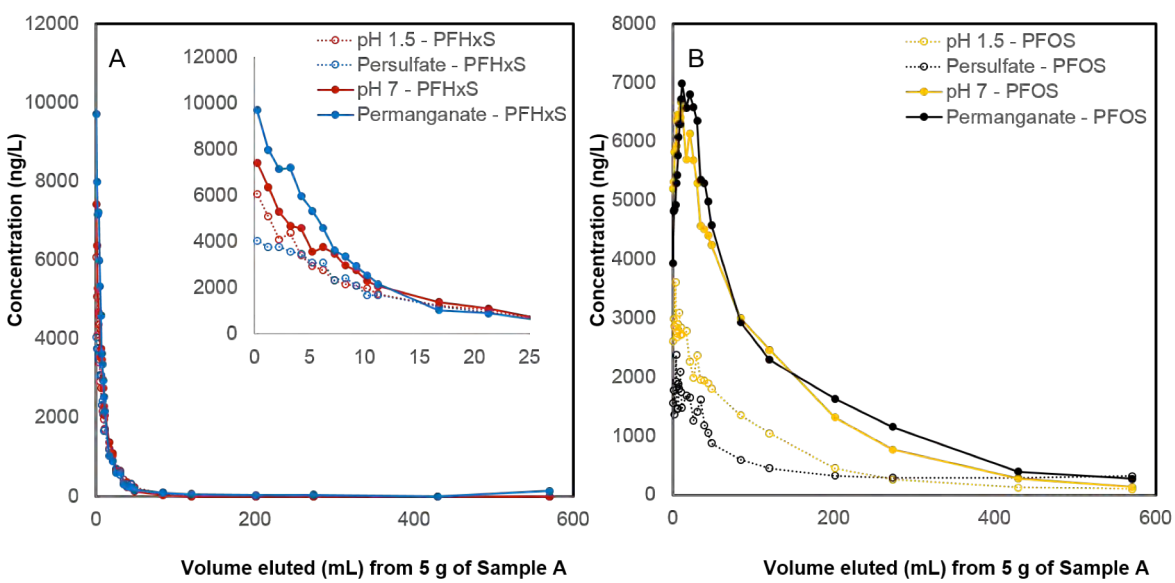

Figure 6-8. Comparison of desorption profiles of PFHxS (**A**) and PFOS (**B**) from Sample A upon application of artificial groundwater under both neutral and acidic conditions as well as when permanganate and persulfate are included in the AGW. Inset in **A** provides the desorption profile for PFHxS within the first 25 mL of applied AGW.

In the case of the PFCAs, desorption profiles for PFHxA and PFOA are provided in **Figure 6-9** with mass recovery calculation results provided in **Table 6-8**. With respect to PFOA, the impacts of persulfate and permanganate on PFOA desorption were similar to those observed for PFHxS: a slight decrease in the effluent concentration was observed for persulfate (as compared to the pH control), whereas a slight increase in PFOA was observed for permanganate application (**Figure 6-9B**). However, the effects of the chemical oxidants was quite different in terms of the mass recovered in the aqueous phase. For PFOA and persulfate, less mass was recovered in the aqueous phase as compared to the pH control, though it is difficult to ascertain as to whether this was due to partial destruction of PFOA. In light of the earlier results of McKenzie *et al.,* (2015, 2016), destruction of PFOA is unlikely. The effects of permanganate on PFAA release, however, were much more dramatic for PFOA than for PFHxS, as twice as much PFOA was released with the addition of permanganate as compared to the pH control (151% vs. 75%). Given the significant levels of PFOA precursors in this sample (**Figure 6-1**), production of PFOA from oxidation of PFOA precursors by permanganate is not particularly surprising.

In contrast, persulfate and permanganate both initially increased the concentrations of PFHxA in the column effluents (**Figure 6-9A**), suggesting that there are either a more diverse suite of PFHxA precursors and/or they are more easily converted to PFHxA upon the application of chemical oxidants. While the persulfate treatment eventually led to a PFHxA effluent profile and mass recovery (59% vs. 50%; **Table 6-8**) similar to the pH control, permanganate clearly had a more complicated and significant impact on PFHxA release. Importantly, recovery of PFHxA in the permanganate columns was ~800%, indicating a very large pool of PFHxA precursors were present that were amenable to permanganate oxidation. Further, the column effluent concentration of PFHxA remained consistently higher over the course of the experiment (as compared to the pH control), and even displayed a pronounced "bump" between 150 mL and 400 mL of released AGW. As this temporary increase in PFHxA was present in both replicate columns, it is likely real and is likely the result of slow desorption and transformation kinetics of a particular PFHxA precursor or group of precursors. Clearly, this high degree of conversion to PFHxA and slow release warrant further investigation a complete understanding of PFHxA release from source zones treated with permanganate is desired.

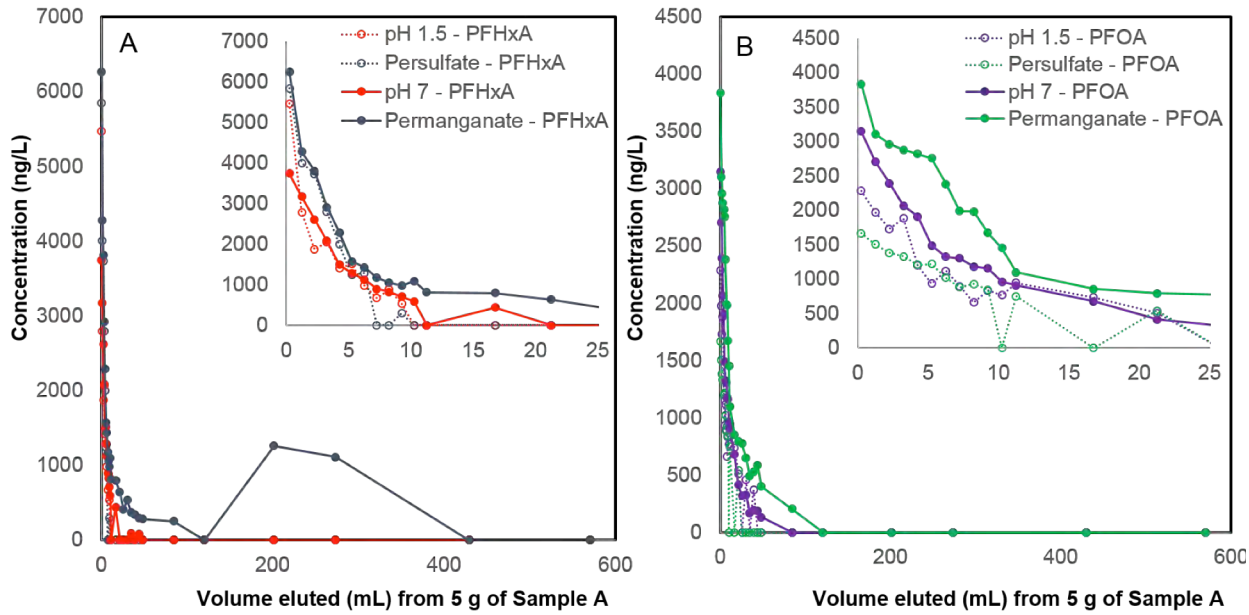

Figure 6-9. Comparison of desorption profiles of PFHxA (**A**) and PFOA (**B**) from Sample A upon application of artificial groundwater under both neutral and acidic conditions as well as when permanganate and persulfate are included in the AGW. Insets provide the desorption profiles within the first 25 mL of applied AGW.

6.4.5.3 Column Desorption Conclusions

The results of the column desorption experiments indicate that while some PFAAs are rapidly released from AFFF-impacted soils, others (particularly PFOS and PFHxS) may be released much more slowly. The effect of pH on PFAA release is quite clear, with lower pH conditions resulting in slower and less complete release. With respect to chemical oxidants, persulfate appears to impact the release of PFAAs from AFFF-impacted soils primarily through pH effects, whereas permanganate appears to enhance both the release of PFAAs as well as the conversion of some PFAA precursors to PFAAs. These results suggest that ongoing release of PFAAs from source zones may be a particularly important component to consider in an assessment of an AFFF-impacted site. Further, these data suggest that permanganate may be an effective agent for converting and releasing PFAAs and PFAA precursors present in AFFF-impacted soils.

6.4.6 Overall Conclusions and Implications

6.4.6.1 Desorption

Because of the uncertainty about the exact chemical structures of the compounds contributing to the apparent PFAA precursor desorption kinetics, any explanation of their slower desorption rates is somewhat speculative. However, one possible explanation is that PFAA precursors are typically larger than the PFCAs they generate upon oxidation (Place and Field, 2012; Houtz and Sedlak, 2012); PFCAs and PFSAs, which have only a carboxylate or sulfonate group, respectively, at the end of the perfluorinated carbon chain, are small relative to many other AFFF components. Potential precursor compounds measured in AFFF can have considerably larger structures attached to the perfluorinated carbon chain such as nonfluorinated alkanes, alcohols, ketones, sulfones, phosphates, amines, and others (Backe *et al.,* 2013; Place and Field, 2012;

Houtz and Sedlak, 2012). Increasing the size of a molecule will generally render it more hydrophobic and thus more likely to have a higher affinity for the solid phase (Schwarzenbach *et al.,* 2003). Negative correlations between molecular volume and k_s, and positive correlations between molecular volume and the size of the slow fraction have been observed in studies with neutral compounds including chlorinated benzenes, PAHs, and PCBs (Cornelissen *et al.,* 1997; Cornelissen *et al.,* 1998). These studies imply that the increased size of PFAA precursors as compared to PFAAs will slow desorption, but the effect of charged functional groups is an added complication. As discussed above, both PFCAs and PFSAs show negative correlations between the lengths of the perfluorinated carbon chains and desorption rate constants, indicating that the size of these compounds is a factor is determining their desorption rates. This suggests that the slower desorption observed in PFAA precursors as compared to PFCAs may be due to their larger size, but the destruction of size information inherent in the TOP assay means that this experiment cannot confirm this.

The charged functional groups on precursor compounds may also play a role in controlling the sorption of PFAA precursors, particularly in regards to sorption on NOM and clay minerals. NOM and clay minerals are both sources of negatively charges surfaces at environmental pH and this can have a strong effect on sorption of charged contaminants (Barnier *et al.,* 2014; Tülp *et al.,* 2009; Nielsen *et al.,* 1997). PFCAs and PFSAs are all negatively charged in the environment, but some precursor compounds contain amine groups which are likely cations at environmental pH (Backe *et al.,* 2013; Place and Field, 2012). Electrostatic attraction between organic matter or mineral surfaces and cationic functional groups on precursor compounds could significantly increase the affinity of these compounds to sorb to sediments (Nielsen *et al.,* 1997; Lee *et al.,* 1997; Zachara *et al.,* 1986). Unfortunately, this explanation has a number of possible complications: not all precursors found in AFFF formulations have cationic functional groups (Place and Field, 2012); the electrostatic attraction will be highly dependent on pH (Nielsen *et al.,* 1997; Lee *et al.,* 1997); and inorganic cations in the aqueous phase might compete with PFAA precursors for limited sorption sites (Schwarzenbach *et al.,* 2003).

6.4.6.2 Implications for Source Zones

A recent site characterization of the Ellsworth AFB site mapped widespread surface soil and aquifer solid contamination as well as a large groundwater plume (McGuire *et al.,* 2014) To help place the results of the present study in context, it is illustrative to examine the relative mass distribution (i.e. sorbed vs aqueous phase) of PFAAs at this site. Integrating maps of contaminant concentrations using Surfer 11 (GoldenSoftware) allows for rough calculations of contaminant mass in the sediment and groundwater plumes. To approximate the PFAA mass associated with solid and groundwater phases at Ellsworth AFB, a number of assumptions were made about site characteristics based on sampling at the site (McGuire *et al.,* 2014). Soil/sediment was split into three layers, surface soil (0.6 m thick), subsurface soil (5.0 m thick), and aquifer solids (3.0 m thick). Aquifer solids were assumed to be saturated and the water table was set at the aquifer solids/subsurface soil boundary. Soil class at the site was clay/clay loam so sediment and soil was assumed to have a dry bulk density of 1500 kg/m^3, aquifer solids were assumed to have a porosity of 0.4. PFAA contamination has been measured in surface soil, aquifer solids, and groundwater[1] and concentrations in the subsurface soil were calculated as the mean of the surface soil and aquifer solids concentrations. Maps of PFAA concentrations were converted to

3D wireframe plots and integrated using Surfer 11 (GoldenSoftware). From these integration results and the assumed site properties listed above the total mass of PFAAs in each compartment could be calculated. The results of these calculations are given in **Table 6-9.**

These calculations indicate that large proportions of total PFAA mass are associated with the surface soil and subsurface sediment. For example, approximately 93% of PFOA and >99% of PFOS are associated with the solid phases rather than in the groundwater. The rate at which these compounds are mobilized from the solid phase will dictate whether surface soils will serve as short or long term sources of groundwater contamination. While insufficient data are available to perform similar calculations of PFAA precursor masses, all the samples studied had notable concentrations of precursors, indicating that any measurements focusing only on PFCAs and PFSAs will miss a significant proportion of the total fluorochemical load at AFFF impacted sites.

Table 6-9. Distribution of Contaminant Mass at Ellsworth AFB by Compartment

Contaminant	Surface Soil	Subsurface Soil	Aquifer Solids	Groundwater
PFBA	8%	61%	20%	10%
PFPeA	10%	60%	21%	10%
PFHxA	6%	53%	33%	8%
PFHpA	6%	52%	34%	9%
PFOA	9%	60%	24%	7%
PFBS	9%	59%	22%	10%
PFHxS	9%	60%	27%	5%
PFOS	14%	73%	13%	0%

7. REPORTING, DISSEMINATION, AND CONCLUSIONS

7.1 Reporting and Dissemination

7.1.1 Reporting

This project also included two non-experimental tasks: *Task 5: Data Analysis*; and *Task 6: Reporting and Dissemination*. The data analysis conducted as part of this project has been reported in the previous chapters of this report.

With respect to reporting and dissemination, this task included the monthly financial reporting and quarterly progress reports required by SERDP, an interim version of this report, and annual in-progress review (IPR) meetings. IPR presentations for this project occurred on 2/16/2012, 5/7/2013, 5/5/2014, and 5/4/2015. In addition, the findings of the research are being disseminated through preparation of journal manuscripts and via presentations at professional conferences.

7.1.2 Dissemination

The results of this project are directly contributing to two new and/or imminent ESTCP projects, ER-201574-T2 and ER-201633. In addition, it is anticipated that these results will contribute to a number of ongoing and/or future SERDP projects (i.e., SERDP ER-2128, SERDP ER-2424, etc.).

A listing of the more than 30 public presentations made as part of this project is provided below.

1. Higgins, C.P. "Understanding the Transport of Perfluorochemicals in Groundwater at AFFF-Impacted Sites" SERDP and ESTCP Webinar Series. 28 January, 2016 (Presentation).
2. Higgins, C.P. "Poly- and Perfluoroalkyl Substances (PFASs) at Aqueous Film-Forming Foam Impacted Sites" Department of Toxicology and Pharmacology, East Carolina University, Greenville, North Carolina. 27 January, 2016 (Presentation).
3. Higgins, C.P. "Fate and Transport of Poly- and Perfluoroalkyl Substances (PFASs) under Conditions Relevant to Aqueous Film-Forming Foam Impacted Sites" Department of Civil and Environmental Engineering, University of Rhode Island. 30 September, 2015. (Presentation).
4. Higgins, C.P. "The Role of Polyfluoroalkyl Substances in Understanding Perfluoroalkyl Acid Contamination at Aqueous Film Forming Foam Sites" 2015 SciX. Providence, Rhode Island. 29 September, 2015 (Presentation)
5. Higgins, C.P. "Environmental Fate and Transport of Poly-and Perfluoroalkyl Substances at Aqueous Film-Forming Foam Impacted Sites" 2015 Tersus Enviromental Remediation Seminar Series. Lakewood, Colorado. 23 September, 2015 (Presentation)
6. Higgins, C.P. Fate and Transport of Perfluorochemicals under Conditions Relevant to Aqueous Film-Forming Foam Impacted Sites. 2015 RemTEC Summit. Westminster, Colorado. 3 March, 2015. (Presentation).

7. Higgins, C.P. "Environmental Fate and Transport of Perfluorochemicals under Conditions Relevant to Aqueous Film-Forming Foam Impacted Sites" Department of Chemistry, University of Toronto, Toronto, Ontario. 5 February, 2015. (Presentation).
8. McKenzie, E.R., Siegrist, R.L., McCray, J.E. and C.P. Higgins. "In situ chemical oxidation effects on the fate and transport of PFAAs in 1-D porous media column studies." 35th SETAC North America Annual Meeting. Vancouver, Canada. 9-13 November, 2014. (Presentation).
9. Higgins, C.P. "Environmental Fate and Transport of Perfluorochemicals under Conditions Relevant to Aqueous Film-Forming Foam Impacted Sites" Department of Civil, Environmental, and Geo-Engineering Warren Lecture Series, University of Minnesota. Minneapolis, Minnesota. 26 September, 2014. (Presentation).
10. McKenzie, E.R., Siegrist, R.L., McCray, J.E. and C.P. Higgins. "Chemical oxidant and NAPL co-contaminant effects on perfluoroalkyl acid transport." Gordon Research Conference on Environmental Sciences: Water. 22-27 June, 2014. Plymouth, New Hampshire. (Poster).
11. Guelfo, J.L., McKenzie, E.R., and C.P. Higgins. "Factors Impacting Groundwater Fate and Transport of Perfluoroalkyl Acids at AFFF-impacted Sites." 24th SETAC Europe Annual Meeting. Basel, Switzerland. 11-15 May, 2014. (Presentation).
12. Higgins. C.P. Field Sampling Methods for Site Characterization. Federal Contaminated Sites Action Plan (FCSAP) Workshop on Management of Perfluoroalkylated Compounds at Federal Contaminated Sites. 19-20 February, 2014. Ottawa, Ontario, Canada (Presentation).
13. Higgins, C.P. McGuire. M.E., Schaefer, C., Richards, T., Backe, W., Field, J.A., Houtz, E., Sedlak, D., Guelfo, J.L, Wunsch, A. Evidence of Remediation-Induced Alteration of Subsurface Poly- and Perfluoroalkyl Substance (PFAS) Distribution at a Former Firefighter Training Area. Groundwater Resources Association of California Symposium on Emerging Contaminants. 4-5 February, 2014. Concord, California (Presentation).
14. Guelfo, J.L., Wunsch, A., McCray, J.E. and C.P. Higgins. "Transport Potential of Perfluoroalkyl Substances (PFASs) at AFFF-impacted Sites: 1-Dimensional Column Studies." 34th SETAC North America Annual Meeting. Nashville, Tennessee. 17-21 November, 2013. (Presentation).
15. McKenzie, E.R., Kudryk, l., Guelfo, J.L., Siegrist, R.L. and C.P. Higgins "Implications of In Situ Chemical Oxidation on PFAAs Fate and Transport in Porous Media." 34th SETAC North America Annual Meeting. Nashville, Tennessee. 17-21 November, 2013. (Presentation).
16. Sepulvado, J.G., and C.P. Higgins. "Transport Potential of Perfluoroalkyl Substances (PFASs) at Aqueous Film-Forming Foam (AFFF)-Impacted Sites: 1- Dimensional Column Studies." Association of Environmental Engineering and Science Professors National Meeting. 14-16 July, 2013. Golden, Colorado. (Presentation)
17. McKenzie, E.R., Kudryk, L., Sepulvado, J.G., Siegrist, R.L., and C.P. Higgins. "In situ chemical oxidation effects on poly- and perfluoroalkyl substance fate and transport." Association of Environmental Engineering and Science Professors National Meeting. 14-16 July, 2013. Golden, Colorado. (Poster)
18. Weathers, T.S., C.P. Higgins, and J.O. Sharp. "Emerging Contamanants from the Microscopic Perspective: The Effects of Perfluoroalkyl Substances on the Common Soil

Microbe." American Society for Microbiology Meeting, 18-21 May, 2013. Denver, CO. (Poster).

19. Sepulvado, J.G., McGuire, M. and C.P. Higgins. "Fate and Transport of Short-Chain PFASs: Batch, Column, and Field Perspectives from AFFF-impacted Sites." 23rd SETAC Europe Annual Meeting. 12-16 May, 2013. Glasgow, Scotland. (Poster).
20. Sepulvado, J.G. and C.P. Higgins. "Transport Potential of Perfluoroalkyl Acids (PFAAs) at AFFF-impacted Sites: 1-Dimensional Column Studies." 26th Rocky Mountain SETAC Annual Meeting. 18-19 April, 2013. Denver, Colorado. (Presentation).
21. Weathers, T.S., C.P. Higgins, and J.O. Sharp. "Implications for subsurface transport during co-contaminant bioremediation in the presence of perfluoroalkyl substances." Remediation Technology Summit, 4-6 March, 2013. Westminster, CO. (Poster).
22. Sepulvado, J.G., McGuire, M. and C.P. Higgins. "Fate and Transport of Short-Chain PFASs: Batch, Column, and Field Perspectives from AFFF-impacted Sites" Colorado School of Mines Graduate Student Association Conference on Earth & Energy Research. 21-22 February, 2013. Golden, Colorado. (Presentation).
23. Weathers, T.S., C.P. Higgins, and J.O. Sharp. "Exploring the relationships between the common soil microbe and perfluoroalkyl substances in batch systems: Implications for bioremediation and contaminant transport" Conference on Earth and Energy Research, 21-22 February, 2013. Golden, CO. (Presentation).
24. Sepulvado, J.G. and C.P. Higgins. "Transport Potential of Perfluoroalkyl Substances (PFASs) at AFFF-impacted Sites: Batch Sorption and Initial 1-D Column Experiments" 33rd SETAC North America Annual Meeting, 11-15 November, 2012. Long Beach, California. (Poster).
25. Sepulvado, J.G., McGuire, M. and C.P. Higgins. "Groundwater Transport Potential of Perfluorinated Compounds at Aqueous Film-forming Foam (AFFF)- Impacted Sites" Gordon Research Conference on Environmental Sciences: Water. 24-29 June, 2012. Plymouth, New Hampshire. (Poster)
26. McGuire, M., Sepulvado, J.G., Christensen, K., Schaefer, C., and C.P. Higgins. "Site Characterization of Aqueous Film-Forming Foam Impacted Groundwater at a Fire Training Facility." Conference on Earth and Energy Research, 29 March, 2012. Golden, Colorado (Poster)
27. Higgins, C.P. "Sorptive Behavior of Perfluorochemicals in Matrices Relevant to Aqueous Film-Forming Foam Impacted Sites" Department of Civil, Environmental, and Architectural Engineering, University of Colorado- Boulder. 20 February, 2012. Boulder, Colorado. (Presentation).
28. Sepulvado, J. and C.P. Higgins. "Sorption of Perfluorochemicals to Matrices Relevant to Sites Impacted by Aqueous Film-Forming Foam" Groundwater Resources Association of California Conference on Emerging Contaminants. 7-8 February, 2012. Concord, California (Presentation).
29. Higgins, C.P., and J.A. Field. "Impacts of Subsurface Biogeochemistry on Perfluoroalkyl Chemical Transport Potential." Strategic Environmental Research and Development Program Annual Symposium, 30 November – 2 December, 2011. Washington, District of Columbia. (Poster).
30. Higgins, C.P., Sepulvado, J.G., Christensen, K., Weathers, T., Sharp, J.O., McCray, J.E., and R.L. Siegrist "Perfluoroalkyl Chemicals in Groundwater at Aqueous Film Forming

Foam (AFFF)-impacted Sites: A State of Knowledge Assessment." Strategic Environmental Research and Development Program Annual Symposium, 30 November – 2 December, 2011. Washington, District of Columbia. (Poster).

31. Sepulvado, J.G. and C.P. Higgins. "Subsurface Transport of Perfluorochemicals at Sites Impacted by Aqueous Film-Forming Foam." 32nd SETAC North America Annual Meeting, 13-17 November, 2011. Boston, Massachusetts. (Poster)

The findings of this project have also been published in five peer-reviewed journals (to date):

1. McKenzie, E.R., Siegrist, R.L., McCray, J.E. and C.P. Higgins. 2016. The influence of a non-aqueous phase liquid (NAPL) and chemical oxidant application on perfluoroalkyl acid (PFAA) fate and transport. *Water Research.* 92: 199-207. DOI:10.1016/j.watres.2016.01.025
2. Weathers, T.S., Harding-Marjanovic, K., Higgins, C.P., Alvarez-Cohen, L., and J.O. Sharp. 2016. Perfluoroalkyl acids inhibit reductive dechlorination of TCE by repressing Dehalococcoides. *Environmental Science & Technology.* 50 (1): 240-248. DOI:10.1021/acs.est.5b04854
3. Weathers, T.S., Higgins, C.P., and J.O. Sharp. 2015. Enhanced biofilm production by a toluene degrading Rhodococcus observed after exposure to perfluoroalkyl acids. *Environmental Science & Technology,* 49 (9): 5458–5466 DOI:10.1021/es5060034
4. McKenzie, E.R., Siegrist, R.L., McCray, J.E. and C.P. Higgins. 2015. Effects of Chemical Oxidants on Perfluoroalkyl Acid (PFAA) Transport in 1-D Porous Media Columns. *Environmental Science & Technology.* 49 (3): 1681–1689 DOI:10.1021/es503676p
5. Guelfo, J.L. and C.P. Higgins. 2013. Subsurface transport potential of perfluoroalkyl acids at aqueous film-forming foam (AFFF)-impacted sites. *Environmental Science & Technology,* 47 (9):4164–4171. DOI:10.1021/es3048043

Though not directly within the scope of this project, SERDP support for this project enabled members of the project team to contribute to a number of additional publications:

1. Rich, C.D., Blaine, A.C., Hundal, L.S., and C.P. Higgins. 2015. Bioaccumulation of perfluoroalkyl acids by earthworms (*Eisenia feotida*) from contaminated soils. *Environmental Science & Technology.* 49 (2): 881–888. DOI:10.1021/es504152d
2. McGuire. M.E., Schaefer, C., Richards, T., Backe, W., Field, J.A., Houtz, E., Sedlak, D., Guelfo, J.L, Wunsch, A. and C.P. Higgins. 2014. Evidence of Remediation-Induced Alteration of Subsurface Poly- and Perfluoroalkyl Substance (PFAS) Distribution at a Former Firefighter Training Area. *Environmental Science & Technology,* 48 (12): 6644-6652. DOI:10.1021/es5006187
3. Houtz, E.F., Higgins, C.P., Field, J.A., and D.L. Sedlak. 2013. Persistence of Perfluoroalkyl Acid Precursors in AFFF-Impacted Groundwater and Soil. *Environmental Science & Technology,* 47 (15), 8187−8195. DOI:10.1021/es4018877

4. Harding-Marjanovic, K. C., Yi, S., Weathers, T. S., Sharp, J. O., Sedlak, D. L., and L. Alvarez-Cohen. Effects of aqueous film-forming foam (AFFF) on trichloroethene (TCE) degradation by a *Dehalococcoides* enrichment culture. 2015, Submitted.

Finally, a number of manuscripts are still being refined, and will be submitted for publication in the near future:

1. Guelfo, J.L., Wunsch, A., McCray, J.E. and C.P. Higgins. Transport Potential of Perfluoroalkyl Acids (PFAAs) at AFFF-impacted Sites: Column Experiments and Modeling. *Manuscript in Preparation.*
2. Azzolini, D.C., Roberts, S.R. and C.P. Higgins. Desorptive behavior of perfluoroalkyl acids and perfluoroalkyl acid precursors from aqueous film-forming foam impacted soils. *Manuscript in Preparation.*
3. Weather, T.S.., Higgins, C.P., and J.O. Sharp. Interactions between a common soil microbe and perfluoroalkyl substances in batch systems. *Manuscript in Preparation.*

7.2 Summary and Conclusions

The overall goal of this research was to evaluate the relative importance of key physicochemical and biological parameters in determining the fate and transport of PFAAs in groundwater in the presence of co-contaminants and during remediation of co-contaminants. The presence of specific PFAAs and their polyfluorinated precursors in groundwater, notably the PFAAs at AFFF-impacted fire training areas has raised concerns about the risk these PFAAs may pose to human health. Unfortunately, there are serious data gaps with respect to our understanding of the behavior of PFAAs in groundwater systems, particularly in the presence of co-contaminants present at AFFF-impacted sites. The research conducted as part of this project has served to close some of these gaps. In particular, sorption and transport of PFAAs will be impacted by the presence of co-contaminants, particularly non-aqueous phase liquids (NAPLs; Guelfo and Higgins, 2013; McKenzie *et al.,* 2016). These interactions are complex, but the overall data suggest that NAPL presence at a site may further retard PFAA transport, assuming limited mobility of the NAPL. What is not clear, however, is the extent to which polyfluorinated precursors also interact with NAPLs

Moreover, prior to the start of this project, little was known about how PFAA fate and transport would be affected when AFFF-impacted sites are subject to *in situ* remediation aimed at attenuating co-contaminants. When microbial co-contaminant remediation technologies are employed, the interactions between PFAAs and the microbial populations are complex. For hydrocarbon-degrading populations, PFAAs do not appear to significantly affect hydrocarbon degradation (Weathers *et al.,* 2015), though the PFAAs do appear to induce biofilm formation (Weathers *et al.,* 2015) which may subsequently impact PFAA transport (*Section 5*). Conversely, high levels of PFAAs does appear to interfere with microbial dehalogenation reactions (Weathers *et al.,* 2016). The extent to which these types of interactions are also relevant for polyfluorinated PFAA precursors remains unknown, though impacts are suspected (Harding-Marjanovic *et al.,*

submitted) Further research, using actual AFFF-impacted soils, groundwater, and/or aquifer materials, may help evaluate the extent to which the microbially mediated remediation technologies impact PFAA fate and transport.

With respect to ISCO remediation technologies for co-contaminants, the results of this study suggest ISCO, particularly the application of persulfate and permanganate, will significantly impact PFAA fate and transport. Notably, in the case of persulfate, the effects appear to be primarily driven by the low pH that results from persulfate application (McKenzie *et al.,* 2015; McKenzie *et al.,* 2016; *Section 6*). Catalyzed hydrogen peroxide and permanganate, however, appear to either not impact of speed up the transport of PFAAs (McKenzie *et al.,* 2015; 2016). Of particular note is the apparent capacity of permanganate to not only mobilize PFAAs from AFFF-impacted soil, but also to facilitate significant conversion of some polyfluorinated precursors to PFAAs (*Section 5*). Coupled with the apparent slower desorption kinetics of polyfluorinated precursors, these data collectively suggest that additional studies related to PFAA release from source zones is warranted.

Overall, the results of this project should significantly aid the environmental restoration community's effort to develop conceptual site models of PFAAs at AFFF-impacted sites as well as move closer to modeling PFAA plumes at these sites. PFAA fate and transport under conditions relevant to AFFF-impacted sites is a complex topic, and though fundamental questions have been addressed through this project, many more questions remain. With further study, the results of this project should meaningfully contribute to modeling and site assessment guidelines that can be used by engineers and contaminant hydrologists for practical implementation.

8. REFERENCES

3M. 1999. Fluorochemical use, distribution and release overview.

3M. 2005. 3M material safety data sheet FC-203CF Light Water (TM) AFFF 3%. St. Paul, MN.

Aguilera, A., V. Souza-Egipsy, P. San Martín-Úriz, and R. Amils. 2008. Extraction of extracellular polymeric substances from extreme acidic microbial biofilms. *Applied Microbiology and Biotechnology*. 78(6): 1079–1088.

Ahrens, L., 2011. Polyfluoroalkyl compounds in the aquatic environment: a review of their occurrence and fate. *Journal of Environmental Monitoring*. 13(1): 20-31.

Alvarez, P. and W. Illman. 2006. Bioremediation and Natural Attenuation: Process Fundamentals and Mathematical Models. Honoken, NJ, Wiley Interscience.

An, Y. J. and S. W. Jeong 2001. Interactions of perfluorinated surfactant with polycyclic aromatic hydrocarbons: Critical micelle concentration and solubility enhancement measurements. *Journal of Colloid and Interface Science*. 242(2): 419-424.

An, Y. J., E. R. Carraway, et al., 2002. Solubilization of polycyclic aromatic hydrocarbons by perfluorinated surfactant micelles. *Water Research*. 36(1): 300-308.

ANSI. 1995. American National Standard, ANSI/ASQC E4-1994. Milwaukee, WI., American Society for Quality Control.

APHA-AWWA-WPCF. 1998. Standard Methods for the Examination of Water and Wastewater, 20th ed. Washington, DC, APHA-AWWA-WPCF.

Arp, H., C. Niederer, and K. Goss. 2006. Predicting the partitioning behavior of various highly fluorinated compounds. *Environmental Science and Technology.* 40: 7298-7304.

ASTM. 1991a. Annual Book of ASTM Standards Volume 04.08: Soil and Rock, Dimension Stone, Geosynthetics. Philadelphia, PA, ASTM.

ASTM. 1991b. Standard Practice for Sampling Waste and Soils for Volatile Organics. Annual Book of ASTM Standards, Vol. 11.04: 108-111.

Aulenta, F., Canosa, A., Majone, M., Panero, S., Reale, P., Rossetti, S. 2008. Trichloroethene Dechlorination and H 2 Evolution Are Alternative Biological Pathways of Electric Charge Utilization by a Dechlorinating Culture in a Bioelectrochemical System. *Environmental Science and Technology.* 42 (16): 6185–6190.

Backe, W.J., Day, T.C., Field, J.A. 2013. Zwitterionic, cationic, and anionic fluorinated chemicals in aqueous film forming foam formulations and groundwater from US military

bases by nonaqueous large-volume injection HPLC-MS/MS. *Environmental Science and Technology.* 47(10): 5226-5234.

Ballapragada, B., H. Stensel, et al., 1997. Effect of hydrogen on reductive dechlorination of chlorinated ethenes. *Environmental Science and Technology.* 31(6): 1728-1734.

Banks, R., B. Smart, and J. Tatlow. 1994. Organofluorine Chemistry Principles and Applications. New York: Plenum Press.

Barnier, C., Ouvrard, S., Robin, C., Morel, J. L. 2014. Desorption kinetics of PAHs from aged industrial soils for availability assessment. *Science of the Total Environment*. 470-471, 639-645.

Bergey, D. H., Holt, J. G. 1994. Bergey's manual of determinative bacteriology; Williams & Wilkins: Baltimore, 1994.

Biddle, A., Stewart, L., Blanchard, J., Leschine, S. 2013. Untangling the Genetic Basis of Fibrolytic Specialization by Lachnospiraceae and Ruminococcaceae in Diverse Gut Communities. *Diversity*. 5 (3): 627–640.

Blaine, A. C., Rich, C. D., Sedlacko, E. M., Hundal, L. S., Kumar, K., Lau, C., Mills, M. A., Harris, K. M., Higgins, C. P. 2014. Perfluoroalkyl acid distribution in various plant compartments of edible crops grown in biosolids-amended soils. *Environmental Science and Technology.* 48 (14): 7858–7865.

Brusseau, M. L. 1992a. Nonequilibrium transport of organic chemicals: The impact of pore-water velocity. *Journal of Contaminant Hydrology*. 9(4): 353–368

Brusseau, M. L. 1992b. Transport of rate-limited sorbing solutes in heterogeneous porous-media - application of a one-dimensional multifactor nonideality model to field data. *Water Resources Research.* 28(9): 2485–2497.

Brusseau, M. L. 1994. Transport of reactive contaminants in heterogeneous porous-media, *Reviews in Geophysics*. 32(3): 285–313.

Brusseau, M. L., P. S. C. Rao, R. E. Jessup, and J. M. Davidson. 1989. Flow interruption: A method for investigating sorption nonequilibrium. *Journal of Contaminant Hydrology*. 4(3): 223–240.

Brusseau, M. L., R. E. Jessup, and P. S. C. Rao. 1991a. Nonequilibrium sorption of organic chemicals: elucidation of rate-limiting processes. *Environmental Science and Technology.* 25(1): 134–142.

Brusseau, M. L., T. Larsen, and T. H. Christensen. 1991b. Rate-limited sorption and nonequilibrium transport of organic chemicals in low organic carbon aquifer materials. *Water Resources Research.* 27(6): 1137–1145.

Buck, R. C., Franklin, J., Berger, U., Conder, J. M., Cousins, I. T., de Voogt, P., Jensen, A. A., Kannan, K., Mabury, S. A., van Leeuwen, S. P. 2011. Perfluoroalkyl and polyfluoroalkyl substances in the environment: Terminology, classification, and origins. *Integrated Environmental Assessment and Management.* 7 (4): 513–541.

Bugna, G., J. Chanton, T. Stauffer, W. MacIntyre, and E. Libelo. 2005. Partitioning microbial respiration between jet fuel and native organic matter in an organic-rich long time-contaminated aquifer. *Chemosphere.* 60 (2): 177–187.

Burns, D., D. Ellis, H. Li, C. McMurdo, and E. Webster. 2008. Experimental pK(a) determination for perfluorooctanoic acid (PFOA) and the potential impact of pK(a) concentration dependence on laboratory-measured partitioning phenomena and environmental modeling. *Environmental Science and Technology.* 42: 9283–9288.

Bustin, S. A. 2001. Quantification of mRNA using real-time reverse transcription PCR (RT-PCR): Trends and problems. *Journal of Molecular Endocrinology*. 29 (1): 23–39.

Bustin, S. A., Benes, V., Garson, J. A., Hellemans, J., Huggett, J., Kubista, M., Mueller, R., Nolan, T., Pfaffl, M. W., Shipley, G. L., et al. 2009. The MIQE guidelines: Minimum information for publication of quantitative real-time PCR experiments. *Clinical Chemistry*. 55 (4): 611–622.

Cain, R., G. Johnson, et al., 2000. Partitioning tracer tests for evaluating remediation performance. *Ground Water*. 38(5): 752-761.

Cameron, D. and A. Klute. 1997. Convective-dispersive solute transport with a combined equilibrium and kinetic adsorption model. *Water Resources Research*. 13: 183–188.

Cao, B., Ahmed, B., Kennedy, D. W., Wang, Z., Shi, L., Marshall, M. J., Fredrickson, J. K., Isern, N. G., Majors, P. D., Beyenal, H. 2011. Contribution of extracellular polymeric substances from Shewanella sp. HRCR-1 biofilms to U(VI) immobilization. *Environmental Science and Technology.* 45 (13): 5483–5490.

Caporaso, J. G., Bittinger, K., Bushman, F. D., DeSantis, T. Z., Andersen, G. L., Knight, R. 2010. PyNAST: a flexible tool for aligning sequences to a template alignment. *Bioinformatics*. 26 (2): 266–267.

Caporaso, J. G., Kuczynski, J., Stombaugh, J., Bittinger, K., Bushman, F. D., Costello, E. K., Fierer, N., Peña, A. G., Goodrich, J. K., Gordon, J. I., et al., 2010. QIIME allows analysis of high-throughput community sequencing data. *Nature Methods*. 7 (5): 335–336.

Carter, M. 1993. Soil Sampling and Methods of Analysis. Ann Arbor, MI, Lewis Publishers.

Chai, Y., Kochetkov, A., Reible, D. D. 2006. Desorption resistance of polycyclic aromatic hydrocarbons and duration of exposure. *Environmental Toxicology and Chemistry*. 25, (11): 2827–2833.

Chen, H., S. Chen, X. Quan, Y. Zhao, and H. Zhao. 2009. Sorption of perfluorooctane sulfonate (PFOS) on oil and oil-derived black Ccarbon: Influence of solution pH and [Ca2+]. *Chemosphere.* 77(10): 1406–1411.

Christ, J., C. Ramsburg, et al., 2005. Coupling aggressive mass removal with microbial reductive dechlorination for remediation of DNAPL source zones: A review and assessment. *Environmental Health Perspectives*. 113(4): 465-477.

Christensen, K., J. King, et al., (in review). NAPL dissolution in an experimental fractured sandstone network.

Conder, J.M., Hoke, R.A., De Wolf, W., Russell, M.H., Buck, R.C., 2008. Are PFCAs bioaccumulative? A critical review and comparison with regulatory lipophilic compounds. *Environmental Science and Technology.* 42(4): 995-1003.

Cornelissen, G., Rigterink, H., ten Hulscher, D. E. M., Vrind, B. A., van Noort, P. C. M. 2001. A simple Tenax extraction method to determine the availability of sediment-sorbed organic compounds. *Environmental Toxicology and Chemistry*. 20 (4): 706-711.

Cornelissen, G., van Noort, P. C. M., Govers, H. A. J. 1998. Mechanism of Slow Desorption of Organic Compounds from Sediments: A Study Using Model Sorbents. *Environmental Science and Technology.* 32: 3124-3131.

Cornelissen, G., van Noort, P. C. M., Govers, H. A. J., 1997. Desorption Kinetics of Chlorobenzenes, Polycyclic Aromatic Hydrocarbons, and Polychlorinated Biphenyls: Sediment Extraction with Tenax and Effects of Contact Time and Solute Hydrophobicity. *Environmental Toxicology and Chemistry*. 16 (7): 1351–1357.

Cozzarelli, I. M., B. A. Bekins, et al., 2001. Progression of natural attenuation processes at a crude-oil spill site: 1. Geochemical evolution of the plume. *Journal of Contaminant Hydrology*. 53(3-4): 369-385.

Crimi, M. and R. Siegrist. 2005. Factors affecting effectiveness and efficiency of DNAPL destruction using potassium permanganate and catalyzed hydrogen peroxide. *Journal of Environmental Engineering-ASCE*. 131(12): 1724-1732.

Cupples, A. M., Spormann, A. M., McCarty, P. L. 2003. Growth of a Dehalococcoides-Like Microorganism on Vinyl Chloride and cis-Dichloroethene as Electron Acceptors as Determined by Competitive PCR. *Applied and Environmental Microbiology*. 69(2): 953–959.

Cusack, F., Lappin-Scott, H., Singh, S., De Rocco, M., Costerton, J. W. 1990. Advances in microbiology to enhance oil recovery. *Applied Biochemistry and Biotechnology*. 24-25(1): 885–898.

D'Agostino, L. A., Mabury, S. A. 2014. Identification of Novel Fluorinated Surfactants in Aqueous Film Forming Foams and Commercial Surfactant Concentrates. *Environmental Science and Technology.* 48 (1): 121-129.

De Philippis, R., Vincenzini, M. 1998. Exocellular polysaccharides from cyanobacteria and their possible applications. *FEMS Microbioly Reviews.* 22 (3): 151–175.

Deeb, R. A., Hu, H.-Y., Hanson, J. R., Scow, K. M., Alvarez-Cohen, L. 2001. Substrate interactions in BTEX and MTBE mixtures by an MTBE-degrading isolate. *Environmental Science and Technology.* 35 (2): 312–317.

Deeb, R. A., Sharp, J. O., Stocking, A., McDonald, S., West, K. A., Laugier, M., Alvarez, P. J. J., Kavanaugh, M. C., Alvarez-Cohen, L. 2002. Impact of ethanol on benzene plume lengths: Microbial and modeling studies. *Journal of Environmental Engineering*. 128 (9): 868–875.

DeSantis, T. Z., Hugenholtz, P., Larsen, N., Rojas, M., Brodie, E. L., Keller, K., Huber, T., Dalevi, D., Hu, P., Andersen, G. L. 2006. Greengenes, a Chimera-Checked 16S rRNA Gene Database and Workbench Compatible with ARB. *Applied and Environmental Microbiology*. 72 (7): 5069–5072.

Dinglasan, M. J. A., Ye, Y., Edwards, E. A., Mabury, S. A. 2004. Fluorotelomer alcohol biodegradation yields poly- and perfluorinated acids. *Environmental Science and Technology.* 38: 2857-2864.

Eaton, A., L. Clesceri, et al., 2005. Standard Methods for the Examination of Water and Wastewater. Washington, DC., American Public Health Association.

Edgar, R. C. 2010. Search and clustering orders of magnitude faster than BLAST. *Bioinformatics*. 26(19): 2460–2461.

Edgar, R. C., Haas, B. J., Clemente, J. C., Quince, C., Knight, R. 2011. UCHIME improves sensitivity and speed of chimera detection. *Bioinformatics*. 27 (16): 2194–2200.

Edwards, E., L. Wills, et al., 1992. Anaerobic degradation of toluene and xylene by aquifer microorganisms under sulfate-reducing conditions. *Applied and Environmental Microbiology*. 58(3): 794-800.

Ekpanyaskun, P. 2006. Transcriptomic analysis of Rhodococcus sp. RHA1 responses to heat shock and osmotic stress. Electronic Thesis, University of British Columbia: UBCV, 2006.

Ellis, D., E. Lutz, et al., 2000. Bioaugmentation for accelerated in situ anaerobic bioremediation. *Environmental Science and Technology.* 34(11): 2254-2260.

Evangelou, V. P. 1998. Environmental Soil and Water Chemistry. John Wiley & Sons: New York, 1998.

Fennell, D., A. Carroll, et al., 2001. Assessment of indigenous reductive dechlorinating potential at a TCE-contaminated site using microcosms, polymerase chain reaction analysis, and site data. *Environmental Science and Technology.* 35(9): 1830-1839.

Ferrey, M., J. Wilson, et al., 2012. Behavior and Fate of PFOA ad PFOS in Sandy Aquifer Sediment. *Ground Water Monitoring & Remediation*.

Fetter, C. W. 1999. Contaminant Hydrogeology, 2nd Edition; Waveland Press, Inc.: Long Grove, IL.

Fierer, N., Lauber, C. L., Zhou, N., McDonald, D., Costello, E. K., Knight, R. 2010. Forensic identification using skin bacterial communities. *Proceedings of the National Academy of Sciences*. 107 (14): 6477–6481.

Finette, B. A., Subramanian, V., Gibson, D. T. 1984. Isolation and characterization of Pseudomonas putida PpF1 mutants defective in the toluene dioxygenase enzyme system. *Journal of Bacteriology*. 160 (3): 1003–1009.

Fire, A. 2010. Material Safety Data Sheet #AMS120 for Tridol M 3% AFFF. Exton, PA

Fluoropolymer Manufacturers Group. 2003. Detecting and Quantifying Low Levels of Fluoropolymer Polymerization Aids - A Guidance Document. Washington, DC.

Freberg, B. I., Haug, L. S., Olsen, R., Daae, H. L., Hersson, M., Thomsen, C., Thorud, S., Becher, G., Molander, P., Ellingsen, D. G. 2010. Occupational exposure to airborne perfluorinated compounds during professional ski waxing. *Environmental Science and Technology.* 44(19): 7723–7728.

Freeborn, R. A., West, K. A., Bhupathiraju, V. K., Chauhan, S., Rahm, B. G., Richardson, R. E., Alvarez-Cohen, L. 2005. Phylogenetic Analysis of TCE-Dechlorinating Consortia Enriched on a Variety of Electron Donors. *Environmental Science and Technology.* 39 (21): 8358–8368.

Freedman, D. and J. Gossett. 1989. Biological reductive dechlorination of tetrachloroethylene and trichloroethylene to ethylene under methanogenic conditions. *Applied and Environmental Microbiology*. 55(9): 2144-2151.

Gaudin, A. and D. Fuerstenau. 1995. Quartz flotation with anionic collectors. *Transactions of AIME*. 202: 958-962.

Gellrich, V., T. Stahl, and T. P. Knepper. 2012. Behavior of perfluorinated compounds in soils during leaching experiments, *Chemosphere.* 87(9): 1052–1056.

George, C., Chovelon, J.M. 2002. A laser flash photolysis study of the decay of SO4-and Cl2-radical anions in the presence of Cl- in aqueous solutions. *Chemosphere.* 47(4): 385-393.

Goncalves, E., H. Hara, D. Miyazawa, J. Davies, L. Eltis, and W. Mohn. 2006. Transcriptomic assessment of isozymes in the biphenyl pathway of Rhodococcus sp. strain RHA1. *Applied and Environmental Microbiology*. 72(9): 6183–6193.

Goss, K. U. 2008. The pK(a) values of PFOA and other highly fluorinated carboxylic acids. *Environmental Science and Technology.* 42(2): 456-458.

Guelfo, J. L. Subsurface fate and transport of poly- and perfluoroalkyl substances. Colorado School of Mines, 2013.

Guelfo, J. L., and C. P. Higgins. 2013. Subsurface Transport Potential of Perfluoroalkyl Acids at Aqueous Film-Forming Foam (AFFF)-Impacted Sites. *Environmental Science and Technology.* 47(9): 4164–4171.

Guelfo, J., Wunsch, A., McCray, J., Higgins, C. P., Transport Potential of Perfluoroalkyl Acids (PFAAs) at AFFF-impacted Sites: Column Experiments and Modeling. *Manuscript in preparation.*

Hansen, K., H. Johnson, J. Eldridge, J. Butenhoff, and L. Dick. 2002. Quantitative characterization of trace levels of PFOS and PFOA in the Tennessee River. *Environmental Science and Technology.* 36(8): 1681–1685.

Harding-Marjanovic, K. C., Yi, S., Weathers, T. S., Sharp, J. O., Sedlak, D. L., Alvarez-Cohen, L. Effects of aqueous film-forming foam (AFFF) on trichloroethene (TCE) degradation by a Dehalococcoides enrichment culture. 2015, Submitted.

Harris, J. K., De Groote, M. A., Sagel, S. D., Zemanick, E. T., Kapsner, R., Penvari, C., Kaess, H., Deterding, R. R., Accurso, F. J., Pace, N. R. 2007. Molecular identification of bacteria in bronchoalveolar lavage fluid from children with cystic fibrosis. *Proceedings of the National Academy of Sciences*. 104: 20529–20533.

Hassan, A., J. Frank, and K. Qvist. 2002. Direct observation of bacterial exopolysaccharides in dairy products using confocal scanning laser microscopy. *Journal of Dairy Science*. 85(7): 1705–1708.

He, J., Holmes, V. F., Lee, P. K. H., Alvarez-Cohen, L. 2007. Influence of Vitamin B12 and Cocultures on the Growth of Dehalococcoides Isolates in Defined Medium. *Applied and Environmental Microbiology*. 73 (9): 2847–2853.

Hendrickson, E. R., Payne, J. A., Young, R. M., Starr, M. G., Perry, M. P., Fahnestock, S., Ellis, D. E., Ebersole, R. C. 2002. Molecular Analysis of Dehalococcoides 16S Ribosomal DNA from Chloroethene-Contaminated Sites throughout North America and Europe. *Applied and Environmental Microbiology*. 68 (2): 485–495.

Higgins, C. P., McLeod, P. B., Macmanus, L. A., Luthy, R. G. 2007. Bioaccumulation of perfluorochemicals in sediments by the aquatic oligochaete Lumbriculus variegatus. *Environmental Science and Technology.* 41 (13): 4600–4606.

Higgins, C., J. Field, C. Criddle, and R. Luthy. 2005. Quantitative determination of perfluorochemicals in sediments and domestic sludge. *Environmental Science and Technology.* 39(11): 3946–3956.

Higgins, C.P., Luthy, R.G., 2006. Sorption of perfluorinated surfactants on sediments. *Environmental Science and Technology.* 40(23): 7251-7256.

Higgins, C.P., Luthy, R.G., 2007. Modeling sorption of anionic surfactants onto sediment materials: an a priori approach for perfluoroalkyl surfactants and linear alkylbenzene sulfonates. *Environmental Science and Technology.* 41(9): 3254-3261.

Holmes, V. F., He, J., Lee, P. K. H., Alvarez-Cohen, L. 2006. Discrimination of Multiple Dehalococcoides Strains in a Trichloroethene Enrichment by Quantification of Their Reductive Dehalogenase Genes. *Applied and Environmental Microbiology*. 72 (9): 5877–5883.

Homme, C. L., Sharp, J. O. 2013. Differential microbial transformation of nitrosamines by an inducible propane monooxygenase. *Environmental Science and Technology.* 47:7388–7395.

Hori, H., Hayakawa, E., Einaga, H., Kutsuna, S., Koike, K., Ibusuki, T., Kiatagawa, H., Arakawa, R., 2004. Decomposition of environmentally persistent perfluorooctanoic acid in water by photochemical approaches. *Environmental Science and Technology.* 38(22): 6118-6124.

Hori, H., Yamamoto, A., Hayakawa, E., Taniyasu, S., Yamashita, N., Kutsuna, S., 2005. Efficient decomposition of environmentally persistent perfluorocarboxylic acids by use of persulfate as a photochemical oxidant. *Environmental Science and Technology.* 39(7): 2383-2388.

Houtz, E. F., Higgins, C. P., Field, J. A., Sedlak, D. L., 2013. Persistence of Perfluoroalkyl Acid Precursors in AFFF-Impacted Groundwater and Soil. *Environmental Science and Technology.* 47 (15): 8187-8195.

Houtz, E. F., Sedlak, D. L. 2012. Oxidative Conversion as a Means of Detecting Precursors to Perfluoroalkyl Acids in Urban Runoff. *Environmental Science and Technology.* 46: 9342-9349.

Huang, K., R. Couttenye, and G. Hoag. 2002. Kinetics of heat-assisted persulfate oxidation of methyl tert -butyl ether (MTBE). *Chemosphere.* 49(4):413-420.

Hug, L. A., Beiko, R. G., Rowe, A. R., Richardson, R. E., Edwards, E. A. 2012. Comparative metagenomics of three Dehalococcoides-containing enrichment cultures: the role of the non-dechlorinating community. *BMC Genomics*.13 (1): 327.

Huling, S. and B. Pivetz. 2006. Engineering Issue Paper: In-Situ Chemical Oxidation. U.S. Environmental Protection Agency (USEPA) Office of Research and Development. Cincinnati, OH.

Hunter, R. C., Beveridge, T. J. 2005. High-Resolution Visualization of Pseudomonas aeruginosa PAO1 Biofilms by Freeze-Substitution Transmission Electron Microscopy. *Journal of Bacteriology*. 187: 7619–7630.

ITRC. 2005. Technical and Regulatory Guidance for In situ Chemical Oxidation of Contaminated Soil and Groundwater, 2nd ed (ISCO-2). Prepared by the ITRC In situ Chemical Oxidation Team.

Jeong, S., M. Wander, et al., 2008. The role of condensed carbonaceous materials on the sorption of hydrophobic organic contaminants in subsurface sediments. *Environmental Science and Technology.* 42(5): 1458-1464.

Jinkerson, R. Anthrone Total Sugar and Polysaccharide Content Assay.

Johnson, M. D., Keinath II, T. M., Weber Jr., W. J. 2001. A Distributed Reactivity Model for Sorption by Soils and Sediments. 14. Characterization and Modeling of Phenanthrene Desorption Rates. *Environmental Science and Technology.*35:1688-1695.

Johnson, R. L., Anschutz, A. J., Smolen, J. M., Simcik, M. F., Penn, R. L. 2007. The Adsorption of Perfluorooctane Sulfonate onto Sand, Clay, and Iron Oxide Surfaces. *Journal of Chemical and Engineering Data*. 52:1165-1170.

Jonker, M., A. Sinke, J. Brils, and A. Koelmans. 2003. Sorption of polycyclic aromatic hydrocarbons to oil contaminated sediment: unresolved complex? *Environmental Science and Technology.* 37(22): 5197–5203.

Jonker, M., and A. Barendregt. 2006. Oil is a sedimentary supersorbent for polychlorinated biphenyls. *Environmental Science and Technology.* 40(12): 3829–3835.

Kalin, R. 2004. Engineered passive bioreactive barriers: risk-managing the legacy of industrial soil and groundwater pollution. *Current Opinions in Microbiology*. 7 (3): 227–238.

Kan, A. T., Gongmin, F., Tomson, M. B., 1994. Adsorption/Desorption Hysteresis in Organic Pollutant and Soil/Sedirnent Interaction. *Environmental Science and Technology.* 28: 859-867.

Kao, C. M., Chen, S. C., Liu, J. K. 2001. Development of a biobarrier for the remediation of PCE-contaminated aquifer. *Chemosphere.* 43 (8): 1071–1078.

Kao, C., and J. Prosser. 1999. Intrinsic bioremediation of trichloroethylene and chlorobenzene: field and laboratory studies. *Journal of Hazardous Materials.* 69(1): 67–79.

Kauck, E. and A. Diesslin. 1951. Some Properties of Perfluorocarboxylic Acids. *Industrial and Engineering Chemistry.* 43: 2332-2334.

Kearse, M., Moir, R., Wilson, A., Stones-Havas, S., Cheung, M., Sturrock, S., Buxton, S., Cooper, A., Markowitz, S., Duran, C., et al. 2012. Geneious Basic: An integrated and extendable desktop software platform for the organization and analysis of sequence data. *Bioinformatics*. 28 (12): 1647–1649.

Kelley, C., B. Hammer, and R. Coffin. 1997. Concentrations and stable isotope values of BTEX in gasoline-contaminated groundwater. *Environmental Science and Technology.* 31(9): 2469–2472.

Key, B., R. Howell, and C. Criddle. 1997. Fluorinated organics in the biosphere. *Environmental Science and Technology.* 31(9): 2445–2454.

Key, B., R. Howell, et al., 1998. Defluorination of organofluorine sulfur compounds by Pseudomonas sp. strain D2. *Environmental Science and Technology.* 32(15): 2283-2287.

Kile, D., and C. Chiou. 1989. Water solubility enhancements of DDT and trichlorobenzene by some surfactans below and above the critical micelle concentration. *Environmental Science and Technology.* 23(7): 832–838.

Kissa, E. 2001. Fluorinated Surfactants and Repellents, Second Edition Revised and Expanded, Vol. 97, Marcel Dekker, Inc., New York, NY.

Kita, A., Takiguchi, N., Kato, J. 2009. Cloning and characterization of sigA and sigB genes from Rhodococcus opacus strain B4: Involvement of sigB in organic solvent tolerance. *Journal of Environmental Biotechnology.* 9 (1): 43–50.

Klute, A. 1986. Methods of Soil Analysis, Part 1. Physical and Mineralogical Methods. Madison, WI, Soil Sci. Soc. Am.

Kolthoff, I. and E. Sandell. 1969. Quantitative Chemical Analysis. New York., Macmillan.

Kuklenyik, Z, J. Reich, J. Tully, L. Needham, and A. Calafat. 2004. Automated solid-phase extraction and measurement of perfluorinated organic acids and amides in human serum and milk. *Environmental Science and Technology.* 38(13): 3698–3704.

La Mesa, C., and B. Sesta. 1987. Micelles in perfluorinated surfactant solutions. *Journal of Physical Chemistry.* 91: 1450–1454.

Lau, C., Anitole, K., Hodes, C., Lai, D., Pfahles-Hutchens, A., Seed, J., 2007. Perfluoroalkyl acids: a review of monitoring and toxicological findings. *Toxicological Sciences.* 99(2): 366-394.

LeBlanc, J., E. Goncalves, and W. Mohn. 2008. Global response to desiccation stress in the soil actinomycete Rhodococcus jostii RHA1. *Applied and Environmental Microbiology*. 74(9): 2627–2636.

Lee, H., Mabury, S. A., 2011. A Pilot Survey of Legacy and Current Commercial Fluorinated Chemicals in Human Sera from United States Donors in 2009. *Environmental Science and Technology.* 45: 8067–8074.

Lee, L. S., Nyman, A. K., Li, H., Nyman, M. C., Jafvert, C. 1997. Initial Sorption of Aromatic Amines to Surface Soils. *Environmental Toxicology and Chemistry*. 16(8): 1575–1582.

Lee, L., P. Rao, M. Brusseau, and R. Ogwada. 1988. Nonequilibrium sorption of organic contaminants during flow through columns of aquifer materials. *Environmental Toxicology and Chemistry* 7: 779–793.

Lee, Y., Lo, S., Kuo, J., Hsieh, C., 2012a. Decomposition of perfluorooctanoic acid by microwaveactivated persulfate: Effects of temperature, pH, and chloride ions. *Frontiers of Environmental Science and Engineering.* 6(1): 17-25.

Lee, Y.C., Lo, S.L., Chiueh, P. T., Liou, Y. H., Chen, M. L., 2010. Microwave-hydrothermal decomposition of perfluorooctanoic acid in water by iron-activated persulfate oxidation. *Water Research*. 44(3): 886-892.

Lee, Y.C., Lo, S.L., Chiueh, P.T., Chang, D.G., 2009. Efficient decomposition of perfluorocarboxylic acids in aqueous solution using microwave-induced persulfate. *Water Research*. 43(11): 2811-2816.

Lee, Y.C., Lo, S.L., Kuo, J., Lin, Y.L., 2012b. Persulfate oxidation of perfluorooctanoic acid under the temperatures of 20-40 degrees C. *Chemical Engineering Journal.* 198: 27-32.

Li, X. Y., Yang, S. F. 2007. Influence of loosely bound extracellular polymeric substances (EPS) on the flocculation, sedimentation and dewaterability of activated sludge. *Water Research*. 41(5): 1022–1030.

Liang, C., Bruell, C.J., Marley, M.C., Sperry, M.L., 2004. Persulfate oxidation for in situ remediation of TCE. II. Activated by chelated ferrous ion. *Chemosphere.* 55: 1225-1233.

Liang, C., C. Huang, et al., 2008. A rapid spectrophotometric determination of persulfate anion in ISCO. *Chemosphere.* 73(9): 1540-1543.

Liang, C., Wang, Z.-S., Bruell, C. J. 2007. Influence of pH on persulfate oxidation of TCE at ambient temperatures. *Chemosphere.* 66 (1): 106-113.

Lindstrom, A.B., Strynar, M.J., Libelo, E.L., 2011. Polyfluorinated compounds: past, present, and future. *Environmental Science and Technology.* 45:7954-7961.

Liu, C.S., Higgins, C.P., Wang, F., Shih, K., 2012a. Effect of temperature on oxidative transformation of perfluorooctanoic acid (PFOA) by persulfate activation in water. *Sepuration and Purification Technology*. 91: 46-51.

Liu, C.S., Shih, K., Wang, F., 2012b. Oxidative decomposition of perfluorooctanesulfonate in water by permanganate. *Sepuration and Purification Technology*. 87:95-100.

Love, M. I., Huber, W., Anders, S. 2014. Moderated estimation of fold change and dispersion for RNA-seq data with DESeq2. *Genome Biology*. 15 (12).

Luo, Y., M. Durenkamp, M. De Nobili, Q. Lin, B.J. Devonshire, and P. Brookes. 2013. Microbial biomass growth, following incorporation of biochars produced at 350 °C or 700 °C, in a silty-clay loam soil of high and low pH. *Soil Biology and Biochemistry*. 57: 513–523.

Luthy, R., G. Aiken, M. Brusseau, S. Cunningham, P. Gschwend, J. Pignatello, M. Reinhard, S. Traina, W. Weber, and J. Westall. 1997. Sequestration of hydrophobic organic contaminants by geosorbents. *Environmental Science and Technology.* 31(12): 3341–3347.

Marchesi, J. R., White, G. F., House, W. A., Russell, N. J. 1994. Bacterial cell hydrophobicity is modified during the biodegradation of anionic surfactants. *FEMS Microbiology Letters*. 124 (3): 387–392.

Martin, J. W., Whittle, D. M., Muir, D. C. G., Mabury, S. A. 2004. Perfluoroalkyl Contaminants in a Food Web from Lake Ontario. *Environmental Science and Technology.* 38(20): 5379–5385.

Maymo-Gatell, X., Chien, Y., Gossett, J. M., Zinder, S. H. 1997. Isolation of a Bacterium That Reductively Dechlorinates Tetrachloroethene to Ethene. *Science*. 276 (1568): 1568–1571.

McCray, J. and M. Brusseau. 1998. Cyclodextrin-enhanced in situ flushing of multiple-component immiscible organic liquid contamination at the field scale: Mass removal effectiveness. *Environmental Science and Technology.* 32(9): 1285-1293.

McCray, J. and M. Brusseau. 1999. Cyclodextrin enhanced in situ flushing of multiple-component immiscible organic liquid contamination at the field scale: Analysis of dissolution behavior. *Environmental Science and Technology.* 33(1): 89-95.

McCray, J. and P. Dugan. 2002. Nonideal equilibrium dissolution of trichloroethene from a decane-based nonaqueous phase liquid mixture: Experimental and modeling investigation. *Water Resources Research*. 38(7)

McCray, J., G. Bai, et al., 2001. Biosurfactant-enhanced solubilization of NAPL mixtures. *Journal of Contaminant Hydrology*. 48(1-2): 45-68.

McCray, J., G. Tick, et al., 2010b. Innovative remediation of NAPL source zones: Lessons learned from legacy field studies. invited paper in review for *Ground Water*.

McCray, J., J. Marr, et al., 2010a. Final report for SERDP ER-1486, Polymer enhanced remediation in heterogeneous media. Golden, CO.

McCray, J., T. Boving, et al., 2000. Cyclodextrin-enhanced solubilization of organic contaminants with implications for aquifer remediation. *Ground Water Monitoring and Remediation*. 20(1): 94-103.

McDonald, D., Price, M. N., Goodrich, J., Nawrocki, E. P., DeSantis, T. Z., Probst, A., Andersen, G. L., Knight, R., Hugenholtz, P. 2012. An improved Greengenes taxonomy with explicit ranks for ecological and evolutionary analyses of bacteria and archaea. *ISME Journal*. 6 (3): 610–618.

McGuire, M. E., Schaefer, C., Richards, T., Backe, W. J., Field, J. A., Houtz, E., Sedlak, D. L., Guelfo, J., Wunsch, A., Higgins, C. P., 2014. Evidence of remediation-induced alteration of subsurface poly- and perfluoroalkyl substance distribution at a former firefighter training area. *Environmental Science and Technology.* 48(12): 6644-6652.

McKenzie, E. R., Siegrist, R. L., McCray, J. E., Higgins, C. P. 2016. The influence of a non-aqueous phase liquid (NAPL) and chemical oxidant application on perfluoroalkyl acid (PFAA) fate and transport. *Water Research*. 92: 199-207

McKenzie, E.R., Siegrist, R.L., McCray, J.E., Higgins, C.P. 2015. Effects of chemical oxidants on perfluoroalkyl acid transport in one-dimensional porous media columns. *Environmental Science and Technology.* 49(3): 1681-1689.

McLeod, M. P., Warren, R. L., Hsiao, W. W. L., Araki, N., Myhre, M., Fernandes, C., Miyazawa, D., Wong, W., Lillquist, A. L., Wang, D., et al. 2006. The complete genome of Rhodococcus sp. RHA1 provides insights into a catabolic powerhouse. *Proceedings of the National Academy of Sciences*. 103 (42): 15582–15587.

Men, Y., Feil, H., VerBerkmoes, N. C., Shah, M. B., Johnson, D. R., Lee, P. K. H., West, K. A., Zinder, S. H., Andersen, G. L., Alvarez-Cohen, L. 2012. Sustainable syntrophic growth of Dehalococcoides ethenogenes strain 195 with Desulfovibrio vulgaris Hildenborough and Methanobacterium congolense: global transcriptomic and proteomic analyses. *ISME Journal.* 6 (2): 410–421.

Men, Y., Lee, P. K. H., Harding, K. C., Alvarez-Cohen, L. 2013. Characterization of four TCE-dechlorinating microbial enrichments grown with different cobalamin stress and methanogenic conditions. *Applied Microbiology and Biotechnology*. 2013, 97 (14): 6439–6450.

Meuser, J. E., Boyd, E. S., Ananyev, G., Karns, D., Radakovits, R., Narayana Murthy, U. M., Ghirardi, M. L., Dismukes, G. C., Peters, J. W., Posewitz, M. C. 2011. Evolutionary

significance of an algal gene encoding an [FeFe]-hydrogenase with F-domain homology and hydrogenase activity in Chlorella variabilis NC64A. *Planta*. 234 (4): 829–843.

Miller, C. T., Pedit, J. A. 1992. Use of a Reactive Surface-Diffusion Model To Describe Apparent Sorption-Desorption Hysteresis and Abiotic Degradation of Lindane in a Subsurface Material. *Environmental Science and Technology.* 26: 1417-1427.

Miller, R. O., Kissel, D. E. 2010. Comparison of Soil pH Methods on Soils of North America. *Soil Science Society of America Journal.* 74 (1): 310–316.

Mitchell, S. M., Ahmad, M., Teel, A. L., Watts, R. J. 2013. Degradation of perfluorooctanoic acid by reactive species generated through catalyzed H2O2 propagation reactions. *Environmental Science and Technology Letters*. 1 (1): 117-121.

Moody, C. A., G. N. Hebert, S. H. Strauss, and J. A. Field. 2003, Occurrence and persistence of perfluorooctanesulfonate and other perfluorinated surfactants in groundwater at a fire-training area at Wurtsmith Air Force Base, Michigan, USA. *Journal of Environmental Monitoring*. 5(2): 341–345.

Moody, C. A., Martin, J. W., Kwan, W. C., Muir, D. C. G., Mabury, S. A. 2002. Monitoring perfluorinated surfactants in biota and surface water samples following an accidental release of fire-fighting foam into Etobicoke Creek. *Environmental Science and Technology.* 36: 545–551.

Moody, C., J. Martin, W. Kwan, D. Muir, and S. Mabury. 2002. Monitoring perfluorinated surfactants in biota and surface water samples following an accidental release of fire-fighting foam into Etobicoke Creek. *Environmental Science and Technology.* 36:4

Moody, C.A., Field, J.A., 1999. Determination of perfluorocarboxylates in groundwater impacted by fire-fighting activity. *Environmental Science and Technology.* 33(16): 2800-2806.

Moody, C.A., Field, J.A., 2000. Perfluorinated surfactants and the environmental implications of their use in fire-fighting foams. *Environmental Science and Technology.* 34(18): 3864-3870.

Morikawa, M. 2006. Beneficial biofilm formation by industrial bacteria Bacillus subtilis and related species. *Journal of Biosciences and Bioengineering*. 101 (1): 1–8.

Moriwaki, H., Y. Takagi, et al., 2005. Sonochemical decomposition of perfluorooctane sulfonate and perfluorooctanoic acid. *Environmental Science and Technology.* 39(9): 3388-3392.

Morris, D. 1948. Quantitative determination of carbohydrates with dreywood's anthrone reagent. *Science.* 107: 254–255.

Müller, C. E., De Silva, A. O., Small, J., Williamson, M., Wang, X., Morris, A., Katz, S., Gamberg, M., Muir, D. C. G. 2011. Biomagnification of perfluorinated compounds in a

remote terrestrial food chain: Lichen-Caribou-wolf. *Environmental Science and Technology.* 45, (20): 8665–8673.

Neeves, K. B., Illing, D. A. R., Diamond, S. L. 2010. Thrombin flux and wall shear rate regulate fibrin fiber deposition state during polymerization under flow. *Biophysical Journal.* 98 (7):1344–1352.

Nguyen, T. V., Reinhard, M., Gin, K. Y.-H. 2013. Rate laws and kinetic modeling of N-ethyl perfluorooctane sulfonamidoethanol (N-EtFOSE) transformation by hydroxyl radical in aqueous solution. *Water Research*. 47: 2241-2250.

Nielsen, T., Siigur, K., Helweg, C., Jørgensen, O., Hansen, P. E., Kirso, U. 1997. Sorption of Polycyclic Aromatic Compounds to Humic Acid As Studied by High-Performance Liquid Chromatography. *Environmental Science and Technology.* 31: 1102-1108.

Nilsson, H., Kärrman, A., Rotander, A., van Bavel, B., Lindström, G., Westberg, H., 2013. Biotransformation of fluorotelomer compound to perfluorocarboxylates in humans. *Environment International.* 51: 8-12.

Ochoa-Herrera, V., R. Sierra-Alvarez, et al., 2008. Reductive defluorination of perfluorooctane sulfonate. *Environmental Science and Technology.* 42(9): 3260-4.

Oh, S., Wang, Q., Shin, W. S., Song, D.-I. 2013. Sorption and desorption kinetics of PAHs in coastal sediment. *Korean Journal of Chemical Engineering.* 30 (1): 145-153.

Ortiz, E., M. Kraatz, and R. G. Luthy. 1999. Organic phase resistance to dissolution of polycyclic aromatic hydrocarbon compounds. *Environmental Science and Technology.* 33(2): 235–242.

Pan, G., Jia, C., Zhao, D., You, C., Chen, H., Jiang, G., 2009. Effect of cationic and anionic surfactants on the sorption and desorption of perfluorooctane sulfonate (PFOS) on natural sediments. *Environmental Pollution.* 157(1): 325-330.

Patrauchan, M. A., Miyazawa, D., LeBlanc, J. C., Aiga, C., Florizone, C., Dosanjh, M., Davies, J., Eltis, L. D., Mohn, W. W. 2012. Proteomic analysis of survival of Rhodococcus jostii RHA1 during carbon starvation. *Applied and Environmental Microbiology*.78 (18): 6714–6725.

Patterson, B., F. Pribac, C. Barber, G. Davis, and R. Gibbs. 1993. Biodegradation and retardation of PCE and BTEX compounds in aquifer material from western Australia using large-scale columns. *Journal of Contaminant Hydrology*. 14: 261–278.

Perry, M., L. MacLean, M. Patrauchan, and E. Vinogradov. 2007. The Structure of the exocellular polysaccharide produced by Rhodococcus sp. RHA1. *Carbohydrate Research.* 342(15): 2223–2229.

Petri, B.G., Siegrist, R.L., Crimi, M.L., 2008. Effects of groundwater velocity and permanganate concentration on DNAPL mass depletion rates during in situ oxidation. *Journal of Environmental Engineering-ASCE*. 134(1): 1-13.

Pfaffl, M. W. 2001. A new mathematical model for relative quantification in real-time RT-PCR. *Nucleic Acids Research.* 29 (9): 45e – 45.

Pfaffl, M. W., Horgan, G. W., Dempfle, L. 2002. Relative expression software tool (REST) for group-wise comparison and statistical analysis of relative expression results in real-time PCR. *Nucleic Acids Research.* 30 (9).

Pfeiffer, T., Bonhoeffer, S. 2003. An evolutionary scenario for the transition to undifferentiated multicellularity. *Proceedings of the National Academy of Sciences*. 100 (3): 1095–1098.

Phelps, C. and L. Young. 1999. Anaerobic biodegradation of BTEX and gasoline in various aquatic sediments. *Biodegradation.* 10(1): 15-25.

Pignatello, J. J. 2012. Dynamic interactions of natural organic matter and organic compounds. *Journal of Soils and Sediments.* 1241-1256.

Pignatello, J. J., and B. Xing 1996, Mechanisms of Slow Sorption of Organic Chemicals to Natural Particles. *Environmental Science and Technology.* 30(1): 1–11.

Pintelon, T. R. R., Picioreanu, C., van Loosdrecht, M. C. M., Johns, M. L. 2012. The effect of biofilm permeability on bio-clogging of porous media. *Biotechnology and Bioengineering*. 109 (4): 1031–1042.

Place, B. J., and J. A. Field 2012): Identification of Novel Fluorochemicals in Aqueous Film-Forming Foams Used by the US Military. *Environmental Science and Technology.* 46(13): 7120–7127.

Plumlee, M. H., McNeill, K., Reinhard, M. 2009. Indirect photolysis of perfluorochemicals: hydroxyl radical-initiated oxidation of N-ethyl perfluorooctane sulfonamido acetate (N-EtFOSAA) and other perfluoroalkanesulfonamides. *Environmental Science and Technology.* 43: 3662-3668.

Prevedouros, K., Cousins, I.T., Buck, R.C., Korzeniowski, S.H., 2006. Sources, fate and transport of perfluorocarboxylates. *Environmental Science and Technology.* 40(1): 32-44.

Price, M. N., Dehal, P. S., Arkin, A. P. 2010. FastTree 2 – Approximately Maximum-Likelihood Trees for Large Alignments. *PLoS ONE*. 5 (3): e9490.

Rambaut, A. 2015. FigTree v1.4.2; http://tree.bio.ed.ac.uk/software/figtree/

Reinhard, M., S. Shang, et al., 1997. In situ BTEX biotransformation under enhanced nitrate- and sulfate-reducing conditions. *Environmental Science and Technology.* 31(1): 28-36.

Rhoads, K. R., Janssen, E. M. L., Luthy, R. G., Criddle, C. S. 2008. Aerobic biotransformation and fate of N-ethyl perfluorooctane sulfonamidoethanol (N-EtFOSE) in activated sludge. *Environmental Science and Technology.*42: 2873-2878.

Richardson, R. E., Bhupathiraju, V. K., Song, D. L., Goulet, T. A., Alvarez-Cohen, L. 2002. Phylogenetic Characterization of Microbial Communities That Reductively Dechlorinate TCE Based upon a Combination of Molecular Techniques. *Environmental Science and Technology.* 36 (12): 2652–2662.

Robbins, G., S. Wang, and J. Stuart. 1993. Using the static headspace method to determine Henry's Law constants. *Analytical Chemistry*. 65(21): 3113–3118.

Rosenmai, A. K., Nielsen, F. K., Pedersen, M., Hadrup, N., Trier, X., Christensen, J. H., Vinggaard, A. M. 2013. Fluorochemicals used in food packaging inhibit male sex hormone synthesis. *Toxicology and Applied Pharmacology*. 266: 132–142.

Rotander, A., Toms, L.-M. L., Aylward, L., Kay, M., Mueller, J. F. 2015. Elevated levels of PFOS and PFHxS in firefighters exposed to aqueous film forming foam (AFFF). *Environment International.* 82: 28–34.

Rouwenhorst, R., J. Frank Jzn, W. Scheffers, and J. van Dijken. 1991. Determination of protein concentration by total organic carbon analysis. *Journal of Biochemical and Biophysical Methods*. 22(2): 119–128.

Sabatini, D., J. Harwell, et al., 1999. Surfactant selection criteria for enhanced subsurface remediation. in: Innovative Subsurface Remediation: Field Testing of Physical, Chemical and Characterization Technologies. M. Brusseau, D. Sabatini, J. Gierke and M. Annable. Washington, D.C, ACS Symposium Series 725, American Chemical Society: 8-23.

Sakamoto, M. 2014. The Family Porphyromonadaceae. In: The Prokaryotes; Rosenberg, E., DeLong, E. F., Lory, S., Stackebrandt, E., Thompson, F., Eds., Springer Berlin Heidelberg: Berlin, Heidelberg, 2014; pp 811–824.

Saleh-Lakha, S., Shannon, K. E., Goyer, C., Trevors, J. T. 2011. Challenges in quantifying microbial gene expression in soil using quantitative reverse transcription real-time PCR. *Journal of Microbiology Methods.* 85 (3): 239–243.

Sander, M., Y. F. Lu, and J. J. Pignatello. 2006. Conditioning-annealing studies of natural organic matter solids linking irreversible sorption to irreversible structural expansion. *Environmental Science and Technology.* 40: 170.

Sanin, S., F. Sanin, and J. Bryers. 2003. Effect of starvation on the adhesive properties of xenobiotic degrading bacteria. *Process Biochemistry.* 38: 909–914.

Schaefer, C., A. Callaghan, et al., 2009. Dense nonaqueous phase liquid architecture and dissolution in discretely fractured sandstone blocks. *Environmental Science and Technology.* 43(6): 1877-1883.

Scheutz, C., Durant, N. D., Broholm, M. M. 2014. Effects of bioaugmentation on enhanced reductive dechlorination of 1,1,1-trichloroethane in groundwater: a comparison of three sites. *Biodegradation*. 25 (3): 459–478.

Schultz, M., D. Barofsky, and J. Field. 2004. Quantitative determination of fluorotelomer sulfonates in groundwater by LC MS/MS. *Environmental Science and Technology.* 38 (6): 1828–1835.

Schwarzenbach, R. P., Gschwend, P. M., Imboden, D. M. 2003. Environmental Organic Chemistry. 2 ed., John Wiley & Sons: New York, 2003.

Seacat, A. M. 2002. Subchronic toxicity studies on perfluorooctanesulfonate potassium salt in cynomolgus monkeys. *Toxicological Sciences.* 68 (1): 249–264.

Seo, H. and J. McCray. 2002. Interfacial tension of chlorinated aliphatic DNAPL mixtures as a function of organic phase composition. *Environmental Science and Technology.* 36(6): 1292-1298.

Sepulvado, J., A. Blaine, L. S. Hundal, and C. P. Higgins. 2011. Occurrence and fate of perfluorochemicals in soil following the land application of municipal biosolids. *Environmental Science and Technology.* 45(19):8106–8112.

Sharp, J. O., Sales, C. M., Alvarez-Cohen, L. 2010. Functional characterization of propane-enhanced N-nitrosodimethylamine degradation by two actinomycetales. *Biotechnology and Bioengineering*. 107 (6): 924–932.

Sharp, J., C. Sales, J. LeBlanc, J. Liu, T. Wood, L. Eltis, W. Mohn, and L. Alvarez-Cohen. 2007. An inducible propane monooxygenase is responsible for n-nitrosodimethylamine degradation by Rhodococcus sp. strain RHA1. *Applied and Environmental Microbiology*. 73(21): 6930–6938.

Sharp, J., T. Wood, and L. Alvarez-Cohen. 2005. Aerobic biodegradation of n-nitrosodimethylamine (NDMA) by axenic bacterial strains. *Biotechnology and Bioengineering*. 89(5): 608–618.

Siegrist, R., M. Crimi, et al., 2008. Chemical oxidation for clean up of contaminated *Ground Water*. Methods and techniques for cleaning-up contaminated sites. in: NATO Science for Peace and Security Series. M. Annable, M. Teodorescu, P. Hlavinek and L. Diels. Dordrecht, The Netherlands, Springer Publishing: 45-58.

Siegrist, R., M. Urynowicz, O. West, M. Crimi, and K. Lowe. 2001. Principles and Practices of In situ Chemical Oxidation Using Permanganate. Columbus, OH, Battelle Press.

Siegrist, R.L., Crimi, M., Simpkin, T.J. 2011. In situ chemical oxidation for groundwater remediation. SERDP and ESTCP Remediation Technology Monograph Series. Springer Publishing. New York, NY.

Simunek, J., and Van Genuchten, M.T. 2005. The HYDRUS-2D software package for simulating two-dimensional movement of water, heat, and multiple solutes in variably saturated media. Version 2.0, Department of Environmental Sciences University of California Riverside, Riverside, CA.

Simunek, J., Sejna, M., Saito, H., Sakai, M., and Van Genuchten, M.T. 2013): The HYDRUS-1D Software Package for Simulating the One-Dimensional Movement of Water, Heat, and Multiple Solutes in Variably-Saturated Media, Department of Environmental Sciences University of California Riverside, Riverside, CA.

Šimůnek, J., van Genuchten, M.T., Sejna, M., 2008. Development and applications of the HYDRUS and STANMOD software packages and related codes. *Vadose Zone Journal.* 7(2): 587-600.

Sivan, A., M. Szanto, and V. Pavlov. 2006. Biofilm development of the polyethylene-degrading bacterium Rhodococcus ruber. *Applied Microbiology and Biotechnology*. 72(2): 346–352.

Smith, M., J. Silva, et al., 2008. Compatibility of polymers and chemical oxidants for enhanced groundwater remediation. *Environmental Science and Technology.* 42(24): 9296-9301.

Smits, K. M., T. Sakaki, A. Limsuwat, and T. H. Illangasekare 2009, Thermal Conductivity of Sands under Varying Moisture and Porosity in Drainage-Wetting Cycles, *Vadose Zone Journal*. 9(1): 172–180.

Sparks, D., A. Page, et al., 1996. Methods of Soil Analysis: Part 3 - Chemical Methods. Madison, WI, Soil Science Society of America.

Steenland, K., Fletcher, T., Savitz, D.A., 2010. Epidemiologic evidence on the health effects of perfluorooctanoic acid (PFOA). *Environmental Health Perspectives*. 118(8): 1100-1108.

Stewart, P. S., Franklin, M. J. 2008. Physiological heterogeneity in biofilms. *Nature Reviews Microbiology*. 6 (3): 199–210.

Sun, S., and S. Boyd. 1991. Sorption of polychlorobiphenyl (PCB) congeners by residual PCB-oil phases in soils. *Journal of Environmental Quality.* 20(3): 557–561.

Taki, H., Syutsubo, K., Mattison, R. G., Harayama, S. 2006. Identification and characterization of o-xylene-degrading Rhodococcus spp. which were dominant species in the remediation of o-xylene-contaminated soils. *Biodegradation.* 18 (1): 17–26.

Tan, K. 1996. Soil Sampling, Preparation, and Analysis. Marcel Dekker, Inc., New York, NY.

Tang, C.Y., Fu, Q.S., Gao, D., Criddle, C.S., Leckie, J.O. 2010. Effect of solution chemistry on the adsorption of perfluorooctane sulfonate onto mineral surfaces. *Water Research*. 44(8): 2654-2662.

Taniyasu, S., K. Kannan, et al., 2008. Analysis of trifluoroacetic acid and other short-chain perfluorinated acids (C2-C4) in precipitation by liquid chromatography-tandem mass spectrometry: Comparison to patterns of long-chain perfluorinated acids (C5-C18). *Analytica Chimica Acta.* 619(2): 221-230.

Taniyasu, S., Yamashita, N., Yamazaki, E., Petrick, G., Kurunthachalam, K., 2013. The environmental photolysis of perfluorooctanesulfonate, perfluorooctanoate, and related fluorochemicals. *Chemosphere.* 90: 1686-1692.

Tao, Q., D. Wang, and H. Tang. 2006. Effect of surfactants at low concentrations on the sorption of atrazine by natural sediment. *Water Environment Research.* 78(7): 653–660.

Templeton, A. S., Knowles, E. J., Eldridge, D. L., Arey, B. W., Dohnalkova, A. C., Webb, S. M., Bailey, B. E., Tebo, B. M., Staudigel, H. 2009. A seafloor microbial biome hosted within incipient ferromanganese crusts. Nature Geoscience. 2 (12): 872–876.

Tulp, H., K. Fenner, R. Schwarzenbach, and K. Goss. 2009. pH-dependent sorption of acidic organic chemicals to soil organic matter. *Environmental Science and Technology.* 43(24): 9189–9195.

Turner, A., Xu, J. 2008. Influence of ionic surfactants on the flocculation and sorption of palladium and mercury in the aquatic environment. *Water Research*. 42 (1-2): 318–326.

Urynowicz, M. and R. Siegrist. 2005. Interphase mass transfer during chemical oxidation of TCE DNAPL in an aqueous system. *Journal of Contaminant Hydrology*. 80(3-4): 93-106.

USEPA. 1986. Test Methods for the Evaluation of Solid Waste, Physical/Chemical Methods SW- 846, 3rd ed. Washington, DC.

USEPA. 1990. Second update to SW-846 Methods Section. Washington, DC.

USEPA. 2009. Provisional Health Advisories for Perfluorooctanoic Acid (PFOA) and Perfluorooctane Sulfonate (PFOS). http://www.epa.gov/region4/water/documents/pha-PFOA_PFOS.pdf.

USEPA. 2012. Emerging Contaminants - Perfluorooctane Sulfonate (PFOS) and Perfluorooctanoic Acid (PFOA). http://www.epa.gov/fedfac/pdf/emerging_contaminants_pfos_pfoa.pdf.

USEPA. 2013. Emerging contaminants - Perfluorooctane Sulfonate (PFOS) and Perfluorooctanoic Acid (PFOA). http://www.epa.gov/sites/production/files/2014-04/documents/factsheet_contaminant_pfos_pfoa_march2014.pdf

Van de Vijver, K., P. Hoff, K. Das, W. Van Dongen, E. Esmans, T. Jauniaux, J. Bouquegneau, R. Blust, and W. De Coen. 2003. Perfluorinated chemicals infiltrate ocean waters: Link between exposure levels and stable isotope ratios in marine mammals. *Environmental Science and Technology.* 37(24): 5545–5550.

Van Genuchten, M. 1981. Non-Equilibrium Transport Parameters from Miscible Displacement Experiments; U.S. Department of Agriculture: U.S. Salinity Laboratory, Riverside, CA.

Van Genuchten, M. T., and R. J. Wagenet. 1989. Two-Site/Two-Region Models for Pesticide Transport and Degradation: Theoretical Development and Analytical Solution. *Soil Science Society of America Journal.* 53(5): 1303.

Vandergeize, R., and L. Dijkhuizen. 2004. Harnessing the catabolic diversity of rhodococci for environmental and biotechnological applications. *Current Opinion in Microbiology*. 7(3): 255–261.

Vázquez-Baeza, Y., Pirrung, M., Gonzalez, A., Knight, R. 2013. EMPeror: a tool for visualizing high-throughput microbial community data. *GigaScience.* 2 (1): 16.

Vecitis, C., H. Park, et al., 2009. Treatment technologies for aqueous perfluorooctanesulfonate (PFOS) and perfluorooctanoate (PFOA). *Frontiers of Environmental Science and Engineering in China.* 3(2): 129-151.

Velten, S., Hammes, F., Boller, M., and Egli, T., 2007. Rapid and direct estimation of active biomass on granular activated carbon through adenosine tri-phosphate (ATP) determination. *Water Research*. 41: 1973-1983

Wang, J., Y. Li, Y. Liu, H. Zhang, and J. Dai. 2010. Disturbance of perfluorooctanoic acid on development and behavior in drosphila larvae. *Environmental Toxicology and Chemistry*. 29(9): 2117–2122.

Wang, N., Liu, J., Buck, R. C., Korzeniowski, S. H., Wolstenholme, B. W., Folsom, P. W., Sulecki, L. M. 2011. 6:2 Fluorotelomer sulfonate aerobic biotransformation in activated sludge of waste water treatment plants. *Chemosphere.* 82: 853-858.

Wang, Q., Garrity, G. M., Tiedje, J. M., Cole, J. R. 2007. Naive Bayesian Classifier for Rapid Assignment of rRNA Sequences into the New Bacterial Taxonomy. *Applied and Environmental Microbiology*. 73 (16): 5261–5267.

Wang, Y., Zhang, P., Pan, G., Chen, H., 2008. Ferric ion mediated photochemical decomposition of perfluorooctanoic acid (PFOA) by 254 nm UV light. *Journal of Hazardous Materials.* 160(1):181-186.

Washington, J. W., Yoo, H., Ellington, J. J., Jenkins, T. M., Libelo, E. L. 2010. Concentrations, Distribution, and Persistence of Perfluoroalkylates in Sludge-Applied Soils near Decatur, Alabama, USA. *Environmental Science and Technology.* 44 (22): 8390–8396.

Weathers, T. S., Higgins, C. P., Sharp, J. O. 2015. Enhanced Biofilm Production by a Toluene-Degrading Rhodococcus Observed after Exposure to Perfluoroalkyl Acids. *Environmental Science and Technology.*49 (9): 5458–5466.

Weaver, R., S. Angle, et al., 1994. Methods of Soil Analysis: Part 2 - Microbiological and Biochemical Properties. Soil Sci. Soc. Am. Madison, WI.

Weber Jr., W. J., Huang, W., Yu, H., 1998. Hysteresis in the sorption and desorption of hydrophobic organic contaminants by soils and sediments 2. Effects of soil organic matter heterogeneity. *Journal of Contaminant Hydrology*. 31: 149-165.

Wolff, S.P., 1994. Ferrous ion oxidation in the presence offFerric ion indicator xylenol orange for measurement of hydroperoxides. *Methods in Enzymology.* 233: 182-189.

Xu, L., Krenitsky, D. M., Seacat, A. M., Butenhoff, J. L., Anders, M. W. 2004. Biotransformation of N-ethyl-N-(2-hydroxyethyl)perfluorooctanesulfonamide by rat liver microsomes, cytosol, and slices and by expressed rat and human cytochromes P450. *Chemical Research in Toxicology.* 17 (6): 767–775.

Yan, J., Im, J., Yang, Y., Loffler, F. E. 2013. Guided cobalamin biosynthesis supports Dehalococcoides mccartyi reductive dechlorination activity. *Philosophical Transactions of The Royal Society B Biological Sciences.* 368 (1616): 20120320–20120320.

Yang, Y., Zeyer, J. 2003. Specific Detection of Dehalococcoides Species by Fluorescence In Situ Hybridization with 16S rRNA-Targeted Oligonucleotide Probes. *Applied and Environmental Microbiology*. 69 (5): 2879–2883.

Ye, J., Coulouris, G., Zaretskaya, I., Cutcutache, I., Rozen, S., Madden, T. L. 2012. Primer-BLAST: A tool to design target-specific primers for polymerase chain reaction. *BMC Bioinformatics*. 13 (1):134.

You, J., Landrum, P. F., Lydy, M. J. 2006. Comparison of Chemical Approaches for Assessing Bioavailability of Sediment-Associated Contaminants. *Environmental Science and Technology.* 40: 6348-6353.

Yu, Q., R. Q. Zhang, et al., 2009. Sorption of perfluorooctane sulfonate and perfluorooctanoate on activated carbons and resin: Kinetic and isotherm study. *Water Research*. 43(4): 1150-1158.

Zachara, J. M., Ainsworth, C. C., Felice, L. J., Resch, C. T. 1986. Quinoline Sorption to Subsurface Materials: Role of pH and Retention of the Organic Cation. *Environmental Science and Technology.* .20 (6): 620-627.

Zhang, X., P. Bishop, and B. Kinkle. 1999. Comparison of extraction methods for quantifying extracellular polymers in biofilm. *Water Science and Technology.* 39(7): 211–218.

APPENDICES

Appendix A-1

Soil Isotherm Parameters and Interpolated K_d Values

Loamy Sand (A) PFAS Isotherms										
Analyte Name	Aqueous Min (µg/L)	Aqueous Max (µg/L)	Solid Min (µg/kg)	Solid Max (µg/kg)	Obs.	Log K_f (mg/kg) $(mg/L)^{-n}$	±	n	±	R^2
PFBA	8.72	1097.33	4.861	100.16	12	-1.00	0.1	0.74	0.06	0.98
PFPeA	18.26	906.0	3.05	74.7	12	-1.08	0.04	0.84	0.04	1.00
PFHxA	15.86	1302.0	1.96	149.08	12	-0.86	0.09	0.95	0.08	0.99
PFHpA	14.87	1176.0	5.15	272.03	12	-0.57	0.05	0.92	0.04	1.00
PFOA- Mix	2.72	920.67	1.29	271.40	15	-0.44	0.12	0.88	0.08	0.98
PFOA-Only	2.81	738.0	1.35	368.47	15	-0.25	0.08	0.98	0.05	0.99
PFNA	1.66	712.67	5.79	433.23	15	-0.19	0.13	0.81	0.08	0.97
PFDA	2.69	449.33	24.50	745.57	12	0.12	0.04	0.68	0.03	1.00
PFUnA	0.39	75.93	33.89	842.68	12	0.56	0.08	0.61	0.03	0.99
PFBS	2.61	1071.33	1.61	227.92	15	-0.64	0.07	0.81	0.04	0.99
PFHxS	2.56	1092.00	1.62	280.61	15	-0.52	0.13	0.80	0.09	0.97
PFOS-Mix	0.66	425.33	3.46	638.53	15	0.13	0.11	0.77	0.05	0.99
PFOS-Only	0.54	286.00	2.65	751.44	15	0.36	0.05	0.88	0.02	1.00

A Interpolated K_d								
C_w (nM)	C_w (mg/L)	C_s (mg/kg)	Interp K_d (L/kg)	Log K_d @ 5nm	C_w (mg/L)	C_s (mg/kg)	Interp K_d (L/kg)	Log K_d @ 350 µg/L
5	0.0011	0.00064	0.61	-0.22	0.35	0.05	0.13	-0.88
5	0.0013	0.00031	0.24	-0.63	0.35	0.03	0.10	-1.01
5	0.0016	0.00029	0.19	-0.73	0.35	0.05	0.15	-0.84
5	0.0018	0.0008	0.44	-0.35	0.35	0.10	0.29	-0.54
5	0.0021	0.00153	0.74	-0.13	0.35	0.14	0.41	-0.39
5	0.0021	0.00131	0.63	-0.20	0.35	0.20	0.57	-0.24
5	0.0023	0.00475	2.05	0.31	0.35	0.27	0.79	-0.10
5	0.0026	0.0223	8.69	0.94	0.35	0.64	1.82	0.26
5	0.0028	0.1025	36.41	1.56	0.35	1.92	5.48	0.74
5	0.0015	0.00119	0.80	-0.10	0.35	0.10	0.28	-0.55
5	0.002	0.00208	1.04	0.02	0.35	0.13	0.37	-0.43
5	0.0025	0.01306	5.23	0.72	0.35	0.60	1.71	0.23
5	0.0025	0.01161	4.65	0.67	0.35	0.92	2.62	0.42

Loam (B) PFAS Isotherms										
Analyte Name	Aqueous Min (µg/L)	Aqueous Max (µg/L)	Solid Min (µg/kg)	Solid Max (µg/kg)	Obs.	Log K_f (mg/kg) $(mg/L)^{-n}$	±	n	±	R^2
PFBA	8.72	982.0	13.65	328.03	12	-0.53	0.05	0.65	0.04	0.99
PFPeA	20.54	918.0	5.73	289.52	12	-0.51	0.09	0.98	0.09	0.98
PFHxA	13.80	1234.67	4.01	172.91	12	-0.85	0.05	0.81	0.05	0.99
PFHpA	13.87	1058.67	2.52	542.64	12	-0.28	0.03	0.85	0.02	1.00
PFOA- Mix	1.58	618.0	4.35	1174.01	15	0.26	0.09	0.89	0.05	0.99
PFOA-Only	1.44	500.67	4.39	987.62	15	0.25	0.07	0.89	0.04	0.99
PFNA	0.59	358.00	5.79	1784.97	15	0.70	0.10	0.87	0.05	0.99
PFDA	0.30	107.73	32.00	2510.18	12	0.97	0.14	0.69	0.06	0.98
PFUnA	NM	NM	NM	NM	NM	NM	NM	NM	NM	NM
PFBS	1.88	938.0	3.69	701.22	15	-0.13	0.05	0.82	0.03	1.00
PFHxS	0.97	770.67	6.36	1306.82	15	0.21	0.05	0.78	0.03	1.00
PFOS-Mix	0.15	107.73	6.55	1970.90	15	1.15	0.08	0.85	0.03	1.00
PFOS-Only	0.09	72.73	5.30	1558.55	15	1.11	0.05	0.83	0.02	1.00

NM = Sorption could not be measured because aqueous concentrations were below detection.

B Interpolated K_d								
C_w (nM)	C_w (mg/L)	C_s (mg/kg)	Interp K_d (L/kg)	Log K_d @ 5nm	C_w (mg/L)	C_s (mg/kg)	Interp K_d (L/kg)	Log K_d @ 350 µg/L
5	0.0011	0.00339	3.18	0.50	0.35	0.15	0.42	-0.37
5	0.0013	0.00048	0.36	-0.44	0.35	0.11	0.32	-0.50
5	0.0016	0.00076	0.49	-0.31	0.35	0.06	0.17	-0.76
5	0.0018	0.00243	1.34	0.13	0.35	0.21	0.61	-0.22
5	0.0021	0.00719	3.48	0.54	0.35	0.71	2.02	0.31
5	0.0021	0.00723	3.50	0.54	0.35	0.70	1.99	0.30
5	0.0023	0.0256	11.06	1.04	0.35	2.00	5.72	0.76
5	0.0026	0.151	58.91	1.77	0.35	4.50	12.86	1.11
5	0.0028	NM	NM	NM	0.35	NM	NM	NM
5	0.0015	0.00351	2.35	0.37	0.35	0.31	0.90	-0.05
5	0.002	0.0125	6.27	0.80	0.35	0.71	2.03	0.31
5	0.0025	0.0861	34.49	1.54	0.35	5.76	16.46	1.22
5	0.0025	0.0914	36.63	1.56	0.35	5.46	15.61	1.19

Sandy Clay Loam (C) PFAS Isotherms										
Analyte Name	Aqueous Min (µg/L)	Aqueous Max (µg/L)	Solid Min (µg/kg)	Solid Max (µg/kg)	Obs.	Log K_f (mg/kg) $(mg/L)^{-n}$	±	n	±	R^2
PFBA	0.15	431.33	0.17	340.84	15	-0.18	0.09	0.97	0.04	0.99
PFPeA	0.21	599.33	0.14	335.79	15	-0.31	0.06	0.99	0.03	1.00
PFHxA	0.21	391.33	0.07	178.54	15	-0.34	0.04	1.05	0.02	1.00
PFHpA	0.42	857.33	0.23	433.41	15	-0.33	0.04	1.00	0.02	1.00
PFOA	0.37	661.33	0.28	733.56	15	0.02	0.09	1.08	0.04	0.99
PFNA	0.14	367.33	0.31	746.18	15	0.26	0.06	0.99	0.03	1.00
PFDA	0.04	173.20	0.25	883.25	15	0.68	0.02	0.98	0.01	1.00
PFUnA	NM	NM	NM	NM	NM	NM	NM	NM	NM	NM
PFBS	0.56	1000.67	0.27	685.04	15	-0.19	0.03	1.05	0.01	1.00
PFHxS	0.37	847.33	0.28	758.85	15	-0.06	0.01	1.01	0.01	1.00
PFOS	0.13	311.33	0.76	1201.49	15	0.55	0.03	0.94	0.01	1.00

NM = Sorption could not be measured because aqueous concentrations were below detection.

C Interpolated K_d								
C_w (nM)	C_w (mg/L)	C_s (mg/kg)	Interp K_d (L/kg)	Log K_d @ 5nm	C_w (mg/L)	C_s (mg/kg)	Interp K_d (L/kg)	Log K_d @ 350 µg/L
5	0.0011	0.00084	0.79	-0.10	0.35	0.24	0.68	-0.17
5	0.0013	0.00069	0.53	-0.28	0.35	0.17	0.49	-0.31
5	0.0016	0.00051	0.33	-0.49	0.35	0.15	0.43	-0.36
5	0.0018	0.00086	0.47	-0.33	0.35	0.16	0.47	-0.33
5	0.0021	0.00133	0.64	-0.19	0.35	0.34	0.96	-0.02
5	0.0023	0.00439	1.89	0.28	0.35	0.64	1.83	0.26
5	0.0026	0.0138	5.36	0.73	0.35	1.70	4.85	0.69
5	0.0026	NM	NM	NM	0.35	NM	NM	NM
5	0.0015	0.00068	0.46	-0.34	0.35	0.21	0.61	-0.22
5	0.002	0.0016	0.80	-0.10	0.35	0.30	0.86	-0.07
5	0.0025	0.0128	5.11	0.71	0.35	1.32	3.78	0.58

Loamy Sand (A)+1.46 g TCE PFAS Isotherms										
Analyte Name	Aqueous Min (µg/L)	Aqueous Max (µg/L)	Solid Min (µg/kg)	Solid Max (µg/kg)	Obs.	Log K_f (mg/kg) $(mg/L)^{-n}$	±	n	±	R^2
PFBA	0.49	427.33	0.81	351.11	15	-0.18	0.11	0.92	0.05	0.99
PFPeA	0.19	556.0	0.24	197.51	15	-0.27	0.18	0.89	0.08	0.97
PFHxA	2.55	426.67	0.65	168.78	12	-0.39	0.02	1.08	0.01	1.00
PFHpA	5.67	983.33	1.86	440.43	12	-0.38	0.04	1.06	0.03	1.00
PFOA	3.15	696.0	2.37	547.98	12	-0.24	0.13	0.89	0.06	0.99
PFNA	0.21	424.0	0.71	554.14	15	-0.03	0.13	0.89	0.06	0.99
PFDA	0.06	785.57	0.78	785.57	15	0.46	0.13	0.88	0.05	0.99
PFUnA	0.12	63.40	2.09	616.58	12	0.90	0.13	0.90	0.05	0.99
PFBS	4.47	1168.0	3.0	606.96	12	-0.29	0.04	0.97	0.03	1.00
PFHxS	0.43	974.67	0.32	643.45	15	-0.21	0.02	0.98	0.01	1.00
PFOS	0.19	293.33	0.61	969.97	15	0.52	0.03	1.01	0.01	1.00

A + TCE Interpolated K_d								
C_w (nM)	C_w (mg/L)	C_s (mg/kg)	Interp K_d (L/kg)	Log K_d @ 5nm	C_w (mg/L)	C_s (mg/kg)	Interp K_d (L/kg)	Log K_d @ 350 µg/L
5	0.0011	0.00119	1.12	0.05	0.35	0.25	0.72	-0.14
5	0.0013	0.00144	1.10	0.04	0.35	0.21	0.60	-0.22
5	0.0016	0.00038	0.24	-0.61	0.35	0.13	0.37	-0.43
5	0.0018	0.00052	0.29	-0.54	0.35	0.14	0.39	-0.41
5	0.0021	0.00231	1.12	0.05	0.35	0.23	0.65	-0.19
5	0.0023	0.0042	1.82	0.26	0.35	0.37	1.05	0.02
5	0.0026	0.015	5.86	0.77	0.35	1.14	3.25	0.51
5	0.0028	0.0406	14.426	1.16	0.35	3.08	8.79	0.94
5	0.0015	0.00097	0.65	-0.19	0.35	0.19	0.53	-0.27
5	0.002	0.0014	0.70	-0.15	0.35	0.22	0.63	-0.20
5	0.0025	0.0079	3.17	0.50	0.35	1.15	3.29	0.52

Loam (B) + 1.46 g TCE PFAS Isotherms										
Analyte Name	Aqueous Min (µg/L)	Aqueous Max (µg/L)	Solid Min (µg/kg)	Solid Max (µg/kg)	Obs.	Log K_f (mg/kg) $(mg/L)^{-n}$	±	n	±	R^2
PFBA	0.26	598.0	0.41	413.81	15	-0.14	0.28	1.07	0.18	0.94
PFPeA	3.01	550.67	1.86	364.97	12	-0.27	0.21	1.04	0.14	0.97
PFHxA	0.14	336.0	0.15	216.38	15	-0.34	0.18	0.93	0.08	0.98
PFHpA	4.29	774.67	3.25	585.37	12	-0.19	0.17	1.03	0.12	0.97
PFOA	0.32	642.67	0.80	881.67	15	0.001	0.14	0.91	0.07	0.98
PFNA	0.04	280.67	0.65	1106.82	15	0.42	0.14	0.83	0.05	0.99
PFDA	1.81	54.13	24.58	1111.52	9	1.54	0.16	1.14	0.08	1.00
PFUnA	NM	NM	NM	NM	NM	NM	NM	NM	NM	NM
PFBS	0.60	1270.67	0.60	726.15	15	-0.36	0.15	0.92	0.08	0.98
PFHxS	0.18	988.00	0.60	996.55	15	-0.11	0.15	0.86	0.07	0.98
PFOS	0.04	140.80	1.08	2016.87	15	1.01	0.15	0.90	0.05	0.99

NM = Sorption could not be measured because aqueous concentrations were below detection.

B + TCE Interpolated K_d								
C_w (nM)	C_w (mg/L)	C_s (mg/kg)	Interp K_d (L/kg)	Log K_d @ 5nm	C_w (mg/L)	C_s (mg/kg)	Interp K_d (L/kg)	Log K_d @ 350 µg/L
5	0.0011	0.00049	0.46	-0.34	0.35	0.24	0.68	-0.17
5	0.0013	0.00055	0.42	-0.38	0.35	0.18	0.51	-0.29
5	0.0016	0.00116	0.74	-0.13	0.35	0.17	0.50	-0.30
5	0.0018	0.00099	0.54	-0.26	0.35	0.22	0.63	-0.20
5	0.0021	0.00361	1.75	0.24	0.35	0.39	1.10	0.04
5	0.0023	0.0172	7.41	0.87	0.35	1.10	3.15	0.50
5	0.0026	0.0384	14.95	1.17	0.35	10.41	29.75	1.47
5	0.0023	NM	NM	NM	0.35	NM	NM	NM
5	0.0015	0.0011	0.73	-0.13	0.35	0.17	0.48	-0.32
5	0.002	0.00374	1.87	0.27	0.35	0.32	0.90	-0.05
5	0.0025	0.0464	18.58	1.27	0.35	3.98	11.37	1.06

Loamy Sand (A) PFAS Isotherms + 100 mg/L SDS										
Analyte Name	Aqueous Min (µg/L)	Aqueous Max (µg/L)	Solid Min (µg/kg)	Solid Max (µg/kg)	Obs.	Log K_f (mg/kg) $(mg/L)^{-n}$	±	n	±	R^2
PFBA	0.17	472.00	0.10	1.90	15	-0.21	0.05	0.99	0.02	1.00
PFPeA	2.07	596.00	1.85	365.57	12	-0.23	0.01	0.93	0.01	1.00
PFHxA	2.16	487.33	1.76	241.56	12	-0.33	0.03	0.92	0.02	1.00
PFHpA	0.46	966.00	0.29	535.14	15	-0.26	0.02	0.98	0.01	1.00
PFOA	0.37	851.33	0.27	520.95	15	-0.19	0.07	0.96	0.03	1.00
PFNA	0.25	620.67	0.31	518.81	15	-0.08	0.03	0.94	0.01	1.00
PFDA	0.09	343.33	0.40	750.04	15	0.33	0.03	0.91	0.01	1.00
PFUnA	0.27	95.87	3.16	780.10	12	0.79	0.17	0.90	0.07	0.99
PFBS	0.55	1298.67	0.55	598.75	15	-0.32	0.02	0.91	0.01	1.00
PFHxS	0.39	1014.67	0.41	635.07	15	-0.19	0.02	0.93	0.01	1.00
PFOS	0.12	376.00	0.41	637.22	15	0.21	0.03	0.91	0.01	1.00

A + SDS Interpolated K_d								
C_w (nM)	C_w (mg/L)	C_s (mg/kg)	Interp K_d (L/kg)	Log K_d @ 5nm	C_w (mg/L)	C_s (mg/kg)	Interp K_d (L/kg)	Log K_d @ 350 µg/L
5	0.0011	0.00069	0.64	-0.19	0.35	0.22	0.63	-0.20
5	0.0013	0.00123	0.93	-0.03	0.35	0.22	0.64	-0.20
5	0.0016	0.00126	0.80	-0.10	0.35	0.18	0.51	-0.29
5	0.0018	0.00111	0.61	-0.21	0.35	0.19	0.56	-0.26
5	0.0021	0.00174	0.84	-0.07	0.35	0.24	0.67	-0.17
5	0.0023	0.00276	1.19	0.08	0.35	0.31	0.88	-0.06
5	0.0026	0.00921	3.59	0.56	0.35	0.82	2.33	0.37
5	0.0026	0.0289	11.27	1.05	0.35	2.42	6.90	0.84
5	0.0015	0.00131	0.87	-0.06	0.35	0.18	0.52	-0.28
5	0.002	0.00194	0.97	-0.01	0.35	0.24	0.69	-0.16
5	0.0025	0.00685	2.74	0.44	0.35	0.62	1.76	0.25

Loam (B) PFAS Isotherms + 100 mg/L SDS										
Analyte Name	Aqueous Min (µg/L)	Aqueous Max (µg/L)	Solid Min (µg/kg)	Solid Max (µg/kg)	Obs.	Log K_f (mg/kg) $(mg/L)^{-n}$	±	n	±	R^2
PFBA	0.21	408.00	0.14	343.59	15	-0.03	0.03	1.03	0.01	1.00
PFPeA	1.94	568.00	2.42	461.23	12	-0.08	0.03	0.94	0.02	1.00
PFHxA	2.14	428.00	2.17	345.69	12	-0.12	0.02	0.96	0.01	1.00
PFHpA	0.30	808.00	0.56	734.26	15	-0.03	0.04	0.93	0.02	1.00
PFOA	0.13	587.00	0.60	930.64	15	0.13	0.08	0.84	0.03	1.00
PFNA	0.10	256.00	0.71	1126.98	15	0.60	0.02	0.94	0.01	1.00
PFDA	0.03	121.07	0.68	1292.35	15	0.97	0.03	0.90	0.01	1.00
PFUnA	NM	NM	NM	NM	NM	NM	NM	NM	NM	NM
PFBS	0.44	893.00	0.94	793.18	15	-0.05	0.04	0.93	0.03	1.00
PFHxS	0.05	616.00	1.04	1210.85	15	0.17	0.10	0.77	0.04	0.99
PFOS	0.05	80.33	1.09	1362.76	15	1.17	0.02	0.95	0.01	1.00

NM = Sorption could not be measured because aqueous concentrations were below detection.

B + SDS Interpolated K_d								
C_w (nM)	C_w (mg/L)	C_s (mg/kg)	Interp K_d (L/kg)	Log K_d @ 5nm	C_w (mg/L)	C_s (mg/kg)	Interp K_d (L/kg)	Log K_d @ 350 µg/L
5	0.0011	0.0008	0.75	-0.13	0.35	0.31	0.89	-0.05
5	0.0013	0.00165	1.26	0.10	0.35	0.31	0.89	-0.05
5	0.0016	0.00157	1.00	0.00	0.35	0.28	0.80	-0.10
5	0.0018	0.00272	1.50	0.18	0.35	0.35	1.01	0.01
5	0.0021	0.00748	3.62	0.56	0.35	0.56	1.60	0.20
5	0.0023	0.0134	5.78	0.76	0.35	1.48	4.24	0.63
5	0.0026	0.0436	16.99	1.23	0.35	3.62	10.36	1.02
5	0.0026	NM	NM	NM	0.35	NM	NM	NM
5	0.0015	0.002	1.36	0.13	0.35	0.33	0.95	-0.02
5	0.002	0.0125	6.28	0.80	0.35	0.66	1.89	0.28
5	0.0025	0.0502	20.11	1.30	0.35	5.48	15.65	1.19

Sandy Clay Loam (C) PFAS Isotherms + 100 mg/L SDS										
Analyte Name	Aqueous Min (µg/L)	Aqueous Max (µg/L)	Solid Min (µg/kg)	Solid Max (µg/kg)	Obs.	Log K_f (mg/kg) $(mg/L)^{-n}$	±	n	±	R^2
PFBA	0.14	460.67	0.15	304.36	15	1.17	0.14	0.94	0.06	0.99
PFPeA	0.18	519.33	0.14	369.10	15	-0.32	0.12	0.97	0.05	0.99
PFHxA	0.24	446.00	0.25	272.41	15	-0.42	0.14	0.92	0.06	0.99
PFHpA	0.47	842.67	0.31	805.60	15	-0.21	0.11	1.01	0.06	0.99
PFOA	0.38	583.33	0.26	1416.73	15	0.18	0.14	1.13	0.07	0.99
PFNA	0.19	395.33	0.38	1200.30	15	0.33	0.11	1.03	0.05	0.99
PFDA	0.06	200.47	0.30	2041.57	15	1.02	0.04	1.08	0.01	1.00
PFUnA	NM	NM	NM	NM	NM	NM	NM	NM	NM	NM
PFBS	0.54	787.33	0.32	854.50	15	-0.11	0.09	1.05	0.05	0.99
PFHxS	0.34	726.67	0.31	1282.43	15	0.01	0.14	1.03	0.07	0.99
PFOS	0.16	259.33	0.76	1858.27	15	0.73	0.10	1.03	0.04	1.00

NM = Sorption could not be measured because aqueous concentrations were below detection.

C + SDS Interpolated K_d								
C_w (nM)	C_w (mg/L)	C_s (mg/kg)	Interp K_d (L/kg)	Log K_d @ 5nm	C_w (mg/L)	C_s (mg/kg)	Interp K_d (L/kg)	Log K_d @ 350 µg/L
5	0.0011	0.0233	21.83	1.34	0.35	5.51	15.74	1.20
5	0.0013	0.00075	0.57	-0.24	0.35	0.17	0.49	-0.31
5	0.0016	0.00102	0.65	-0.19	0.35	0.15	0.42	-0.38
5	0.0018	0.00103	0.57	-0.25	0.35	0.21	0.61	-0.21
5	0.0021	0.00143	0.69	-0.16	0.35	0.46	1.32	0.12
5	0.0023	0.00423	1.83	0.26	0.35	0.73	2.09	0.32
5	0.0026	0.0162	6.33	0.80	0.35	3.33	9.50	0.98
5	0.0026	NM	NM	NM	0.35	NM	NM	NM
5	0.0015	0.00083	0.56	-0.25	0.35	0.26	0.74	-0.13
5	0.002	0.00175	0.88	-0.06	0.35	0.35	1.01	0.00
5	0.0025	0.0112	4.50	0.65	0.35	1.84	5.24	0.72

Loamy Sand (A) PFAS Isotherms + 100 mg/L AO										
Analyte Name	Aqueous Min (µg/L)	Aqueous Max (µg/L)	Solid Min (µg/kg)	Solid Max (µg/kg)	Obs.	Log K_f (mg/kg) $(mg/L)^{-n}$	±	n	±	R^2
PFBA	0.13	458.67	0.09	442.30	15	0.03	0.04	1.04	0.02	1.00
PFPeA	0.24	548.00	0.05	433.38	15	0.02	0.10	1.17	0.05	1.00
PFHxA	0.27	403.33	0.03	218.43	15	-0.13	0.09	1.20	0.04	1.00
PFHpA	0.52	884.00	0.08	562.78	15	-0.17	0.07	1.17	0.04	1.00
PFOA	0.45	724.67	0.07	833.55	15	0.17	0.11	1.25	0.06	0.99
PFNA	0.21	393.33	0.12	670.86	15	0.34	0.10	1.13	0.04	1.00
PFDA	0.05	196.67	0.13	1079.78	15	0.83	0.08	1.10	0.03	1.00
PFUnA	NM	NM	NM	NM	NM	NM	NM	NM	NM	NM
PFBS	0.58	984.67	0.20	888.16	15	0.02	0.13	1.09	0.07	0.99
PFHxS	0.34	806.00	0.14	875.01	15	0.10	0.10	1.10	0.05	0.99
PFOS	0.09	353.33	0.32	1250.33	15	0.54	0.07	0.98	0.03	1.00

NM = Sorption could not be measured because aqueous concentrations were below detection.

A + AO Interpolated K_d								
C_w (nM)	C_w (mg/L)	C_s (mg/kg)	Interp K_d (L/kg)	Log K_d @ 5nm	C_w (mg/L)	C_s (mg/kg)	Interp K_d (L/kg)	Log K_d @ 350 µg/L
5	0.0011	0.00085	0.80	-0.10	0.35	0.36	1.03	0.01
5	0.0013	0.00045	0.34	-0.46	0.35	0.31	0.88	-0.06
5	0.0016	0.00033	0.21	-0.68	0.35	0.21	0.61	-0.22
5	0.0018	0.00043	0.23	-0.63	0.35	0.20	0.56	-0.25
5	0.0021	0.00067	0.32	-0.49	0.35	0.40	1.15	0.06
5	0.0023	0.00228	0.99	-0.01	0.35	0.66	1.90	0.28
5	0.0026	0.0095	3.70	0.57	0.35	2.13	6.09	0.78
5	0.0023	NM	NM	NM	0.35	NM	NM	NM
5	0.0015	0.00088	0.59	-0.23	0.35	0.34	0.96	-0.02
5	0.002	0.00137	0.69	-0.16	0.35	0.40	1.14	0.06
5	0.0025	0.01	4.02	0.60	0.35	1.25	3.56	0.55

Loam (B) PFAS Isotherms + 100 mg/L AO										
Analyte Name	Aqueous Min (µg/L)	Aqueous Max (µg/L)	Solid Min (µg/kg)	Solid Max (µg/kg)	Obs.	Log K_f (mg/kg) $(mg/L)^{-n}$	±	n	±	R^2
PFBA	0.16	453.33	0.40	161.79	15	-0.23	0.19	0.85	0.09	0.97
PFPeA	0.27	627.33	0.26	175.33	15	-0.32	0.16	0.91	0.08	0.98
PFHxA	0.26	459.33	0.18	89.37	15	-0.50	0.17	0.91	0.08	0.98
PFHpA	0.36	978.00	0.44	260.34	15	-0.33	0.14	0.88	0.07	0.98
PFOA	0.22	618.00	0.72	582.87	15	0.15	0.14	0.91	0.06	0.99
PFNA	0.06	225.07	0.58	558.82	15	0.56	0.17	0.89	0.06	0.98
PFDA	0.13	63.73	4.53	726.77	12	1.08	0.24	0.86	0.10	0.98
PFUnA	NM	NM	NM	NM	NM	NM	NM	NM	NM	NM
PFBS	0.66	794.00	2.31	367.93	15	-0.11	0.17	0.81	0.09	0.96
PFHxS	0.06	580.67	0.98	506.61	15	0.09	0.17	0.76	0.97	0.97
PFOS	0.20	85.87	1.37	791.88	12	0.98	0.26	0.81	0.11	0.97

NM = Sorption could not be measured because aqueous concentrations were below detection.

B + AO Interpolated K_d								
C_w (nM)	C_w (mg/L)	C_s (mg/kg)	Interp K_d (L/kg)	Log K_d @ 5nm	C_w (mg/L)	C_s (mg/kg)	Interp K_d (L/kg)	Log K_d @ 350 µg/L
5	0.0011	0.00177	1.67	0.22	0.35	0.24	0.68	-0.16
5	0.0013	0.00112	0.85	-0.07	0.35	0.18	0.53	-0.28
5	0.0016	0.00089	0.57	-0.24	0.35	0.12	0.35	-0.46
5	0.0018	0.0018	0.99	0.00	0.35	0.18	0.53	-0.28
5	0.0021	0.00495	2.40	0.38	0.35	0.54	1.53	0.19
5	0.0023	0.0161	6.95	0.84	0.35	1.43	4.08	0.61
5	0.0026	0.0706	27.50	1.44	0.35	4.88	13.94	1.14
5	0.0023	NM	NM	NM	0.35	NM	NM	NM
5	0.0015	0.00392	2.62	0.42	0.35	0.33	0.95	-0.02
5	0.002	0.0113	5.66	0.75	0.35	0.56	1.60	0.20
5	0.0025	0.0751	30.10	1.48	0.35	4.06	11.60	1.06

Sandy Clay Loam (C) PFAS Isotherms + 100 mg/L AO										
Analyte Name	Aqueous Min (µg/L)	Aqueous Max (µg/L)	Solid Min (µg/kg)	Solid Max (µg/kg)	Obs.	Log K_f (mg/kg) $(mg/L)^{-n}$	±	n	±	R^2
PFBA	0.14	444.67	0.46	461.15	15	-0.24	0.18	0.86	0.08	0.97
PFPeA	0.19	537.33	0.16	476.96	15	-0.20	0.09	0.98	0.04	0.99
PFHxA	0.23	392.00	0.10	258.91	15	-0.28	0.08	1.04	0.04	1.00
PFHpA	0.35	674.00	0.41	819.49	15	0.05	0.03	1.01	0.02	1.00
PFOA	0.21	239.27	0.59	1978.06	15	0.98	0.03	1.15	0.01	1.00
PFNA	0.06	139.00	0.46	1788.75	15	1.28	0.10	1.08	0.04	1.00
PFDA	0.13	126.13	4.33	1784.11	12	1.20	0.27	0.87	0.10	0.97
PFUnA	NM	NM	NM	NM	NM	NM	NM	NM	NM	NM
PFBS	0.42	710.00	0.47	1339.82	15	0.24	0.03	1.05	0.02	1.00
PFHxS	0.18	235.33	0.85	2420.37	15	1.07	0.02	1.10	0.01	1.00
PFOS	0.04	89.60	1.19	2212.01	15	1.53	0.20	0.97	0.07	0.99

NM = Sorption could not be measured because aqueous concentrations were below detection.

C+AO Interpolated K_d								
C_w (nM)	C_w (mg/L)	C_s (mg/kg)	Interp K_d (L/kg)	Log K_d @ 5nm	C_w (mg/L)	C_s (mg/kg)	Interp K_d (L/kg)	Log K_d @ 350 µg/L
5	0.0011	0.00157	1.47	0.17	0.35	0.23	0.67	-0.17
5	0.0013	0.00093	0.71	-0.15	0.35	0.22	0.64	-0.19
5	0.0016	0.00065	0.42	-0.38	0.35	0.18	0.50	-0.30
5	0.0018	0.00196	1.08	0.03	0.35	0.39	1.12	0.05
5	0.0021	0.00779	3.77	0.58	0.35	2.84	8.11	0.91
5	0.0023	0.0276	11.90	1.08	0.35	6.13	17.52	1.24
5	0.0026	0.0864	33.68	1.53	0.35	6.34	18.12	1.26
5	0.0023	NM	NM	NM	0.35	NM	NM	NM
5	0.0015	0.00182	1.22	0.09	0.35	0.57	1.63	0.21
5	0.002	0.0123	6.17	0.79	0.35	3.67	10.50	1.02
5	0.0025	0.1025	41.07	1.61	0.35	12.31	35.16	1.55

Appendix A-2

Summary of Freundlich n-values measured in PFAS and PFAS+ Co-contaminant Isotherms

Analyte	A n	±	A+ TCE n	±	A+ SDS n	±	A+AO n	±	B n	±	B+ TCE n	±	B+ SDS n	±	B+AO n	±	C n	±	C+ SDS n	±	C+AO n	±
PFBA	0.74	0.06	0.92	0.05	0.99	0.02	1.04	0.02	0.65	0.04	1.07	0.18	1.03	0.01	0.85	0.09	0.97	0.04	0.94	0.06	0.86	0.08
PFPeA	0.84	0.04	0.89	0.08	0.93	0.01	1.17	0.05	0.98	0.09	1.04	0.14	0.94	0.02	0.91	0.08	0.99	0.03	0.97	0.05	0.98	0.04
PFHxA	0.95	0.08	1.08	0.01	0.92	0.02	1.20	0.04	0.81	0.05	0.93	0.08	0.96	0.01	0.91	0.08	1.05	0.02	0.92	0.06	1.04	0.04
PFHpA	0.92	0.04	1.06	0.03	0.98	0.01	1.17	0.04	0.85	0.02	1.03	0.12	0.93	0.02	0.88	0.07	1.00	0.02	1.01	0.06	1.01	0.02
PFOA	0.88	0.08	0.89	0.06	0.96	0.03	1.25	0.06	0.89	0.05	0.91	0.07	0.84	0.03	0.91	0.06	1.08	0.04	1.13	0.07	1.15	0.01
PFNA	0.81	0.08	0.89	0.06	0.94	0.01	1.13	0.04	0.87	0.05	0.83	0.05	0.94	0.01	0.89	0.06	0.99	0.03	1.03	0.05	1.08	0.04
PFDA	0.68	0.03	0.88	0.05	0.91	0.01	1.10	0.03	0.69	0.06	1.14	0.08	0.90	0.01	0.86	0.10	0.98	0.01	1.08	0.01	0.87	0.10
PFUnA	0.61	0.03	0.90	0.05	0.90	0.07	NM	NM	NM	NM	NM	NM	NM	NM	NM	NM	NM	NM	NM	NM	NM	NM
PFBS	0.81	0.04	0.97	0.03	0.91	0.01	1.09	0.07	0.82	0.03	0.92	0.08	0.93	0.03	0.81	0.09	1.05	0.01	1.05	0.05	1.05	0.02
PFHxS	0.80	0.09	0.98	0.01	0.93	0.01	1.10	0.05	0.78	0.03	0.86	0.07	0.77	0.04	0.76	0.97	1.01	0.01	1.03	0.07	1.10	0.01
PFOS	0.77	0.05	1.01	0.01	0.91	0.01	0.98	0.03	0.85	0.03	0.90	0.05	0.95	0.01	0.81	0.11	0.94	0.01	1.03	0.04	0.97	0.07

NM = Sorption could not be measured because aqueous concentrations were below detection.

Appendix A-2

Summary of Freundlich n-values measured in PFAS and PFAS+ Co-contaminant Isotherms

Analyte	A n	±	A+ TCE n	±	A+ SDS n	±	A+AO n	±	B n	±	B+ TCE n	±	B+ SDS n	±	B+AO n	±	C n	±	C+ SDS n	±	C+AO n	±
PFBA	0.74	0.06	0.92	0.05	0.99	0.02	1.04	0.02	0.65	0.04	1.07	0.18	1.03	0.01	0.85	0.09	0.97	0.04	0.94	0.06	0.86	0.08
PFPeA	0.84	0.04	0.89	0.08	0.93	0.01	1.17	0.05	0.98	0.09	1.04	0.14	0.94	0.02	0.91	0.08	0.99	0.03	0.97	0.05	0.98	0.04
PFHxA	0.95	0.08	1.08	0.01	0.92	0.02	1.20	0.04	0.81	0.05	0.93	0.08	0.96	0.01	0.91	0.08	1.05	0.02	0.92	0.06	1.04	0.04
PFHpA	0.92	0.04	1.06	0.03	0.98	0.01	1.17	0.04	0.85	0.02	1.03	0.12	0.93	0.02	0.88	0.07	1.00	0.02	1.01	0.06	1.01	0.02
PFOA	0.88	0.08	0.89	0.06	0.96	0.03	1.25	0.06	0.89	0.05	0.91	0.07	0.84	0.03	0.91	0.06	1.08	0.04	1.13	0.07	1.15	0.01
PFNA	0.81	0.08	0.89	0.06	0.94	0.01	1.13	0.04	0.87	0.05	0.83	0.05	0.94	0.01	0.89	0.06	0.99	0.03	1.03	0.05	1.08	0.04
PFDA	0.68	0.03	0.88	0.05	0.91	0.01	1.10	0.03	0.69	0.06	1.14	0.08	0.90	0.01	0.86	0.10	0.98	0.01	1.08	0.01	0.87	0.10
PFUnA	0.61	0.03	0.90	0.05	0.90	0.07	NM	NM	NM	NM	NM	NM	NM	NM	NM	NM	NM	NM	NM	NM	NM	NM
PFBS	0.81	0.04	0.97	0.03	0.91	0.01	1.09	0.07	0.82	0.03	0.92	0.08	0.93	0.03	0.81	0.09	1.05	0.01	1.05	0.05	1.05	0.02
PFHxS	0.80	0.09	0.98	0.01	0.93	0.01	1.10	0.05	0.78	0.03	0.86	0.07	0.77	0.04	0.76	0.97	1.01	0.01	1.03	0.07	1.10	0.01
PFOS	0.77	0.05	1.01	0.01	0.91	0.01	0.98	0.03	0.85	0.03	0.90	0.05	0.95	0.01	0.81	0.11	0.94	0.01	1.03	0.04	0.97	0.07

NM = Sorption could not be measured because aqueous concentrations were below detection.

Appendix A-3

Aqueous PFAS Concentrations Measured in the Presence of Varying Concentrations of SDS. Reactors were prepared with 0.5 mg/L PFASs and 0, 0.5, 10, 50, and 100 mg/L SDS. Note that Y-axis scales were varied based on aqueous PFAS concentrations measured.

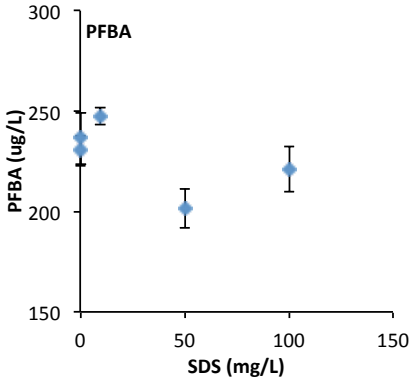

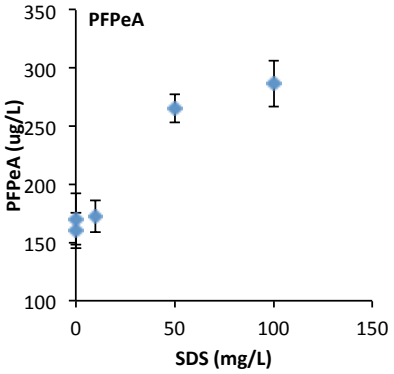

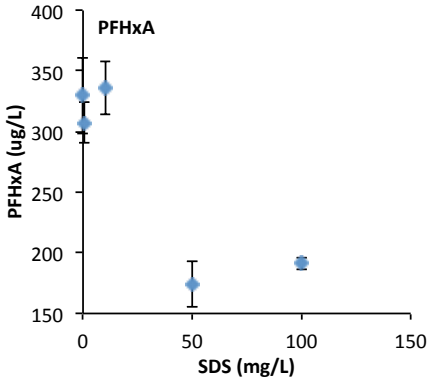

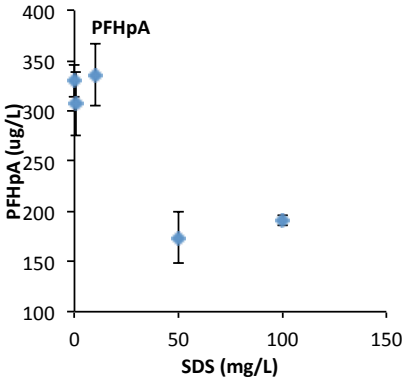

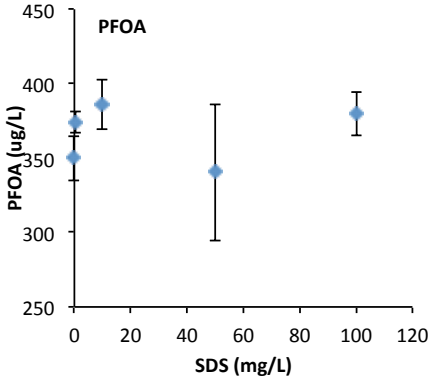

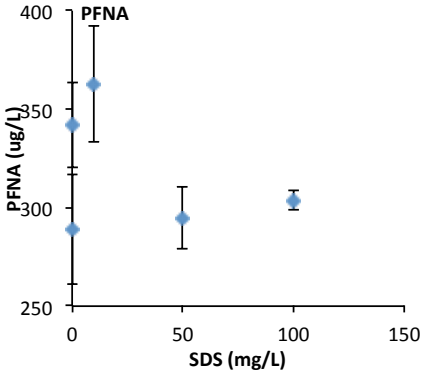

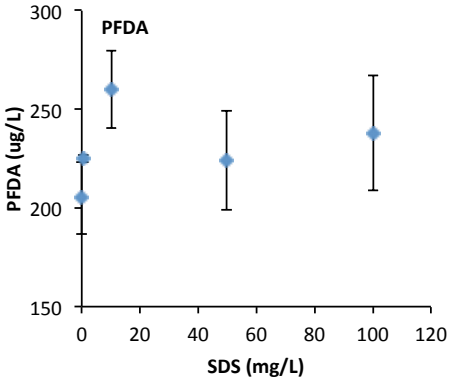
PFDA
PFDA (ug/L)
300
250
200
150
0
20
40
60
80
100
120
SDS (mg/L)

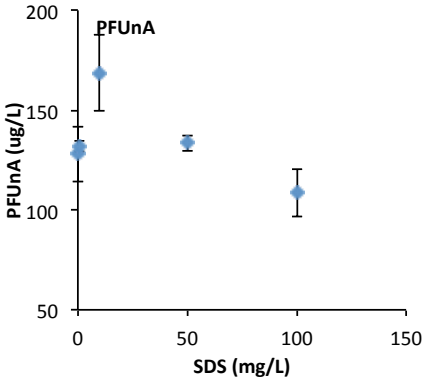
PFUnA
PFUnA (ug/L)
200
150
100
50
0
50
100
150
SDS (mg/L)

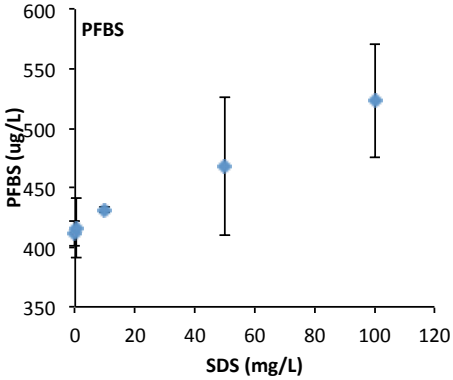
PFBS
PFBS (ug/L)
600
550
500
450
400
350
0
20
40
60
80
100
120
SDS (mg/L)

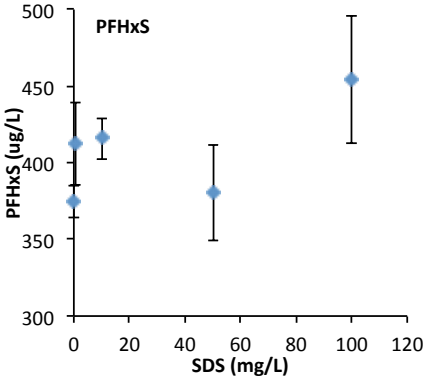
PFHxS
PFHxS (ug/L)
500
450
400
350
300
0
20
40
60
80
100
120
SDS (mg/L)

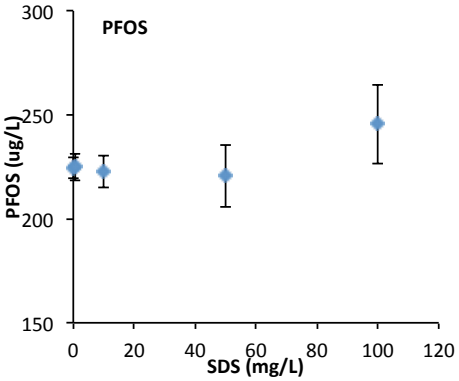
PFOS
PFOS (ug/L)
300
250
200
150
0
20
40
60
80
100
120
SDS (mg/L)

Appendix A-4

Aqueous PFAS Concentrations Measured in the Presence of Varying Concentrations of AO. Reactors were prepared with 0.5 mg/L PFASs and 0, 0.5, 10, 50, and 100 mg/L AO. Note that Y-axis scales were varied based on aqueous PFAS concentrations measured.

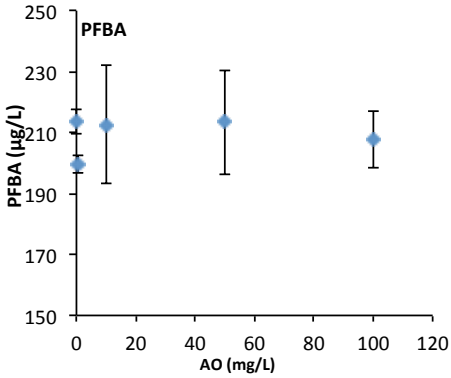

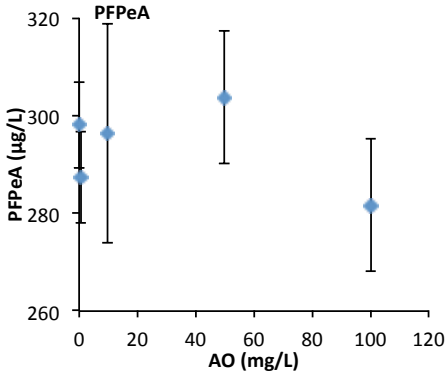

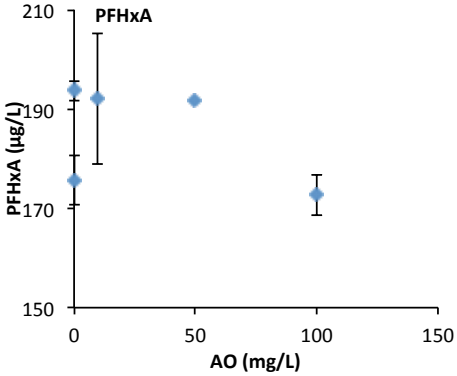

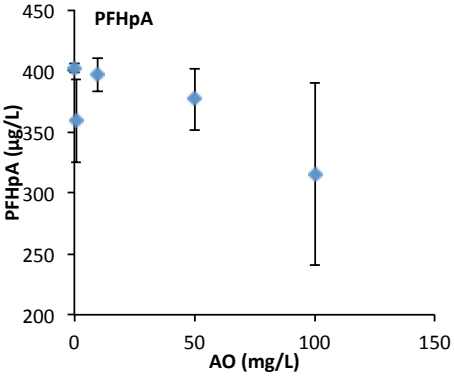

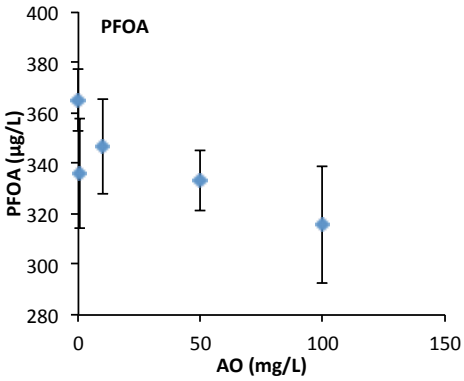

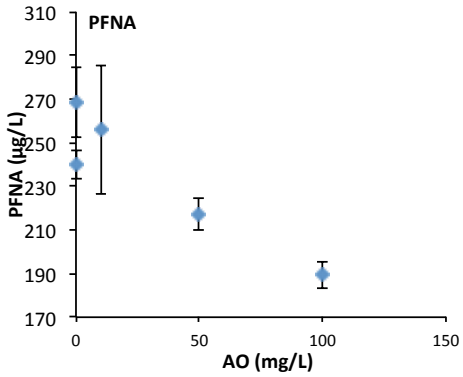

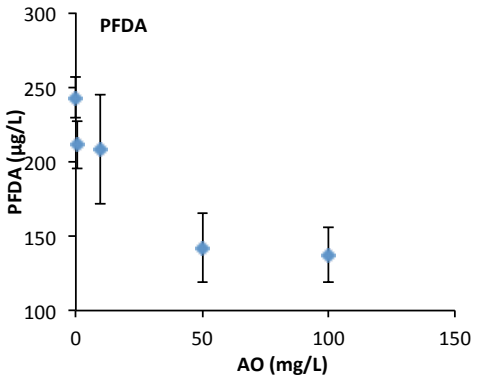
PFDA
PFDA (µg/L)
300
250
200
150
100
0
50
100
150
AO (mg/L)

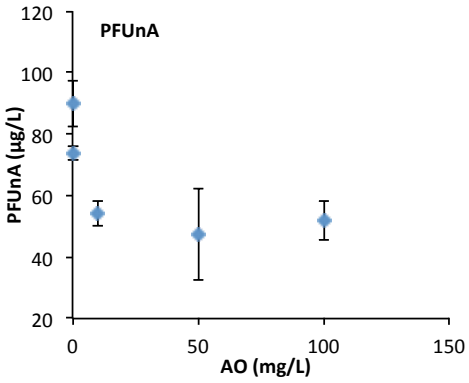
PFUnA
PFUnA (µg/L)
120
100
80
60
40
20
0
50
100
150
AO (mg/L)

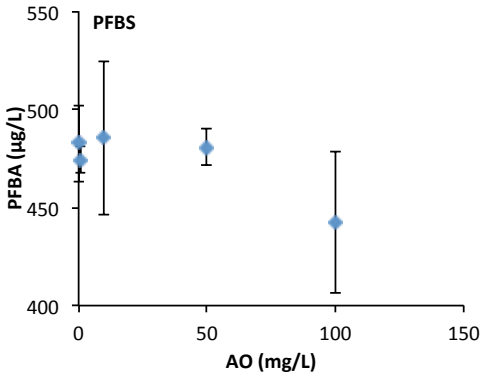
PFBS
PFBA (µg/L)
550
500
450
400
0
50
100
150
AO (mg/L)

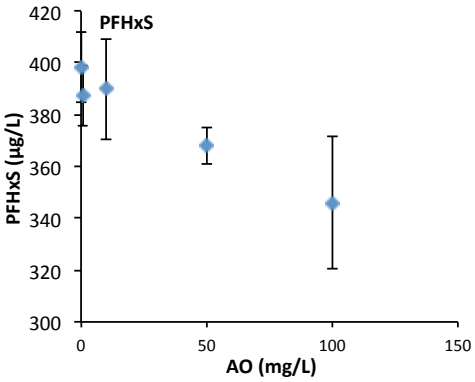
PFHxS
PFHxS (µg/L)
420
400
380
360
340
320
300
0
50
100
150
AO (mg/L)

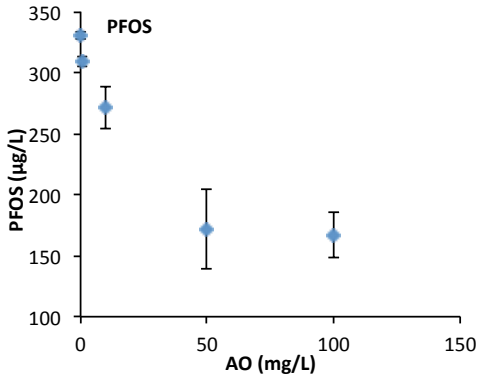
PFOS
PFOS (µg/L)
350
300
250
200
150
100
0
50
100
150
AO (mg/L)

Appendix B

Dual-Indexed Primer Specifications used in Chapter 4.

```
501-508 PCR primer design – forward primer:
<Illumina adapter><i5 index>< primer pad><linker><V4 16Sf>
Illumina adapter: AATGATACGGCGACCACCGAGATCTACAC
      i5 index: NNNNNNNN
      Primer pad: TATGGTAATT
      Linker: GT
V4 16Sf: GTGCCAGCMGCCGCGGTAA

701-712 PCR primer design – reverse primer:
<Illumina adapter><i7 index>< primer pad><linker><V4 16Sr>
      Illumina adapter: CAAGCAGAAGACGGCATACGAGAT
      i7 index: NNNNNNNN
      Primer pad: AGTCAGTCAG
      Linker: CC
V4 16Sr: GGACTACHVGGGTWTCTAAT
```

The amplification program began with initial denaturation for two minutes at 95°C, followed by the amplification cycles that included 95°C for 20 seconds, 55°C for 15 seconds, and 72°C for 5 minutes. The final extension occurred at 72°C for 10 minutes and ended with a final hold at 4°C.

```
Sequencing Post-Processing Scripts
#Join paired ends
multiple_split_libraries_fastq.py -i /joined_renamed_tw
-o /split_out_tw --demultiplexing_method sampleid_by_file --
include_input_dir_path --remove_filepath_in_name
--read_indicator .join.

#Pick open reference OTUs[3-6]
pick_open_reference_otus.py -i seqs.fna
-r /macqiime/greengenes/gg_13_8_otus/rep_set/97_otus.fasta
-o /open_ref_otus
-p /pick_open_ref_otus_parameters.txt -m usearch61

#OTU table summary
biom summarize-table
-i  /open_ref_otus/otu_table_mc2_w_tax.biom
-o  /open_ref_otus/otu_table_summary

#Divide samples for different projects and summarize table
filter_samples_from_otu_table.py
-i /open_ref_otus/otu_table_mc2_w_tax.biom
-o /open_ref_otu/otu_table_tw_erd.biom
--sample_id_fp /erd_sample_ids.txt

biom summarize-table
-i /otu_table_tw_erd.biom
-o /otu_table_summary_tw_erd
```

```
#Rarify OUT table to lowest count
single_rarefaction.py
-i /otu_table_tw_erd.biom
-o /otu_table_tw_erd_21761.biom
-d 21761

#Summarize rarefied and non-rarefied OTU tables
summarize_taxa_through_plots.py
-i /otu_table_tw_erd_21761.biom
-o /wf_taxa_summary_tw_erd_21761
-m /150107_illumina_mapping_tsw.txt

summarize_taxa_through_plots.py
-i /otu_table_tw_erd.biom
-o /wf_taxa_summary_tw_erd_norare
-m /150107_illumina_mapping_tsw.txt

#Make .tre file[7]
make_phylogeny.py -i /rep_set_aligned_pfiltered.fasta
-o /rep_st_tw.tre

#Set alpha diversity parameters
echo "alpha_diversity:metrics shannon,PD_whole_tree,chao1,observed_species" >
alpha_params.txt

#Calculate alpha diversity on rarefied and non-rarefied
alpha_rarefaction.py
-i /otu_table_tw_erd_21761.biom
-m /150107_illumina_mapping_tsw_erd.txt
-o /wf_arare_tw_erd/
-p alpha_params.txt
-t /rep_st_tw.tre

alpha_rarefaction.py
-i /otu_table_tw_erd.biom
-m /150107_illumina_mapping_tsw_erd.txt
-o wf_arare_tw_erd_norare/
-p alpha_params.txt
-t /rep_st_tw.tre

#Calculate beta diversity on rarefied and non-rarefied
beta_diversity_through_plots.py
-i /otu_table_tw_erd_21761.biom
-m /150107_illumina_mapping_tsw_erd.txt
-o /wf_bdiv_tw_erd_21761
-t /rep_st_tw.tre

beta_diversity_through_plots.py
-i /otu_table_tw_erd.biom
-m /150107_illumina_mapping_tsw_erd.txt
-o /wf_bdiv_tw_erd_norare
-t /rep_st_tw.tre
```

```
#Filter samples for comparison
filter_samples_from_otu_table.py
-i /otu_table_mc2_w_tax.biom
-o /otu_table_tw_erd_AllMix.biom
--sample_id_fp /erd_sample_ids_AllMix.txt

# This is to further separate files (e.g. AllMix = all PFAAs and 0, PFSA =
sulfonates and 0, 22ppm means only samples at 22 (sulfonates and allmix)
filter_samples_from_otu_table.py
-i /otu_table_mc2_w_tax.biom
-o /otu_table_tw_erd_PFSA.biom
--sample_id_fp /erd_sample_ids_PFSA.txt

filter_samples_from_otu_table.py
-i /otu_table_mc2_w_tax.biom
-o /otu_table_tw_erd_22ppm.biom
--sample_id_fp /erd_sample_ids_22ppm.txt

filter_samples_from_otu_table.py
-i /otu_table_mc2_w_tax.biom
-o /otu_table_tw_erd_66ppm.biom
--sample_id_fp /erd_sample_ids_66ppm.txt

filter_samples_from_otu_table.py
-i  /otu_table_mc2_w_tax.biom
-o /otu_table_tw_erd_110ppm.biom
--sample_id_fp /erd_sample_ids_110ppm.txt

# Filter samples to >0.001 abundance, repeated for each OTU table
filter_otus_from_otu_table.py
-i /otu_table_tw_erd_All_no_10.biom
-o /otu_table_tw_erd_All_no_10_minfrac_001.biom
--min_count_fraction 0.001

# Summarize by taxa and convert to integers, repeated for each OTU table
summarize_taxa.py
-i /otu_table_tw_erd_All_no_10_minfrac_001.biom
-o otu_table_All_no_10_taxa_abs_minfrac_001.biom
-a

# Convert to json file format, repeated for each OTU table
biom convert -i /otu_table_tw_erd_All_no_10_minfrac_001_L6.biom
-o /otu_table_tw_erd_All_no_10_minfrac_001_L6_json.biom
--table-type="OTU table"
--to-json

# Differential abundance using DeSeq, repeated for each comparison[8]
differential_abundance.py
-i /otu_table_tw_erd_All_no_10_minfrac_001_L6_json.biom
-o /All_NoPFAAv10_tax_L6_minfrac_001_DEseq.txt
-m /150107_illumina_mapping_tsw_erd.txt -c PFAA -x 10ppm -y NoPFAA
-a DESeq2_nbinom -d

# Make new .tre file to use with FIGtree
```

```
make_phylogeny.py
-i /rep_set_aligned_pfiltered.fasta
-o /rep_st_tw_fig.tre

# Prune tree file
filter_tree.py
-i /rep_st_tw_fig.tre
-o erd_minfrac001_pruned.tre
-t /erd_minfrac001_tips_to_keep.txt

# Create distance matrices (then manually change their names)
beta_diversity.py -i /otu_table_tw_erd_AllMix_minfrac_001.biom
-m weighted_unifrac -o /beta_div/ -t /rep_st_tw.tre

# Adonis statistical test[9]
compare_categories.py --method adonis
-i /weighted_unifrac_otu_table_tw_erd_AllMix_minfrac_001.txt
-m 150107_illumina_mapping_tsw_erd_AllMix.txt -c PFAA -o /adonis/ -n 999

# ANOSIM statistical test
compare_categories.py --method anosim
-i /weighted_unifrac_otu_table_tw_erd_AllMix_minfrac_001.txt
-m /150107_illumina_mapping_tsw_erd_AllMix.txt -c PFAA -o /anosim/ -n 999

# Redo adonis and ANOSIM without 110
# Remove 110
filter_samples_from_otu_table.py
-i /otu_table_tw_erd_AllMix_minfrac_001.biom
-o /otu_tab_erd_AllMix_minfrac_001_no110.biom
-m /150107_illumina_mapping_tsw_erd_AllMix_stats.txt
-s 'Location:Dechlor'

# Redo beta div without 110, manually rename file
beta_diversity.py -i /otu_tab_erd_AllMix_minfrac_001_no110.biom
-m weighted_unifrac -o /beta_div/ -t /rep_st_tw.tre

# Run tests without 110
compare_categories.py --method adonis
-i /weighted_unifrac_otu_tab_erd_AllMix_minfrac_001_no110.txt
-m /150107_illumina_mapping_tsw_erd_AllMix_stats_no110.txt -c PFAA
-o /adonis/ -n 999

compare_categories.py --method anosim
-i /weighted_unifrac_otu_tab_erd_AllMix_minfrac_001_no110.txt
-m /150107_illumina_mapping_tsw_erd_AllMix_stats_no110.txt -c PFAA
-o /anosim/ -n 999
```